NONLINEAR FILTERING, PARAMETER ESTIMATION AND DECOMPOSITION OF LARGE RAINFALL-RUNOFF MODELS

by
CARLOS E. PUENTE ANGULO
and
RAFAEL L. BRAS

RALPH M. PARSONS LABORATORY
HYDROLOGY AND WATER RESOURCE SYSTEMS

DEPARTMENT OF CIVIL ENGINEERING
MASSACHUSETTS INSTITUTE OF TECHNOLOGY

Report No. 297

The work upon which this publication is based
was sponsored by the Hydrologic Research Laboratory,
National Weather Service,
U.S. Department of Commerce

October 1984

MIT

DEPARTMENT
OF
CIVIL
ENGINEERING

SCHOOL OF ENGINEERING
MASSACHUSETTS INSTITUTE OF TECHNOLOGY
Cambridge, Massachusetts 02139

R -84-13

OSP 89310

NONLINEAR FILTERING, PARAMETER ESTIMATION AND DECOMPOSITION OF LARGE RAINFALL-RUNOFF MODELS

by

Carlos E. Puente Angulo

and

Rafael L. Bras

RALPH M. PARSONS LABORATORY

HYDROLOGY AND WATER RESOURCE SYSTEMS

Report Number 297

The work upon which this publication is based was sponsored by the Hydrologic Research Laboratory, National Weather Service, U.S. Department of Commerce

October 1984

ABSTRACT

Three topics related to the real time forecasting of river flows are studied. First, the usefulness of nonlinear filtering procedures in connection with a conceptual rainfall-runoff model is investigated. By means of a case study it is determined that only filters which employ future information to correct the past (smoothers) could potentially improve forecasts over the simpler extended Kalman filter. The quality of the predictions is heavily dependent on the nature of the assigned error of the conceptual rainfall-runoff model.

The second topic deals with the estimation of the conceptual model error using the maximum likelihood method and consistency conditions on model residuals. The utility of the procedures is tested in practical applications. It is shown the simplified maximum likelihood procedure gives excellent forecasting results independent on the initial conditions, but raises some questions as to the sensitivity of the soil moisture accounting part of the model.

The third topic deals with the forecasting on a basin composed of several interconnected sub-basins. Decomposition procedures are proposed to forecast on sub-basins separately, using upstream flow predictions as inputs to downstream basins. When tested in practice, these methods provide reliable and inexpensive forecasts.

ACKNOWLEDGEMENTS

This work was sponsored by the Hydrologic Research Laboratory of the National Weather Service, U. S. Department of Commerce, under Cooperative Agreement NA 80AA-H-00D44. The valuable interaction with the HRL's staff is gratefully acknowledged. Special mention is due to Dr. Michael Hudlow, to Dr. George Smith, to Dr. Edward Johnson, and for his many contributions to Dr. Konstantine Georgakakos.

The comments and suggestions of Professors Daniele Veneziano, Juan Valdes, and Fred Schweppe are gratefully acknowledged.

Discussions with Dr. Pedro Restrepo, Stephanos Andreou, Aristotelis Mantoglou, Fadi Karaa, Aris Georgakakos, Mario Diaz-Granados, Alvaro Aldama, Maria Gini, Jorge Ramirez, Efstratios Vomvoris, and Dr. Roman Budzianowski have been useful and therefore they are rightfully appreciated.

The efficient typing of this report is due to Elaine Healy.

TABLE OF CONTENTS

ABSTRACT.....ii

ACKNOWLEDGEMENTS.....iii

TABLE OF CONTENTS.....iv

LIST OF FIGURES.....vii

LIST OF TABLES.....xv

LIST OF SYMBOLS.....xviii

Chapter 1 INTRODUCTION.....1
1.1 Scope of Study.....1
1.2 Literature Review.....2
1.3 Report Outline.....6

Chapter 2 A CONCEPTUAL RAINFALL-RUNOFF MODEL.....7
2.1 Introduction.....7
2.2 The Station Precipitation Model.....7
2.3 The Soil Moisture Accounting Model.....9
2.4 The Channel Router Model.....14
2.5 Summary of the Rainfall-Runoff Model Structure.....15
2.6 Stochastic Representation of the Rainfall-Runoff Process.....16

Chapter 3 STATE ESTIMATION OF NONLINEAR DYNAMIC SYSTEMS.....19
3.1 Introduction.....19
3.2 Linearized Kalman Filter.....20
3.2.1 Extended Kalman Filter.....24
3.3 Iterated Extended Kalman Filter.....26
3.4 Extended Linear Filter-Smoother and Iterated Extended Linear Filter-Smoother.....29
3.5 Second Order Gaussian Filter.....34

Chapter 4 PRACTICAL USE OF APPROXIMATE NONLINEAR FILTERS.....39
4.1 Introduction.....39
4.2 Description of the Drainage Basin and of the Available Data.....39
4.3 Review of the Comparison Indices.....45
4.4 Case Study Results.....47
4.4.1 One-Step Ahead Predictions.....47
4.4.2 Extended Forecasting.....73
4.5 Summary.....88

Chapter 5 THE ESTIMATION OF THE DYNAMICS NOISE SPECTRAL DENSITY MATRIX OF A NONLINEAR DYNAMIC SYSTEM..... 89
5.1 Introduction..... 89
5.2 Problem Definition..... 90
5.3 Procedures to Find the Spectral Density Matrix..... 92
5.4 Approximate Estimators of the Spectral Density Matrix, Q(t)..... 96
5.4.1 Maximum Likelihood for System with Transition Matrix Non-Dependent on Q(t)..... 96
5.4.1.1 Implementation Considerations.....101
5.4.1.2 An Approximate Maximum Likelihood Solution Which Uses Second Order Likelihood Derivatives.....102
5.4.1.3 An Explicit Sub-Optimal and Simple Estimate.....103
5.4.2 Estimation of Q(t) from Consistency of One-Step Ahead Residuals.....105
5.4.2.1 Further Conditions on Residuals Useful in Estimating Q.....107
5.5 Summary.....109

Chapter 6 PRACTICAL ESTIMATION OF THE DYNAMICS NOISE SPECTRAL DENSITY MATRIX.....110
6.1 Introduction.....110
6.2 Approximate Maximum Likelihood Results.....110
6.2.1 Sensitivity of the Estimation on the Number of Data Points.....118
6.2.2 Local Sensitivity of the Approximate Maximum Likelihood Estimate.....123
6.2.3 Sensitivity of the Approximate Maximum Likelihood Estimate on the Upper Bounds.....141
6.2.4 Results from the Sub-Optimal Explicit Maximum Likelihood Estimator.....149
6.3 Results for Q Matrices Estimated from Consistency Conditions.....149
6.4 Summary.....157

Chapter 7 FILTERING OF LARGE SCALE BASINS.....160
7.1 Introduction.....160
7.2 Block Diagonal Decomposition Filters.....164

Chapter 8 PRACTICAL USE OF DECOMPOSITION PROCEDURES.....171
8.1 Introduction.....171
8.2 Description of the Drainage Basin and of the Available Data.....171
8.3 Deterministic Discharge Predictions on the Large Scale Basin.....178
8.4 Stochastic Predictions on the Large Scale Basin.....183
8.5 Summary.....204

Chapter 9 CONCLUSIONS AND RECOMMENDATIONS.....205
9.1 Summary of Results.....205
9.2 Recommendations for Future Research.....209
9.3 Computational Considerations.....212

REFERENCES.....214

Appendix A RAINFALL-RUNOFF MODEL FIRST ORDER LINEARIZATION MATRICES.....221

Appendix B RAINFALL-RUNOFF MODEL SECOND ORDER EXPANSION MATRICES.....228

Appendix C BROAD COMPARISON OF DISCHARGE PREDICTIONS USING DIFFERENT SPECTRAL DENSITY MATRICES.....237

Appendix D APPROXIMATE MAXIMUM LIKELIHOOD ESTIMATION ON THE POTOMAC BASIN.....253

LIST OF FIGURES

2.1 Rainfall-Runoff Model Schematic Diagram

3.1 Extended Kalman Filter Structure, EKF

3.2 Iterated Extended Kalman Filter Structure, IEKF-3 (with three local iterations)

3.3 Extended Linear Filter-Smoother Structure, ELFS-1 (with one smoothing cycle)

3.4 Iterated Extended Linear Filter-Smoother Structure, IELFS-3,1 (with one smoothing cycle and three local iterations)

4.1 Deterministic Prediction of Precipitation, Bird Creek, April-May 1960

4.2 Stochastic Prediction of Precipitation, Bird Creek, April-May 1960, Q-4

4.3 Deterministic Prediction of Discharge, Bird Creek, April-May 1960

4.4 Stochastic Prediction of Discharge, Bird Creek, April-May 1960, EKF, Q-4

4.5 Stochastic Prediction of Discharge, Bird Creek, April-May 1960, IEKF-6, Q-4

4.6 Stochastic Prediction of Discharge, Bird Creek, April-May 1960, ELFS-1, Q-4

4.7 Stochastic Prediction of Discharge, Bird Creek, April-May 1960, ELFS-2, Q-4

4.8 Stochastic Prediction of Discharge, Bird Creek, April-May 1960, IELFS-6,2, Q-4

4.9 Stochastic Prediction of Discharge, Bird Creek, April-May 1960, SOGF, Q-4

4.10 Stochastic Prediction of Discharge, Bird Creek, April-May 1960, EKF, Q-0

4.11 Stochastic Prediction of Discharge, Bird Creek, April-May 1960, ELFS-2, Q-0

4.12 Stochastic Prediction of Discharge, Bird Creek, April-May 1960, EKF, Q-3

4.13 Stochastic Prediction of Discharge, Bird Creek, April-May 1960, ELFS-2, Q-3

4.14 Predicted Trajectories of Upper Zone Tension Volume, Q-3

4.15 Predicted Trajectories of Upper Zone Free Volume, Q-3

4.16 Predicted Trajectories of Lower Zone Tension Volume, Q-3

4.17 Predicted Trajectories of Lower Zone Free Primary Volume, Q-3

4.18 Predicted Trajectories of Lower Zone Free Secondary Volume, Q-3

4.19 Predicted Trajectories of Additional Impervious Volume, Q-3

4.20 Predicted Trajectories of Upper Zone Tension Volume, Q-4

4.21 Predicted Trajectories of Upper Zone Free Volume, Q-4

4.22 Predicted Trajectories of Lower Zone Tension Volume, Q-4

4.23 Predicted Trajectories of Lower Zone Free Primary Volume, Q-4

4.24 Predicted Trajectories of Lower Zone Free Secondary Volume, Q-4

4.25 Predicted Trajectories of Additional Impervious Volume, Q-4

4.26 Extended Forecast of Discharge, Bird Creek, May 1960, Q-3, 6 hrs, EKF

4.27 Extended Forecast of Discharge, Bird Creek, May 1960, Q-3, 12 hrs, EKF

4.28 Extended Forecast of Discharge, Bird Creek, May 1960, Q-3, 6 hrs, ELFS-2

4.29 Extended Forecast of Discharge, Bird Creek, May 1960, Q-3, 12 hrs, ELFS-2

4.30 Extended Forecast of Discharge, Bird Creek, May 1960, Q-4, 6 hrs, EKF

4.31 Extended Forecast of Discharge, Bird Creek, May 1960, Q-4, 12 hrs, EKF

4.32 Extended Forecast of Discharge, Bird Creek, May 1960, Q-4, 6 hrs, ELFS-2

4.33 Extended Forecast of Discharge, Bird Creek, May 1960, Q-4, 12 hrs, ELFS-2

6.1 Stochastic Prediction of Discharge, Bird Creek, May 1960, EKF, Q-4

6.2 Stochastic Prediction of Discharge, Bird Creek, May 1960, EKF, Q-6

6.3 Stochastic Prediction of Discharge, Bird Creek, May 1960, EKF, Q-7

6.4 Stochastic Prediction of Discharge, Bird Creek, May 1960, EKF, Q-0

6.5 Stochastic Prediction of Discharge, Bird Creek, May 1960, EKF, Q-8

6.6 Stochastic Prediction of Discharge, Bird Creek, May 1960, EKF, Q-9

6.7 Stochastic Prediction of Discharge, Bird Creek, May 1960, EKF, Q-10

6.8 Stochastic Prediction of Discharge, Bird Creek, May 1960, EKF, Q-12

6.9 Stochastic Prediction of Discharge, Bird Creek, May 1960, EKF, Q-11

6.10 Stochastic Prediction of Discharge, Bird Creek, May 1960, EKF, Q-13

6.11 Stochastic Prediction of Precipitation, Bird Creek, May 1960, Q-8, with Q(1,1) = 0

6.12 Stochastic Prediction of Precipitation, Bird Creek, May 1960, Q-8

6.13 Precipitation Residuals Standard Deviations, Bird Creek, May 1960, Q-8

6.14 Predicted Trajectory of Condensed Water Volume, May 1960, Q-8, only channel non-zero

6.15 Predicted Trajectory of Upper Zone Tension Volume, May 1960, Q-8, only channel non-zero

6.16 Predicted Trajectory of Upper Zone Free Volume, May 1960, Q-8, only channel non-zero

6.17 Predicted Trajectory of Lower Zone Tension Volume, May 1960, Q-8, only channel non-zero

6.18 Predicted Trajectory of Lower Zone Free Primary Volume, May 1960, Q-8 only channel non-zero

6.19 Predicted Trajectory of Lower Zone Free Secondary Volume, May 1960, Q-8, only channel non-zero

6.20 Predicted Trajectory of Additional Impervious Volume, May 1960, Q-8 only channel non-zero

6.21 Predicted Trajectory of Volume on First Reservoir, May 1960, Q-8, only channel non-zero

6.22 Predicted Trajectory of Volume on Second Reservoir, May 1960, Q-8, only channel non-zero

6.23 Predicted Trajectory of Volume on Third Reservoir, May 1960, Q-8, only channel non-zero

6.24 Filter Gains for the First Reservoir State, May 1960, Q-8, only channel non-zero

6.25 Filter Gains for the Third Reservoir State, May 1960, Q-8, only channel non-zero

6.26 Extended Forecast of Discharge, Bird Creek, May 1960, Q-8, only channel non-zero, 6 hrs

6.27 Extended Forecast of Discharge, Bird Creek, May 1960, Q-8, only channel non-zero, 12 hrs

6.28 Extended Forecast of Discharge, Bird Creek, May 1960, Q-8, only channel non-zero, 18 hrs

6.29 Stochastic Prediction of Discharge, Bird Creek, May 1960, Q-15

6.30 Stochastic Prediction of Discharge, Bird Creek, May 1960, Q-15 only channel non-zero

6.31 Adaptive Discharge Predictions, Bird Creek, May 1960, Q-0, States X_p, S_2, every time step

6.32 Adaptive Discharge Predictions, Bird Creek, May 1960, Q-4, States X_p, S_1, every time step

6.33 Adaptive Discharge Predictions, Bird Creek, May 1960, Q-8, States X_p, S_3, every time step

6.34 Adaptive Discharge Predictions, Bird Creek, May 1960, Q-4, States X_p, S_2, every 4 time steps

7.1 Filter Gains for the Condensed Water Volume, May 1960, Q-4

7.2 Filter Gains for the Upper Zone Free Volume, May 1960, Q-4

7.3 Filter Gains for the Additional Impervious Storage, May 1960, Q-4

7.4 Filter Gains for the Third Channel State, May 1960, Q-4

7.5 Hypothetical Large Scale Basin

7.6 Schematic Representation of a Large Scale Basin

8.1 Sub-basin Network for the Potomac River Basin with Outlet at Millville

8.2 Deterministic Prediction of Discharge, Lynnwood, Observed Rainfall as Input, October-November 1970

8.3 Deterministic Prediction of Discharge, Front Royal, Observed Rainfall as Input, October-November 1970

8.4 Deterministic Prediction of Discharge, Cootes Store, Observed Rainfall as Input, October-November 1970

8.5 Deterministic Prediction of Discharge, Strasburg, Observed Rainfall as Input, October-November 1970

8.6 Deterministic Prediction of Discharge, Millville, Observed Rainfall as Input, October-November 1970

8.7 Stochastic Prediction of Precipitation, Lynnwood, October 12 to November 30, 1970

8.8 Stochastic Prediction of Precipitation, Front Royal, October 12 to November 30, 1970

8.9 Stochastic Prediction of Precipitation, Cootes Store, October 12 to November 30, 1970

8.10 Stochastic Prediction of Precipitation, Strasburg, October 12 to November 30, 1970

8.11 Stochastic Prediction of Precipitation, Millville, October 12 to November 30, 1970

8.12 Stochastic Prediction of Discharge, Lynnwood, Decomposition Procedure of Puente, et al., October 12 to November 30, 1970

8.13 Stochastic Prediction of Discharge, Front Royal, Decomposition Procedure of Puente, et al., October 12 to November 30, 1970

8.14 Stochastic Prediction of Discharge, Cootes Store, Decomposition Procedure of Puente, et al., October 12 to November 30, 1970

8.15 Stochastic Prediction of Discharge, Strasburg, Decomposition Procedure of Puente, et al., October 12 to November 30, 1970

8.16 Stochastic Prediction of Discharge, Millville, Decomposition Procedure of Puente, et al., October 12 to November 30, 1970

8.17 Stochastic Prediction of Discharge, Lynnwood, Decomposition Procedure of Georgakakos, October 12 to November 30, 1970

8.18 Stochastic Prediction of Discharge, Front Royal, Decomposition Procedure of Georgakakos, October 12 to November 30, 1970

8.19 Stochastic Prediction of Discharge, Cootes Store, Decomposition Procedure of Georgakakos, October 12 to November 30, 1970

8.20 Stochastic Prediction of Discharge, Strasburg, Decomposition Procedure of Georgakakos, October 12 to November 30, 1970

8.21 Stochastic Prediction of Discharge, Millville, Decomposition Procedure of Georgakakos, October 12 to November 30, 1970

8.22 Stochastic Prediction of Discharge, Lynnwood, Global Filter in Two Levels, October 12 to November 30, 1970

8.23 Stochastic Prediction of Discharge, Front Royal, Global Filter in Two Levels, October 12 to November 30, 1970

8.24 Stochastic Prediction of Discharge, Cootes Store, Global Filter in Two Levels, October 12 to November 30, 1970

8.25 Stochastic Prediction of Discharge, Strasburg, Global Filter in Two Levels, October 12 to November 30, 1970

8.26 Stochastic Prediction of Discharge, Millville, Global Filter in Two Levels, October 12 to November 30, 1970

8.27 Stochastic Prediction of Discharge, Lynnwood, Global Filter, October 12 to November 30, 1970

8.28 Stochastic Prediction of Discharge, Front Royal, Global Filter, October 12 to November 30, 1970

8.29 Stochastic Prediction of Discharge, Cootes Store, Global Filter, October 12 to November 30, 1970

8.30 Stochastic Prediction of Discharge, Strasburg, Global Filter, October 12 to November 30, 1970

8.31 Stochastic Prediction of Discharge, Millville, Global Filter, October 12 to November 30, 1970

C.1 Stochastic Prediction of Discharge, Bird Creek, Run No. 1, EKF, Q-8 only channel non-zero

C.2 Stochastic Prediction of Discharge, Bird Creek, Run No. 1, EKF, Q-4

C.3 Stochastic Prediction of Discharge, Bird Creek, Run No. 2, EKF, Q-8 only channel non-zero

C.4 Stochastic Prediction of Discharge, Bird Creek, Run No. 2, EKF, Q-4

C.5 Stochastic Prediction of Discharge, Bird Creek, Run No. 3, EKF, Q-8 only channel non-zero

C.6 Stochastic Prediction of Discharge, Bird Creek, Run No. 3, EKF, Q-4

C.7 Stochastic Prediction of Discharge, Bird Creek, Run No. 4, EKF, Q-8 only channel non-zero

C.8 Stochastic Prediction of Discharge, Bird Creek, Run No. 4, EKF, Q-4

C.9 Stochastic Prediction of Discharge, Bird Creek, Run No. 5, EKF, Q-8 only channel non-zero

C.10 Stochastic Prediction of Discharge, Bird Creek, Run No. 5, EKF, Q-4

C.11 Stochastic Prediction of Discharge, Bird Creek, Run No. 6, EKF, Q-8 only channel non-zero

C.12 Stochastic Prediction of Discharge, Bird Creek, Run No. 6, EKF, Q-4

C.13 Stochastic Prediction of Discharge, Bird Creek, Run No. 7, EKF, Q-8 only channel non-zero

C.14 Stochastic Prediction of Discharge, Bird Creek, Run No. 7, EKF, Q-4

C.15 Stochastic Prediction of Discharge, Bird Creek, Run No. 8, EKF, Q-8 only channel non-zero

C.16 Stochastic Prediction of Discharge, Bird Creek, Run No. 8, EKF, Q-4

C.17 Histogram of the Difference in Time Between Predicted and Observed Peak

C.18 Histogram of the Percent Error in Forecasting Hydrograph Peak Magnitude

D.1 Stochastic Prediction of Discharge, Lynnwood, Decomposition Procedure of Georgakakos, October 12 to November 30, 1970, Maximum Likelihood

D.2 Stochastic Prediction of Discharge, Front Royal, Decomposition Procedure of Georgakakos, October 12 to November 30, 1970, Maximum Likelihood

D.3 Stochastic Prediction of Discharge, Cootes Store, Decomposition Procedure of Georgakakos, October 12 to November 30, 1970, Maximum Likelihood

D.4 Stochastic Prediction of Discharge, Strasburg, Decomposition Procedure of Georgakakos, October 12 to November 30, 1970, Maximum Likelihood

D.5 Stochastic Prediction of Discharge, Millville, Decomposition Procedure of Georgakakos, October 12 to November 30, 1970, Maximum Likelihood

D.6 Stochastic Prediction of Discharge, Lynnwood, Decomposition Procedure of Puente, et al., October 12 to November 30, 1970, Maximum Likelihood

D.7 Stochastic Prediction of Discharge, Front Royal, Decomposition Procedure of Puente, et al., October 12 to November 30, 1970, Maximum Likelihood

D.8 Stochastic Prediction of Discharge, Cootes Store, Decomposition Procedure of Puente, et al., October 12 to November 30, 1970, Maximum Likelihood

D.9 Stochastic Prediction of Discharge, Strasburg, Decomposition Procedure of Puente, et al., October 12 to November 30, 1970, Maximum Likelihood

D.10 Stochastic Prediction of Discharge, Millville, Decomposition Procedure of Puente, et al., October 12 to November 30, 1970, Maximum Likelihood

LIST OF TABLES

2.1 Soil Moisture Accounting Model Variables

4.1 Linearization Matrices for the Rainfall-Runoff Model

4.2 Parameter Values for the Rainfall-Runoff Model

4.3 Rainfall-Runoff Initial Mean and Initial Standard Deviations

4.4 Rainfall-Runoff Model Spectral Density Standard Deviations

4.5 Rainfall-Runoff Model Observation Error Covariance Matrix

4.6 Residual Statistics and Least Squares Performance Indices for Precipitation

4.7 Residual Statistics for Discharge

4.8 Normalized Residuals Statistics for Discharge

4.9 Least Squares Performance Indices for Discharge

4.10 CPU Execution Time of the Nonlinear Filters

4.11 Extended Forecasting Least Squares Indices for Precipitation

4.12 Extended Forecasting Least Squares Indices for Discharge, EKF

4.13 Extended Forecasting Least Squares Indices for Discharge, ELFS-2

6.1 Initial Spectral Density Standard Deviations and Upper Bounds

6.2 Approximate Maximum Likelihood Spectral Density Standard Deviations

6.3 Discharge Residuals Statistics for Q Matrices Obtained by Approximate Maximum Likelihood, 124 Data Points

6.4 Discharge Normalized Residuals Statistics for Q Matrices Obtained by Approximate Maximum Likelihood, 124 Data Points

6.5 Discharge Least Squares Indices and Model Log-Likelihood for Q Matrices Obtained by Approximate Maximum Likelihood, 124 Data Points

6.6 Discharge Residuals Statistics for Q Matrices Obtained by Approximate Maximum Likelihood, 40 and 84 Data Points

6.7 Discharge Normalized Residuals Statistics for Q Matrices Obtained by Approximate Maximum Likelihood, 40 and 84 Data Points

6.8 Discharge Least Squares Indices and Model Log-Likelihood for Q Matrices Obtained by Approximate Maximum Likelihood, 40 and 84 Data Points

6.9 Discharge Least Squares Indices and Model Log-Likelihood One Dimensional Sensitivity, Q of Level 8

6.10 Discharge Least Squares Indices and Model Log-Likelihood High Dimensional Sensitivity, Q of Level 8

6.11 Upper Bounds Sensitivity and Their Corresponding Approximate Maximum Likelihood Standard Deviation Estimates

6.12 Discharge Least Squares Indices and Model Log-Likelihood for Variable Upper Bounds

6.13 Discharge Least Squares Indices.
Adaptive Estimation of Q Matrix Every Time Step

6.14 Discharge Least Squares Indices.
Adaptive Estimation of Q Matrix, Variable Estimation Lag

6.15 Discharge Least Squares Indices.
Adaptive Estimation of Q Matrix Using Consistency Conditions of Higher Lags

7.1 Decomposition Algorithm of Puente, et al. (1983)

7.2 Decomposition Algorithm of Georgakakos (1983)

8.1 Potomac River Sub-Basins Characteristics

8.2 Discharge Average, Maximum and Minimum Values for the Potomac River Basin, October 1969 to September 1971

8.3 Model Parameter Values for the Different Sub-Basins on the Potomac Basin

8.4 Initial State Means for the Different Sub-Basins on the Potomac Basin

8.5 Spectral Density Matrix Diagonal Standard Deviations for the Different Sub-Basins on the Potomac Basin

C.1 Time Intervals Used in Comparisons

C.2 Discharge Residual Statistics for Different Runs

C.3 Discharge Normalized Residual Statistics for Different Runs

C.4 Discharge Least Squares Indices for Different Runs

LIST OF SYMBOLS

Symbol	Description
$A(t_{k+1})$	Second order correction on gain matrix, $A(t_{k+1}) = [a_{ij}]$
A^T	Transpose of matrix A
$\underline{a}_c$	Channel model parameters
a_i	Outflow coefficient of reservoir i, $a_o := 0$
$\underline{a}_p$	Precipitation model parameters
$\underline{a}_s$	Soil model parameters
B_k	Residuals covariance matrix at time t_k
$C_i(k)$	Lag-i correlation matrix at time t_k
C_1	Maximum drainage from lower zone free aquifers
C_2	Fraction of maximum drainage from lower zone free aquifers provided by the primary component
D	Determination coefficient
d'_ℓ	Lower zone primary instantaneous drainage coefficient [1/HR]
d''_ℓ	Lower zone secondary instantaneous drainage coefficient [1/HR]
d_u	Upper zone instantaneous drainage coefficient [1/HR]
E	Efficiency coefficient
EKF	Extended Kalman filter
ELFS-r	Extended linear filter-smoother with r smoothing cycles
E[•]	Expectation Operator

F^d	Downstream dynamics linearization matrix with respect to upstream discharge input
$F(\cdot)$	First order dynamic linearization matrix with respect to the states
$F^u(\cdot)$	First order dynamic linearization matrix with respect to the inputs
$\underline{f}(\cdot)$	Dynamic function of nonlinear system
$\underline{f}_c(\cdot)$	Channel dynamic function
$f_p(\cdot)$	Precipitation dynamic function
$\underline{f}_s(\cdot)$	Soil dynamic function
$f_z(\cdot,\cdot,\cdot)$	Joint probability density function of the observations
$G^{st}_{k\|k-1}$	Covariance matrix of predicted states derivatives with respect to the s^{th} and t^{th} unknown parameters
$H(\cdot)$	First order observation linearization matrix with respect to the states
$H_k(\cdot)$	Observation linearization matrix at time t_k
$H^u(\cdot)$	First order observations linearization matrix with respect to the inputs
$\underline{h}(\cdot)$	Observation function of nonlinear system
$h_c(\cdot)$	Discharge observation function
$h_p(\cdot)$	Mean areal precipitation observation function
I	Identity matrix
$I(\underline{u}_p,\underline{a}_p)$	Input rate of moisture into clouds
IEKF-ℓ	Iterated extended Kalman filter with ℓ iterations
IELFS-ℓ,r	Iterated extended linear filter-smoother with ℓ iterations and r smoothing cycles
$J_N(\cdot)$	Conditional information matrix of N observations
K_{k+1}	Gain matrix at time t_{k+1}
K_{b_k}	Backwards gain matrix at time t_k

L	Extrapolation coefficient
$L_N(\cdot,\cdot,\cdot)$	Logarithm of the likelihood function of N observations
$\ell(\cdot)$	Likelihood function
m	Exponent parameter on channel model
m_1, m_2, m_3	Exponent parameters on soil model
N	Number of time steps
n	Number of nonlinear reservoirs
$O(\underline{u}_p, \underline{a}_p)$	Output rate of moisture from clouds
P	Persistence coefficient
$P(t \mid t_k)$	Error covariance matrix at time t from information up to time t_k
$P_b(\tau)$	Backwards predicted error covariance matrix at time τ
$P_b'(t_k)$	Backwards updated error covariance matrix at time t_k
P_f	Fraction of percolated water assigned to the lower zone free water aquifers
P_i	Input fraction to reservoir i
P_o	Surface pressure, or initial error covariance matrix
$P_s(t_k \mid t_k)$	Smoothed error covariance matrix at time t_k
P_{ij}	(i,j) element of $P(t_{k+1} \mid t_k)$
$Q(t)$	Spectral density matrix of noise $\underline{w}(t)$ at time t
$Q'(t)$	Spectral density matrix of noise $\underline{w}'(t)$ at time t
$Q^d(t)$	Assigned spectral density matrix of downstream sub-basin
$Q^d(t)'$	Discharge input related spectral density matrix of downstream sub-basin

Q_k	Discrete dynamics noise covariance matrix
$Q_u(t)$	Covariance matrix of the inputs at time t
$Q'_u(t)$	Variance of upstream discharge input at time t
$R(t_k)$	Covariance matrix of noise $\underline{v}(t_k)$ at time t_k
$R'(t_k)$	Covariance matrix of noise $\underline{v}'(t_k)$ at time t_k
S	Sum of squares of observations from predictions
S(i,j,k)	Second order derivatives of k^{th} dynamic function with respect to states i and j
S_i	Volume storage in reservoir i
S_o	Sum of squares of observations from their mean
SOGF	Second order Gaussian filter
$T(i,j,\ell)$	Second order derivatives of ℓ^{th} observations function with respect to states i and j
T_d	Surface dew point temperature
$[t_k,t]$	Time
T_o	Surface temperature
$\underline{u}(t)$	Inputs of nonlinear dynamic system at time t
$\underline{u}^*(t)$	Input linearization trajectory at time t
u_c	Total channel inflow per unit time
u_e	Instantaneous evapotranspiration demand [MM/HR]
$\underline{u}_p$	Vector of inputs of precipitation model, $\underline{u}_p^T = [T_o\ P_o\ T_o]$
$\underline{v}(t_k)$	Noise in observation equation at time t_k
$\underline{v}'(t_k)$	Noise in linearized observation equation at time t_k

$\underline{w}(t)$	Noise in dynamic equation at time t
$\underline{w}'(t)$	Noise in linearized dynamic equation at time t
$\overline{\underline{w}}_k$	Discrete dynamics noise on interval (t_k, t_{k+1})
$\underline{X}(t)$	State of nonlinear dynamic system at time t
$\underline{X}^*(t)$	State linearization trajectory at time t
$\hat{\underline{X}}(t \mid t_k)$	State estimate at time t from information up to time t_k
$\hat{\underline{X}}_b(\tau)$	Backwards predicted state estimate at time τ
$\hat{X}_b'(t_k)$	Backwards updated estimate at time t_k
$\underline{X}_c$	States of channel model
$\hat{\underline{X}}_o$	Initial state mean
X_p	Water equivalent mass in a cloud column
$\underline{X}_s$	States of soil model
$\hat{\underline{X}}_s(t_k \mid t_k)$	Smoothed estimate at time t_k
X_1	Upper zone water tension content [MM], $0 \leq X_1 \leq X_1^o$
X_1^o	Upper zone tension water capacity [MM]
X_2	Upper zone free water content [MM], $0 \leq X_2 \leq X_2^o$
X_2^o	Upper zone free water capacity [MM]
X_3	Lower zone tension water content [MM], $0 \leq X_3 \leq X_3^o$
X_3^o	Lower zone tension water capacity [MM]

X_4	Lower zone primary free water content [MM], $0 \leq X_4 \leq X_4^o$
X_4^o	Lower zone primary free water capacity [MM]
X_5	Lower zone secondary free water content [MM], $0 \leq X_5 \leq X_5^o$
X_5^o	Lower zone secondary free water capacity [MM]
X_6	Additional impervious storage [MM]
y	Fraction of lower zone elements which is empty
$\underline{Z}(t_k)$	Observation of dynamic system at time t_k
Z_c	Discharge rate at drainage outlet
$Z_\ell(t)$	Extrapolated estimate of observation at time t
$Z_o(t)$	Observation at time t
$\hat{Z}_o(t_i)$	Observation prediction at time t_i
$\overline{Z}_o$	Sample average of observations over time
Z_p	Precipitation volume rate at the ground
$Z_r(t)$	Predicted observation at time t from regression of observations and predictions
β_1	Fraction of basin that becomes impervious when tension water requirements are met
β_2	Fraction of basin permanently impervious
$\Delta\underline{X}_k$	Updated minus predicted state estimate vector at time t_k
$\Delta\underline{Z}_{k+\ell}$	ℓ^{th}-step ahead predicted residuals at time $t_{k+\ell}$

$\delta_{\ell m}$	Delta function
ε	Parameter in percolation function
ε_1	Ratio of updraft velocity to square root of potential thermal energy
ε_4	Average diameter of particles in a cloud
$\underline{\eta}_i$	State updated estimate after i iterations on observatio function
θ	Exponent on percolation function
μ	Parameter of fraction of base flow not appearing in river flow
$\hat{\underline{\xi}}_j$	Estimate of the unknown spectral density matrix elements after j iterations
ξ^s	s^{th} unknown of spectral density matrix
τ	Backwards time, $t = t_{k+1} - \tau$
$\hat{\phi}(\underline{u}_p, \underline{a}_p)$	Precipitation rate function
$\Phi_k(t_{k+1}, t_k)$	System transition matrix between times t_k and t_{k+1}
Φ_k	Short notation of $\Phi_k(t_{k+1}, t_k)$
$\hat{\Phi}_k(t_k)$	Transition matrix associated with time t_k
$\underline{\partial}^2(F,P)$	Second order terms in second order filter, $\partial_i^2 = \text{trace}\ \{[\frac{\partial^2 f_i}{\partial x_j \partial x_k}] \cdot P\}$

Chapter 1

INTRODUCTION

1.1 Scope of Study

It is important to properly forecast river flows. Obvious needs arise in the operation of flood control reservoirs, in the planning of actions during times of floods, and in the maintenance of minimum flow levels for navigation and water quality purposes.

This work studies three topics related to the real time forecasting of river flows:

a. Assessment of the usefulness of nonlinear forecasting techniques,

b. Development of procedures to properly quantify the errors of the rainfall-runoff model being used, and

c. Development of techniques to forecast flows in a large scale basin composed of several sub-basins.

The forecasting of river flows requires the use of mathematical models to approximate the very complex process that transforms rainfall into runoff. This transformation is known to be of nonlinear nature, partly due to dependence on antecedent moisture conditions. This inherent nonlinearity has led to the development of several nonlinear rainfall-runoff models. The first topic of study deals with procedures that follow such nonlinearities, as opposed to techniques that require a linearized rainfall-runoff representation.

The type of hydrologic model that is used in this work belongs to the class of conceptual models. These models do not represent the physical laws exactly, but rather express them in a simplified way. In any typical stochastic forecasting procedure, i.e., Kalman filter, the predictions are a function of model error or the level of confidence (trust) given to the model. Model error is hard to quantify. It basically measures the differences between reality and the model that approximates it. The second topic on this work deals with the proper quantification of such differences in order to obtain more accurate flow predictions.

The third problem addressed in this work concerns the efficient forecasting of river flows on a large scale basin, composed of several interconnected sub-basins. Dimensionality problems are common when attempts are made to simultaneously predict at all points. By properly dealing with sub-basins separately, computational savings may be obtained and the overall quality of the predictions could be maintained.

1.2 Literature Review

This section reviews work done in forecasting river flows, using conceptual hydrologic models and a filtering mechanism. A review of the use of models which are based only on input-output data representations (black-box or systems-theoretic models) is not presented here. For such a case, the reader is referred to Sorooshian (1983).

The first attempt to use conceptual models within a stochastic filtering framework was that of Kitanidis and Bras (1978). These authors developed the state-space formulation of the National Weather Service River Forecast System (NWSRFS-Sacramento) model, Peck (1976), and used it together with a linear router model to obtain six hours lead discharge predictions using evapotranspiration and precipitation records as known inputs. The obtained results showed the advantage of updating the model states from discharge observations (stochastic filtering approach) as opposed to a deterministic propagation of the model dynamics.

Due to the existence of discontinuous threshold type functions on the original Sacramento model formulation, Kitanidis and Bras (1978) used not only Taylor linearizations but also stochastic linearizations in order to apply Kalman filtering techniques. The use of the Sacramento model, in a stochastic mode, gave better extended forecasts (for lead times greater than six hours) than black-box models with time varying parameters.

The model parameters employed by Kitanidis and Bras (1978) were computed using the manual calibration procedure described in Peck (1976). Methods to obtain such parameters automatically, using the maximum likelihood approach, have been suggested by Goldstein and Larimore (1980), Restrepo-Posada and Bras (1982), and Sorooshian, et al. (1982). These procedures differ on the way the maximization problem is numerically solved. Although these works show the potential of the maximum likelihood approach, the existence of non-unique optima,

extended likelihood valleys, high correlation between some parameters and non-identifiable parameters are recognized problems.

More realistic channel models than the single linear reservoir used by Kitanidis and Bras (1978) have been proposed. Georgakakos and Bras (1980) developed a nonlinear channel router which, when used in connection with the Sacramento model, preserves the most important characteristics of the hydrograph. A method to obtain the channel model parameters was also given by these authors. Goldstein and Larimore (1980) used canonical correlation principles to obtain a reduced order state-space representation of the unit hydrograph.

Georgakakos and Bras (1982) developed a station precipitation model in state-space form. Based on surface temperature, pressure and dew point temperature, their model produces as output the precipitation rate. By coupling such a model with the Sacramento model and the nonlinear channel router of Georgakakos and Bras (1980), a general and realistic rainfall-runoff model was obtained. Results obtained using the model in a stochastic filtering framework indicated that the coupling of the precipitation to the soil and channel models by the filter is of considerable value to river flow forecasting.

Bergstrom and Forsman (1973) and Bergstrom (1975) developed a simple nonlinear conceptual hydrologic model, HBV-2, that produces the outflow discharge from a basin, using daily precipitation records as a known input. Such model, which explicitly takes into account snow melting, was employed by Fjeld and Aam (1980) to produce daily

discharge predictions using the Kalman filtering methodology. By approximating the optimal gains for a given level of trust on the model equations, these authors avoided the need of propagating in time the error covariance matrix of the model five states. When daily discharge forecasts were used as inputs to control a hydroelectric power system in Norway, significant savings of water and energy were obtained.

Takara et al. (1983) developed an algorithm for real time forecasting of flows on a basin composed by several sub-basins. Precipitation is modelled in an stochastic fashion, and its predictions are obtained using a moving average method. The dynamics on the sub-basins are approximated as nonlinear reservoirs that have effective (lagged) rainfall as input. The channel routing is made by using a cascade of nonlinear reservoirs. Because the sub-basins are interconnected, the ordering on the river network (upstream to downstream) is followed to obtain the predictions using the extended Kalman filter. The updatings of the composite storage vector, that represents the basin, are done from available discharge observations. In a case study at the Yura River in Japan, Takara et al. (1983) found satisfactory one-hour lead results using their real time algorithm with colored noise in the model dynamics. The quality of the flow predictions decreased as the lead time was increased to four hours.

1.3 Report Outline

The organization of this report is as follows. Chapter 2 describes the rainfall-runoff model to be used in this work. The way model error is introduced is also discussed in this chapter. Chapter 3 presents the theoretical aspects of the nonlinear filtering procedures. Chapter 4 includes the results of using the nonlinear filters and the rainfall-runoff model in a case study. Precedures to properly quantify the errors of the rainfall-runoff model are developed in Chapter 5. Results of applying such methods to a case study are presented in Chapter 6. Chapter 7 describes efficient techniques to forecast precipitation and river flows in a large scale basin. The results found using such procedures are included in Chapter 8. The conclusions and recommendations for future research are given in Chapter 9.

Chapter 2

A CONCEPTUAL RAINFALL-RUNOFF MODEL

2.1 Introduction

This chapter describes the conceptual rainfall-runoff model employed in this work. The hydrologic response of a basin is approximated by coupling a station precipitation model, a soil moisture accounting procedure and a channel routing scheme.

The rainfall-runoff model produces as output the precipitation rate over the area of interest and the discharge at the outlet of the basin. The model is driven by four inputs: temperature, pressure, dew point temperature, and the potential evapotranspiration over the basin area.

A brief description of the model equations in state-space form is given in the following sections of this chapter.

2.2 The Station Precipitation Model

The first component of the rainfall-runoff model is the station precipitation model of Georgakakos and Bras (1982). This spatially lumped parameter model has as inputs the surface temperature, T_o, pressure, P_o, and dew point temperature, T_d. It produces as output the precipitation volume rate over the basin.

The model is based on atmospheric thermodynamics and cloud microphysics principles. The dynamic equation is a balance equation for the condensed water equivalent mass within a cloud column, X_p:

$$\frac{dX_p}{dt} = I(\underline{u}_p, \underline{a}_p) - O(\underline{u}_p, \underline{a}_p)X_p \qquad (2.1)$$

The function $I(\underline{u}_p,\underline{a}_p)$ represents the rate of moisture input into the clouds. It is computed from the pseudo-adiabatic ascent of surface air characterized by the input vector of meteorological variables $\underline{u}_p^T = [T_o\ P_o\ T_d]$. The function $O(\underline{u}_p, \underline{a}_p)$ is the output rate of moisture from the cloud column per unit of equivalent water mass. Two output components are considered by this function: water that leaves the column's top due to updraft velocity, and water that leaves the cloud's bottom, basically composed by the larger droplets.

The vector $\underline{a}_p$ denotes the precipitation model parameters, $\underline{a}_p^T = [\varepsilon_1,\varepsilon_4]$. The parameter ε_1 is the ratio of the updraft velocity to the square root of the potential thermal energy per unit mass of ascending air at the height of average updraft velocity. If ε_1 increases, the updraft velocity increases giving a higher moisture input rate $I(\underline{u}_p,\underline{a}_p)$, a higher moisture output at the cloud's top and a lower moisture output at the cloud's bottom, which overall tends to give lower mass output $O(\underline{u}_p,\underline{a}_p)X_p$. The input mass of condensed water is distributed in different droplet diameters according to an exponential particle size distribution. The average diameter of particles in the cloud is the second parameter ε_4. If ε_4 increases, the heavier the particles become and consequently the higher the mass output.

The observation equation of the model gives the precipitation volume rate at the ground, Z_p:

$$Z_p = \hat{\phi}(\underline{u}_p, \underline{a}_p)X_p \qquad (2.2)$$

The precipitation rate function $\hat{\phi}(\underline{u}_p,\underline{a}_p)$ accounts for that part of the water mass which on leaving the cloud bottom reaches the ground. Evaporation of the falling particles, below the cloud, is taken into account by this function. The parameter vector affects $\hat{\phi}(\underline{u}_p,\underline{a}_p)$ the same way as it affects $O(\underline{u}_p,\underline{a}_p)$, i.e., a higher ε_1 reduces the precipitation rate while a higher ε_4 increases it.

The actual expressions for the functions $I(\underline{u}_p,\underline{a}_p)$, $O(\underline{u}_p,\underline{a}_p)$ and $\hat{\phi}(\underline{u}_p,\underline{a}_p)$ are given in Georgakakos and Bras (1982).

2.3 The Soil Moisture Accounting Model

The second component of the rainfall-runoff model is a modified version of the NWSRFS or Sacramento Model derived by Peck (1976). The representative soil-column in the basin is divided in six components. The balance equations of the water volumes stored in the different elements represent the soil model dynamic equations. The model is driven by the precipitation and evapotranspiration rates over the basin, and produces as the output the water flow into the river, which after routing will give the outflow discharge from the basin.

The original Sacramento model contains threshold type functions to account for the dynamics of some of its components, i.e., these components respond only when a threshold storage is reached. In the

modified version these discontinuous functions are replaced by continuous power functions, which consequently allow responses at all times with higher values of element discharge as the threshold is approached.

The Sacramento model variables and parameters are summarized in Table 2.1. The model equations are:

UPPER ZONE TENSION ELEMENT

$$\frac{dX_1}{dt} = \left[1 - \left(\frac{X_1}{X_1^o}\right)^{m_1}\right] \hat{\phi}\, X_p - u_e \frac{X_1}{X_1^o} \tag{2.3}$$

UPPER ZONE FREE ELEMENT

$$\frac{dX_2}{dt} = \left(\frac{X_1}{X_1^o}\right)^{m_1} \hat{\phi}\, X_p \left[1 - \left(\frac{X_2}{X_2^o}\right)^{m_2}\right] - d_u X_2 - C_1(1 + \varepsilon y^{\theta}) \frac{X_2}{X_2^o} \tag{2.4}$$

LOWER ZONE TENSION ELEMENT

$$\frac{dX_3}{dt} = C_1(1 + \varepsilon y^{\theta}) \frac{X_2}{X_2^o} (1 - P_f) \left[1 - \left(\frac{X_3}{X_3^o}\right)^{m_3}\right] - u_e\left(1 - \frac{X_1}{X_1^o}\right) \frac{X_3}{X_1^o + X_3^o} \tag{2.5}$$

LOWER ZONE FREE PRIMARY ELEMENT

$$\frac{dX_4}{dt} = -d'_{\ell} X_4 + C_1(1 + \varepsilon y^{\theta}) \frac{X_2}{X_2^o} \left[1 - (1 - P_f)\left\{1 - \left(\frac{X_3}{X_3^o}\right)^{m_3}\right\}\right]$$

$$\cdot\left[\left(C_2 \frac{X_5}{X_5^o} - 1\right) \frac{X_4}{X_4^o} + 1\right] \qquad (2.6)$$

LOWER ZONE FREE SECONDARY ELEMENT

$$\frac{dX_5}{dt} = -d''_{\ell} X_5 + C_1(1 + \varepsilon y^{\theta}) \frac{X_2}{X_2^o} \left[1 - (1 - P_f)\left\{1 - \left(\frac{X_3}{X_3^o}\right)^{m_3}\right\}\right]$$

$$\cdot \left[\left(1 - C_2 \frac{X_5}{X_5^o}\right) \frac{X_4}{X_4^o}\right] \qquad (2.7)$$

ADDITIONAL IMPERVIOUS STORAGE ELEMENT

$$\frac{dX_6}{dt} = \left[1 - \left(\frac{X_6 - X_1}{X_3^o}\right)^2 \left(\frac{X_1}{X_1^o}\right)^{m_1}\right]\hat{\phi} X_p - u_e\left(1 - \frac{X_1}{X_1^o}\right)\left(\frac{X_6 - X_1}{X_1^o + X_3^o}\right)$$

$$- u_e \frac{X_1}{X_1^o} - \left[1 - \left(\frac{X_6 - X_1}{X_3^o}\right)^2\right]\left(\frac{X_2}{X_2^o}\right)^{m_2}\left(\frac{X_1}{X_1^o}\right)^{m_1} \hat{\phi} X_p \qquad (2.8)$$

Table 2.1

Soil Moisture Accounting Model Variables

Symbol	Description
	STATE VARIABLES
X_1	Upper zone tension water content [MM]
X_2	Upper zone free water content [MM]
X_3	Lower zone tension water content [MM]
X_4	Lower zone free primary water content [MM]
X_5	Lower zone free secondary water content [MM]
X_6	Additional impervious storage [MM]
	INPUT VARIABLES
$\hat{\phi} \cdot X_p$	Instantaneous precipitation rate [MM/6HRS]
u_e	Instantaneous evapotranspiration demand [MM/6HRS]
	PARAMETERS
X_1^o	Upper zone tension water capacity [MM]
X_2^o	Upper zone free water capacity [MM]
X_3^o	Lower zone tension water capacity [MM]
X_4^o	Lower zone free primary water capacity [MM]
X_5^o	Lower zone free secondary water capacity [MM]
d_u	Upper zone instantaneous drainage coefficient [1/HRS]

Table 2.1 (continued)

d'_ℓ	Lower zone primary instantaneous drainage coefficient [1/HRS]
d''_ℓ	Lower zone secondary instantaneous drainage coefficient [1/HRS]
ε	Parameter in percolation function
θ	Exponent in percolation function
P_f	Fraction of percolated water assigned to the lower zone free water elements
μ	Parameter of Fraction of base flow not appearing in river flow
β_1	Fraction of the basin that becomes impervious when tension water requirements are met
β_2	Fraction of the basin that is permanently impervious
m_1	Exponent on upper zone tension outflow approximation
m_2	Exponent on upper zone free outflow approximation
m_3	Exponent on lower zone tension outflow approximation
	OUTPUT VARIABLES
u_c	Input volume to the river [MM]
	AUXILIARY VARIABLES
C_1	Maximum drainage from lower zone free aquifers, $C_1 = d'_\ell X_4^o + d''_\ell X_5^o$
y	Fraction of lower zone elements which is empty, $y = 1 - \frac{X_3 + X_4 + X_5}{X_3^o + X_4^o + X_5^o}$
C_2	Fraction of maximum drainage from lower zone free aquifers provided by the primary component, $C_2 = d'_\ell X_4^o / C_1$

INPUT VOLUME TO THE CHANNEL

$$u_c = (d_u X_2 + \frac{d'_\ell X_4 + d''_\ell X_5}{1 + \mu})(1 - \beta_1 - \beta_2) + \hat{\phi} X_p \beta_2$$

$$+ (\frac{X_6 - X_1}{X_3^o})^2 \hat{\phi} X_p (\frac{X_1}{X_1^o})^{m_1} \beta_1 + \hat{\phi} X_p (\frac{X_1}{X_1^o})^{m_1} (\frac{X_2}{X_2^o})^{m_2} (1 - \beta_1 - \beta_2)$$

$$+ [1 - (\frac{X_6 - X_1}{X_3^o})^2] (\frac{X_2}{X_2^o})^{m_2} (\frac{X_1}{X_1^o})^{m_1} \hat{\phi} X_p \beta_1 \qquad (2.9)$$

2.4 The Channel Router Model

The last component of the rainfall-runoff model is the conceptual channel router of Georgakakos and Bras (1980). The channel is modelled as a series of nonlinear reservoirs. The model is driven by the volume of water produced by the soil, and produces as the output the discharge from the basin. The dynamic equations of the router are the balance equations of its components. If S_i denotes the storage on the i^{th} reservoir, the balance equations are:

$$\frac{dS_i}{dt} = P_i u_c + a_{i-1} S_{i-1}^m - a_i S_i^m \,, \quad a_o = 0$$

$$i = 1,2,\ldots,n \qquad (2.10)$$

The constants P_i, a_i, i=1,2,...n, m and the number of reservoirs, n, constitute the router parameters. The instantaneous discharge at the basin outlet, Z_c, is the outflow from the last reservoir, or

$$Z_c = a_n S_n^m \tag{2.11}$$

2.5 Summary of the Rainfall-Runoff Model Structure

The rainfall-runoff model can be summarized in state-space form by the following dynamic and observation equations,

DYNAMIC EQUATIONS:

$$\frac{d}{dt} X_p = f_p(X_p, \underline{u}_p; \underline{a}_p) \qquad \text{RAINFALL}$$

$$\frac{d}{dt} \underline{X}_s = \underline{f}_s(X_p, \underline{X}_s, \underline{u}_p, u_e; \underline{a}_p, \underline{a}_s) \qquad \text{SOIL} \tag{2.12}$$

$$\frac{d}{dt} \underline{X}_c = \underline{f}_c(X_p, \underline{X}_s, \underline{X}_c, \underline{u}_p, u_e; \underline{a}_p, \underline{a}_s, \underline{a}_c) \qquad \text{CHANNEL}$$

OBSERVATION EQUATIONS:

$$Z_p = h_p(X_p, \underline{u}_p; \underline{a}_p) \qquad \text{MEAN AREAL PRECIPITATION}$$

$$Z_c = h_c(\underline{X}_c; \underline{a}_c) \qquad \text{DISCHARGE} \tag{2.13}$$

The variables X_p, $\underline{X}_s$ and $\underline{X}_c$ represent respectively the state variables of the precipitation, soil and channel sections of the model,

$$\underline{X}_s^T = [X_1\ X_2\ X_3\ X_4\ X_5\ X_6]$$
$$\underline{X}_c^T = [S_1\ S_2\ \ldots\ S_n]$$

The input variables of the model are u_e and the vector $\underline{u}_p$. The parameter values of the different model components are respec-

tively $\underline{a}_p$, $\underline{a}_s$, and $\underline{a}_c$. From the previously described expressions for functions f_p, $\underline{f}_s$, $\underline{f}_c$, h_p, and h_c, it can be concluded that the precipitation component is linear with respect to the state X_p, but nonlinear with respect to the inputs; while the soil and channel components are both nonlinear with respect to the states and linear with respect to the inputs. Figure 2.1 summarizes the model processes, states, parameters inputs and observations.

2.6 Stochastic Representation of the Rainfall-Runoff Process

If the conceptual rainfall-runoff model is used in practical applications, the modelled processes will differ from reality. This discrepancy can be attributed to some of the following causes:

a. Errors in the model structure

b. Errors in the model parameters

c. Errors in the model inputs

d. Errors in the model observations

Inaccurate representations of the physical phenomenon result in errors of type (a). The conceptual rainfall-runoff model uses lumped parameters to describe a spatially distributed process and therefore errors in model structure are to be expected. Not properly calibrated parameters give rise to errors of type (b). Errors of types (c) and (d) arise from inaccuracies in the observation mechanisms or in the transformation of actual observations into model observations (e.g., the computation of averaged values from point values).

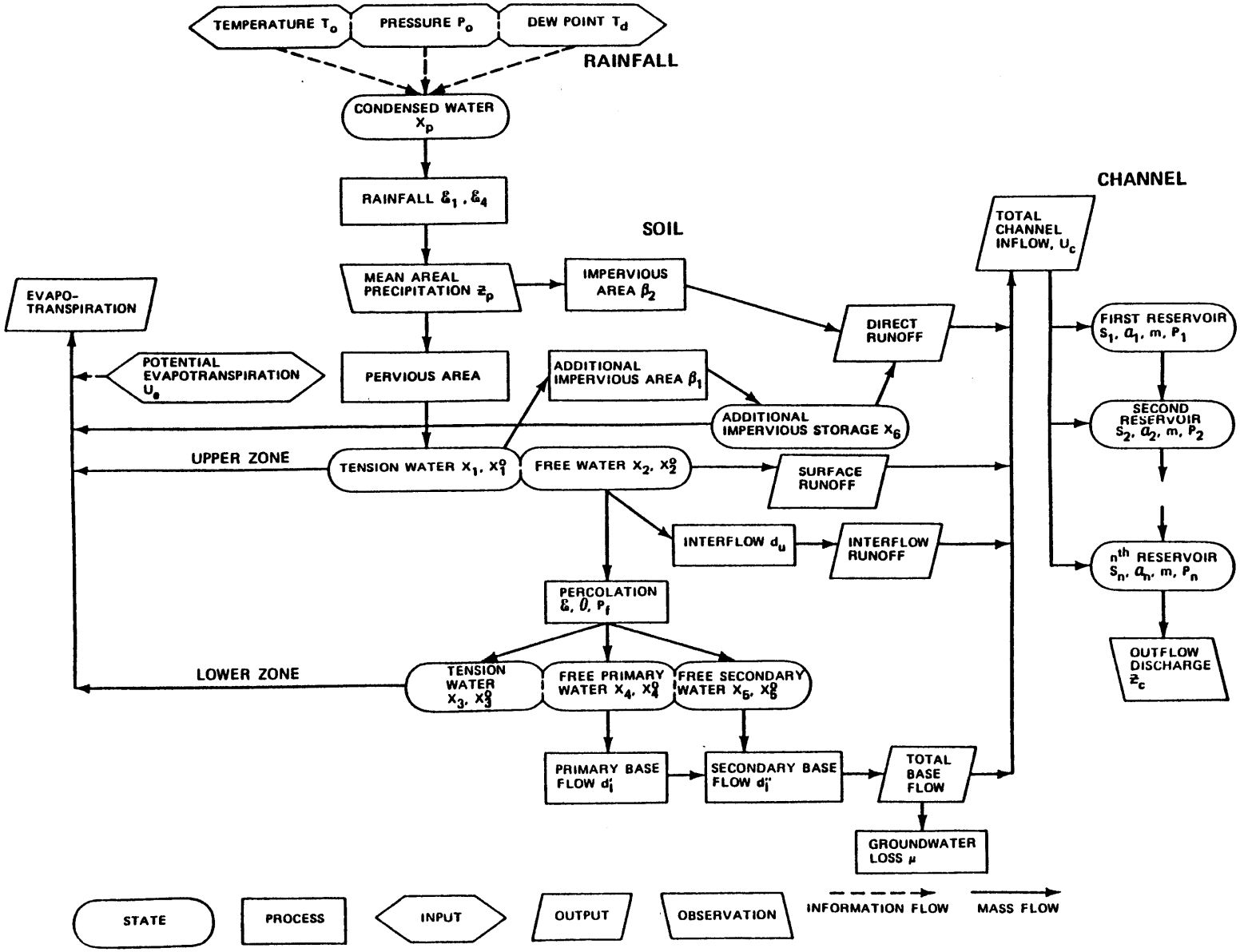

Figure 2.1 Rainfall-Runoff Model Schematic Diagram

Some of the above errors are treated explicitly in this work by interpreting the rainfall-runoff mechanism as a stochastic process.The conceptual rainfall-runoff model becomes a stochastic nonlinear dynamic system with the following dynamic and observation equations:

DYNAMIC EQUATIONS

$$\frac{d}{dt}\underline{X}(t) = \underline{f}(\underline{X}(t), \underline{u}(t), t) + \underline{w}(t) \qquad (2.14)$$

OBSERVATION EQUATIONS

$$\underline{Z}(t_k) = \underline{h}(\underline{X}(t_k), \underline{u}(t_k), t_k) + \underline{v}(t_k) \qquad k=0,1,2,... \qquad (2.15)$$

The stochastic components $\underline{w}(t)$ and $\underline{v}(t_k)$ are typically modelled as zero mean Gaussian processes. The vectors $\underline{X}$, $\underline{u}$ and $\underline{Z}$ represent respectively the states, inputs and observations of the model.

Given the stochastic nature of the additive noises $\underline{w}(t)$ and $\underline{v}(t_k)$, the states and observations, at any particular time, become random variables. The prediction problem then becomes the estimation of the states from the random observations. This problem will be fully explored in Chapter 3.

Chapter 3

STATE ESTIMATION OF NONLINEAR DYNAMIC SYSTEMS

3.1 Introduction

For several reasons, the state estimation of nonlinear dynamic systems is considerably more difficult than that of linear dynamic systems. Under the most reasonable Bayesian criteria, the optimal state estimate is the state's conditional mean given the observations. For linear dynamic systems, if the dynamics and observations noises are Gaussian, then the conditional distribution of the states given the observations is also Gaussian. This implies that the state conditional mean can be obtained from linear operations on the observations via the well known Kalman filter procedure. On the other hand, nonlinear dynamic systems, even with Gaussian dynamics and observation noises, will not result in Gaussian distributions for the conditional states given the observations. This means that it is no longer possible to stay in the domain of correlation theory (means and covariances), but the whole conditional distribution function must be considered. In general, it is not easy to obtain such conditional distribution.

Several approximations to the problem of state estimation (filtering) of nonlinear dynamic systems have been proposed. There are two major groupings of approximations:

a. Those that approximate the whole state conditional distribution function with a finite set of parameters, and

b. Those that approximate the nonlinear functions with linear ones and then apply linear filtering results.

Approximations in group (a) are based on parametrizations of the state conditional distribution function by finite series expansions or the use of distribution functions characterized by a finite number of parameters. Sorenson and Stubberud (1968) propose to approximate the density function in terms of Hermite polynomials (Edgeworth Expansions). Alpsach and Sorenson (1972) suggest the use of Gaussian sums. Common to all of the procedures, within this group, is the need to obtain non-obvious discretizations of the states and the need to store considerable amount of information. For these reasons filters of type (a) will not be considered in conjunction with the rainfall-runoff model.

The approximate estimators of type (b) have been the most popular in practical applications. These filters will be used together with the rainfall-runoff model and will be described in the following.

3.2 Linearized Kalman Filter

The general nonlinear dynamic system with observations at discrete times is given by:

$$\begin{aligned} \frac{d}{dt}\underline{X}(t) &= \underline{f}(\underline{X}(t), \underline{u}(t), t) + \underline{w}(t) \\ \underline{Z}(t_k) &= \underline{h}(\underline{X}(t_k), \underline{u}(t_k), t_k) + \underline{v}(t_k), \qquad k=0,1,2,\ldots \end{aligned} \tag{3.1}$$

where:

$\underline{X}(t)$: state vector at time t

$\underline{u}(t)$: inputs vector at time t

$\underline{Z}(t_k)$: observations vector at time t_k

$\underline{f}(\cdot)$: nonlinear dynamics function

$\underline{h}(\cdot)$: nonlinear observations function

$\underline{w}(t)$: continuous dynamics noise

$\underline{v}(t_k)$: discrete observations noise

The additive noise random components are assumed zero mean independent Gaussian random vectors. $\underline{w}(t)$ has spectral density matrix $Q(t)$ and $\underline{v}(t_k)$ has covariance matrix $R(t_k)$.

In order to apply linear filtering results, the nonlinear dynamics and observations functions are linearized about given state and inputs trajectories $\underline{X}^*(t)$ and $\underline{u}^*(t)$. This results in the following approximation:

$$\frac{d}{dt}\underline{X}(t) = \underline{f}(\underline{X}^*(t),\underline{u}^*(t),t) + F(\underline{X}^*(t),\underline{u}^*(t),t)(\underline{X}(t) - \underline{X}^*(t)) + \underline{w}'(t)$$

$$\underline{Z}(t_k) = \underline{h}(\underline{X}^*(t_k),\underline{u}^*(t_k),t_k) + H(\underline{X}^*(t_k),\underline{u}^*(t_k),t_k)(\underline{X}(t_k) - \underline{X}^*(t_k)) + \underline{v}'(t_k) \qquad (3.2)$$

where $F(\cdot)$ and $H(\cdot)$ are respectively the linearization matrices[1] of the dynamics and observation functions with respect to the states, and

[1] First order derivatives in case of Taylor linearizations

$\underline{w}'(t)$ and $\underline{v}'(t_k)$ are trajectory dependent noise components defined by:

$$\underline{w}'(t) = F^u(\underline{X}^*(t),\underline{u}^*(t),t)(\underline{u}(t)-\underline{u}^*(t)) + \underline{w}(t) \tag{3.3}$$

$$\underline{v}'(t_k) = H^u(\underline{X}^*(t_k), \underline{u}^*(t_k),t_k)(\underline{u}(t_k)-\underline{u}^*(t_k)) + \underline{v}(t_k) \tag{3.4}$$

with $F^u(\cdot)$ and $H^u(\cdot)$ being respectively the linearization matrices[1] of the dynamics and observations functions with respect to the inputs.

If $\underline{u}^*(t)$ is the expected value of the inputs, the noise components are zero mean white Gaussian processes with spectral density matrix $Q'(t)$ and covariance matrix $R'(t_k)$ given by

$$Q'(t) = F^u(\underline{X}^*(t),\underline{u}^*(t),t)\, Q_u(t)\, F^u(\underline{X}^*(t), \underline{u}^*(t),t)^T + Q(t) \tag{3.5}$$

and

$$R'(t_k) = H^u(\underline{X}^*(t_k),\underline{u}^*(t_k),t_k)Q_u(t_k)H^u(\underline{X}(t_k),\underline{u}^*(t_k),t_k)^T + R(t_k) \tag{3.6}$$

where $Q_u(t)$ denotes the inputs covariance matrix at time t.

The linearized Kalman filter for the nonlinear system is obtained by applying the linear Kalman filter to the linear system described by Equations (3.2). If $\hat{\underline{X}}(t|t_k)$ and $P(t|t_k)$ denote the state estimate and its respective error covariance matrix at time t from information up to time t_k, the linearized Kalman filter equations are, Gelb (1974):

---

[1] First order derivatives in case of Taylor linearizations.

STATE ESTIMATE PROPAGATION, $t\in[t_k, t_{k+1})$

$$\frac{d}{dt}\hat{\underline{X}}(t|t_k) = \underline{f}(\underline{X}^*(t),\underline{u}^*(t),t) + F(\underline{X}^*(t),\underline{u}^*(t),t)\cdot[\hat{\underline{X}}(t|t_k) - \underline{X}^*(t)] \tag{3.6}$$

ERROR COVARIANCE PROPAGATION, $t\in[t_k, t_{k+1})$

$$\frac{d}{dt}P(t|t_k) = F(\underline{X}^*(t),\underline{u}^*(t),t)P(t|t_k) + P(t|t_k)F(\cdot,\cdot,\cdot,)^T + Q'(t) \tag{3.7}$$

STATE ESTIMATE UPDATE, k=0,1,...

$$\hat{\underline{X}}(t_{k+1}|t_{k+1}) = \hat{\underline{X}}(t_{k+1}|t_k) + K_{k+1}[\underline{Z}(t_{k+1}) - \underline{h}(\underline{X}^*(t_{k+1}),\underline{u}^*(t_{k+1}),t_{k+1}) - H(\underline{X}^*(t_{k+1}),\underline{u}^*(t_{k+1}),t_{k+1}) \cdot\{\hat{\underline{X}}(t_{k+1}|t_k) - \underline{X}^*(t_{k+1})\}] \tag{3.8}$$

ERROR COVARIANCE UPDATE, k=0,1,...

$$P(t_{k+1}|t_{k+1}) = [I - K_{k+1}\cdot H(\cdot,\cdot,\cdot,)]P(t_{k+1}|t_k)[I - K_{k+1}\cdot H(\cdot,\cdot,\cdot)]^T + K_{k+1}R'(t_{k+1})K_{k+1}^T \tag{3.9}$$

KALMAN GAIN

$$K_{k+1} = P(t_{k+1}|t_k)H(\cdot,\cdot,\cdot)^T[H(\cdot,\cdot,\cdot)P(t_{k+1}|t_k)H(\cdot,\cdot,\cdot)^T + R'(t_{k+1})]^{-1} \tag{3.10}$$

INITIAL CONDITIONS

$$\hat{\underline{X}}(t_o|t_o) = \hat{\underline{X}}_o;\ P(t_o|t_o) = P_o \tag{3.11}$$

If the linearization trajectory is known in advance, the error covariance propagation and gain matrices can be computed off-line, i.e., they do not depend on the current state estimate. Although this represents computational and storage savings, the performance of the filter heavily depends on the proper selection of the linearization trajectory.

3.2.1 Extended Kalman Filter

A way to bypass the need of specifying the state linearization trajectory in advance is to linearize about the current estimates given by the filter. If such trajectory is employed, the error covariance and gain matrices can no longer be pre-computed, but large initial linearization errors are less likely to propagate. Such filtering procedure is called extended Kalman filter, EKF; its algorithm is, Jazwinski (1970):

STATE ESTIMATE PROPAGATION, $t\in[t_k, t_{k+1})$

$$\frac{d}{dt}\hat{\underline{X}}(t|t_k) = \underline{f}(\hat{\underline{X}}(t|t_k),\ \underline{u}^*(t), t) \tag{3.12}$$

ERROR COVARIANCE PROPAGATION, $t\in[t_k, t_{k+1})$

$$\frac{d}{dt}P(t|t_k) = F(\hat{\underline{X}}(t|t_k), \underline{u}^*(t), t)\ P(t|t_k) + P(t|t_k)F(\cdot,\cdot,\cdot)^T + Q'(t) \tag{3.13}$$

STATE ESTIMATE UPDATE, k=0,1,...

$$\hat{\underline{X}}(t_{k+1}|t_{k+1}) = \hat{\underline{X}}(t_{k+1}|t_k) + K_{k+1}[\underline{Z}(t_{k+1}) - \underline{h}(\hat{\underline{X}}(t_{k+1}|t_k), \underline{u}^*(t_{k+1}), t_{k+1})] \tag{3.14}$$

ERROR COVARIANCE UPDATE, k=0,1,...

$$P(t_{k+1}|t_{k+1}) = [I - K_{k+1}H(\hat{\underline{X}}(t_{k+1}|t_k),\ \underline{u}^*(t_{k+1}), t_{k+1})] \cdot P(t_{k+1}|t_k)[I - K_{k+1}H(\cdot,\cdot,\cdot)]^T + K_{k+1}R'(t_{k+1})K_{k+1}^T \tag{3.15}$$

KALMAN GAIN

$$K_{k+1} = P(t_{k+1}|t_k)H(\cdot,\cdot,\cdot)^T [H(\cdot,\cdot,\cdot)P(t_{k+1}|t_k)H(\cdot,\cdot,\cdot)^T + R'(t_{k+1})]^{-1} \tag{3.16}$$

INITIAL CONDITIONS

$$\underline{\hat{X}}(t_o|t_o) = \underline{\hat{X}}_o; \quad P(t_o|t_o) = P_o \tag{3.17}$$

Notice that Equations (3.12) and (3.13) are coupled. The extended Kalman filter structure is shown in Figure 3.1.

3.3 Iterated Extended Kalman Filter

Local iteration algorithms have been developed to approximate the nonlinear filtering problem. Denham and Pines (1966) introduced the iterated extended Kalman filter, IEKF. The propagation stage of this filter is the same as in the extended Kalman filter, but relinearizations are made during the updating stage (to the observations functions) until convergence is reached. The algorithm for this filter is:

STATE ESTIMATE PROPAGATION, $t\in[t_k, t_{k+1})$

$$\frac{d}{dt}\underline{\hat{X}}(t|t_k) = \underline{f}(\underline{\hat{X}}(t|t_k), \underline{u}^*(t), t) \tag{3.18}$$

ERROR COVARIANCE PROPAGATION, $t\in[t_k, t_{k+1})$

$$\frac{d}{dt}P(t|t_k) = F(\underline{\hat{X}}(t|t_k), \underline{u}^*(t), t)P(t|t_k) + P(t|t_k)F(\cdot,\cdot,\cdot)^T + Q'(t) \tag{3.19}$$

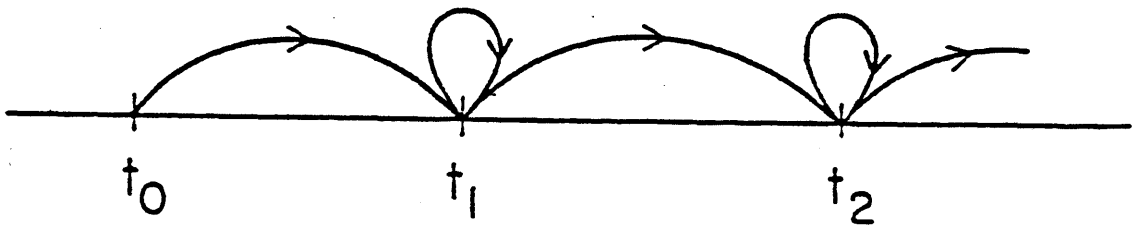

Figure 3.1 Extended Kalman Filter Structure, EKF

UPDATED STATE INITIALIZATION

$$\underline{\eta}_1 = \hat{\underline{X}}(t_{k+1}|t_k) \tag{3.20}$$

UPDATED STATE ITERATIONS, $i=1,2,\ldots,\ell$

$$\underline{\eta}_{i+1} = \hat{\underline{X}}(t_{k+1}|t_k) + K^i_{k+1}[\underline{Z}(t_{k+1}) - \underline{h}(\underline{\eta}_i, \underline{u}^*(t_{k+1}), t_{k+1}) - H(\underline{\eta}_i, \underline{u}^*(t_{k+1}), t_{k+1})\{\hat{\underline{X}}(t_{k+1}|t_k) - \underline{\eta}_i\} \tag{3.21}$$

GAIN MATRIX ITERATIONS, $i=1,2,\ldots,\ell$

$$K^i_{k+1} = P(t_{k+1}|t_k)H(\underline{\eta}_i, \underline{u}^*(t_{k+1}), t_{k+1})^T \cdot [H(\cdot,\cdot,\cdot)P(t_{k+1}|t_k)H(\cdot,\cdot,\cdot)^T + R'(t_{k+1})]^{-1} \tag{3.22}$$

STATE ESTIMATE UPDATE, $k=0,1,\ldots$

$$\hat{\underline{X}}(t_{k+1}|t_{k+1}) = \underline{\eta}_{\ell+1} \tag{3.23}$$

ERROR COVARIANCE UPDATE, $k=0,1,\ldots$

$$P(t_{k+1}|t_{k+1}) = [I - K^\ell_{k+1}H(\underline{\eta}_\ell, \underline{u}^*(t_{k+1}), t_{k+1})]P(t_{k+1}|t_k) \cdot [I - K^\ell_{k+1}H(\cdot,\cdot,\cdot)]^T + K^\ell_{k+1}R'(t_{k+1})K^{\ell T}_{k+1} \tag{3.24}$$

INITIAL CONDITIONS

$$\hat{\underline{X}}(t_o|t_o) = \hat{\underline{X}}_o \; ; \quad P(t_o|t_o) = P_o \tag{3.25}$$

The local iterations limit, ℓ, is defined such that $\underline{n}_{\ell+1} \simeq \underline{n}_{\ell}$. Note that improving the state and error covariance updated values not only affects the current time step, but also future time steps, since such estimated values become the initial conditions for the state and error covariance propagation differential equations. The structure of the iterated extended Kalman filter is represented in Figure 3.2.

3.4 Extended Linear Filter-Smoother and Iterated Extended Linear Filter-Smoother

Information available in the future may be used in the past to decrease linearization errors on the system nonlinear dynamic functions. If future estimates are propagated into the past, better past estimates will be obtained. If such past estimates serve as initial conditions for new estimates in the future, better tracking of the system dynamic nonlinearities will be achieved.

Better past estimates are obtained by using the linearized Kalman filter on the backwards dynamic equations, with the previous forward estimate as the linearization trajectory. For the interval $[t_k, t_{k+1}]$ the backwards filter algorithm is, Gelb (1974):

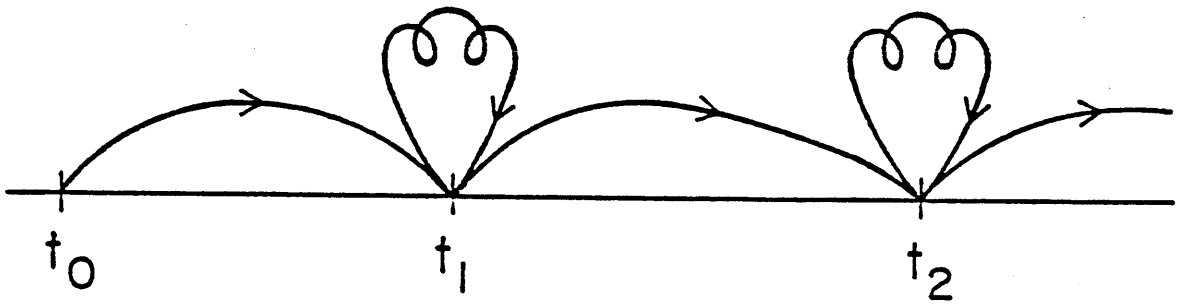

Figure 3.2 Iterated Extended Kalman Filter Structure, IEKF-3 (with three local iterations)

BACKWARDS STATE ESTIMATE PROPAGATION, $\tau\epsilon[0,t_{k+1}-t_k)$, $t = t_{k+1}-\tau$

$$\frac{d}{d\tau}\hat{\underline{X}}_b(\tau) = -\underline{f}(\hat{\underline{X}}(t|t_k),\ \underline{u}^*(t),t) - F(\hat{\underline{X}}(t|t_k),\underline{u}^*(t),t)\cdot[\hat{\underline{X}}_b(\tau) - \hat{\underline{X}}(t|t_k)] \tag{3.26}$$

BACKWARDS ERROR COVARIANCE PROPAGATION, $\tau\epsilon[0,t_{k+1} - t_k)$

$$\frac{d}{d\tau}\ P_b(\tau) = -F(\hat{\underline{X}}(t|t_k),\underline{u}^*(t),t)P_b(\tau) - P_b(\tau)F(\cdot,\cdot,\cdot)^T + Q'(t) \tag{3.27}$$

BACKWARDS STATE ESTIMATE UPDATE

$$\hat{\underline{X}}_b'(t_k) = \hat{\underline{X}}_b(t_{k+1}- t_k) + K_{b_k}[\underline{Z}(t_k) - \underline{h}(\hat{\underline{X}}(t_k|t_k),\underline{u}^*(t_k),t_k) - H(\hat{\underline{X}}(t_k|t_k),\cdot,\cdot)\{\hat{\underline{X}}_b(t_{k+1}-t_k) - \hat{\underline{X}}(t_k|t_k)\}] \tag{3.28}$$

BACKWARDS ERROR COVARIANCE UPDATE

$$P_b'(t_k) = [I - K_{b_k}H(\cdot,\cdot,\cdot)]P_b(t_{k+1} - t_k)[I - K_{b_k}H(\cdot,\cdot,\cdot)]^T + K_{b_k}R'(t_k)K_{b_k}^T \tag{3.29}$$

BACKWARDS GAIN

$$K_{b_k} = P_b(t_{k+1}-t_k)H(\cdot,\cdot,\cdot)^T\cdot [H(\cdot,\cdot,\cdot)P_b(t_{k+1}-t_k)H(\cdot,\cdot,\cdot)^T + R'(t_k)]^{-1} \tag{3.30}$$

After use of this algorithm two estimates at time t_k are known, namely $\hat{\underline{X}}(t_k|t_k)$ and $\hat{\underline{X}}'_b(t_k)$. A new initial condition for forwards dynamic propagation is obtained by weighting these estimates according to their error covariance matrices:

$$\hat{\underline{X}}_s(t_k|t_k) = P_s(t_k|t_k)[P(t_k|t_k)^{-1}\ \hat{\underline{X}}(t_k|t_k) + P'_b(t_k)^{-1}\ \hat{\underline{X}}'_b(t_k)] \tag{3.31}$$

where

$$P_s(t_k|t_k)^{-1} = P(t_k|t_k)^{-1} + P'_b(t_k)^{-1} \tag{3.32}$$

Once these smoothed estimates are obtained, the extended Kalman filter can be used again in the forwards dynamic equations. Because more accurate initial conditions have been obtained at t_k, better estimates at t_{k+1} are expected.

The extended linear filter-smoother, ELFS, is the combination of a forward extended Kalman filter and a backwards linearized Kalman filter. The procedure on any interval may be repeated for a fixed number of backwards-forwards cycles, or for as many cycles until convergence is achieved. The structure of this procedure is shown in Figure 3.3.

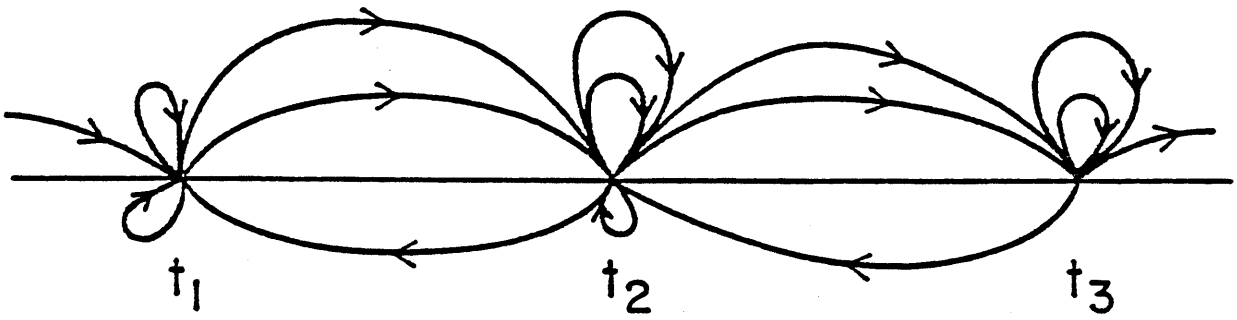

Figure 3.3 Extended Linear Filter-Smoother Structure, ELFS-1 (with one smoothing cycle)

If the iterated extended Kalman filter is used in the forwards dynamic propagations, linearization errors will be reduced on the dynamics function and in the observation function, Wishner, et al. (1968). This filter is named iterated extended Kalman filter-smoother, IELFS. Its structure is shown in Figure 3.4.

3.5 Second Order Gaussian Filter

When using the extended Kalman filter and other nonlinear filtering approximations, first order Taylor expansions are usually used in approximating nonlinear functions. In order to achieve increased accuracy in the computation of the conditional mean of the states, such functions may be approximated by higher order Taylor expansions.

The second order Gaussian filter has the same structure of the extended Kalman filter. The linearization trajectory is also computed by the filter itself. The algorithm for this filter is, Jazwinski (1970):

STATE ESTIMATE PROPAGATION, $t\varepsilon[t_k, t_{k+1})$

$$\frac{d}{dt}\ \underline{\hat{X}}(t|t_k) = \underline{f}(\underline{\hat{X}}(t|t_k), \underline{u}^*(t), t) + \frac{1}{2}\ \underline{\partial}^2(F, P(t|t_k)) \qquad (3.33)$$

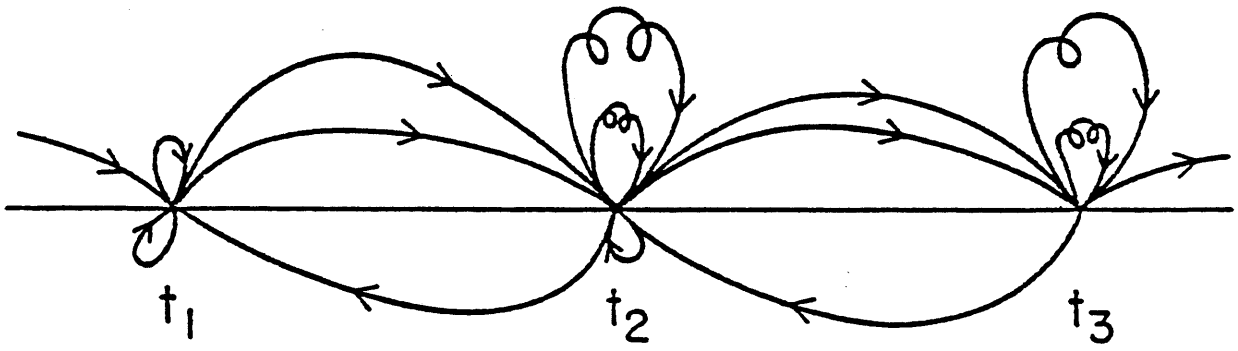

Figure 3.4 Iterated Extended Linear Filter-Smoother Structure, IELFS-3,1 (with one smoothing cycle and three local iterations)

ERROR COVARIANCE PROPAGATION, $t\in[t_k, t_{k+1})$

$$\frac{d}{dt} P(t|t_k) = F(\hat{\underline{X}}(t|t_k), \underline{u}^*(t), t)P(t|t_k) + P(t|t_k)F(\cdot,\cdot,\cdot)^T + Q'(t) \tag{3.34}$$

STATE ESTIMATE UPDATE, k=0,1,...

$$\hat{\underline{X}}(t_{k+1}|t_{k+1}) = \hat{\underline{X}}(t_{k+1}|t_k) + K_{k+1}[\underline{Z}(t_{k+1}) - \underline{h}(\hat{\underline{X}}(t_{k+1}|t_k), \underline{u}^*(t_{k+1}), t_{k+1}) - \frac{1}{2}\underline{\partial}^2(H, P(t_{k+1}|t_k))] \tag{3.35}$$

ERROR COVARIANCE UPDATE, k=0,1,...

$$P(t_{k+1}|t_{k+1}) = [I - K_{k+1}H(\hat{\underline{X}}(t_{k+1}|t_k), \underline{u}^*(t_{k+1}), t_{k+1})] \cdot P(t_{k+1}|t_k)[I - K_{k+1}H(\cdot,\cdot,\cdot)]^T + K_{k+1}R'(t_{k+1})K_{k+1}^T \tag{3.36}$$

GAIN MATRIX

$$K_{k+1} = P(t_{k+1}|t_k)H(\cdot,\cdot,\cdot)^T \cdot [H(\cdot,\cdot,\cdot)P(t_{k+1}|t_k)H(\cdot,\cdot,\cdot)^T + R'(t_{k+1}) + A(t_{k+1})]^{-1} \tag{3.37}$$

INITIAL CONDITIONS

$$\hat{\underline{X}}(t_o|t_o) = \hat{\underline{X}}_o; \quad P(t_o|t_o) = P_o \tag{3.38}$$

The second order terms $\underline{\partial}^2(F,P(t|t_k))$ and $\underline{\partial}^2(H,P(t_{k+1}|t_k))$ are defined component-wise by:

$$\partial_i^2(F,B) = \text{trace}\ \{[\frac{\partial^2 f_i}{\partial X_p \partial X_q}]\cdot B\} \tag{3.39}$$

with $[\frac{\partial^2 f_i}{\partial X_p \partial X_q}]$ the matrix of second order derivatives of the i^{th} component of $\underline{f}$ with respect to the states, evaluated at the current state estimate.

The correction term on the gain, $A(t_{k+1})$, depends on fourth order moments of the system. It is defined by:

$$\begin{aligned} A(t_{k+1}) = \frac{1}{2} E\{&\underline{\partial}^2(H,[\hat{\underline{X}}(t_{k+1}|t_k) - \underline{X}(t_{k+1})][\hat{\underline{X}}(t_{k+1}|t_k) - \underline{X}(t_{k+1})]^T)\cdot \\ &\underline{\partial}^2(H,[\hat{\underline{X}}(t_{k+1}|t_k) - \underline{X}(t_{k+1})][\hat{\underline{X}}(t_{k+1}|t_k) - \underline{X}(t_{k+1})]^T)^T\} \\ &- \frac{1}{2}\underline{\partial}^2(H,P(t_{k+1}|t_k))\underline{\partial}^2(H,P(t_{k+1}|t_k))^T \end{aligned} \tag{3.40}$$

where the expectation may be obtained from Gaussian moment factoring, to give for the (i,j) element of the correction:

$$a_{ij}^{k+1} = \frac{1}{4} \left[\sum_{r,s;m,n} \frac{\partial^2 h_i}{\partial X_r \partial X_s} \left(P_{rm} P_{sn} + P_{rn} P_{sm} \right) \frac{\partial^2 h_j}{\partial X_m \partial X_n} \right] \tag{3.41}$$

with P_{rm} denoting the (r,m) element of $P(t_{k+1} \mid t_k)$.

Chapter 4

PRACTICAL USE OF APPROXIMATE NONLINEAR FILTERS

4.1 Introduction

The results of applying the approximate nonlinear filters and the rainfall-runoff model to a case study are presented in this chapter. One step ahead forecasting as well as extended forecasting are considered.

Residual statistics and the least squares performance indices of Kitanidis and Bras (1978) are used to compare the performance of the different procedures.

Table 4.1 includes the nonzero elements on the linearization matrices of the dynamics and observations of the rainfall-runoff model. The actual expressions for these quantities are given in Appendix A. The second order derivatives, required to use the second order Gaussian filter, are included in Appendix B.

4.2 Description of the Drainage Basin and of the Available Data

The drainage basin under consideration in the present study is the Bird Creek basin near Sperry, Oklahoma. The area of the catchment is 2344 km^2(915.6 mi^2). Discharges every six-hours ("instantaneous") are measured at USGS Station No. 07177500. The average discharge is 20 m^3/sec with maximum recorded discharge of 2535.1

Table 4.1

Linearization Matrices for the Rainfall-Runoff Model

Matrix F

	X_p	X_1	X_2	X_3	X_4	X_5	X_6	S_1	S_2	...	S_{n-1}	S_n
X_p	T											
X_1	T	T										
X_2	T	T	T	T	T	T						
X_3		T	T	T	T	T						
X_4			T	T	T	T						
X_5			T	T	T	T						
X_6	T	T	T				T					
S_1	T	T	T		T	T	T	T				
S_2	T	T	T		T	T	T	T	T			
⋮			⋮				⋮					
S_{n-1}	T	T	T		T	T	T			...	T	
S_n	T	T	T		T	T	T			...	T	T

Matrix H

	X_p	X_1	X_2	X_3	X_4	X_5	X_6	S_1	$..S_2$	...	S_{n-1}	S_n
Z_p	T											
Z												T
c												

Table 4.1 (continued)

Matrix F^u

	T_o	P_o	T_d	u_e
X_p	T	T	T	
X_1	T	T	T	T
X_2	T	T	T	
X_3				T
X_4				
X_5				
X_6	T	T	T	T
S_1	T	T	T	
S_2	T	T	T	
⋮				
S_n	T	T	T	

MATRIX H^u

	T_o	P_o	T_d	u_e
Z_p	T	T	T	
Z_c				

m^3/sec and minimum of 0.22 m^3/sec. Characteristics of the discharge record are high peak and sharp hydrographs in the period from April to September. It is common to have flows rising from near zero to 200-250 m^3/sec in a period of 18 hours.

Instantaneous mean areal temperature, pressure, dew point, and precipitation data were provided by the NWS-Hydrologic Research Laboratory. These data sets were obtained from point observations at Tulsa, Oklahoma, 20 kms southeast of the basin's outlet.

Evapotranspiration demand was obtained from daily potential evapotranspiration data provided by the NWS. Instantaneous evapotranspiration was found by distributing the daily values over time intervals 0-6, 6-11, 12-18, and 18-24 hours, according to 0, 33, 67, and 0 percent, respectively.

There was no snow accumulation nor ablation in the case study.

Table 4.2 includes the values of the parameters for the rainfall-runoff model. These values were fixed in all the computations. The precipitation parameters are those in Georgakakos (1982a). The soil parameters were estimated by the NWS staff based on physiographic characteristics of the basin and input-output data. The channel parameters are those of Georgakakos and Bras (1980), obtained from input-output data for the month of July 1959.

The power functions, that approximate the threshold functions of the original Sacramento model, all have exponents equal to two.

Table 4.2

Parameter Values for the Rainfall-Runoff Model

	SYMBOL	VALUES
PRECIPITATION		
Updraft velocity parameter	ε_1	0.16×10^{-2}
Cloud particle mean diameter	ε_4	0.55×10^{-4}
SOIL		
Upper tension capacity	X_1^o	120.0
Upper free capacity	X_2^o	15.0
Lower tension capacity	X_3^o	160.0
Lower free primary capacity	X_4^o	140.0
Lower free secondary capacity	X_5^o	14.0
Interflow coefficient	d_u	0.0891
Primary drainage coefficient	d_ℓ'	0.0033
Secondary drainage coefficient	d_ℓ''	0.0336
Percolation Parameter	ε	48.0
Percolation Exponent	Θ	2.1
Fraction to lower free	P_f	0.02
Exponents on threshold approximation	m_1, m_2, m_3	2.0
Baseflow percent lost parameter	μ	3.55

Table 4.2 (continued)

	SYMBOL	VALUES
Additional impervious fraction	β_1	0.17
Permanent impervious fraction	β_2	0.001
CHANNEL		
Number of reservoirs	n	3
Input fraction to Reservoir 1	P_1	0.95
Input fraction to Reservoir 2	P_2	0.05
Input fraction to Reservoir 3	P_3	0
Exponent of router	m	0.8
Parameter of Reservoir 1	a_1	1.09
Parameter of Reservoir 2	a_2	1.04
Parameter of Reservoir 3	a_3	1.08

4.3 Review of the Comparison Indices

The least square indices of Kitanidis and Bras (1978) are reviewed in this section. These indices are the coefficients of efficiency, determination, persistence and extrapolation.

The efficiency of a model was defined by Nash and Sutcliffe (1970) as the proportion of the variance on the observed data accounted by the model. The efficiency coefficient is given by:

$$E = \frac{S_o - S}{S_o} \tag{4.1}$$

where S_o measures variability on the observed data and S measures variability of the predictions, over N time steps:

$$S_o = \sum_{i=1}^{N} (Z_o(t_i) - \overline{Z}_o)^2 \tag{4.2}$$

$$S = \sum_{i=1}^{N} (Z_o(t_i) - \hat{Z}_o(t_i))^2 \tag{4.3}$$

with $Z_o(t_i)$ denoting the observation at time t_i, $\hat{Z}_o(t_i)$ the prediction at time t_i and $\overline{Z}_o$ the observation mean over the N time steps.

Values of the efficiency coefficient close to one are indicative of good performance.

Another measure of performance is the determination coefficient of the linear regression line that relates the observations and the predictions. It is defined by:

$$D = 1 - \frac{\sum_{i=1}^{N} (Z_o(t_i) - Z_r(t_i))^2}{S_o} \qquad (4.4)$$

with $Z_r(t_i)$ denoting the estimate at time t_i given by the regression line. The coefficient of determination is always higher than the coefficient of efficiency because the regression line removes systematic errors in the forecast. Again a value of D closer to one is indicative of good performance.

The coefficient of persistance compares the model predictions with predictions given by the previous observation. This coefficient is given by:

$$P = 1 - \frac{S}{\sum_{i=1}^{N} (Z_o(t_i) - Z_o(t_{i-1}))^2} \qquad (4.5)$$

This coefficient takes values less than or equal to one, with one indicating perfect predictions.

The coefficient of extrapolation compares the model predictions with predictions obtained by linearly extrapolating the two most recent observations. If $Z_\ell(t_i)$ denotes the extrapolated estimate to time t_i, from the two most recent observations in the past, the coefficient of extrapolation is then:

$$L = 1 - \frac{S}{\sum_{i=1}^{N} (Z_o(t_i) - Z_\ell(t_i))^2} \qquad (4.6)$$

Once again a value of L closer to one indicates better performance.

4.4 Case Study Results

4.4.1 One-step Ahead Predictions

The months of April and May of 1960 were used to make comparisons among the different approximate nonlinear filters. Similar results were obtained for July 1959 but these results are not reported here.

All stochastic runs, i.e., with filtering, were made with the same set of initial conditions. The initial state mean and its initial diagonal error covariance matrix are included in Table 4.3.

The spectral density matrix Q(t) was assumed diagonal and constant for all times. Several structures for this matrix were considered. Its standard deviations are included in Table 4.4. It was assumed that the inputs were measured without error. This gives the matrix $Q_u(t)$ equal to zero and consequently the spectral density matrix for the linearized system, Q'(t), is the same as Q(t). The input values were also assumed perfectly predictable, i.e., the true inputs at times t_k and t_{k+1} were used to obtain state estimates at time t_{k+1}.

Table 4.3

Rainfall-Runoff Initial Mean and Initial Standard Deviations

State	Mean [mm]	Standard Deviation [mm]
X_p	1.0	0.03
X_1	10.0	0.3
X_2	12.0	0.1
X_3	10.0	0.3
X_4	10.0	0.3
X_5	11.0	0.1
X_6	0.0	0.1
S_1	0.05	0.001
S_2	0.05	0.001
S_3	0.05	0.001

Table 4.4

Rainfall-Runoff Model Spectral Density Standard Deviations

	Q-Level					
State	0	1	2	3	4	5
X_p	2	5	10	20	10	30
X_1	10^{-7}	10^{-6}	10^{-5}	10^{-4}	10^{-1}	0.2
X_2	10^{-4}	10^{-3}	10^{-2}	10^{-1}	10^{-2}	0.2
X_3	0.05	0.5	5	50	5	10
X_4	0.0187	0.187	1.87	18.7	1.87	10
X_5	0.0682	0.682	6.82	68.2	6.82	10
X_6	0.075	0.75	7.5	75	7.5	10
S_1	0.70	0.70	0.70	0.70	1	1
S_2	0.17	0.17	0.17	0.17	1.7	1
S_3	0.17	0.17	0.17	0.17	0.17	0.25

The observations covariance matrix, $R(t) = R(t)'$, for the rainfall-runoff model is given in Table 4.5. The observation errors in discharge are made of a constant error and an error directly proportional to the discharge observation. On the other hand, the precipitation measurements error were assumed not related to precipitation observations, but given by a constant value at all times.

Results of the use of the rainfall-runoff model in a deterministic model (without filtering), to predict instantaneous mean areal precipitation with a 6-hour lead are shown in Figure 4.1. Use of the extended Kalman filter and Q of level 2 give the precipitation predictions depicted in Figure 4.2. Notice the slight improvement due to the use of filtering. The residual statistics (means, variation coefficients, and autocorrelation of different lags) as well as the least squares performance indices for the two procedures are included in Table 4.6.

Because the precipitation portion of the rainfall-runoff model is linear with respect to the state, and the error covariance of the inputs was taken equal to zero, no improvement in prediction of precipitation is expected from the other approximations to nonlinear filtering. Precipitation predictions were also found insensitive to the spectral density matrix changes defined in Table 4.4.

Results for deterministic prediction of discharge are shown in Figure 4.3. The residual statistics (means, variation coefficients, skewness, and autocorrelations of different lags); statistics of the series obtained by normalizing the residuals by their respective

Table 4.5

Rainfall-Runoff Model Observation Error Covariance Matrix

	MAP	Discharge
MAP	1	0
Discharge	0	$(0.05+0.1\ Z_c)^2$

Z_c - Discharge observation

MAP - Mean Areal Precipitation

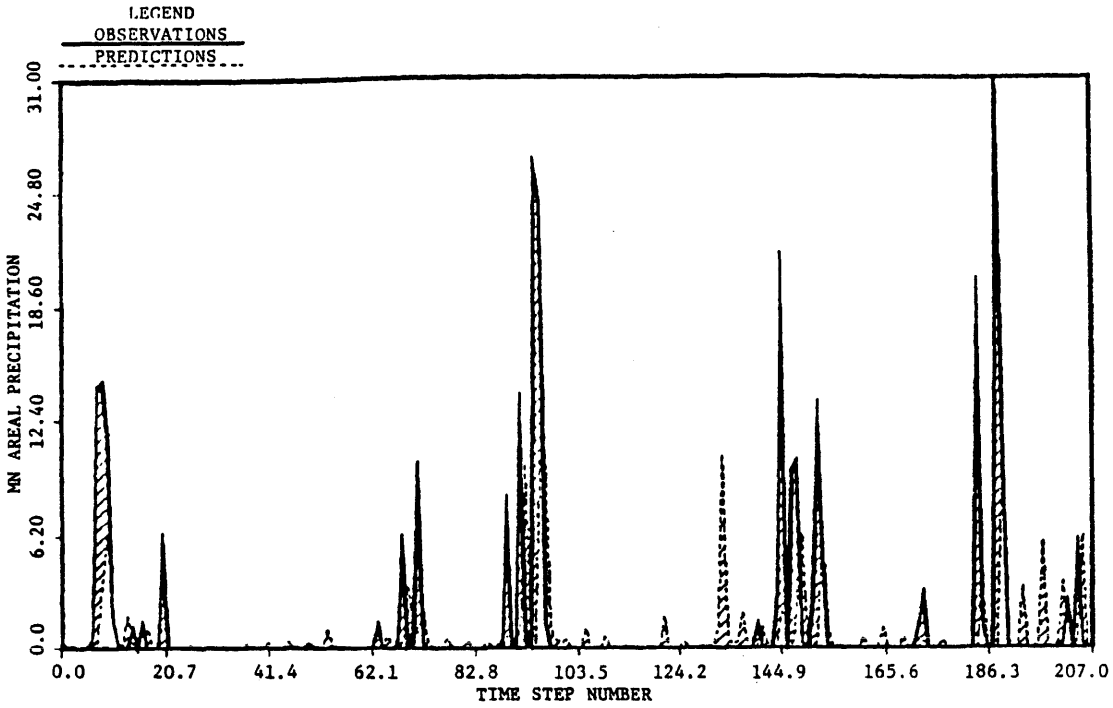

Figure 4.1 Deterministic Prediction of Precipitation, Bird Creek, April-May 1960

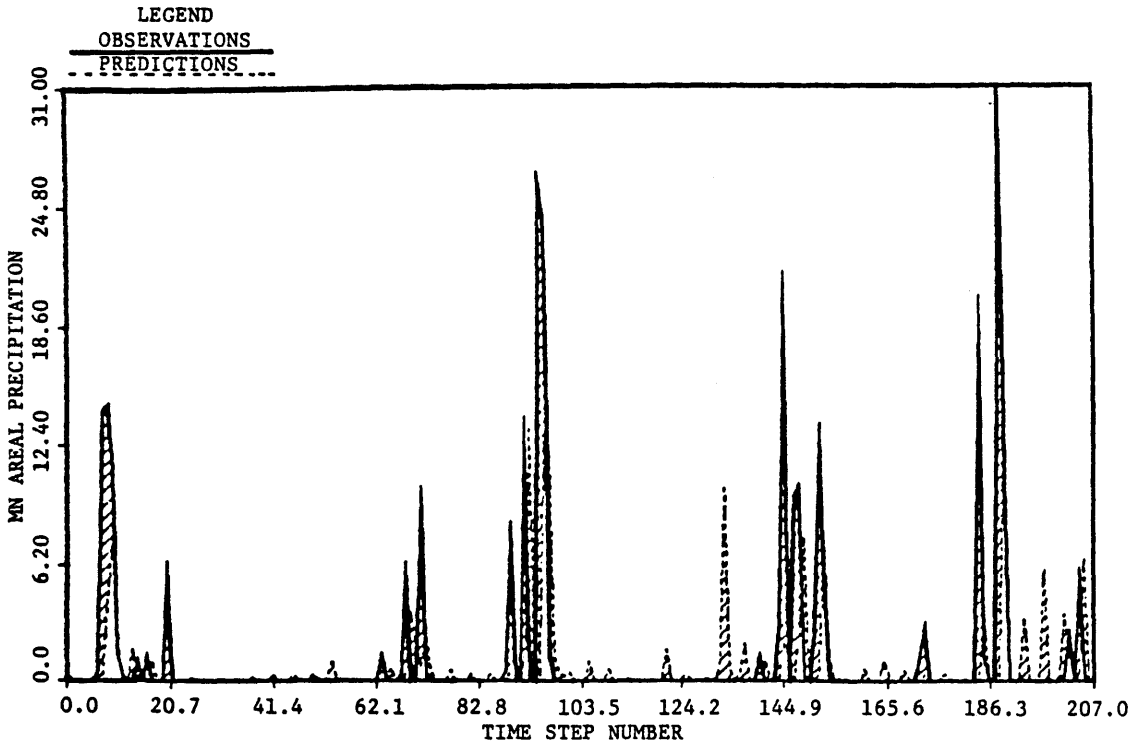

Figure 4.2 Stochastic Prediction of Precipitation, Bird Creek, April-May 1960, Q-4

Table 4.6

Residual Statistics and Least Squares Performance Indices for Precipitation

	Deterministic	EKF
Mean	0.60	0.54
Variation Coefficient	7.04	7.92
Correlation lag 1	0.07	0.03
Correlation lag 2	-0.15	-0.18
Efficiency	0.03	0.02
Determination	0.07	0.08
Persistence	0.26	0.26
Extrapolation	0.71	0.70

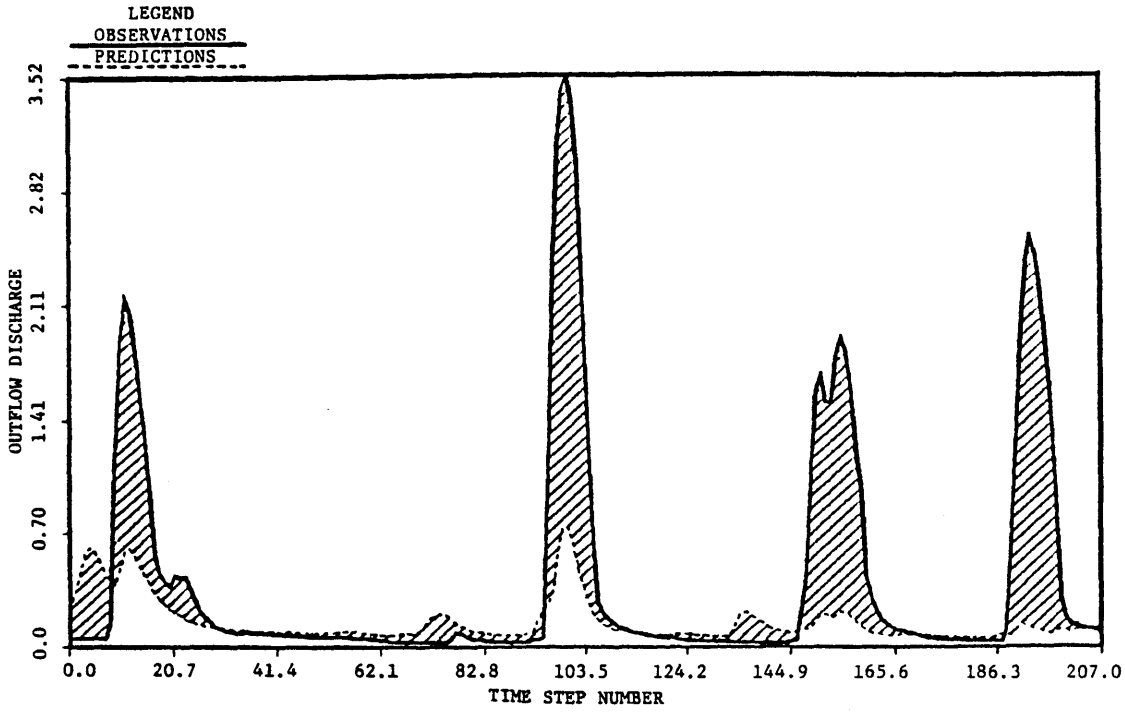

Figure 4.3 Deterministic Prediction of Discharge, Bird Creek, April-May 1960

standard deviations; and the least square indices for these results are given in the first rows of Tables 4.7, 4.8, and 4.9.

The residual statistics, normalized residual statistics and least squares performance indices for discharge, for the different nonlinear filters and for the different spectral density matrices are contained in Tables 4.7, 4.8, and 4.9, respectively.

The following remarks summarize the behavior of the different nonlinear filters in predicting discharge:

1. The approximated nonlinear filters do better in reproducing the discharge hydrograph than predictions obtained from deterministic use of the system dynamics.
2. The extended Kalman filter performance was not improved by the iterated extended Kalman filter (convergent after six iterations) or by the second order Gaussian filter. Because the exponents of the nonlinear reservoirs that constitute the channel have a value of 0.8, second order derivatives in the channel includes terms of the form $(0.8)(-0.2)S_i^{-1.2}$. For low flows these terms give unrealistically high values that have a detrimental effect on the predictions. The second order filter was then restricted only to high flows, defined when the storage of the last reservoir exceeds 0.2, but even for high discharges this filter closely resembles the predictions obtained by using the extended Kalman filter. Figures 4.4, 4.5, and 4.9 show the discharge predictions with these three filters for Q of level 4.

Table 4.7

Residual Statistics for Discharge

Q-Level	Procedure	Mean	Variation Coefficient	Skewness	Autocorrelation Lag-1	Lag-2	Lag-3	Lag-4
DETERMINISTIC		0.26	2.56	2.09	0.96	0.82	0.65	0.46
0	EKF	0.25	2.22	2.61	0.94	0.79	0.60	0.40
	IEKF-6	0.26	2.22	2.61	0.94	0.79	0.60	0.41
	ELFS-1	0.21	2.40	2.70	0.89	0.74	0.54	0.33
	ELFS-2	0.22	2.29	2.58	0.93	0.77	0.57	0.36
	IELFS-6,2	0.22	2.31	2.57	0.93	0.77	0.57	0.36
	SOFG	0.27	2.09	2.60	0.93	0.79	0.60	0.41
1	EKF	0.25	2.22	2.61	0.94	0.79	0.60	0.40
	IEKF-6	0.26	2.22	2.61	0.94	0.79	0.60	0.41
	ELFS-1	0.22	2.33	2.68	0.92	0.77	0.57	0.36
	ELFS-2	0.21	2.23	2.32	0.92	0.76	0.57	0.37
	IELFS-6,2	0.21	2.25	2.32	0.92	0.76	0.57	0.37
	SOGF	0.27	2.09	2.61	0.93	0.79	0.60	0.41

Table 4.7 (continued)

Q-Level	Procedure	Mean	Variation Coefficient	Skewness	Autocorrelation Lag-1	Lag-2	Lag-3	Lag-4
2	EKF	0.25	2.23	2.61	0.94	0.79	0.60	0.40
	IEKF-6	0.26	2.23	2.61	0.94	0.79	0.60	0.41
	ELFS-1	0.21	2.31	2.61	0.92	0.77	0.57	0.35
	ELFS-2	0.19	2.25	2.19	0.91	0.74	0.56	0.38
	IELFS-6,2	0.19	2.26	2.19	0.91	0.74	0.56	0.38
	SOGF	0.27	2.10	2.61	0.93	0.79	0.60	0.41
3	EKF	0.20	2.73	2.65	0.93	0.78	0.58	0.37
	IEKF-6	0.20	2.72	2.65	0.93	0.78	0.58	0.37
	ELFS-1	0.07	5.22	2.84	0.88	0.67	0.43	0.21
	ELFS-2	0.04	6.45	2.71	0.78	0.46	0.26	0.16
	IELFS-6,2	0.05	6.35	2.72	0.78	0.48	0.29	0.18
	SOGF	0.20	2.64	2.67	0.93	0.77	0.58	0.37
	ELFS-3	0.03	7.81	2.82	0.73	0.36	0.15	0.08

Table 4.7 (continued)

Q-Level	Procedure	Mean	Variation Coefficient	Skewness	Autocorrelation Lag-1	Lag-2	Lag-3	Lag-4
4	EKF	0.08	3.56	2.69	0.61	0.69	0.37	0.37
	IEKF-6	0.07	4.22	2.57	0.57	0.69	0.35	0.39
	ELFS-1	0.10	2.14	3.04	0.58	0.36	0.21	0.14
	ELFS-2	0.10	2.13	3.07	0.67	0.40	0.25	0.18
	IELFS-6,2	0.10	2.15	3.05	0.67	0.40	0.26	0.19
	SOGF	0.10	2.64	2.82	0.66	0.63	0.41	0.35
5	EKF	0.14	2.50	2.95	0.87	0.74	0.52	0.34
	IEKF-6	0.13	2.63	2.94	0.85	0.74	0.51	0.34
	ELFS-1	0.14	2.00	3.02	0.82	0.64	0.46	0.29
	ELFS-2	0.10	2.24	2.66	0.66	0.39	0.26	0.26
	IELFS-6,2	0.10	2.14	2.60	0.66	0.38	0.26	0.25
	SOGF	0.16	2.28	2.97	0.87	0.71	0.53	0.35

Table 4.8

Normalized Residuals Statistics for Discharge

0-Level	Procedure	Mean	Variation Coefficient	Skewness	Autocorrelations Lag-1	Lag-2	Lag-3	Lag-4
DETERMINISTIC		0.91	2.30	1.70	0.94	0.80	0.64	0.46
0	EKF	0.88	1.99	1.93	0.92	0.78	0.62	0.45
	IEKF-6	0.94	1.96	1.89	0.92	0.78	0.63	0.46
	ELFS-1	0.70	2.23	1.96	0.87	0.74	0.57	0.39
	ELFS-2	0.76	2.11	1.90	0.91	0.77	0.59	0.41
	IELFS-6,2	0.80	2.09	1.86	0.90	0.76	0.59	0.42
	SOGF	0.90	1.94	2.01	0.91	0.76	0.59	0.42
1	EKF	0.88	1.99	1.92	0.92	0.78	0.62	0.45
	IEKF-6	0.94	1.96	1.88	0.92	0.78	0.63	0.46
	ELFS-1	0.74	2.13	1.94	0.90	0.77	0.59	0.40
	ELFS-2	0.73	2.09	1.81	0.91	0.75	0.58	0.41
	IELFS-6,2	0.76	2.07	1.82	0.89	0.74	0.57	0.41
	SOGF	0.91	1.93	2.00	0.91	0.76	0.59	0.43

Table 4.8 (continued)

Normalized Residuals Statistics for Discharge

Q-Level	Procedure	Mean	Variation Coefficient	Skewness	Autocorrelations Lag-1	Lag-2	Lag-3	Lag-4
2	EKF	0.88	2.00	1.92	0.92	0.78	0.62	0.45
	IEKF-6	0.93	1.97	1.89	0.92	0.78	0.63	0.46
	ELFS-1	0.73	2.12	1.89	0.91	0.76	0.58	0.39
	ELFS-2	0.67	2.15	1.78	0.89	0.72	0.55	0.40
	IELFS-6,2	0.70	2.13	1.81	0.88	0.70	0.54	0.40
	SOGF	0.91	1.92	1.97	0.92	0.77	0.60	0.43
3	EKF	0.63	2.73	1.90	0.91	0.75	0.57	0.39
	IEKF-6	0.69	2.62	1.90	0.91	0.75	0.58	0.41
	ELFS-1	0.13	10.2	1.08	0.82	0.56	0.33	0.14
	ELFS-2	0.07	16.8	1.35	0.72	0.36	0.16	0.08
	IELFS-6,2	0.11	10.1	1.92	0.72	0.38	0.20	0.11
	SOGF	0.66	2.6	1.90	0.91	0.75	0.57	0.39
	ELFS-3	0.04	27.4	1.12	0.69	0.30	0.10	0.04

Table 4.8 (continued)

Normalized Residuals Statistics for Discharge

Q-Level	Procedure	Mean	Variation Coefficient	Skewness	Autocorrelations Lag-1	Lag-2	Lag-3	Lag-4
4	EKF	0.17	4.96	1.80	0.41	0.69	0.26	0.43
	IEKF-6	0.22	4.32	2.21	0.30	0.62	0.20	0.41
	ELFS-1	0.31	2.14	2.42	0.49	0.31	0.16	0.11
	ELFS-2	0.33	2.08	2.66	0.64	0.35	0.20	0.15
	IELFS-6,2	0.39	2.03	3.37	0.54	0.28	0.16	0.12
	SOGF	0.27	2.99	1.92	0.50	0.63	0.31	0.34
5	EKF	0.40	2.44	2.31	0.83	0.73	0.52	0.37
	IEKF-6	0.42	2.42	2.32	0.77	0.70	0.49	0.37
	ELFS-1	0.40	1.94	2.32	0.78	0.59	0.44	0.30
	ELFS-2	0.30	2.25	2.18	0.61	0.32	0.21	0.23
	IELFS-6,2	0.36	2.12	2.81	0.56	0.26	0.17	0.19
	SOGF	0.42	2.35	2.45	0.84	0.70	0.51	0.34

Table 4.9

Least Squares Performance Indices for Discharge

Q-Level	Procedure	Efficiency	Determination	Persistence	Extrapolation
	DETERMINISTIC	0.07	0.37	-8.6	-19.3
0	EKF	0.32	0.80	-5.9	-13.7
	IEKF-6	0.30	0.79	-6.1	-14.1
	ELFS-1	0.49	0.80	-4.2	-10.1
	ELFS-2	0.47	0.85	-4.5	-10.6
	IELFS-6,2	0.46	0.84	-4.6	-10.8
	SOGF	0.28	0.74	-6.3	-14.6
1	EKF	0.32	0.80	-5.9	-13.7
	IEKF-6	0.30	0.79	-6.1	-14.1
	ELFS-1	0.47	0.84	-4.4	-10.5
	ELFS-2	0.54	0.88	-3.7	-8.9
	IELFS-6,2	0.54	0.88	-3.7	-9.1
	SOGF	0.29	0.75	-6.3	-14.5

Table 4.9 (continued)

Q-Level	Procedure	Efficiency	Determination	Persistence	Extrapolation
2	EKF	0.33	0.80	-5.9	-13.7
	IEKF-6	0.31	0.79	-6.1	-14.1
	ELFS-1	0.50	0.86	-4.2	- 9.9
	ELFS-2	0.62	0.89	-2.9	- 7.4
	IELFS-6,2	0.61	0.89	-3.0	- 7.5
	SOGF	0.30	0.76	-6.2	-14.2
3	EKF	0.41	0.74	-5.1	-11.9
	IEKF-6	0.39	0.73	-5.3	-12.3
	ELFS-1	0.75	0.80	-1.5	- 4.4
	ELFS-2	0.85	0.87	-0.5	- 2.2
	IELFS-6,2	0.84	0.87	-0.6	- 2.4
	SOGF	0.41	0.73	-5.1	-11.9
	ELFS-3	0.87	0.88	-0.4	- 1.9

Table 4.9 (continued)

Q-Level	Procedure	Efficiency	Determination	Persistence	Extrapolation
4	EKF	0.86	0.92	-0.44	-2.06
	IEKF-6	0.85	0.91	-0.52	-2.24
	ELFS-1	0.91	0.94	0.04	-1.04
	ELFS-2	0.90	0.93	-0.07	-1.26
	IELFS-6,2	0.90	0.93	-0.04	-1.21
	SOGF	0.85	0.91	-0.56	-2.30
5	EKF	0.76	0.91	-1.5	-4.3
	IEKF-6	0.75	0.91	-1.5	-4.4
	ELFS-1	0.83	0.93	-0.8	-2.7
	ELFS-2	0.89	0.93	-0.1	-1.4
	IELFS-6,2	0.89	0.93	-0.1	-1.4
	SOGF	0.73	0.89	-1.8	-4.9

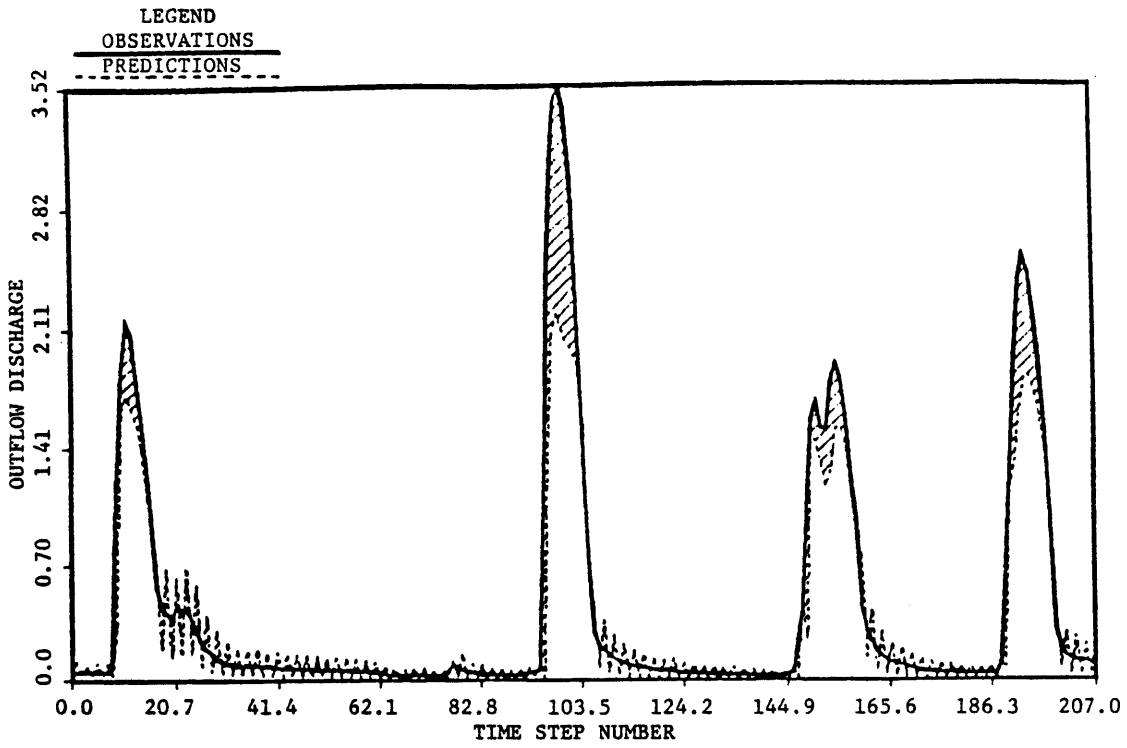

Figure 4.4 Stochastic Prediction of Discharge, Bird Creek, April-May 1960, EKF, Q-4

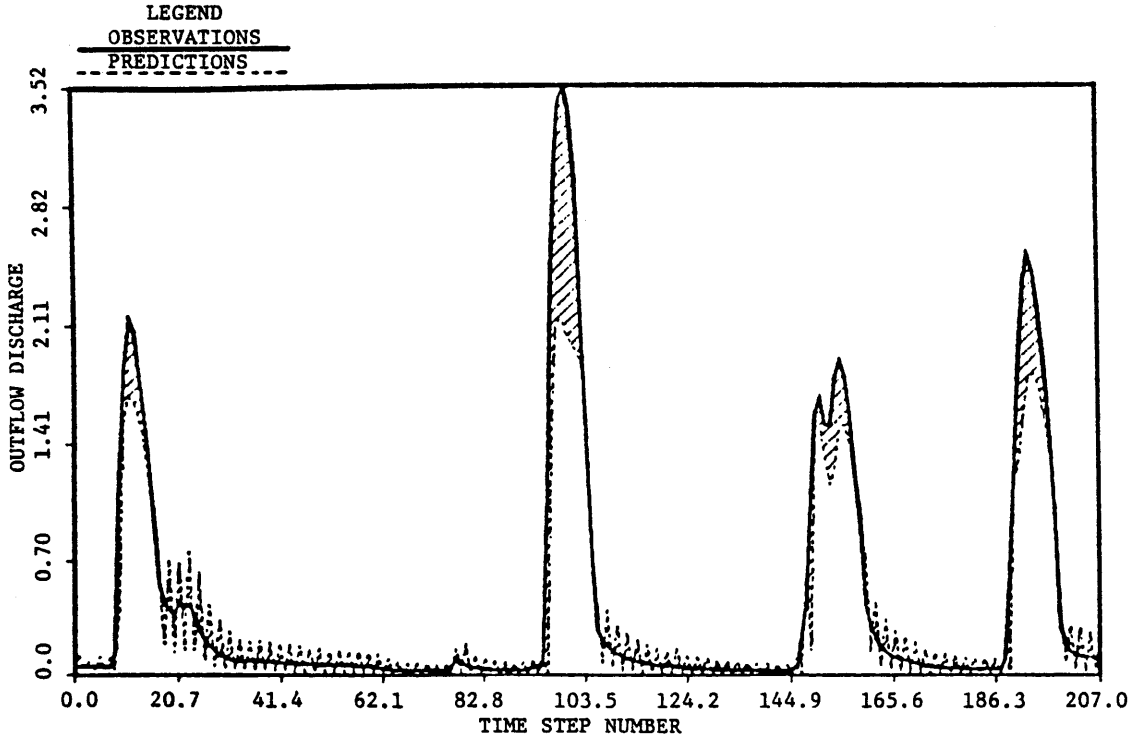

Figure 4.5 Stochastic Prediction of Discharge, Bird Creek, April-May 1960, IEKF-6, Q-4

3. The extended linear filter-smoother, computed after one or two cycles, gives as good or better predictions that the extended Kalman filter. Generally the former gives higher peaks and eliminates low flow oscillations often found by using the extended Kalman filter. See Figures 4.4, 4.6, and 4.7. The extended Kalman filter discharge predictions oscillate when excessive updatings occur. This happens when the predicted variance of the discharge observation is big compared to the discharge observation variance specified by the user. The extended linear filter-smoother predictions oscillate less than those of the extended Kalman filter because the use of future information in the past gives generally lower predicted variances.
4. For Q of levels 0 to 3 the extended Kalman filter gave poor results, as implied by autocorrelations of residuals and normalized residuals close to one, and least squares indices far from one. Although, the quality of the predictions improves as the soil dynamics are trusted less (as Q moves from 0 to 3, see Table 4.4), the peaks remain badly underestimated, see Figures 4.10 and 4.12. The extended linear filter-smoother also underestimates the peaks for spectral density matrices of levels 0 to 2, see Figure 4.11, but for Q of level 3 the predictions obtained by this filter are very good, see Figure 4.13.

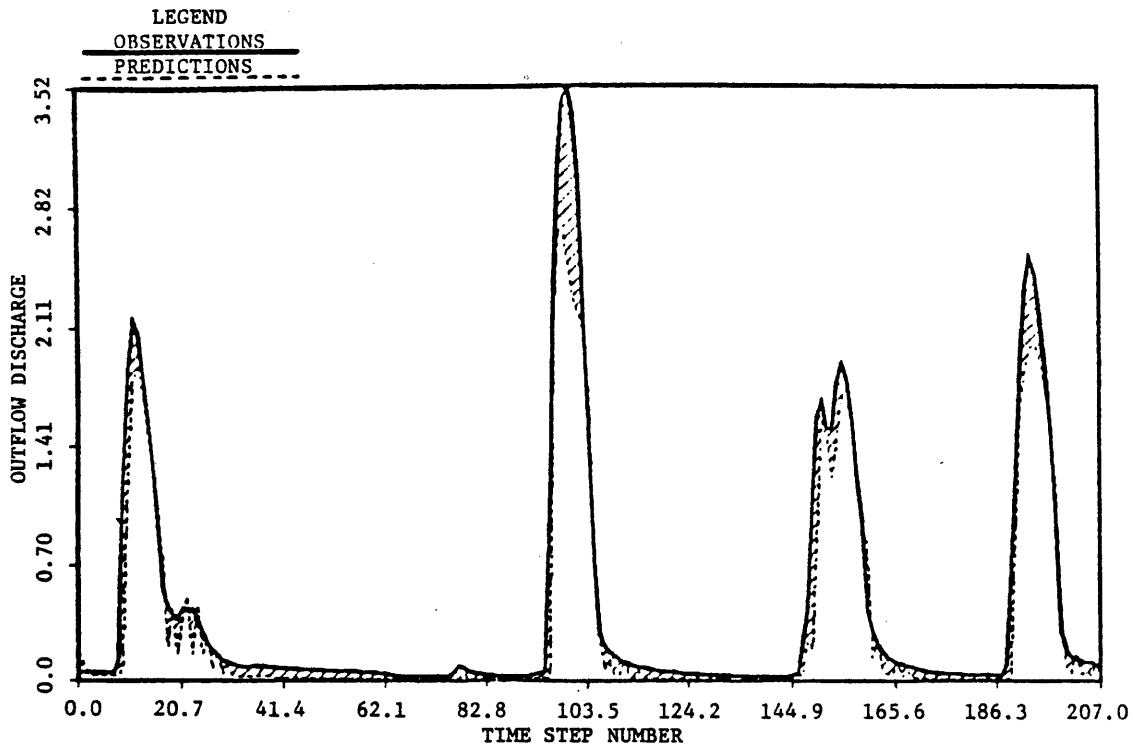

Figure 4.6 Stochastic Prediction of Discharge, Bird Creek, April-May 1960, ELFS-1, Q-4

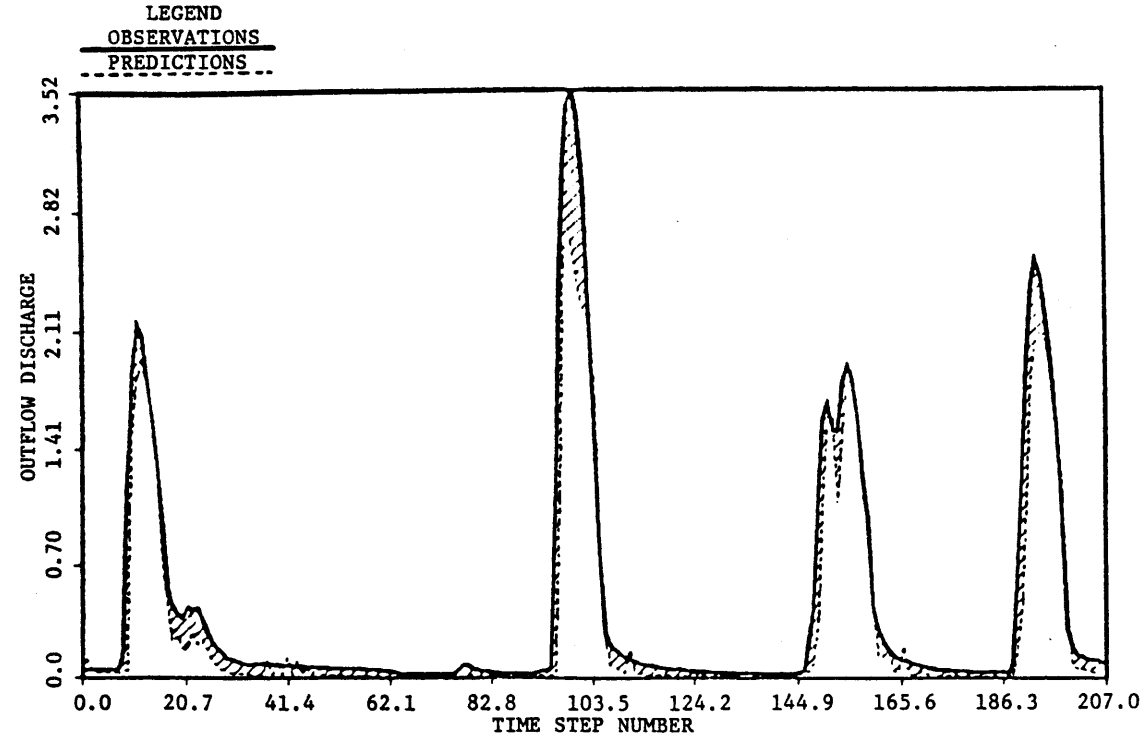

Figure 4.7 Stochastic Prediction of Discharge, Bird Creek, April-May 1960, ELFS-2, Q-4

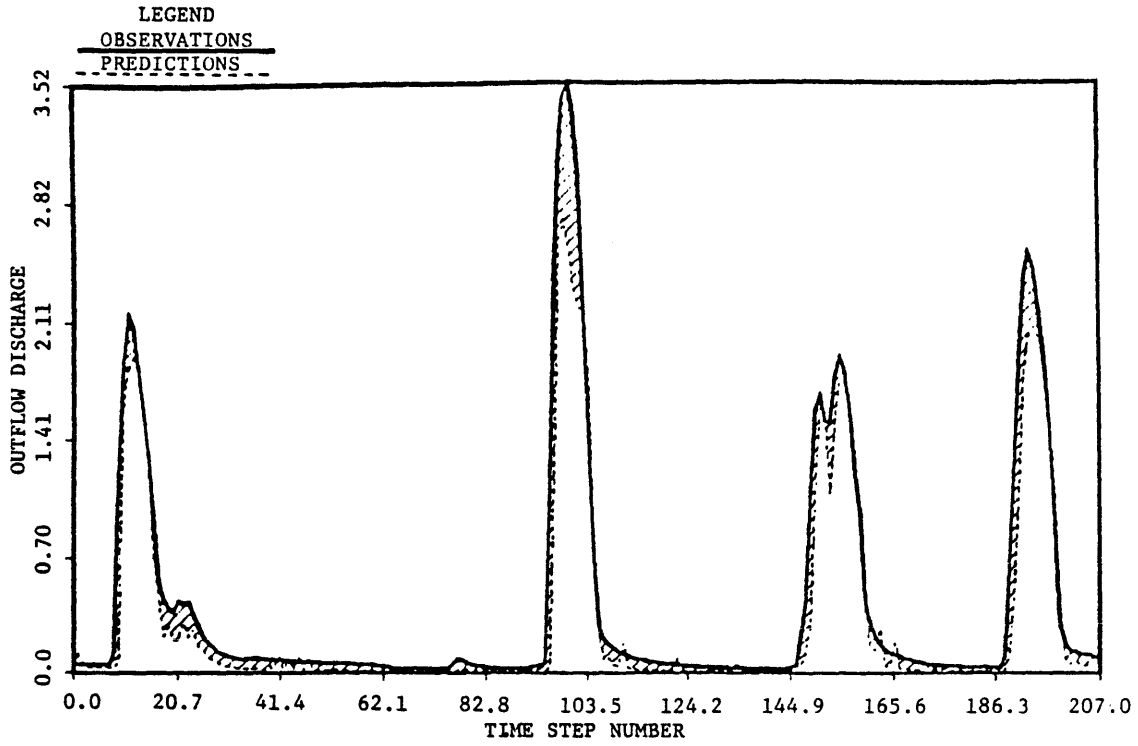

Figure 4.8 Stochastic Prediction of Discharge, Bird Creek, April-May 1960, IELFS-6,2, Q-4

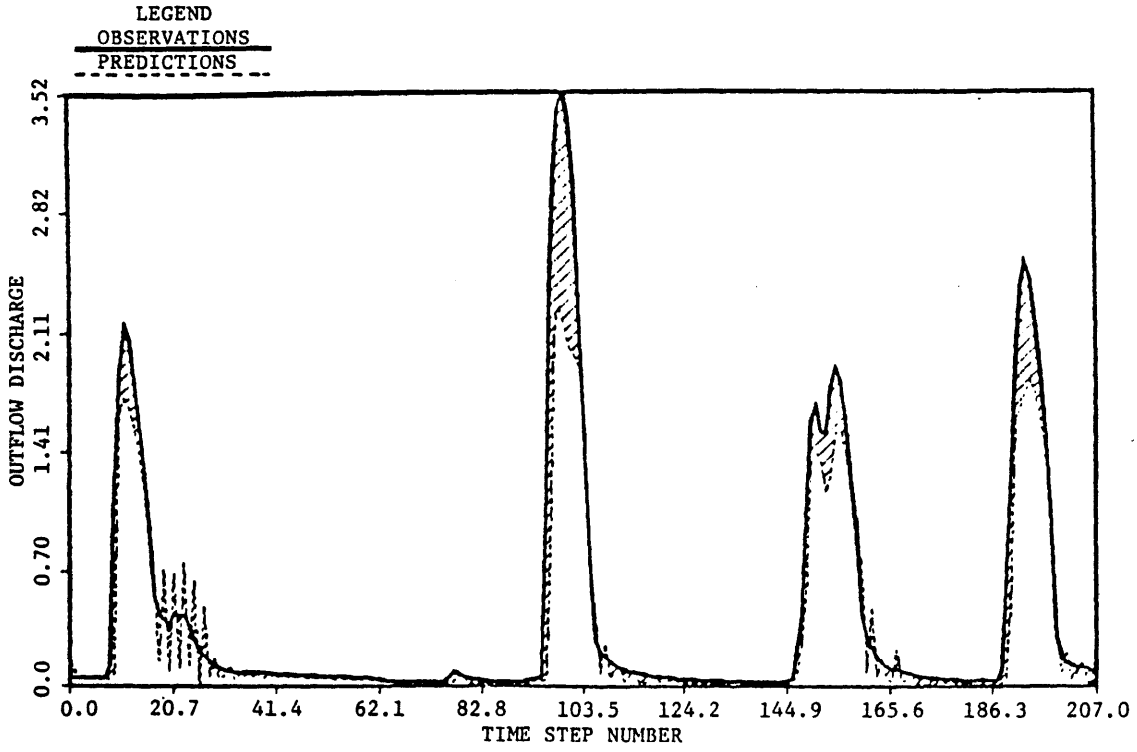

Figure 4.9 Stochastic Prediction of Discharge, Bird Creek, April-May 1960, SOGF, Q-4

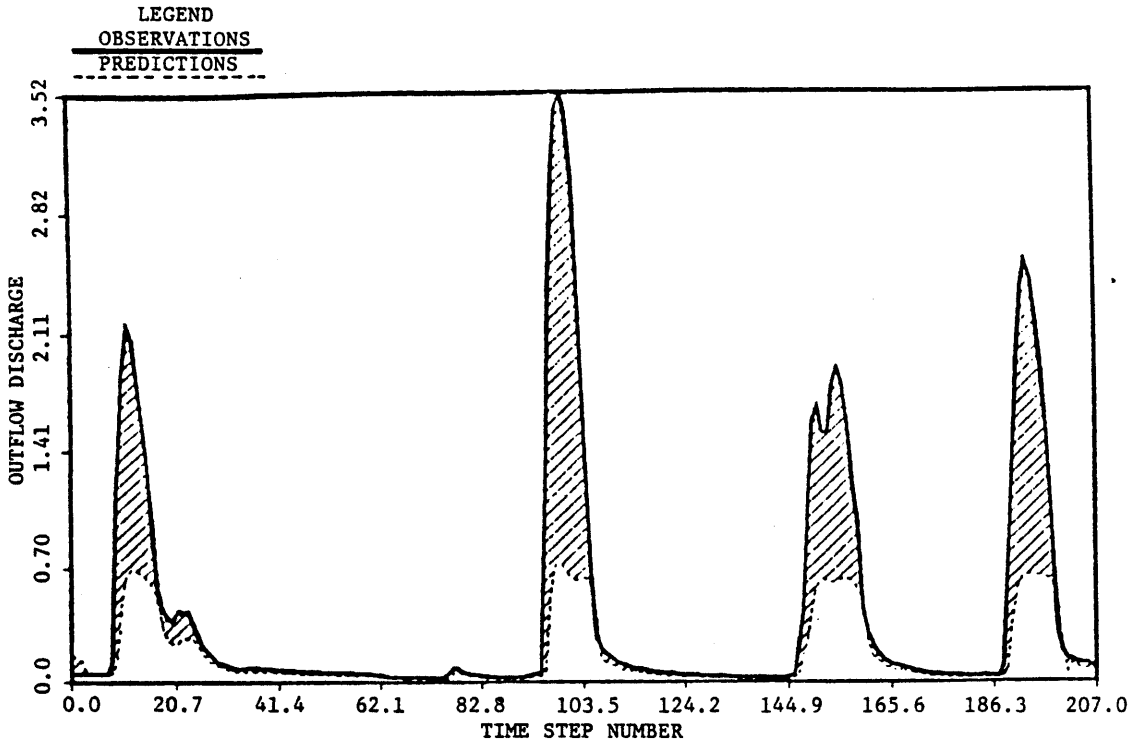

Figure 4.10 Stochastic Prediction of Discharge, Bird Creek, April-May 1960, EKF, Q-0

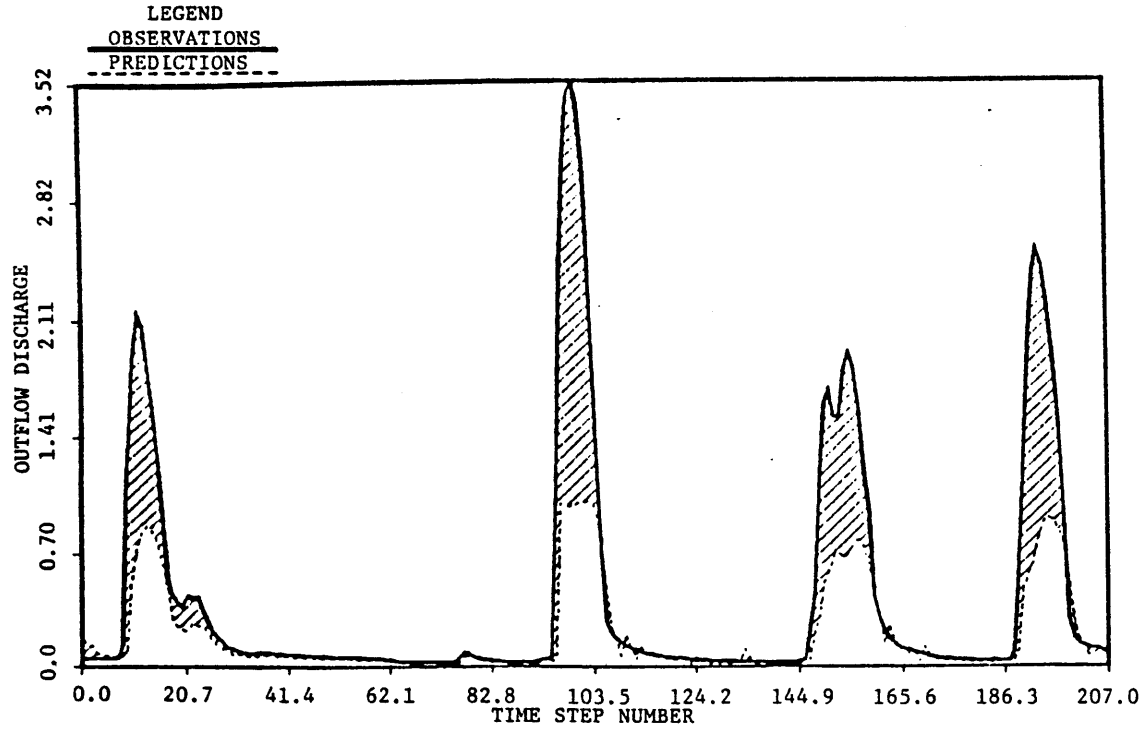

Figure 4.11 Stochastic Prediction of Discharge, Bird Creek, April-May 1960, ELFS-2, Q-0

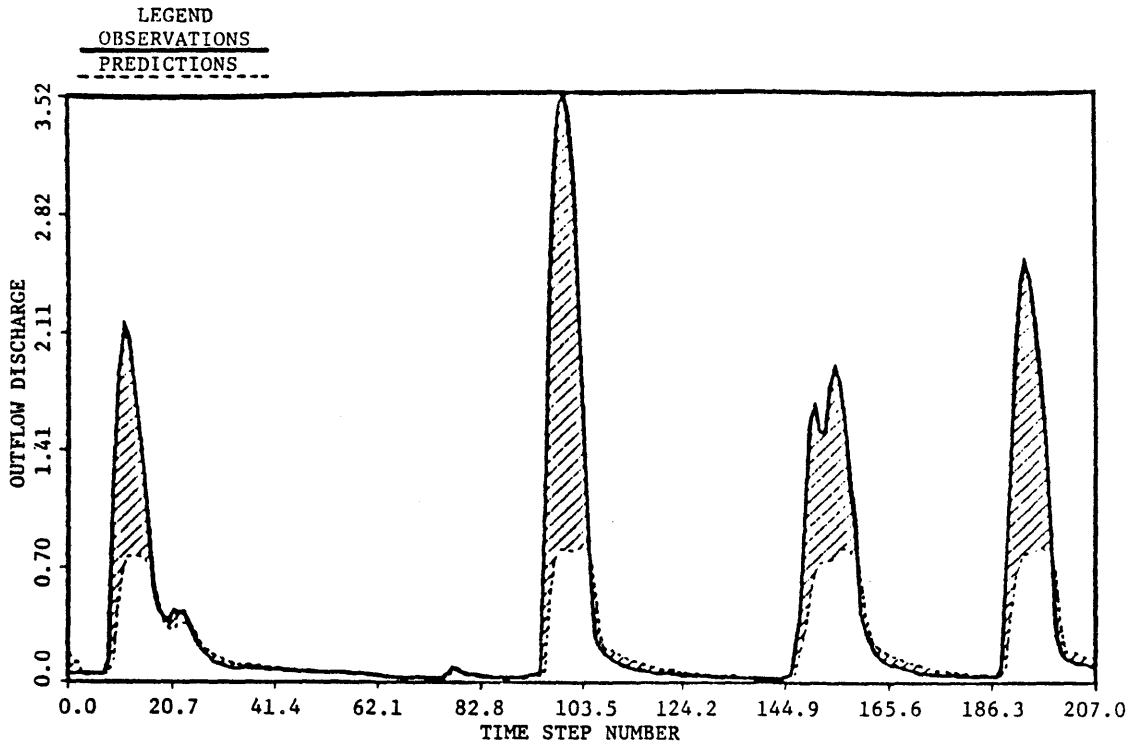

Figure 4.12 Stochastic Prediction of Discharge, Bird Creek, April-May 1960, EKF, Q-3

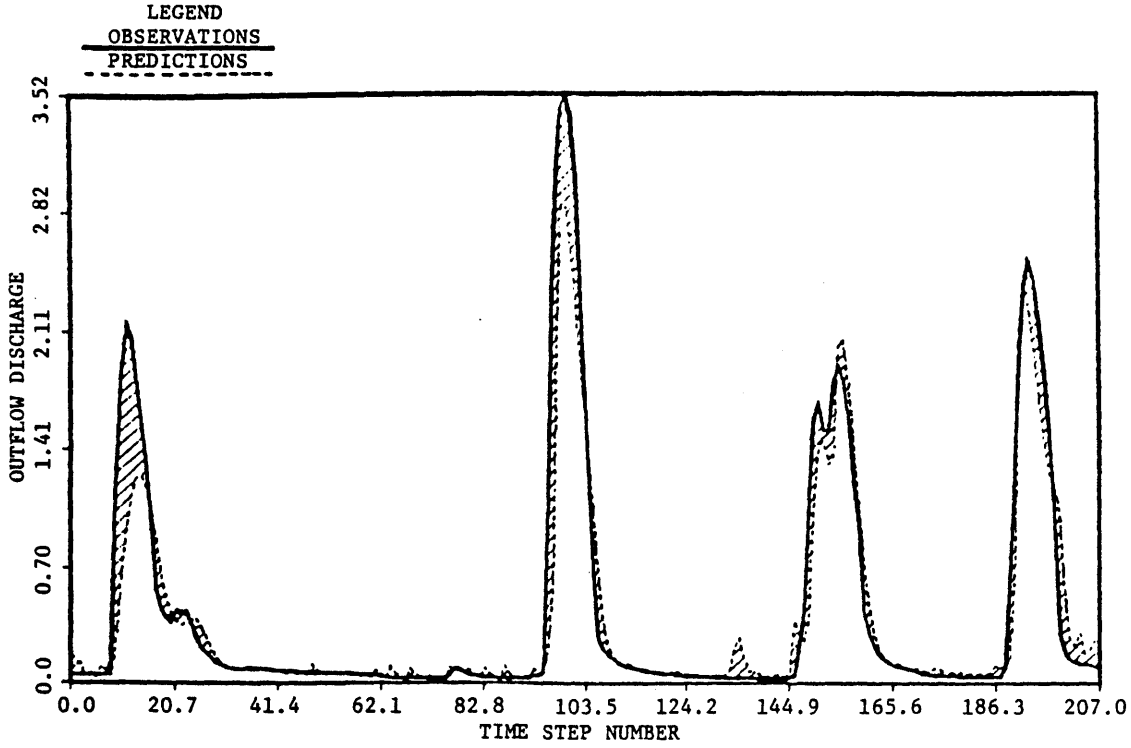

Figure 4.13 Stochastic Prediction of Discharge, Bird Creek, April-May 1960, ELFS-2, Q-3

5. The iterated extended linear filter-smoother gives about the same predictions of the extended linear filter-smoother, see Figures 4.7 and 4.8.
6. For spectral density matrices of levels 4 and 5, all the approximate nonlinear filters give good results, see Figures 4.4 to 4.9. Notice that although the procedures using smoothing give the best results, the extended Kalman filter also performs well.
7. All the approximate nonlinear filters have a timing error in predicting the hydrographs. Usually predictions during the rising limb lag the observations one time step, i.e., 6 hours. The extended Kalman filter follows best the recession portion of the hydrograph, the extended linear filter-smoother often decays one step behind.
8. The computational time is considerably increased by procedures with smoothing due to the numerical integration of the mean and error covariance differential equations, and due to the storage of forward trajectories needed to linearize the backwards differential equations. Table 4.10 includes the CPU execution time required by the different filtering procedures.
9. The means of the state predicted by the extended Kalman filter and the extended linear filter-smoother are in general different. The states in the upper soil zones for the extended Kalman filter contain less water than the ones given

Table 4.10

CPU Execution Time of the Nonlinear Filters

Procedure	Seconds per time step*
EKF	4.4
IEKF-6	5.0
ELFS-1	44.0
ELFS-2	82.5
ELFS-3	121.0
IELFS-6,2	84.2
SOGF	16.7

*At PRIME 750 Computer

by the extended linear filter-smoother, which are closer to saturation. For the deep lower portion of the soil the result tends to be the opposite. See Figure 4.14 to 4.19 for Q of level 3 and Figures 4.20 to 4.25 for Q of level 4. Recall that although the rainfall-runoff model conserves the water volume, the use of the updating step with any filter will "create" additional water whenever is necessary. This updating operation is the difference between the extended Kalman filter and the extended linear filter-smoother. The latter follows the model nonlinear dynamics better and commonly updates more the states in the upper soil, resulting in higher peaks.

4.4.2 Extended Forecasting

Extended forecasts were obtained with the rainfall-runoff model for the month of May 1960. The extended Kalman filter and the extended linear filter-smoother, computed with 2 cycles, were used as the filtering mechanisms.

The initial conditions were obtained by taking the predicted state means and error standard deviations on May 1st from ELFS-2 one-step predictions on the period April to May 1960, found using the initial conditions given in Table 4.3.

Table 4.11 includes the least square performance indices for precipitation. As can be seen there is no decrease in performance as the

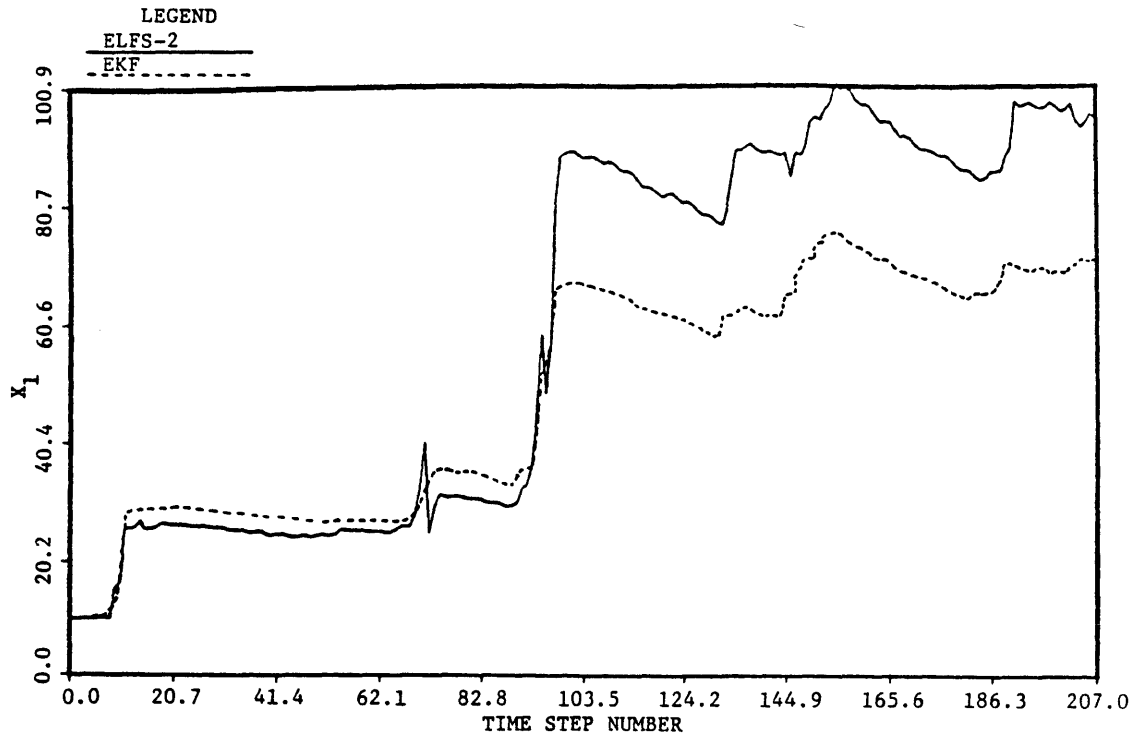

Figure 4.14 Predicted Trajectories of Upper Zone Tension Volume, Q-3

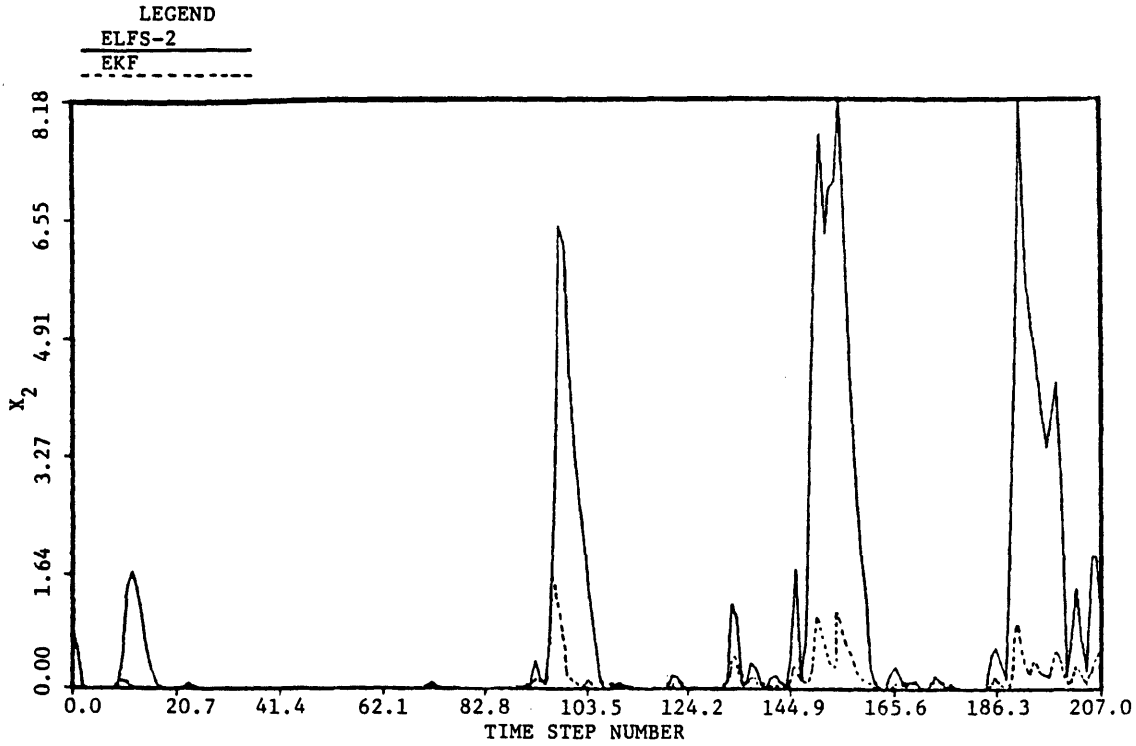

Figure 4.15 Predicted Trajectories of Upper Zone Free Volume, Q-3

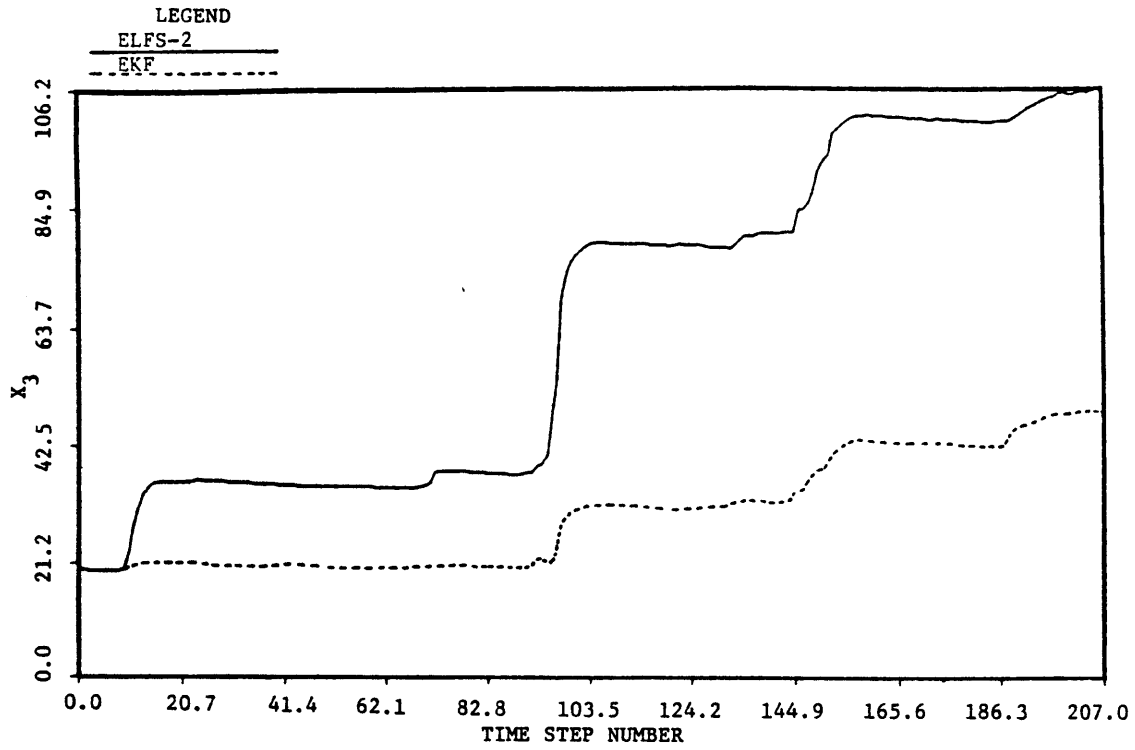

Figure 4.16 Predicted Trajectories of Lower Zone Tension Volume, Q-3

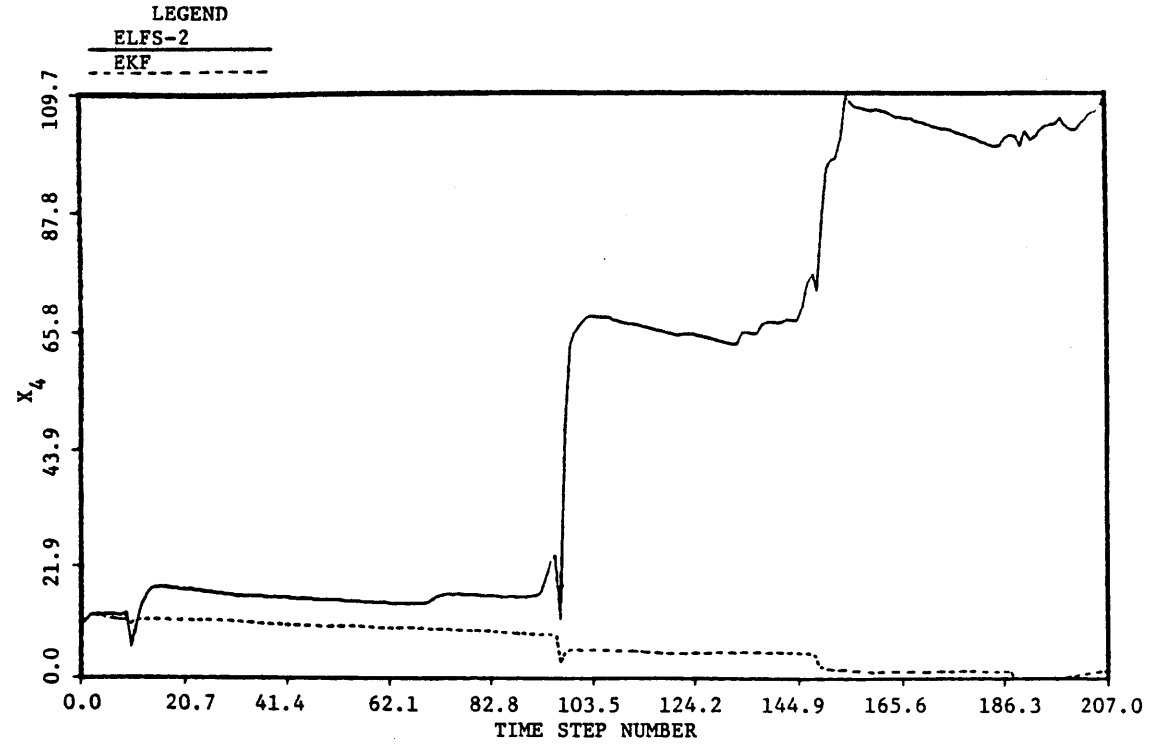

Figure 4.17 Predicted Trajectories of Lower Zone Free Primary Volume, Q-3

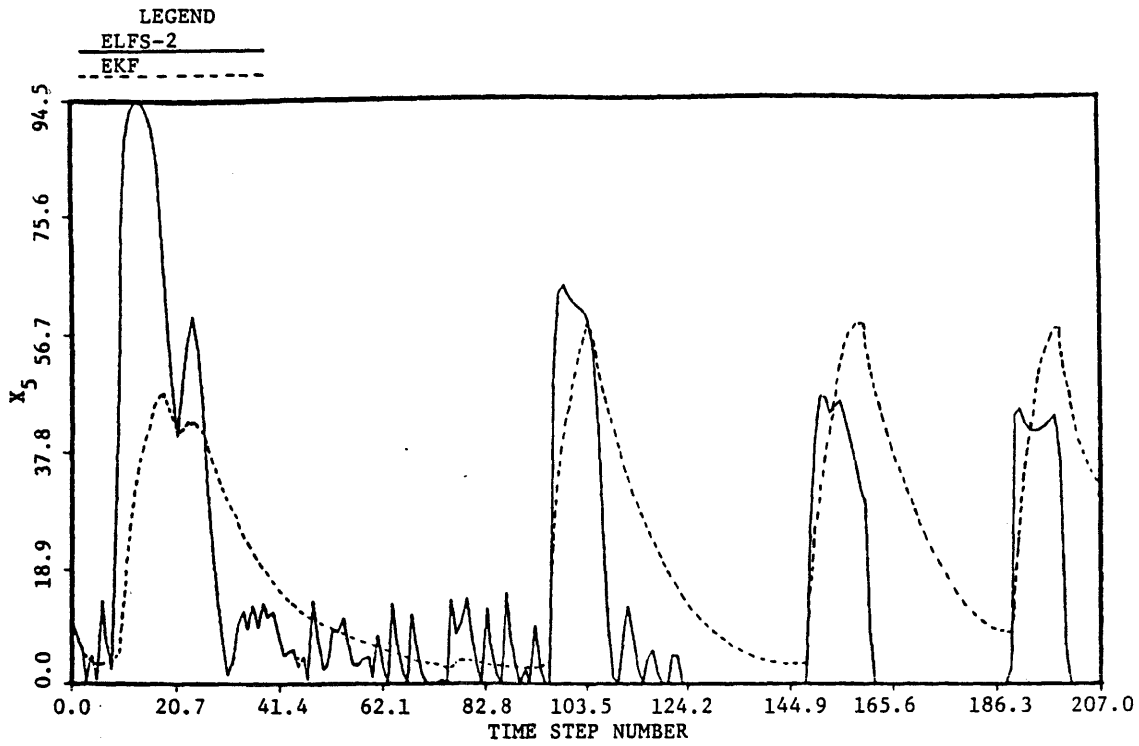

Figure 4.18 Predicted Trajectories of Lower Zone Free Secondary Volume, Q-3

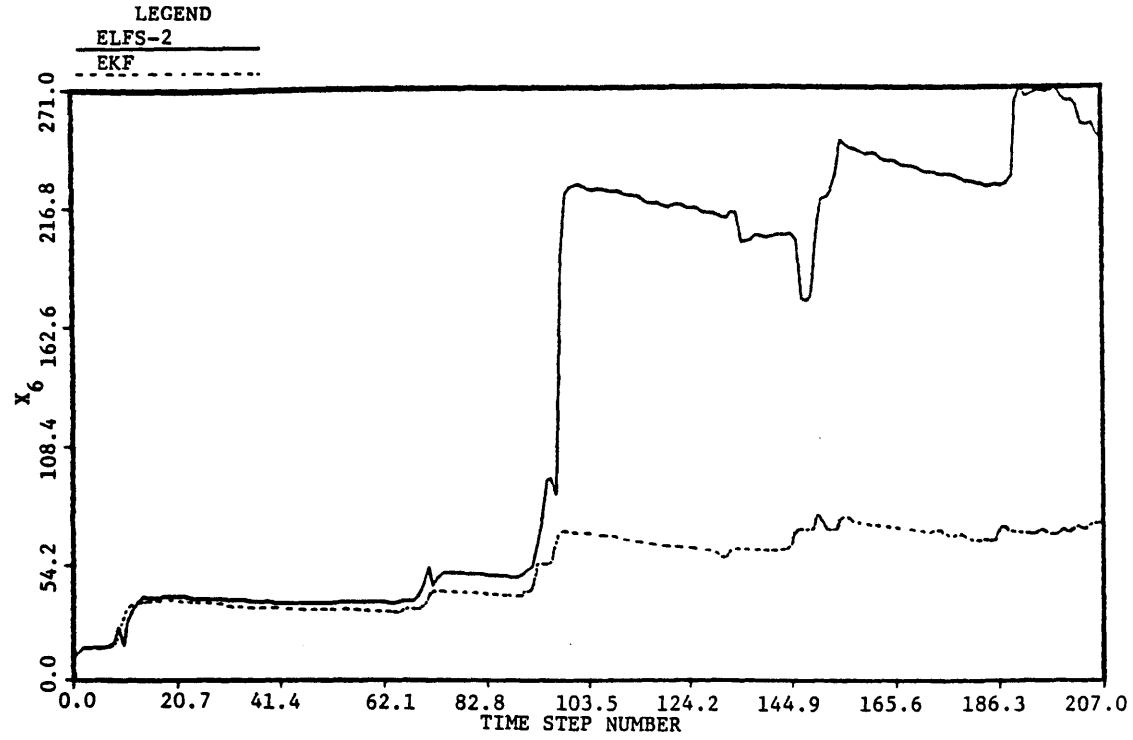

Figure 4.19 Predicted Trajectories of Additional Impervious Volume, Q-3

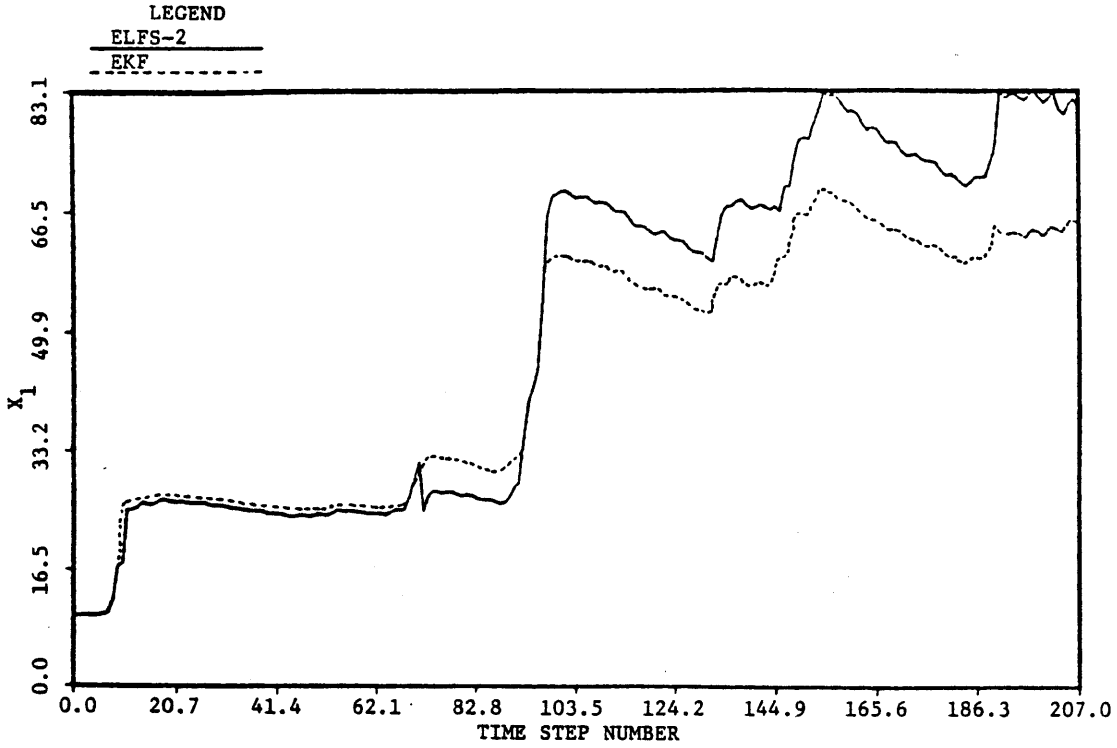

Figure 4.20 Predicted Trajectories of Upper Zone Tension Volume, Q-4

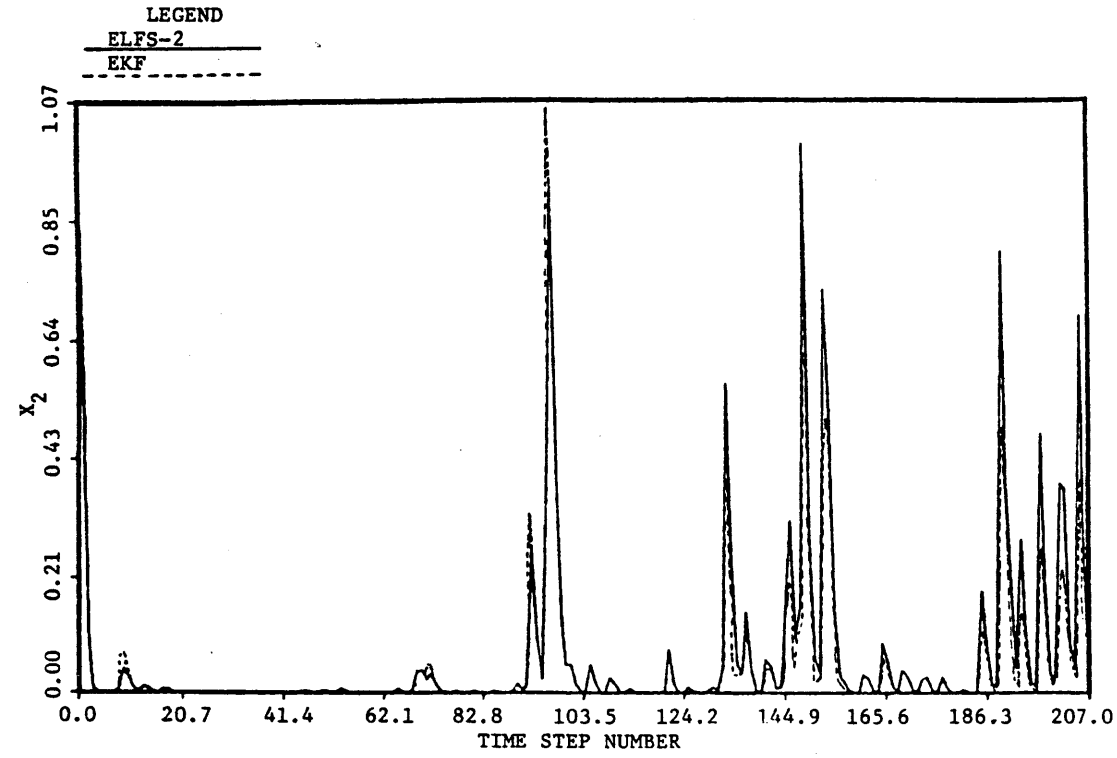

Figure 4.21 Predicted Trajectories of Upper Zone Free Volume, Q-4

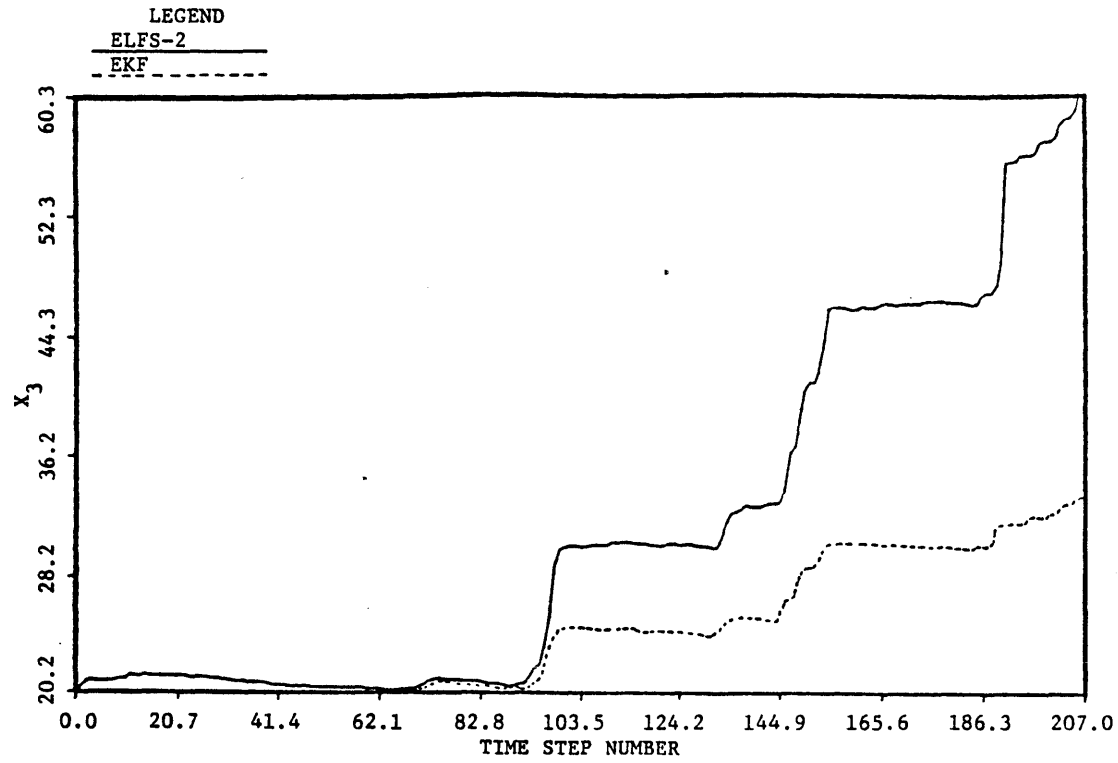

Figure 4.22 Predicted Trajectories of Lower Zone Tension Volume, Q-4

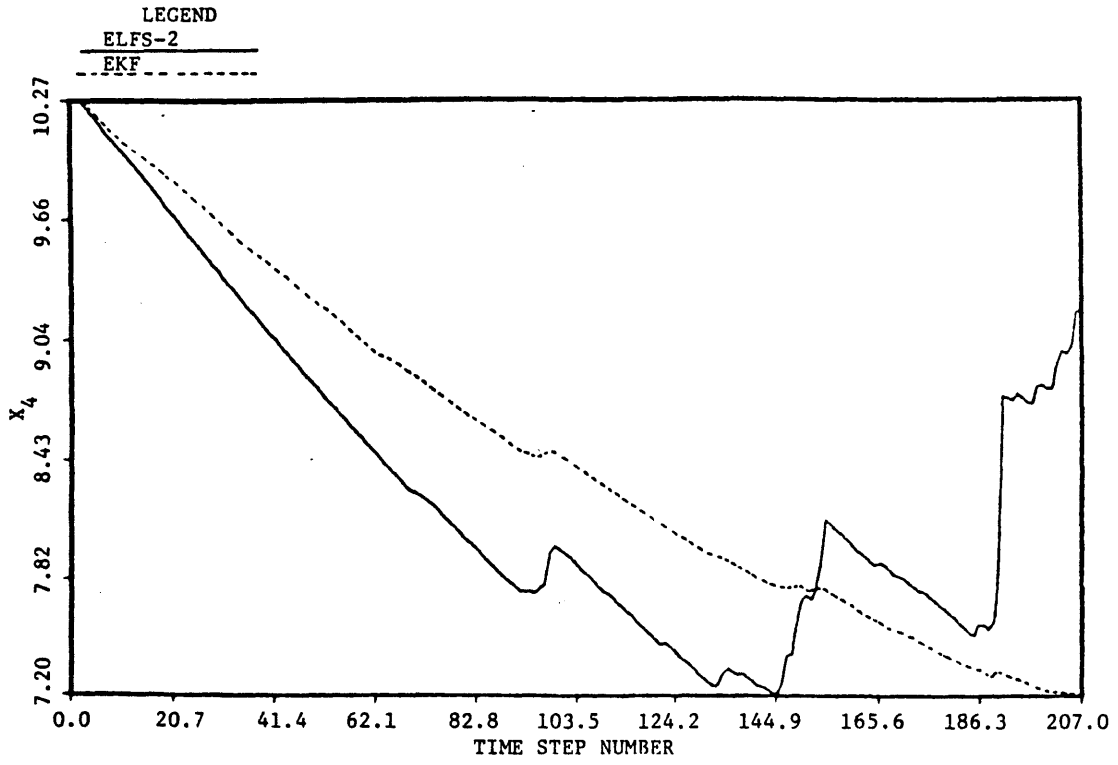

Figure 4.23 Predicted Trajectories of Lower Zone Free Primary Volume, Q-4

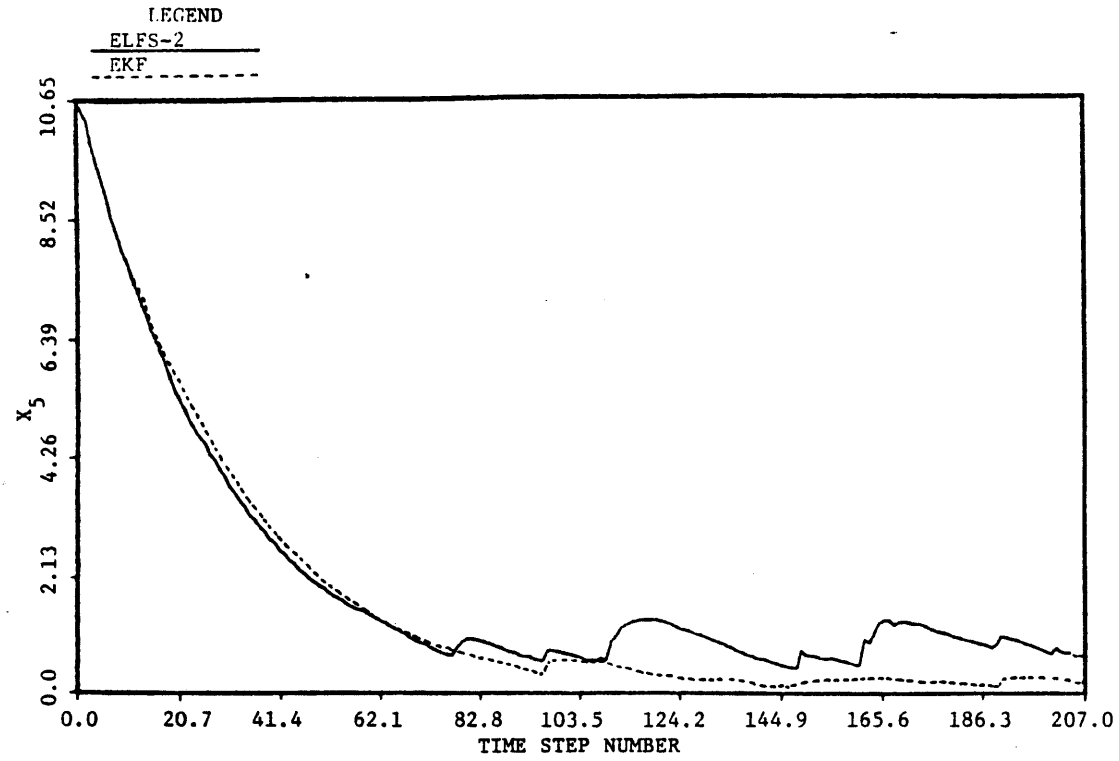

Figure 4.24 Predicted Trajectories of Lower Zone Free Secondary Volume, Q-4

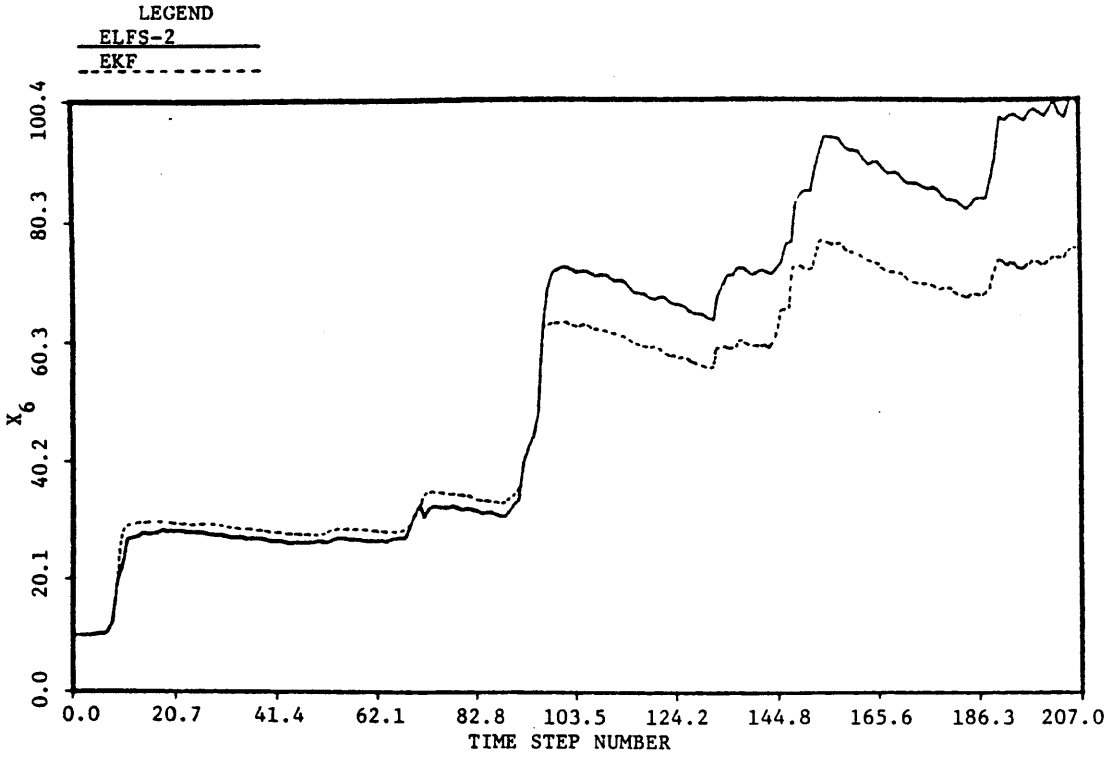

Figure 4.25 Predicted Trajectories of Additional Impervious Volume, Q-4

Table 4.11

Extended Forecasting Least Squares Indices for Precipitation

Lead Time	6 hrs	12 hrs	18 hrs	24 hrs
Efficiency	-0.02	-0.02	-0.02	-0.02
Determination	0.09	0.05	0.05	0.05
Persistence	0.27	0.51	0.42	0.35
Extrapolation	0.71	0.72	0.72	0.72

Q-level 3

lead time increases. Predictions of precipitation 6 hours ahead do not differ much from that 24 hours ahead. Recall that the inputs are assumed known in advance, which means that temperature, pressure and dew point are playing a dominant role in predicting precipitation. This is explained from the fact that characteristic times for rainfall are often less than 6 hours, and then the value of initial conditions is lost after a few hours.

Tables 4.12 and 4.13 contain the least squares performance indices for discharge if the filtering process is respectively the extended Kalman filter and the extended linear filter-smoother. As can be seen the quality of the predictions deteriorates as the lead time increases. The tendencies obtained with one-step ahead predictions are preserved by the extended forecasts, i.e., for Q of level 0 both nonlinear filters give bad predictions, for Q of level 3 the extended linear filter-smoother gives better predictions, and for Q of level 4 both nonlinear filters give the same quality of predictions. See Figures 4.26 to 4.33.

Table 4.12

Extended Forecasting Least Squares Indices for Discharge, EKF

Q-level 0

Lead Time	6 hrs	12 hrs	18 hrs	24 hrs
Efficiency	0.26	0.04	-0.18	-0.31
Determination	0.80	0.69	0.58	0.54
Persistence	-6.51	-10.94	-13.04	-18.96
Extrapolation	-17.08	-22.53	-27.70	-30.92

Q-level 3

Lead Time	6 hrs	12 hrs	18 hrs	24 hrs
Efficiency	0.35	0.18	0.01	-0.13
Determination	0.73	0.52	0.26	0.06
Persistence	-5.57	-10.18	-12.53	-16.84
Extrapolation	-14.83	-19.11	-23.27	-26.32

Q-level 4

Lead Time	6 hrs	12 hrs	18 hrs	24 hrs
Efficiency	0.85	0.58	0.20	-0.12
Determination	0.92	0.81	0.64	0.47
Persistence	-0.54	-2.00	-3.14	-8.24
Extrapolation	-2.72	-9.28	-18.55	-26.27

Table 4.13

Extended Forecasting Least Squares Indices for Discharge, ELFS-2

Q-level 0

Lead Time	6 hrs	12 hrs	18 hrs	24 hrs
Efficiency	0.39	0.11	-0.14	-0.29
Determination	0.82	0.67	0.52	0.42
Persistence	-5.15	-9.12	-13.24	-19.23
Extrapolation	-13.82	-20.71	-26.82	-30.57

Q-level 3

Lead Time	6 hrs	12 hrs	18 hrs	24 hrs
Efficiency	0.65	0.48	0.30	0.13
Determination	0.76	0.59	0.41	0.24
Persistence	-2.52	-4.96	-6.16	-10.20
Extrapolation	-7.48	-11.64	-15.97	-20.16

Q-level 4

Lead Time	6 hrs	12 hrs	18 hrs	24 hrs
Efficiency	0.86	0.56	0.19	-0.11
Determination	0.91	0.69	0.44	0.24
Persistence	-0.36	-1.44	-4.20	-8.20
Extrapolation	-2.28	-9.64	-18.72	-26.16

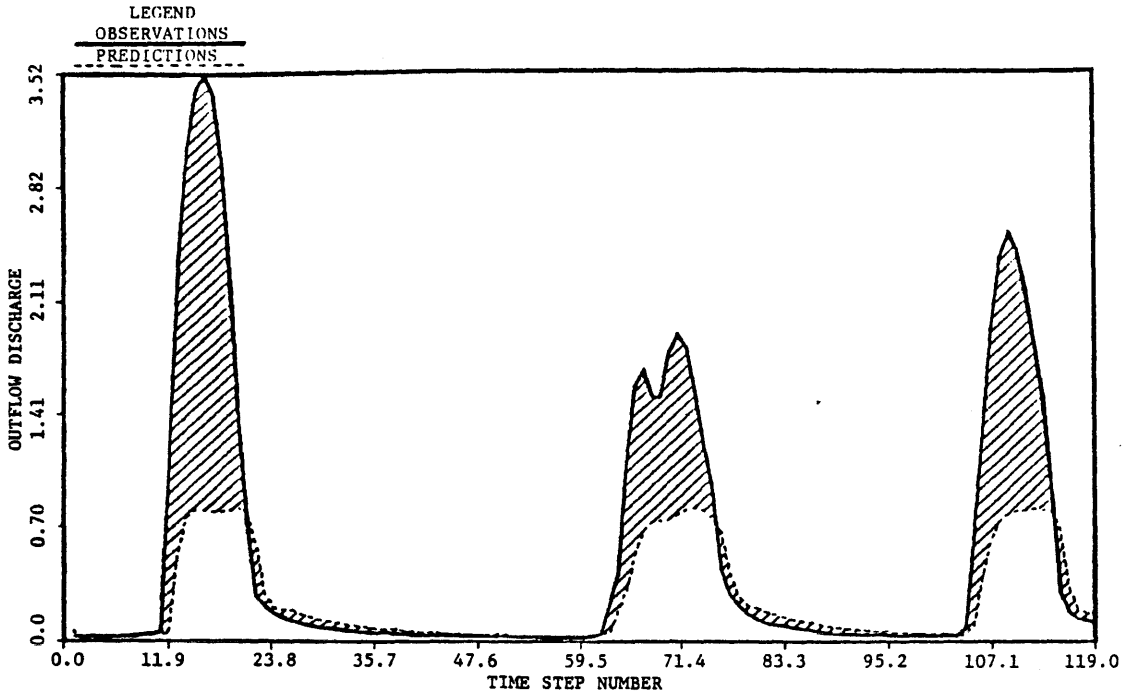

Figure 4.26 Extended Forecast of Discharge, Bird Creek, May 1960, Q-3, 6 hrs, EKF

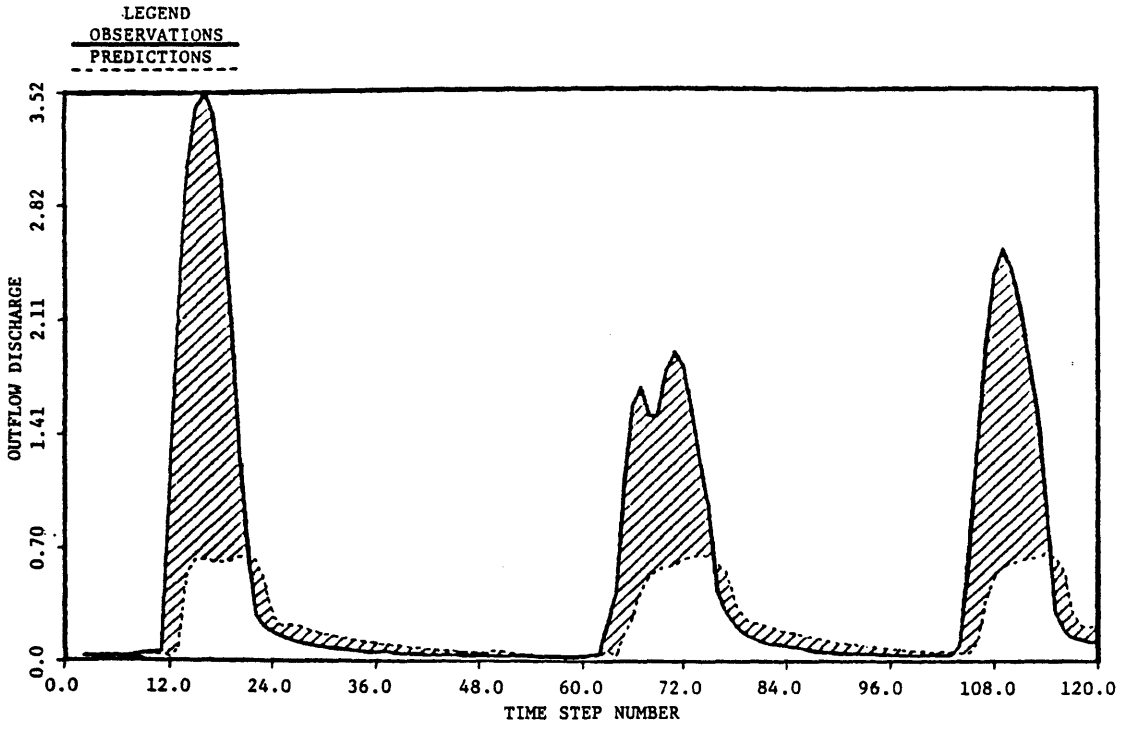

Figure 4.27 Extended Forecast of Discharge, Bird Creek, May 1960, Q-3, 12 hrs, EKF

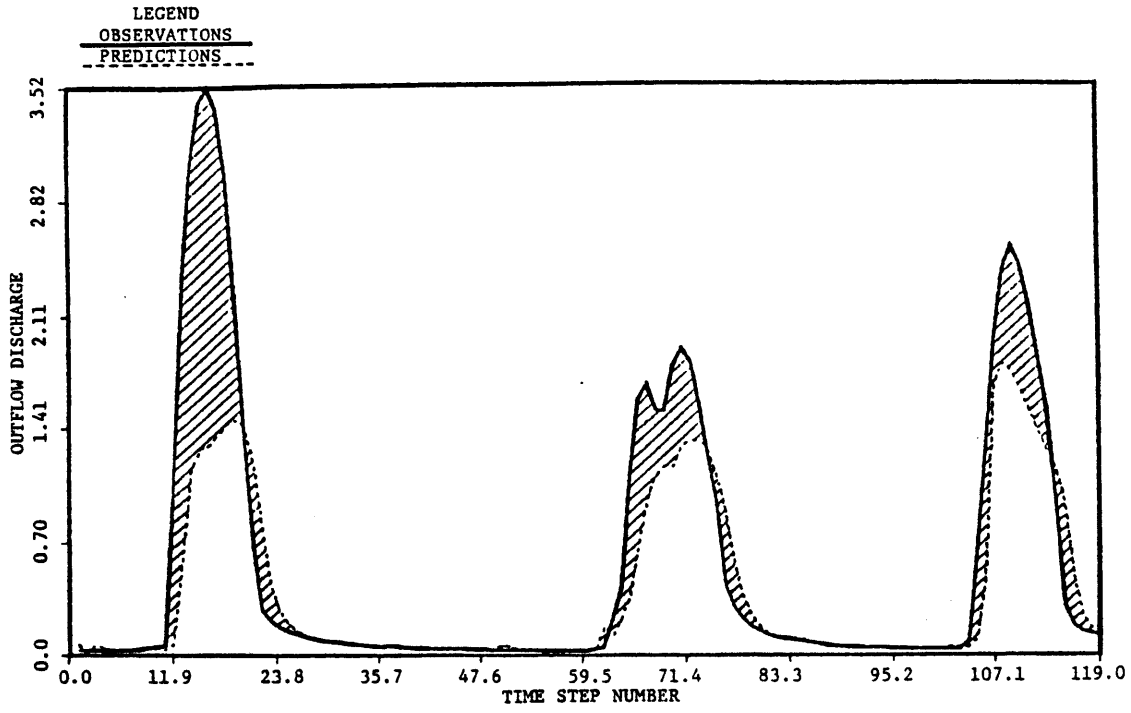

Figure 4.28 Extended Forecast of Discharge, Bird Creek, May 1960, Q-3, 6 hrs, ELFS-2

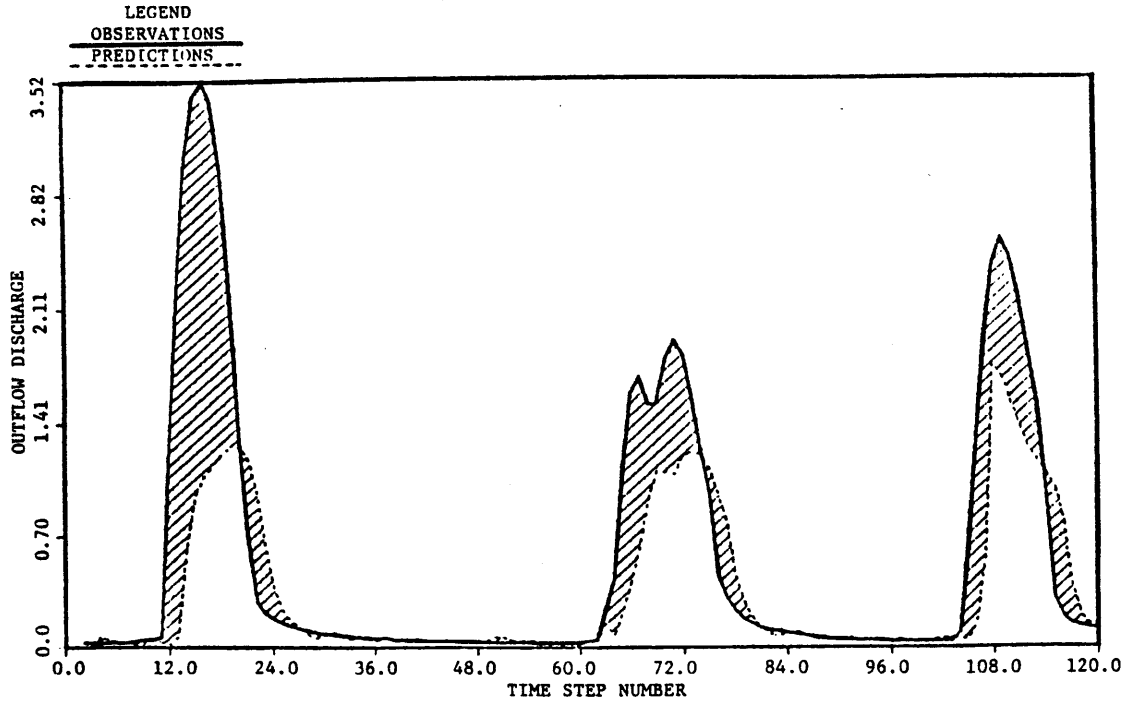

Figure 4.29 Extended Forecast of Discharge, Bird Creek, May 1960, Q-3, 12 hrs, ELFS-2

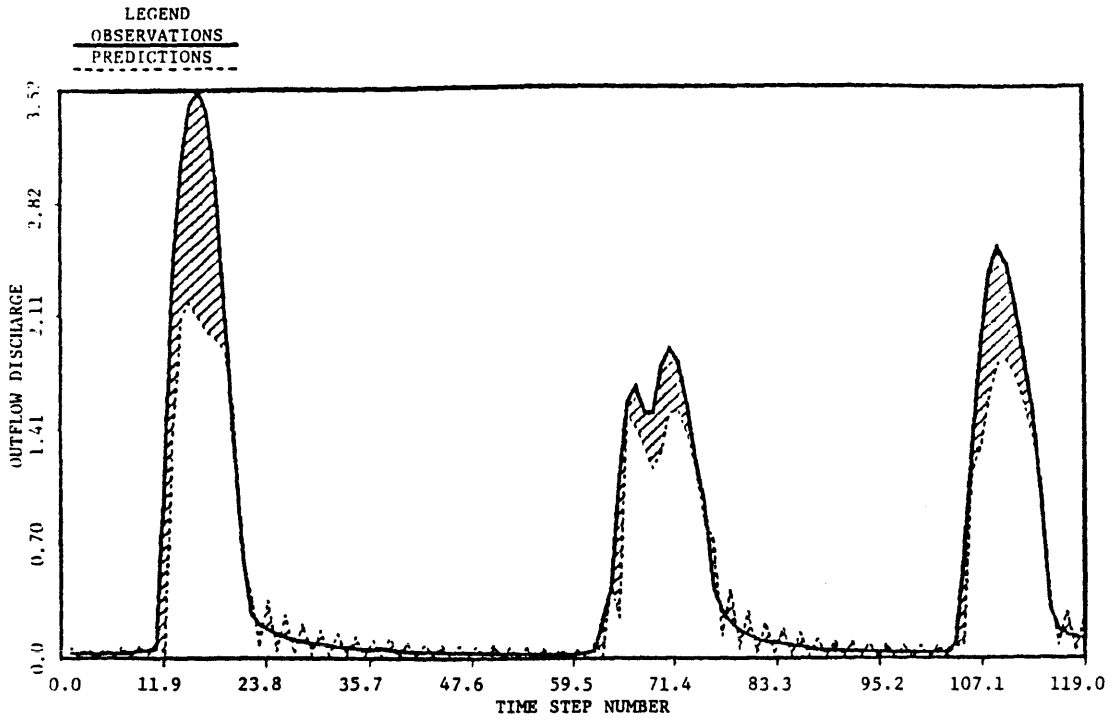

Figure 4.30 Extended Forecast of Discharge, Bird Creek, May 1960, Q-4, 6 hrs, EKF

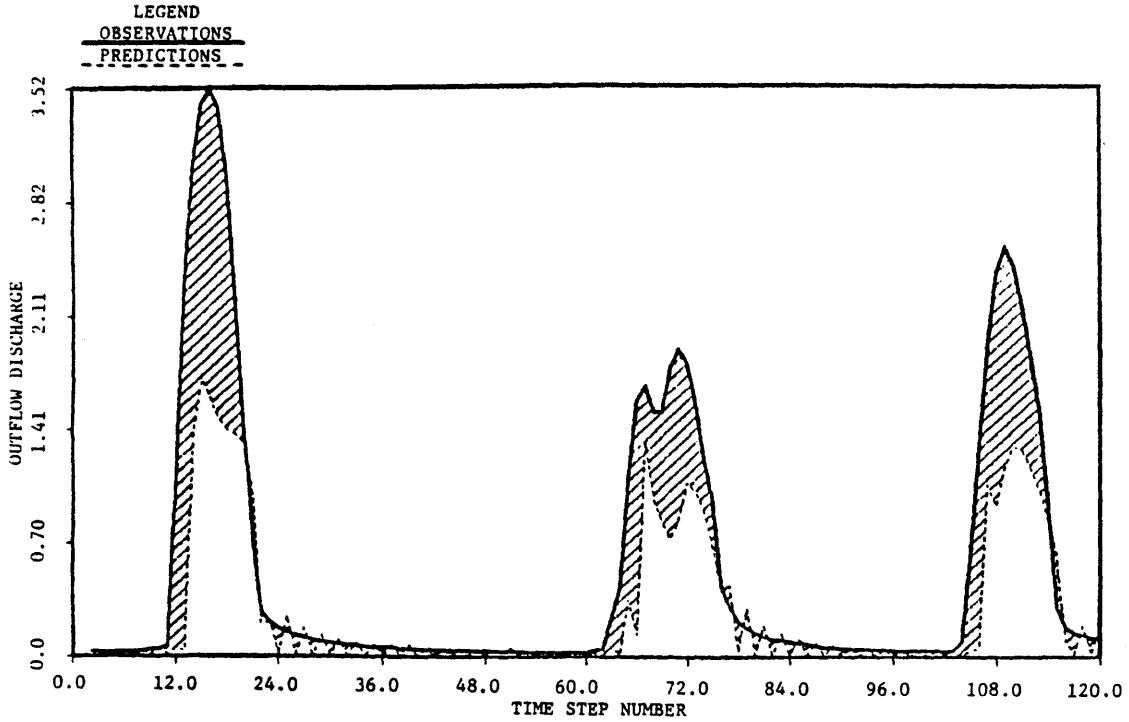

Figure 4.31 Extended Forecast of Discharge, Bird Creek, May 1960, Q-4, 12 hrs, EKF

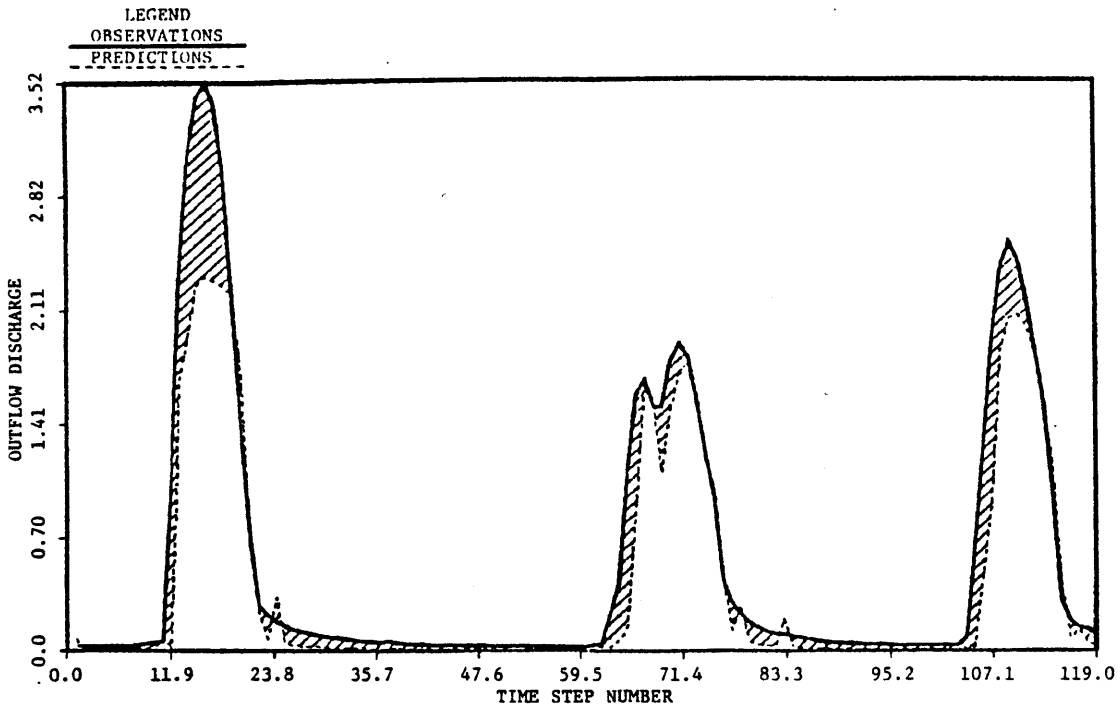

Figure 4.32 Extended Forecast of Discharge, Bird Creek, May 1960, Q-4, 6 hrs, ELFS-2

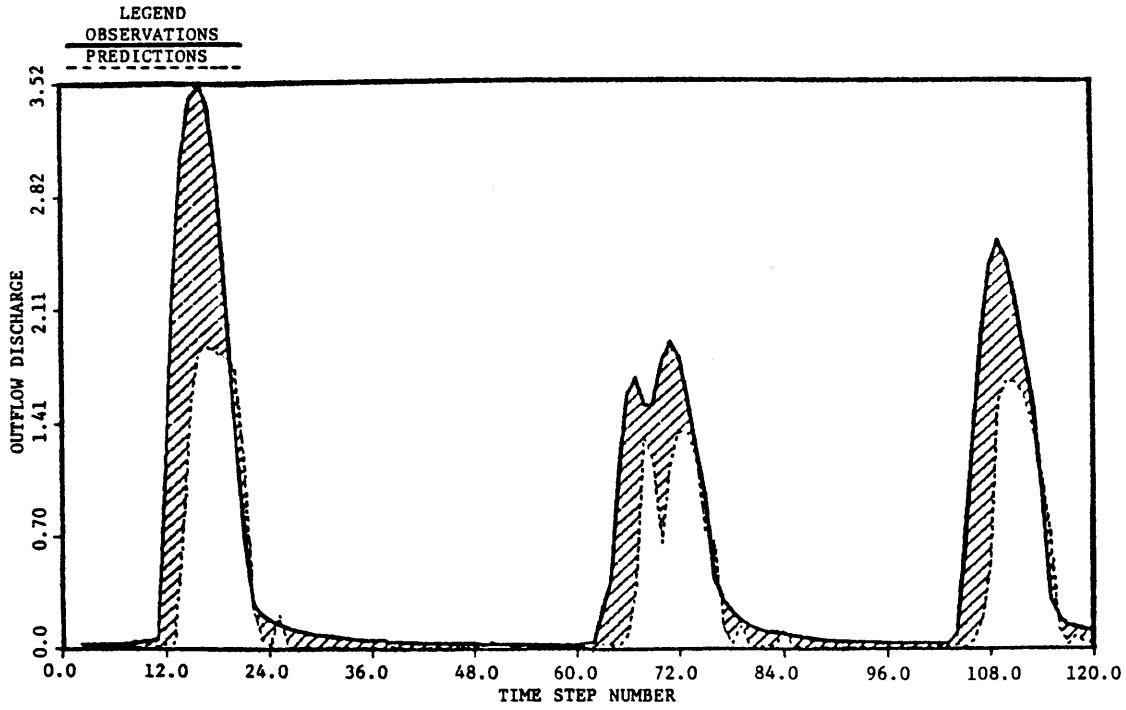

Figure 4.33 Extended Forecast of Discharge, Bird Creek, May 1960, Q-4, 12 hrs, ELFS-2

4.5 Summary

This chapter includes the results of applying the nonlinear filtering procedures and the rainfall-runoff model to a case study. It has been shown that the spectral density matrix of the system dynamics noise plays a key role on the predictions of discharge. Depending on Q, all procedures could give bad or good predictions.

The filtering procedures that include smoothing represent generally improvements over the extended Kalman filter. However, the computational time they require is considerably higher than that of the extended Kalman filter.

As should be expected, extended forecasts decrease in quality as the lead time increases, no matter what nonlinear filtering procedure is being used. Precipitation extended forecasts do not degrade with lead time, but this is due to the unrealistic assumption that the inputs are known in advance.

Chapter 5

THE ESTIMATION OF THE DYNAMICS NOISE SPECTRAL DENSITY MATRIX OF A NONLINEAR DYNAMIC SYSTEM

5.1 Introduction

The use of modern estimation techniques with dynamic systems requires the complete specification of the system parameters. In particular the applicability of nonlinear filtering procedures depends on the knowledge of the parameters of the physical system as well as the parameters that describe the system stochastic behavior. The stochastic components are usually modelled as zero mean independent Gaussian processes that appear in an additive way on the dynamic equations and on the system observation equations. The covariance matrices of these Gaussian processes must be specified by the user before any estimate of the states of the system can be obtained. The covariance matrix related to the observation equations is generally easier to obtain than the covariance matrix related to the additive noise on the dynamic equations. The noise on the observations depends on the expected accuracy of the measurements. The additive noise on the dynamic equations represent the modelling error, or the difference between reality and the model that approximates it, a harder property to quantify.

As the results of Chapter 4 suggest, the spectral density matrix of the dynamics noise plays a key role on the quality of the predictions. The emphasis in this chapter will be on describing simple and non-expensive procedures to estimate such a matrix, under the assumption that all the physical model parameters and the parameters that specify the observations covariance matrix are known.

5.2 Problem Definition

The system under consideration is described by the following equations:

$$\text{Dynamic Equations:} \qquad \frac{d}{dt}\underline{X}(t) = \underline{f}(\underline{X}(t),\underline{u}(t),t) + \underline{w}(t) \qquad (5.1)$$

$$\text{Observation Equations:} \quad \underline{Z}(t_k) = \underline{h}(\underline{X}(t_k),\underline{u}(t_k),t_k) + \underline{v}(t_k) \qquad k=0,1,2,... \qquad (5.2)$$

with $\underline{w}(t)$ and $\underline{v}(t_k)$ being the random components that account for errors in the modelling of the physical system and in the measurements. Vectors $\underline{X}$, $\underline{u}$, and $\underline{Z}$ represent the states, inputs and observations, respectively, of the physical model, and $\underline{f}$ and $\underline{h}$ are generally non-linear functions.

The processes $\underline{w}(t)$ and $\underline{v}(t_k)$ are assumed zero-mean independent Gaussian processes, independent of each other. $\underline{w}(t)$ has spectral density matrix $Q(t)$ and $\underline{v}(t_k)$ has covariance matrix $R(t_k)$,

$$\underline{w}(t) \sim N[\underline{0}, Q(t)] \tag{5.3}$$

$$\underline{v}(t_k) \sim N[\underline{0}, R(t_k)] \tag{5.4}$$

Recall from Chapter 3 that Q(t) plays an additive role in the error covariance propagation term of any of the nonlinear filters. This implies that Q(t) plays a role in the computation of the filter gain used in the updating calculations. Due to the nonlinearity of the dynamic and observation functions $\underline{f}$ and $\underline{h}$, and the subsequent linearization required by the nonlinear filters, the matrix Q(t) also affects future state estimates.

All parameters that affect functions $\underline{f}$ and $\underline{h}$ as well as the parameters of matrices $R(t_k)$ are assumed known. The problem is how to find matrices Q(t) such that overall performance of the filter is improved.

Criteria to judge improvement in performance include:

a. Minimizing the one-step predicted residuals,

b. Maximizing the likelihood of the observations, and

c. Making the behavior of the filter consistent with its expectations.

In the next section these criteria are fully explored. Given that good performance with the extended Kalman filter implies good performance with the other nonlinear filters, the procedures will be tailored to the extended Kalman filter.

5.3 Procedures to Find the Spectral Density Matrix

The first procedure is to find Q(t) such that the sum of squares of the one-step predicted residuals is minimized. This constitutes a nonlinear optimization problem, which may be defined by

$$\min_{Q} \sum_{k=1}^{N} [\underline{Z}(t_k) - \underline{h}(\hat{\underline{X}}(t_k|t_{k-1}),\underline{u}(t_k),t_k)]^T B_k \\ [\underline{Z}(t_k) - \underline{h}(\hat{\underline{X}}(t_k|t_{k-1}),\underline{u}(t_k),t_k)] \qquad (5.5)$$

where B_k represents a weighting matrix.

Finding Q(t) using this formula will require the evaluation of the derivatives of function $\underline{h}$ with respect to Q, which are not readily available. Numerical computation of these derivatives is required, which makes the use of this criteria expensive.

A second alternative consists on finding Q(t) such that the likelihood of the observations given Q(t) is maximized. If Q(t) is assumed constant in time, the problem to be solved is:

$$\max_{Q} \ \ell(\underline{Z}(t_1), \ldots, \underline{Z}(t_N)|Q) \qquad (5.6)$$

or

$$\max_{Q} \ f_Z(\underline{Z}(t_1), \ldots, \underline{Z}(t_N)|Q) \qquad (5.7)$$

where f_Z is the joint probability density function of the observations given Q.

After linearizations of the observation functions, it can be shown that this density function is asymptotically multivariable Gaussian, Abramson (1968). The criteria can then be expressed in terms of the logarithm of the likelihood function as:

$$\max_{Q} -\frac{1}{2} \sum_{k=1}^{N} \{\ell n|B_k| + \Delta\underline{Z}_k^T B_k^{-1} \Delta\underline{Z}_k\} \tag{5.8}$$

where $|B_k|$ represents the determinant of matrix B_k, $\Delta\underline{Z}_k$ represents the one-step predicted residuals and B_k denotes the covariance matrix of the residuals,

$$B_k = R'(t_k) + H_k(\cdot,\cdot,\cdot)P(t_k|t_{k-1})H_k(\cdot,\cdot,\cdot)^T \tag{5.9}$$

The use of this criteria requires the calculation of the derivatives of B_k and $\Delta\underline{Z}_k$ with respect to the unknown Q, and again these are not readily available. Numerical calculation of such derivatives may be obtained at a high cost. These derivatives may also be approximated. Simple approximations will be pursued in the next section. Notice that the second term in Equation (5.8) is a weighted sum of residuals over the N time steps.

A third idea was introduced by Jazwinski (1969) to overcome the problem of filter divergence often found in filtering applications. The object is to estimate Q(t) such that the predictions are consistent with their expectations. The derivation is based on the discrete

version of the extended Kalman filter error covariance propagation, i.e., with Equation (3.13) replaced by:

$$P(t_{k+1}|t_k) = \Phi_k(t_{k+1},t_k)\, P(t_k|t_k)\, \Phi_k^T(t_{k+1},t_k) + \overline{Q}_k \qquad (5.10)$$

where

$$\overline{Q}_k = \int_{t_k}^{t_{k+1}} \Phi_k(t_{k+1},\tau)\, Q'(\tau)\, \Phi_k^T(t_{k+1},\tau)\, d\tau \qquad (5.11)$$

with $Q'(t)$ being the input dependent spectral density matrix after linearizations, and with $\Phi_k(t_{k+1},\tau)$ being the system transition matrix between times τ and t_{k+1}, which results from the solution of,

$$\frac{d\Phi_k(t,\tau)}{dt} = F\left(\underline{\hat{X}}(t|t_k),\ \underline{u}(t),\ t\right) \Phi_k(t,\tau) \qquad (5.12)$$

with initial condition $\Phi_k(\tau,\tau) = I$, where I is the identity matrix.

Define the ℓ-steps ahead predicted residuals by

$$\Delta\underline{Z}_{k+\ell} = \underline{Z}(t_{k+\ell}) - E\{\underline{Z}(t_{k+\ell})|\underline{Z}(t_1),\ \ldots,\ \underline{Z}(t_k)\} \qquad (5.13)$$

i.e., the difference between the actual and predicted observations using information up to ℓ-time steps in the past. Then using the linearized version of the dynamic and observation equations, it is easy to show that the ℓ-steps ahead predicted residuals are, Jazwinski (1969),

$$\Delta \underline{Z}_{k+\ell} = H_{k+\ell}\, \Phi_k(t_{k+\ell}, t_k)\left(\underline{X}(t_k) - \hat{\underline{X}}(t_k \mid t_k)\right)$$

$$+ H_{k+\ell} \sum_{i=1}^{\ell} \Phi_{k+i}(t_{k+\ell}, t_{k+i})\, \overline{\underline{w}}_{k+i-1} + \underline{v}'(t_{k+\ell}) \qquad (5.14)$$

where $\overline{\underline{w}}_{k+\ell-1}$ is the discrete dynamics noise in the interval $[t_{k+\ell-1}, t_{k+\ell})$ defined in terms of the Gaussian process $\underline{w}'(t)$ by

$$\overline{\underline{w}}_{k+\ell-1} = \int_{t_{k+\ell-1}}^{t_{k+\ell}} \Phi_{k+\ell-1}(t_{k+\ell}, \tau)\underline{w}'(\tau)d\tau \qquad (5.15)$$

From Equation (5.14) it is easy to compute the covariance matrix of the predicted residuals, i.e., for $m \geq \ell$

$$E[\Delta \underline{Z}_{k+\ell} \Delta \underline{Z}_{k+m}^T] = H_{k+\ell}\Phi_k(t_{k+\ell}, t_k)P(t_k \mid t_k)\Phi_k^T(t_{k+m}, t_k)H_{k+m}^T$$

$$+ H_{k+\ell}\left\{\sum_{i=1}^{\ell} \Phi_{k+i}(t_{k+\ell}, t_{k+i})\overline{Q}_{k+i-1}\Phi_{k+1}^T(t_{k+m}, t_{k+i})\right\}H_{k+m}^T$$

$$+ R'(t_{k+\ell})\delta_{\ell m} \qquad (5.16)$$

Q(t) is defined such that the expected covariances of the predicted residuals equals the covariance matrix obtained from the filter, i.e., it is defined by the condition:

$$E[\Delta \underline{Z}_{k+\ell} \Delta \underline{Z}_{k+m}^T] \equiv \Delta \underline{Z}_{k+\ell} \Delta \underline{Z}_{k+m}^T \qquad (5.17)$$

for $1 \leq \ell$, $m \leq M$.

Note that condition (5.17) gives a filter with time lag M since k+M observations have to occur in order to obtain the prediction at time k+1. The simple case when M is equal to one is fully developed later in this chapter.

5.4 Approximate Estimators of the Spectral Density Matrix, Q(t)

In this section approximate estimators of matrix Q(t) will be obtained using the approaches of maximum likelihood and of consistency of the residual covariance matrices.

5.4.1 Maximum Likelihood for System with Transition Matrix Non-Dependent on Q(t)

If it is assumed that Φ_k does not depend on the unknown parameters, then the derivatives of the likelihood function may be obtained recursively. Recall that Equation (5.8), for Q(t) constant in time, gives Q as the matrix that maximizes

$$L_N(\underline{Z}(t_1),\ldots,\underline{Z}(t_N)|Q) = -\frac{1}{2}\left(\sum_{k=1}^{N} \ell n|B_k| + \Delta\underline{Z}_k^T B_k^{-1} \Delta\underline{Z}_k\right) \qquad (5.18)$$

The optimal Q matrix may be obtained using Newton's method. The first order derivatives with respect to the unknowns gives

$$\frac{\partial L_N}{\partial \xi^s} = -\frac{1}{2}\left\{\sum_{k=1}^{N} \frac{\partial}{\partial \xi^s} \ell n|B_k| + \frac{\partial}{\partial \xi^s}(\Delta\underline{Z}_k^T B_k^{-1} \Delta\underline{Z}_k)\right\} \qquad (5.19)$$

where ξ^s is the s^{th} unknown of Q. If the observations linearization matrix, H_k, is also non-dependent on Q, these derivatives are

$$\frac{\partial L_N}{\partial \xi^s} = -\frac{1}{2} \sum_{k=1}^{N} \mathrm{Tr}\{(B_k^{-1} - B_k^{-1} \Delta\underline{Z}_k \Delta\underline{Z}_k^T B_k^{-1}) \frac{\partial B_k}{\partial \xi^s} - 2B_k \Delta\underline{Z}_k \frac{\partial \hat{\underline{X}}(t_k | t_{k-1})}{\partial \xi^s} H_k^T\} \quad (5.20)$$

with Tr(A) the trace of matrix A.

The shown derivatives may be obtained as

$$\frac{\partial B_k}{\partial \xi^s} = H_k \frac{\partial P(t_k | t_{k-1})}{\partial \xi^s} H_k^T \quad (5.21)$$

with $\partial P(t_k | t_{k-1})/\partial \xi^s$ satisfying the following recursive equation, Abramson (1968),

$$\frac{\partial P(t_k | t_{k-1})}{\partial \xi^s} = \Phi_{k-1}(t_k, t_{k-1})[I - K_{k-1}H_{k-1}] \frac{\partial P(t_{k-1} | t_{k-2})}{\partial \xi^s} \cdot [I - K_{k-1}H_{k-1}]^T \Phi_{k-1}(t_k, t_{k-1})^T + \frac{\partial \overline{Q}_{k-1}}{\partial \xi^s} \quad (5.22)$$

where $\overline{Q}_{k-1}$ is related to Q as in Equation (5.11).

Similarly, it is easy to show that $\partial \hat{\underline{X}}(t_k | t_{k-1})/\partial \xi^s$ satisfies the following recursive equation:

$$\frac{\partial \hat{\underline{X}}(t_k|t_{k-1})}{\partial \xi^s} = \Phi_{k-1}(t_k, t_{k-1})\{[I - K_{k-1}H_{k-1}] \frac{\partial \hat{\underline{X}}(t_{k-1}|t_{k-2})}{\partial \xi^s} +$$

$$[I - K_{k-1}H_{k-1}] \frac{\partial P(t_{k-1}|(t_{k-2})}{\partial \xi^s} [1 - K_{k-1}H_{k-1}]^T H_{k-1}^T R'(t_{k-1})^{-1} \Delta \underline{Z}_{k-1}\} \tag{5.23}$$

To compute the likelihood derivatives, Equations (5.22) and (5.23) are solved simultaneously with initial conditions

$$\frac{\partial P(t_1|t_0)}{\partial \xi^s} = \frac{\partial \overline{Q}_1}{\partial \xi^s} \tag{5.24}$$

and

$$\frac{\partial \hat{\underline{X}}(t_1|t_0)}{\partial \xi^s} = \underline{0} \tag{5.25}$$

Newton's method updates a given estimate of the unknown vector using the following iterative calculations:

$$\hat{\underline{\xi}}_j = \hat{\underline{\xi}}_{j-1} - \left(\frac{\partial^2 L_N}{\partial \xi^2}\Big|_{\hat{\underline{\xi}}_{j-1}}\right)^{-1} \frac{\partial L_N}{\partial \xi}\Big|_{\hat{\underline{\xi}}_{j-1}} \tag{5.26}$$

where $\hat{\underline{\xi}}_{j-1}$ is the current vector of unknown parameters and $(\partial^2 L_n/\partial \xi^2)$ is the matrix of the likelihood second-order derivatives. Because this matrix is not easily obtained, Abramson (1968) suggests the use of the conditional information matrix which is known to approximate for large N the negative of the second-order derivatives.

Then if the information matrix, J_N, is used, Newton's method becomes

$$\hat{\underline{\xi}}_j = \hat{\underline{\xi}}_{j-1} + J_N(\hat{\underline{\xi}}_{j-1})^{-1} \left.\frac{\partial L_N}{\partial \xi}\right|_{\hat{\underline{\xi}}_{j-1}} \tag{5.27}$$

The conditional information matrix is defined by

$$J_N(\hat{\underline{\xi}}_j) = E\{\left(\frac{\partial L_N(\underline{Z}(t_1),\ldots,\underline{Z}(t_N)\,|\,\xi_j)}{\partial \xi}\right)\left(\frac{\partial L_N(\cdot,\cdot,\cdot)}{\partial \xi}\right)^T \Big|\, \hat{\underline{\xi}}_j\}$$

Abramson (1968) showed that the (s,t) element of the above matrix is

$$J_N(\hat{\xi}_{j-1})^{st} = \frac{1}{2} \sum_{k=1}^{N} \{\mathrm{Tr}\left(B_k^{-1} \frac{\partial B_k}{\partial \xi^s} B_k^{-1} \frac{\partial B_k}{\partial \xi^t}\right) + 2\mathrm{Tr}(B_k^{-1} H_k G_{k|k-1}^{st} H_k^T)\} \tag{5.28}$$

with $G_{k|k-1}^{st}$ a matrix defined by

$$G_{k|k-1}^{st} = E\{\frac{\partial \hat{\underline{X}}(t_k\,|\,t_{k-1})}{\partial \xi^s} \cdot \frac{\partial \hat{\underline{X}}(t_k\,|\,t_{k-1})^T}{\partial \xi^t} \,|\, \hat{\xi}_{j-1}\} \tag{5.29}$$

which in turn satisfies the recursive equation,

$$G^{st}_{k|k-1} = \Phi_{k-1}\{[I - K_{k-1}H_{k-1}]G^{st}_{k-1|k-2}[I - K_{k-1}H_{k-1}]^T +$$

$$[I - K_{k-1}H_{k-1}]\frac{\partial P(t_{k-1}|t_{k-2})}{\partial \xi^s}[I - K_{k-1}H_{k-1}]^T H^T_{k-1} R'(t_{k-1})^{-1} \cdot B_{k-1} \cdot$$

$$R'(t_{k-1})^{-1} H_{k-1}[I - K_{k-1}H_{k-1}]\frac{\partial P(t_{k-1}|t_{k-1})}{\partial \xi^t}[I - K_{k-1}H_{k-1}]^T\}\Phi^T_{k-1}$$

(5.30)

with initial condition

$$G^{st}_{1|0} = 0 \tag{5.31}$$

Although the equations are recursive and appealing for computer implementation, a considerable amount of storage and computations are needed to obtain results. Computational cuts may be obtained if it is assumed that the state covariance derivatives are more important than the state mean derivatives with respect to the unknown parameters. In this case the log-likelihood function derivatives reduce to

$$\frac{\partial L_N}{\partial \xi^s} = -\frac{1}{2}\sum_{k=1}^{N} Tr\{B_k^{-1} - B_k^{-1}\Delta Z_k \Delta Z_k^T B_k^{-1})\frac{\partial B_k}{\partial \xi^s}\} \tag{5.32}$$

with the approximate conditional information matrix given by

$$J_N(\hat{\underline{\xi}}_{j-1})^{st} = \frac{1}{2} \sum_{k=1}^{N} Tr\{B_k^{-1} \frac{\partial B_k}{\partial \xi^s} B_k^{-1} \frac{\partial B_k}{\partial \xi^t}\} \quad (5.33)$$

5.4.1.1. Implementation Considerations

Computational savings are achieved by noticing that the information matrix $J_N(\hat{\underline{\xi}}_{j-1})$, is symmetric.

The discrete noise covariance derivatives $\partial \overline{Q}_k / \partial \xi^s$ are not easy to obtain because they involve the computation of an integral whose integrand $(\Phi_k(t_{k+1},\tau))$ is only numerically obtainable. If the variations of Φ_k on the interval (t_k,t_{k+1}) are small, then $\overline{Q}_k$ may be approximated by

$$\overline{Q}_k \simeq \hat{\Phi}_k(t_k) Q (t_{k+1} - t_k) \hat{\Phi}_k^T(t_k) \quad (5.34)$$

where $\hat{\Phi}_k(t_k)$ is the transition matrix associated with the beginning of the interval, i.e.,

$$\hat{\Phi}_k(t_k) = \exp\{F(\hat{\underline{X}}(t_k|t_k), \underline{u}(t_k), t_k)\} \quad (5.35)$$

This approximation allows an easy computation of the discrete noise covariance derivatives,

$$\frac{\partial \overline{Q}_k}{\partial \xi^s} = \hat{\Phi}_k(t_k) \frac{\partial Q}{\partial \xi^s} (t_{k+1} - t_k) \hat{\Phi}_k(t_k)^T \tag{5.36}$$

where $\partial Q/\partial \xi^s$ is a matrix of zeros except for the location correspondent to the s^{th} unknown, where the value is one.

5.4.1.2 An Approximate Maximum Likelihood Solution Which Uses Second Order Likelihood Derivatives

If it can be further assumed that the most important contribution of the derivatives of the one-step residuals covariance comes from the term involving matrix Q, then

$$\frac{\partial B_k}{\partial \xi^s} = H_k \hat{\Phi}_k(t_k) \frac{\partial Q}{\partial \xi^s} (t_{t+1} - t_k) \hat{\Phi}_k(t_k)^T H_k^T \tag{5.37}$$

which gives the likelihood function derivatives as

$$\frac{\partial L_N}{\partial \xi^s} = -\frac{1}{2} \sum_{k=1}^{N} Tr\{(B_k^{-1} - B_k^{-1} \Delta Z_k \Delta Z_k^T B_k^{-1}) \cdot H_k \hat{\Phi}_k(t_k) \frac{\partial Q}{\partial \xi^s} (t_{k+1} - t_k) \hat{\Phi}_k(t_k)^T H_k^T\} \tag{5.38}$$

From this expression it is easy to compute the second order derivatives, they are:

$$\frac{\partial^2 L_N}{\partial \xi^t \partial \xi^s} = -\frac{1}{2} \sum_{k=1}^{N} \mathrm{Tr}\left\{\frac{\partial}{\partial \xi^t}\left(B_k^{-1} - B_k^{-1}\Delta Z_k \Delta Z_k^T B_k^{-1}\right) \frac{\partial B_k}{\partial \xi^s}\right\} \tag{5.39}$$

but $\partial B_k^{-1}/\partial \xi^t = -B_k^{-1}\partial B_k/\partial \xi^t B_k^{-1}$, and then

$$\frac{\partial^2 L_N}{\partial \xi^t \partial \xi^s} = \frac{1}{2} \sum_{k=1}^{N} \mathrm{Tr}\left\{B_k^{-1} \frac{\partial B_k}{\partial \xi^t} B_k^{-1} \frac{\partial B_k}{\partial \xi^s} - B_k^{-1}\Delta Z_k \Delta Z_k^T B_k^{-1} \frac{\partial B_k}{\partial \xi^t} B_k^{-1} \frac{\partial B_k}{\partial \xi^s}\right.$$

$$\left. - B_k^{-1} \frac{\partial B_k}{\partial \xi^t} B_k^{-1}\Delta Z_k \Delta Z_k^T B_k^{-1} \frac{\partial B_k}{\partial \xi^s}\right\} \tag{5.40}$$

5.4.1.3 An Explicit Sub-Optimal and Simple Estimate

The following derivation follows Abramson (1968). Assume that the state covariance derivatives are more important than the state mean derivatives with respect to the unknown parameters. In this case the likelihood function is given by Equation (5.32) or

$$\frac{\partial L_N}{\partial \xi^s} = -\frac{1}{2} \sum_{k=1}^{N} \mathrm{Tr}\left\{\Delta B_k^{-1} H_k \frac{\partial P(t_k | t_{k-1})}{\partial \xi^s} H_k^T\right\} \tag{5.41}$$

where $\Delta B_k^{-1} = B_k^{-1} - B_k^{-1}\Delta Z_k \Delta Z_k B_k^{-1}$. It can be easily shown that Equation (5.41) is

$$\frac{\partial L_N}{\partial \xi^s} = -\frac{1}{2} \sum_{k=1}^{N} \mathrm{Tr}\left\{H_k^T \Delta B_k^{-1} H_k \frac{\partial P(t_k | t_{k-1})}{\partial \xi^s}\right\} \tag{5.42}$$

But

$$H_k^T \Delta B_k^{-1} H_k = P(t_k|t_{k-1})^{-1}[P(t_k|t_{k-1}) - P(t_k|t_k) - \Delta\underline{X}_k \Delta\underline{X}_k^T]\, P(t_k|t_{k-1})^{-1} \tag{5.43}$$

where $\Delta\underline{X}_k = \hat{\underline{X}}(t_k|t_k) - \hat{\underline{X}}(t_k|t_{k-1})$.

Then the likelihood function derivatives are,

$$\frac{\partial L_N}{\partial \xi^s} = -\frac{1}{2} \sum_{k=1}^{N} \mathrm{Tr}\{P(t_k|t_{k-1})^{-1}[P(t_k|t_{k-1}) - P(t_k|t_k) - \Delta\underline{X}_k \Delta\underline{X}_k^T] \cdot P(t_k|t_{k-1})^{-1} \frac{\partial P(t_k|t_{k-1})}{\partial \xi^s}\} \tag{5.44}$$

If $\partial P(t_k|t_{k-1})/\partial \xi^s$ is given by the term including Q, and if $t_k - t_{k-1} = 1$, then,

$$\frac{\partial L_N}{\partial \xi^s} = -\frac{1}{2} \sum_{k=1}^{N} \mathrm{Tr}\{P(t_k|t_{k-1})^{-1}[\hat{\Phi}_{k-1}(t_{k-1})P(t_{k-1}|t_{k-1})\hat{\Phi}_{k-1}(t_{k-1})^T + \hat{\Phi}_{k-1}(t_{k-1})Q\hat{\Phi}_{k-1}(t_{k-1})^T - P(t_k|t_k) - \Delta\underline{X}_k \Delta\underline{X}_k^T]P(t_k|t_{k-1})^{-1} \cdot \hat{\Phi}_{k-1}(t_{k-1}) \frac{\partial Q}{\partial \xi^s} \hat{\Phi}_{k-1}^T(t_{k-1})\} \tag{5.45}$$

or

$$\frac{\partial L_N}{\partial \xi^s} = -\frac{1}{2} \sum_{k=1}^{N} [\hat{\Phi}_{k-1}^T(t_{k-1}) P(t_k|t_{k-1})^{-1} \{\hat{\Phi}_{k-1}(t_{k-1}) Q \hat{\Phi}_{k-1}(t_{k-1})^T$$

$$- \Delta\underline{X}_k \Delta\underline{X}_k^T - P(t_k|t_k) + \hat{\Phi}_{k-1}(t_{k-1}) P(t_{k-1}|t_{k-1}) \hat{\Phi}_{k-1}(t_{k-1})^T\}$$

$$\cdot P(t_k|t_{k-1})^{-1} \hat{\Phi}_{k-1}(t_{k-1})]^{rt} \qquad (5.46)$$

with (r,t) denoting the location of the s^{th} unknown of Q.

If it is further assumed that $\hat{\Phi}_{k-1}(t_{k-1})$ and $P(t_k|t_{k-1})$ are approximately constant over time, then $\partial L_N/\partial \xi^s = 0$ is satisfied when

$$\sum_{k=1}^{N} \{\hat{\Phi}_{k-1}(t_{k-1}) Q \hat{\Phi}_{k-1}(t_{k-1})^T - \Delta\underline{X}_k \Delta\underline{X}_k^T - P(t_k|t_k)$$

$$+ \hat{\Phi}_{k-1}(t_{k-1}) P(t_{k-1}|t_{k-1}) \hat{\Phi}_{k-1}(t_{k-1})^T\} = 0 \qquad (5.47)$$

from which the following estimator is obtained for the (r,t) element of Q, after j iterations:

$$\hat{Q}_j^{rt} = \frac{1}{N} \{ \sum_{k=1}^{N} \hat{\Phi}_{k-1}(t_{k-1})^{-1} [\Delta\underline{X}_k \Delta\underline{X}_k^T + P(t_k|t_k) - P(t_k|t_{k-1})$$

$$+ \hat{\Phi}_{k-1}(t_{k-1}) \hat{Q}_{j-1} \hat{\Phi}_{k-1}(t_{k-1})^T] (\hat{\Phi}_{k-1}(t_{k-1})^{-1})^T\}^{rt} \qquad (5.48)$$

5.4.2 Estimation of Q(t) from Consistency of One-Step Ahead Residuals

Jazwinski's estimator becomes applicable in real time if Q(t) is constant over two time steps. In this case the consistency condition to be achieved is:

$$E[\Delta\underline{Z}_{k+1} \cdot \Delta\underline{Z}_{k+1}^T] = \Delta\underline{Z}_{k+1} \cdot \Delta\underline{Z}_{k+1}^T \tag{5.49}$$

The expectation of the left-hand side is

$$E[\Delta\underline{Z}_{k+1}\Delta\underline{Z}_{k+1}^T] = H_{k+1}\Phi_k(t_{k+1},t_k)P(t_k|t_k)\Phi_k^T(t_{k+1},t_k)H_{k+1}^T + H_{k+1}\overline{Q}_k H_{k+1}^T + R'(t_{k+1}) \tag{5.50}$$

If $\overline{Q}_k$ is approximated using the transition matrix at the beginning of the interval, condition (5.49) becomes,

$$H_{k+1}\hat{\Phi}_k(t_k)Q(t_k)(t_{k+1} - t_k)\hat{\Phi}_k^T(t_k)\, H_{k+1}^T = \Delta\underline{Z}_{k+1}\Delta\underline{Z}_{k+1}^T - H_{k+1}\hat{\Phi}_k(t_k)P(t_k|t_k)\hat{\Phi}_k(t_k)^T H_{k+1}^T - R(t_{k+1}) \tag{5.51}$$

If $Q(t_{k+1}) \approx Q(t_k)$, this equation provides an estimate to be used the next time step.

If the Q matrix is constant over say L time steps, a smoothed estimate of Q(t) may be obtained solving:

$$\sum_{k=1}^{L} H_{k+1}\hat{\Phi}_k(t_k)Q(t)(t_{k+1} - t_k)\hat{\Phi}_k^T(t_k)H_{k+1}^T = \sum_{k=1}^{L} \Delta\underline{Z}_{k+1}\Delta\underline{Z}_{k+1}^T - \sum_{k+1}^{L} \left(H_{k+1}\hat{\Phi}_k(t_k)P(t_k|t_k)\hat{\Phi}(t_k)^T H_{k+1}^T + R'(t_{k+1})\right) \tag{5.52}$$

In general, the linear Equations (5.51) and (5.52) are not easily solvable for Q, because typically there are more unknowns than equa-

tions. This means not all the elements of Q(t) can be estimated but only as many as the number of independent conditions.

If estimates of Q(t) are obtained adaptively, i.e., changing the matrix every time step, one basically obtains the MISP (mutually interactive state/parameter estimation) estimator as described by O'Connell (1980).

If more elements of Q(t) than the ones obtained from Equations (5.51) or (5.52) are necessary, more consistency conditions must be introduced.

5.4.2.1 Further Conditions on Residuals Useful in Estimating Q

Kitanidis and Bras (1978) used the previously explained consistency of the lag zero covariance of the residuals as well as the consistency on the higher lags correlation of the residuals to estimate a constant in time and diagonal $\overline{Q}$ (in discrete form). The condition they employed is the well known whiteness of the residuals if the filter is optimal. In this section it will be shown how to use such conditions to obtain more equations from which elements of Q (in continuous form) may be obtained.

The whiteness of the residuals condition states that if the filter is optimal the residual correlations of lags other than zero should be zero. The expected correlation matrices are easily computed using Equation (5.14). They are defined by

$$C_i(k) = E[\Delta\underline{Z}_k \Delta\underline{Z}_{k-i}^T] \tag{5.53}$$

These expectations are, Kitanidis and Bras (1978):

$$\begin{aligned} C_1(k) &= H_k \hat{\Phi}_{k-1}[P(t_{k-1}|t_{k-2})H_{k-1}^T - K_{k-1}B_{k-1}] \\ &\vdots \\ C_i(k) &= H_k \hat{\Phi}_{k-1}[I - K_{k-1}H_{k-1}]\hat{\Phi}_{k-2}[I - K_{k-2}H_{k-2}] \cdots \\ &\quad \cdot \hat{\Phi}_{k-i}[P(t_{k-i}|t_{k-i-1})H_{k-i}^T - K_{k-i}B_{k-i}] \end{aligned} \tag{5.55}$$

where B_k denotes the covariance matrix of the residuals.

The whiteness condition is satisfied if for all i:

$$P(t_{k-i}|t_{k-i-1})H_{k-i}^T - K_{k-i}B_{k-i} = 0 \tag{5.56}$$

Premultiplying by H_{k-i} and expanding $P(t_{k-i}|t_{k-i-1})$ gives the necessary condition:

$$\begin{aligned} &H_{k-i}\hat{\Phi}_{k-i-1}(t_{k-i-1})P(t_{k-i-1}|t_{k-i-1})\hat{\Phi}_{k-i-1}(t_{k-i-1})^T H_{k-i}^T \\ &+ H_{k-i}\hat{\Phi}_{k-i-1}(t_{k-i-1})Q(t_k)\hat{\Phi}_{k-i-1}(t_{k-i-1})^T H_{k-i}^T - H_{k-i}K_{k-i}B_{k-i} = 0 \end{aligned} \tag{5.57}$$

If B_{k-i} is assumed given from lag zero conditions, these equations provide the following additional conditions:

$$H_{k-i}\hat{\Phi}_{k-i-1}(t_{k-i-1})Q(t_k)\hat{\Phi}_{k-i-1}(t_{k-i-1})^T H_{k-i}^T = H_{k-i}K_{k-i}\underline{\Delta Z}_{k-i}\underline{\Delta Z}_{k-i}^T$$
$$- H_{k-i}\hat{\Phi}_{k-i-1}(t_{k-i-1})P(t_{k-i-1}\,|\,t_{k-i-1})\hat{\Phi}_{k-i-1}(t_{k-i-1})^T H_{k-i}^T \tag{5.58}$$

for all i.

If applied for say L lags, then the updating of the Q matrix are made every L time steps, with smoothed conditions (5.58) according to the number of equations over the period of L time steps, i.e., L lag-0 equations, L-1 lag-1 equations, and so on.

5.5 Summary

The problem of estimating the spectral noise covariance matrix of a nonlinear stochastic dynamic system has been reviewed. The problem is a nonlinear optimization problem generally solved exactly by numerical methods. Simple approximations based on the maximum likelihood approach and on the consistency of the filter residuals have been presented. Results of applying these procedures to estimate the spectral density matrix of the rainfall-runoff model are given in the next chapter.

Chapter 6

PRACTICAL ESTIMATION OF THE DYNAMICS NOISE SPECTRAL DENSITY MATRIX

6.1 Introduction

The results of applying the spectral density matrix estimation techniques to the rainfall-runoff model are presented in this chapter. One step ahead predictions were obtained for the Bird Creek basin in Oklahoma, using the extended Kalman filter for the month of May 1960.

The physical model parameters were those of Table 4.2, with the observations noise covariance matrix characterized as in Table 4.5. The covariance matrix of the inputs, $Q_u(t)$, was assumed, as in Chapter 4, equal to zero; so that the spectral density matrix for the linearized system equals $Q(t)$.

All predictions were obtained from the same set of initial state mean and standard deviations. The values of such conditions were the same used in extended forecasting in Chapter 4.

6.2 Approximate Maximum Likelihood Results

A constant in time and diagonal spectral density matrix Q was found using the approximate maximum likelihood procedure of Chapter 5. This approximate estimator main assumptions are that the transition matrix, Φ_k, and the linearization matrix of the observations, H_k, both have near zero derivatives with respect to the unknown elements of Q. It is further assumed that predicted error covariance

derivatives are more important than predicted state mean derivatives, and that the most important contribution to the predicted error covariance derivatives comes from the derivatives of the discrete dynamics noise covariance matrix. Under these assumptions the first and second order likelihood derivatives are given by Equations (5.38) and (5.40).

The estimates of the matrix Q were found using Newton's method, i.e., Equation (5.26). Not only second order derivatives but also the conditional information matrix (Equation (5.33)) was used to update the estimates. The estimator was calculated from two different sets of initial conditions: one which is the best matrix Q in Chapter 4, and the other which gave the worst results in Chapter 4; i.e., Q matrices of levels 4 and 0, respectively.

Lower and upper bounds were imposed on the estimates. If the approximate procedure gave negative standard deviations, a value of 10^{-5} was used. It was found that if no upper bound is employed, the procedure often gives unrealistically high standard deviations which when used in the next iteration lead to numerical problems in the integration of the differential equations of the error covariance of the states. The upper bounds were obtained by trial and error by studying the magnitudes of the states of the rainfall-runoff model.

The initial spectral density standard deviations and the upper bounds for each state are given in Table 6.1.

Table 6.1

Initial Spectral Density Standard Deviations and Upper Bounds

State	Q-Level 0	Q-Level 4	Upper Bounds
X_p	2	10	100
X_1	10^{-7}	10^{-1}	60
X_2	10^{-4}	10^{-2}	20
X_3	0.05	5	80
X_4	0.0187	1.87	80
X_5	0.0682	6.82	40
X_6	0.075	7.5	100
S_1	0.70	1	50
S_2	0.17	1.7	50
S_3	0.17	0.17	50

Given that each iteration requires considerable amount of computational time (around 10 CPU minutes for a month of data), a maximum of 25 iterations was allowed. This implies that convergence may not be achieved. The estimate was defined by the spectral density matrix, giving the highest log-likelihood value during the 25 iterations. Since bounds are being used it is possible to fail to have improvement in the log-likelihood value from iteration to iteration. However, higher log-likelihood values than those corresponding to the initial conditions were always found.

Table 6.2 includes the estimated values of the Q matrix under different initial conditions. This Table also includes the number of data points used in the estimation, the mechanism used to iterate with Newton's method and the number of iterations required to obtain the estimates.

Tables 6.3, 6.4, and 6.5 summarize respectively the residual statistics, normalized residual statistics and least squares indices for discharge predictions obtained from Q matrices estimated from a month (124 points) of data; i.e., for Q of levels 6, 7, 8, and 9. Table 6.5 also includes the log-likelihood values for the period.

As is shown the approximate maximum likelihood procedure improves the log-likelihood and the overall quality of the predictions. Better predictions were found if the conditional information matrix is used in Newton's method. In this case the results are excellent independently of the initial condition and with similar convergent values, (see Table 6.2 for Q of levels 6 and 8).

Table 6.2

Approximate Maximum Likelihood Spectral Density Standard Deviations

State	Q-Level 6	7	8	9	10	11	12	13
X_p	100	100	100	100	100	100	100	100
X_1	60	10^{-5}	60	10^{-5}	10^{-5}	60	10^{-5}	10^{-5}
X_2	16.46	10^{-5}	20	20	10^{-5}	10^{-5}	17.9	20
X_3	10^{-5}	80	10^{-5}	10^{-5}	10^{-5}	80	80	80
X_4	10^{-5}	10^{-5}	10^{-5}	80	80	10^{-5}	10^{-5}	10^{-5}
X_5	40	40	40	40	10^{-5}	40	36	40
X_6	10^{-5}	10^{-5}	10^{-5}	100	100	100	100	10^{-5}
S_1	17.97	0.79	13.2	10^{-5}	1.58	5.9	0.54	3.75
S_2	10^{-5}	4.84	10^{-5}	9.9	1.19	10^{-5}	10^{-5}	10^{-5}
S_3	1.31	10^{-5}	0.71	10^{-5}	1.45	2.47	0.76	10^{-5}
Initial Q	4	4	0	0	4	0	4	0
Data Points	124	124	124	124	40	40	84	84
Second Corrections	J	∂^2	J	∂^2	J	J	J	J
Iterations	15	12	16	3	4	3	13	16

∂^2 Second order derivatives
J Conditonal information matrix

Table 6.3

Discharge Residuals Statistics for Q Matrices Obtained by Approximate Maximum Likelihood, 124 Data Points

Q-Level	Second Corrections	Mean	Variation Coefficient	Skewness	Autocorrelations Lag-1	Lag-2	Lag-3	Lag-4
4	Reference	0.117	2.74	2.31	0.70	0.68	0.41	0.33
6	J	-0.120	-3.08	0.24	0.43	-0.17	-0.13	0.06
7	∂^2	0.011	28.6	0.40	-0.22	0.59	-0.01	0.21
0	Reference	0.344	1.94	2.11	0.94	0.79	0.59	0.38
8	J	-0.008	-24.5	0.72	0.32	-0.24	-0.11	0.20
9	∂^2	-0.056	-8.0	-2.1	-0.20	0.12	0.19	-0.05

∂^2 Second order derivatives
J Conditional information matrix

Table 6.4

Discharge Normalized Residuals Statistics for Q Matrices Obtained by Approximate Maximum Likelihood, 124 Data Points

Q-Level	Second Corrections	Mean	Variation Coefficient	Skewness	Autocorrelations Lag-1	Lag-2	Lag-3	Lag-4
4	Reference	0.291	3.27	1.62	0.56	0.68	0.35	0.38
6	J	0.021	8.21	1.37	0.45	-0.08	0.05	0.24
7	∂^2	-0.206	-5.50	-0.13	-0.39	0.60	-0.12	0.25
0	Reference	1.150	1.74	1.49	0.92	0.78	0.61	0.43
8	J	-0.026	-13.92	-0.32	0.37	-0.26	-0.14	0.19
9	∂^2	-0.76	-3.10	-1.60	-0.10	0.10	0.19	-0.05

$\partial 2$ Second order derivatives
J Conditional information matrix

Table 6.5
Discharge Least Squares Indices and Model Log-Likelihood for Q Matrices Obtained by Approximate Maximum Likelihood, 124 Data Points

Q-Level	Second Corrections	Efficiency	Determination	Persistence	Extrapolation	Log Likelihood
4	Reference	0.85	0.92	-0.55	-2.73	-1104.8
6	J	0.96	0.96	0.59	0.00	- 683.2
7	∂^2	0.87	0.87	-0.37	-2.30	- 547.8
0	Reference	0.27	0.80	-6.51	-17.10	-1600.5
8	J	0.94	0.95	0.44	-0.36	- 615.3
9	∂^2	0.73	0.77	-1.71	-5.52	- 760.2

∂^2 Second order derivatives
J Conditional information matrix

Figures 6.1, 6.2, and 6.3 show the discharge lead-one predictions for Q matrices of levels 4, 6, and 7. Notice that although Q of level 7 had a larger likelihood, Q of level 6 gives a better looking hydrograph and hence better least squares indices.

Figures 6.4, 6.5, and 6.6 show the lead-one discharge predictions for Q matrices of levels 0, 8, and 9. Notice the improvement obtained by using the Q matrix from the maximum likelihood procedure.

6.2.1 Sensitivity of the Estimation on the Number of Data Points

In an effort to study the sensitivity of the approximate maximum likelihood method, the procedure was utilized with variable amounts of information. The matrix Q was estimated using 40 and 84 data points from the beginning of May 1960, which correspond respectively to using information of the first and first two discharge peaks on the month.

The estimation was made using the conditional information matrix in Newton's method. The two initial conditions of Table 6.1 were considered. The final estimates (matrices Q of levels 10, 11, 12, and 13), and the number of iterations necessary to obtain them are given in Table 6.2. As is observed in this Table, the initial condition has an effect on the final estimate for the short data set. As the number of data points increases, the effect of the initial condition tends to diminish, with the effect practically disappearing if the whole month is employed.

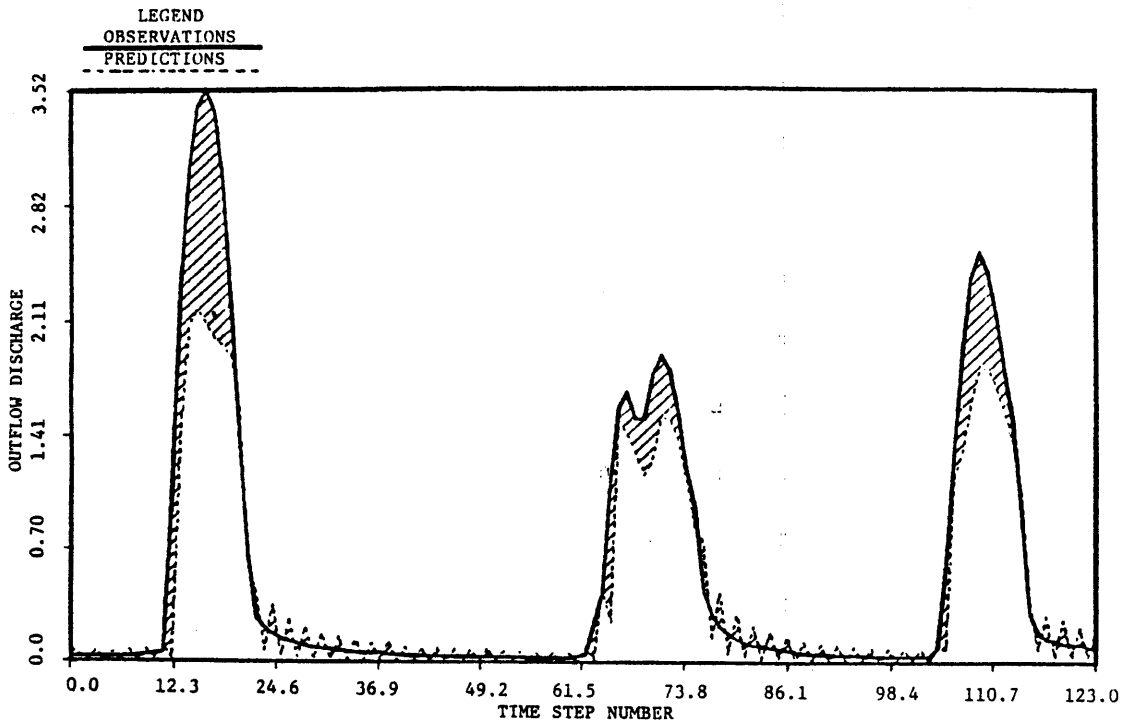

Figure 6.1 Stochastic Prediction of Discharge, Bird Creek, May 1960, EKF, Q-4

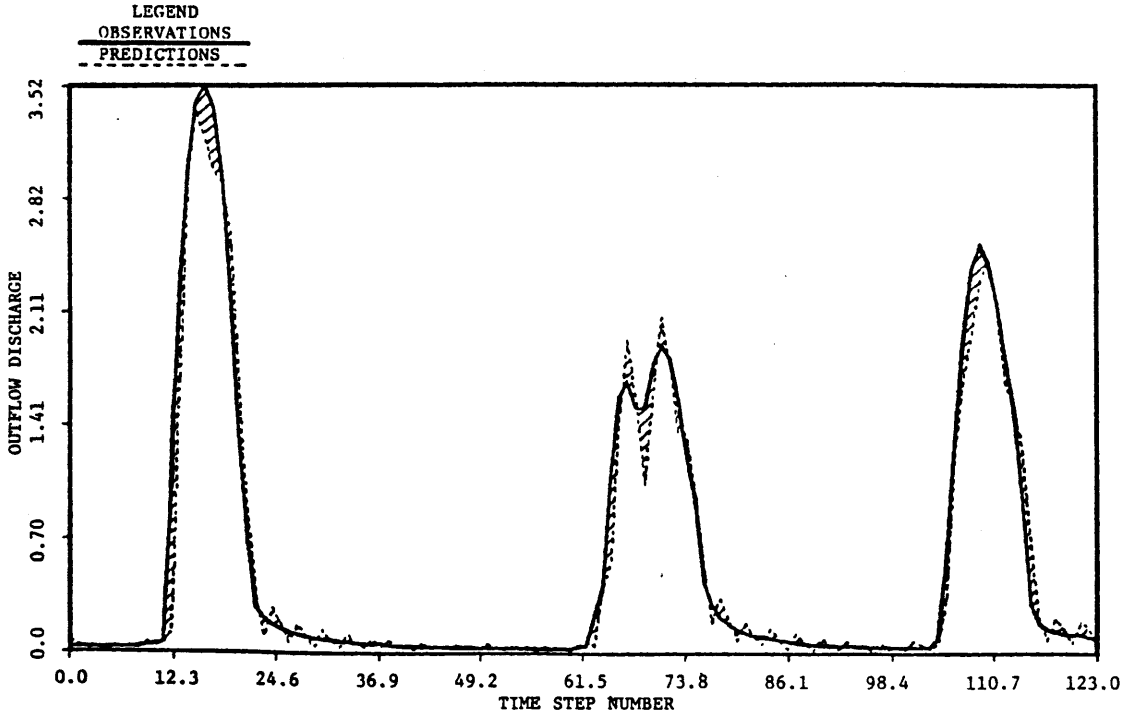

Figure 6.2 Stochastic Prediction of Discharge, Bird Creek, May 1960, EKF, Q-6

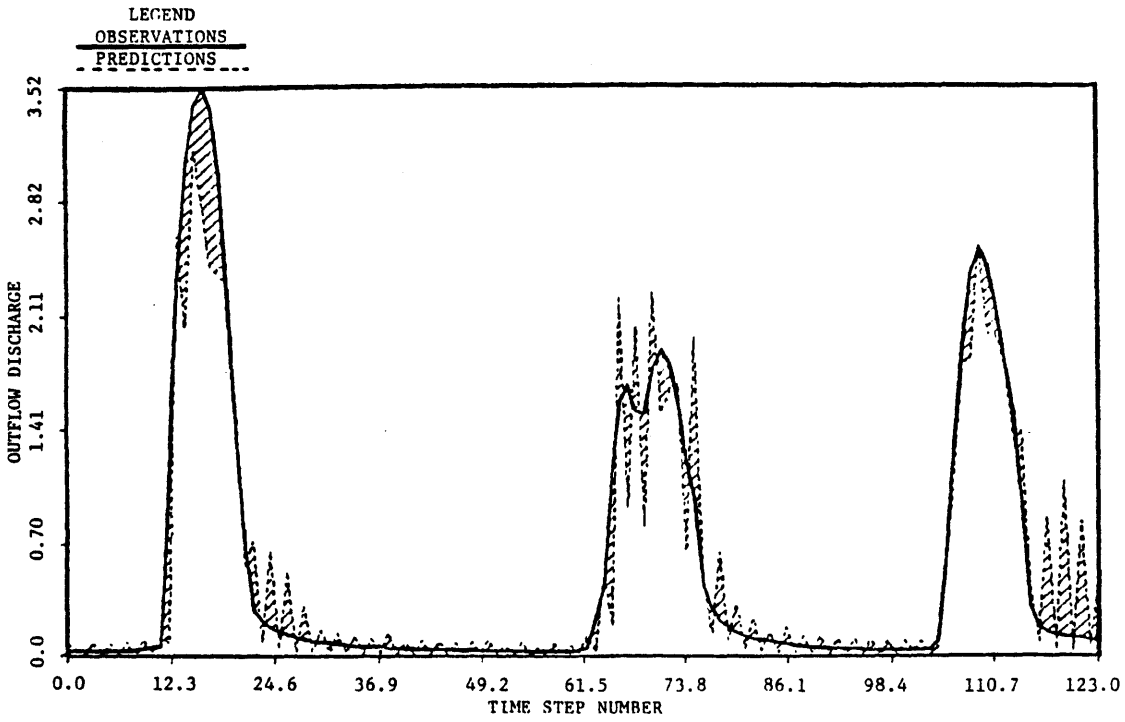

Figure 6.3 Stochastic Prediction of Discharge, Bird Creek, May 1960, EKF, Q-7

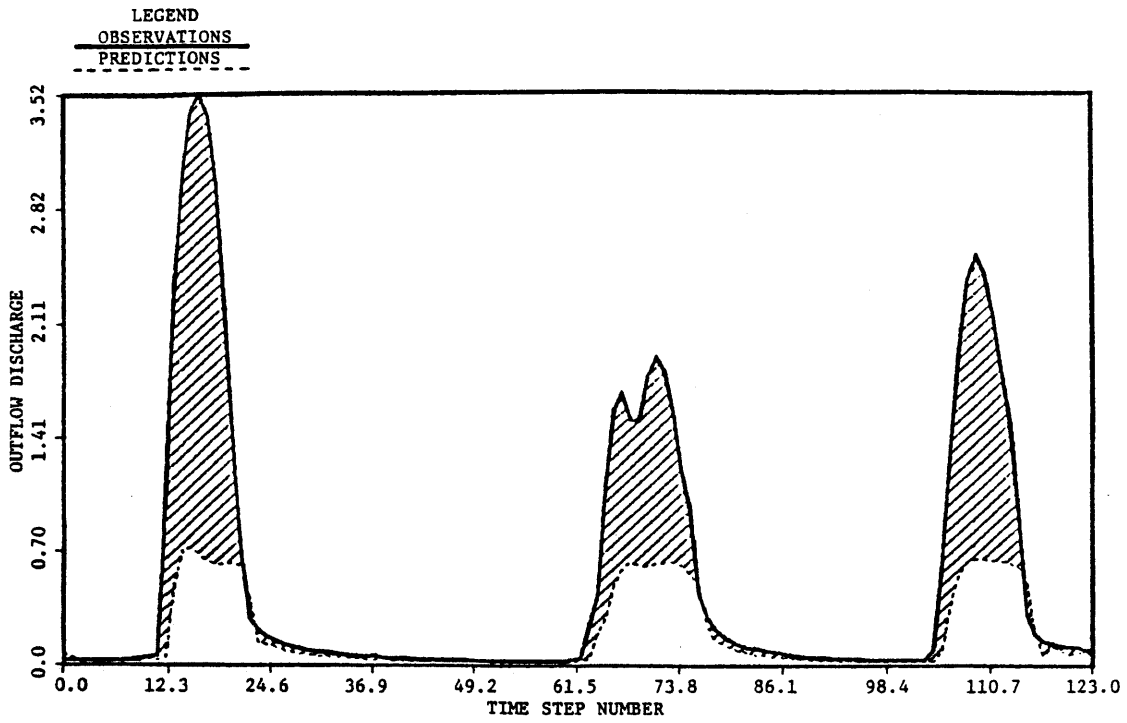

Figure 6.4 Stochastic Prediction of Discharge, Bird Creek, May 1960, EKF, Q-0

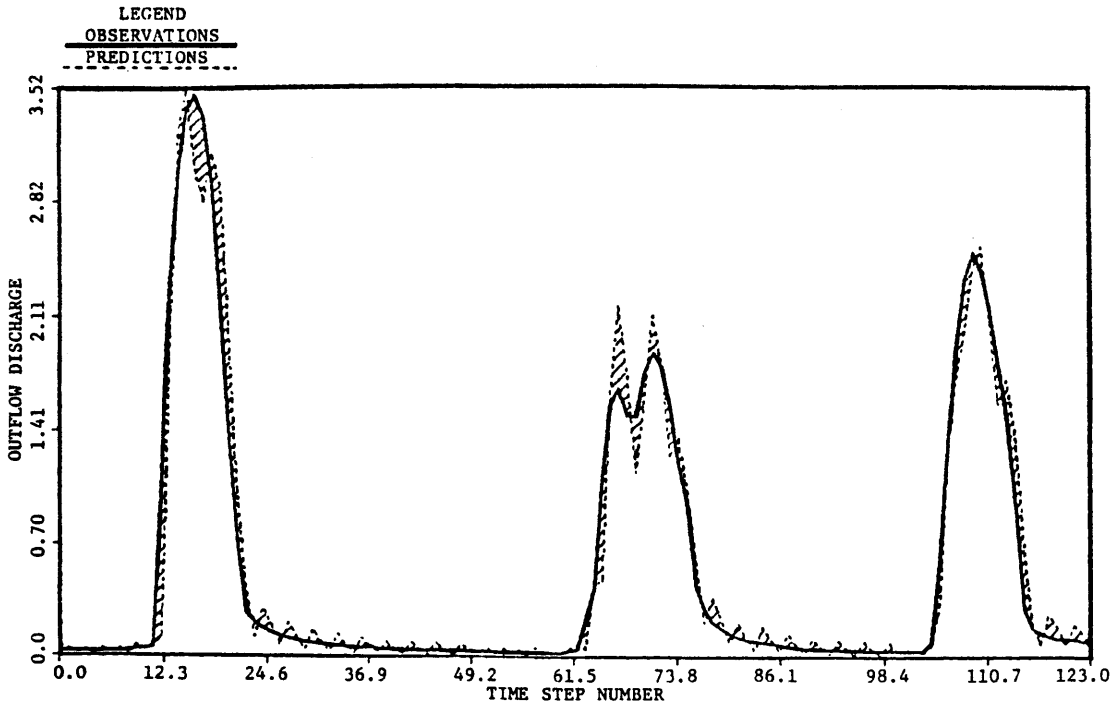

Figure 6.5 Stochastic Prediction of Discharge, Bird Creek, May 1960, EKF, Q-8

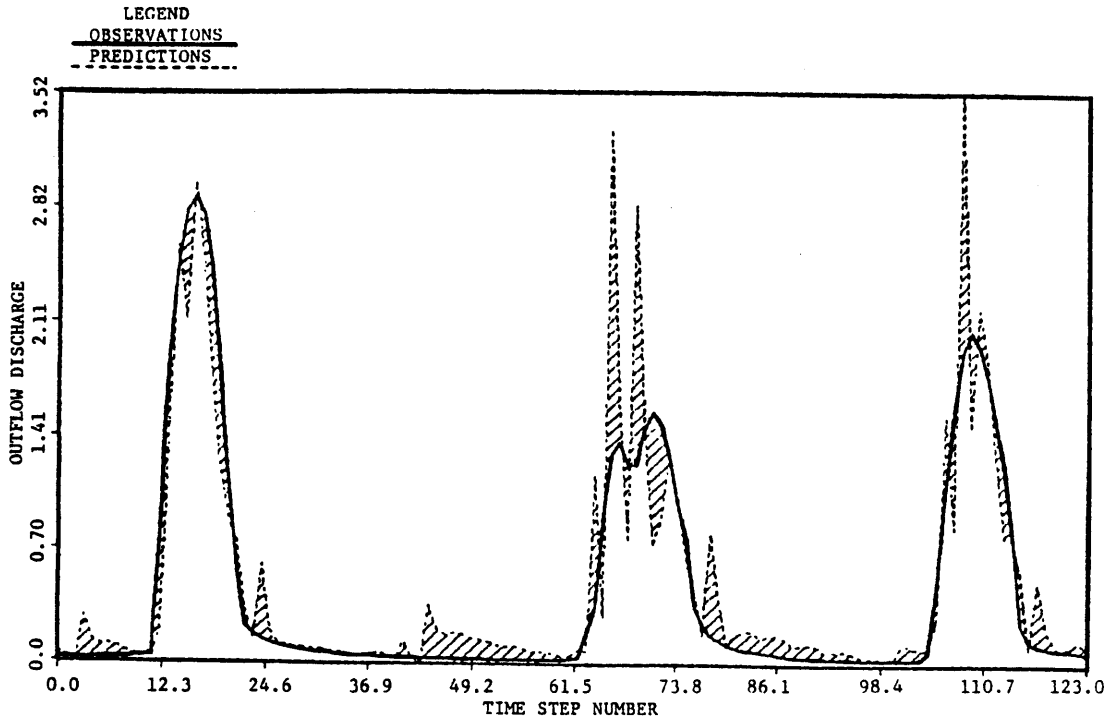

Figure 6.6 Stochastic Prediction of Discharge, Bird Creek, May 1960, EKF, Q-9

Tables 6.6, 6.7, and 6.8 show the residual statistics, normalized residual statistics and least squares indices for the lead-one discharge predictions, when the matrices estimated using short data periods are used to forecast in the whole month of May 1960. Notice that although the model likelihood increases as more data points are used in the estimation of matrix Q, the quality of the statistics of residuals and normalized residuals do not necessarily follow the same pattern.

As can be seen in Figures 6.7 and 6.8 for starting matrix Q of level 4, and in Figures 6.9 and 6.10 for starting matrix Q of level 0; the more data points used in the estimation, the higher the predicted peaks.

6.2.2 Local Sensitivity of the Approximate Maximum Likelihood Estimate

To check the importance of spectral density values equal to the upper or lower bounds, a sensitivity study in the vicinity of the approximate maximum likelihood estimate was performed. The results obtained with the matrix Q of level 8 (see Table 6.2) are presented in this section. Similar results were also obtained for the matrix Q of level 6.

Table 6.9 includes the least squares indices for discharge predictions and the model log-likelihood value when one element of Q of

Table 6.6

Discharge Residuals Statistics for Q Matrices Obtained by Approximate Maximum Likelihood, 40 and 84 Data Points

Q-Level	Second Corrections	Mean	Variation Coefficient	Skewness	Autocorrelations Lag-1	Lag-2	Lag-3	Lag-4
4	Reference	0.117	2.74	2.31	0.70	0.68	0.41	0.33
10	J	0.257	1.77	2.10	0.92	0.75	0.56	0.37
12	J	-0.088	-6.66	-0.06	0.87	0.59	0.24	-0.08
0	Reference	0.344	1.94	2.11	0.94	0.79	0.59	0.38
11	J	0.225	1.85	2.05	0.91	0.74	0.54	0.34
13	J	0.026	13.4	1.99	0.76	0.40	0.16	0.08

J Conditional information matrix

Table 6.7

Discharge Normalized Residuals Statistics for Q Matrices Obtained by Approximate Maximum Likelihood, 40 and 84 Data Points

Q-Level	Second Corrections	Mean	Variation Coefficient	Skewness	Autocorrelations Lag-1	Lag-2	Lag-3	Lag-4
4	Reference	0.291	3.27	1.62	0.56	0.68	0.35	0.38
10	J	0.222	1.91	2.20	0.93	0.76	0.56	0.35
12	J	-0.174	-6.00	-1.36	0.84	0.54	0.20	-0.08
0	Reference	1.150	1.74	1.49	0.92	0.78	0.61	0.43
11	J	0.121	1.98	2.21	0.92	0.75	0.54	0.33
13	J	-0.310	-5.68	-0.33	0.55	0.18	0.12	0.08

J Conditional information matrix

Table 6.8

Discharge Least Squares Indices and Model Log-Likelihood for Q Matrices Obtained by Approximate Maximum Likelihood, 40 and 84 Data Points

Q-Level	Second Corrections	Efficiency	Determination	Persistence	Extrapolation	Log Likelihood
4	Reference	0.85	0.92	-0.55	-2.73	-1104.8
10	J	0.64	0.92	-2.65	-7.79	- 723.1
12	J	0.54	0.60	-3.66	-10.23	- 677.2
0	Reference	0.27	0.80	-6.51	-17.10	-1600.5
11	J	0.71	0.93	-1.97	-6.15	- 772.6
12	J	0.84	0.85	-0.59	-2.83	- 592.0

J Conditional information matrix

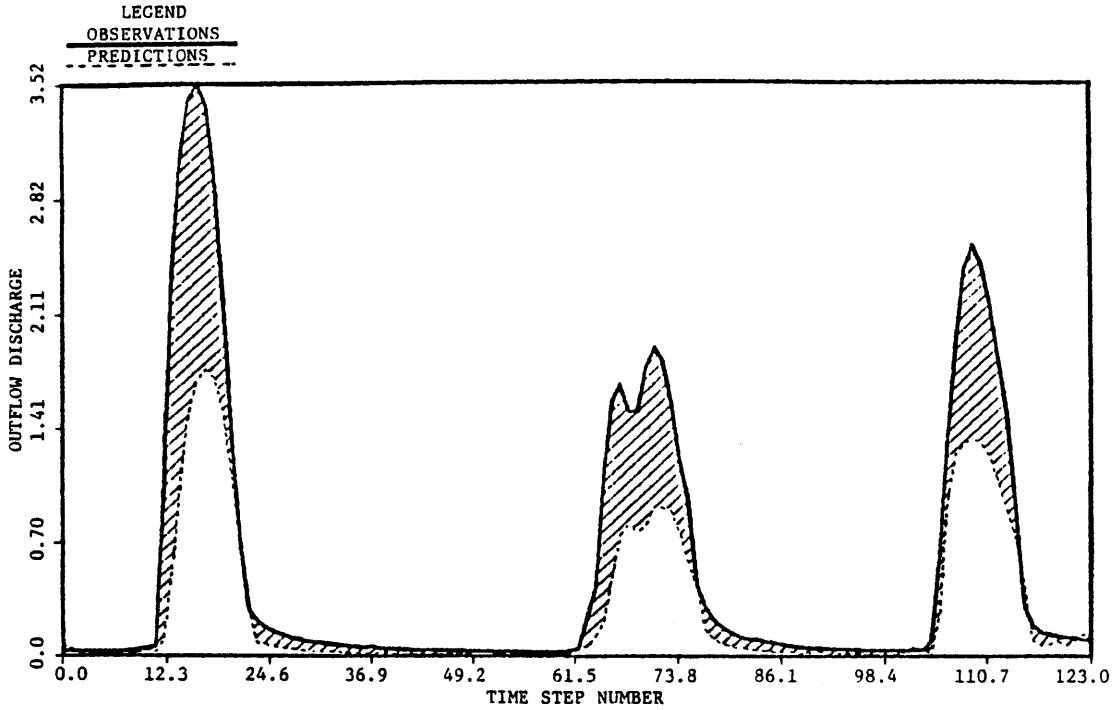

Figure 6.7 Stochastic Prediction of Discharge, Bird Creek, May 1960, EKF, Q-10

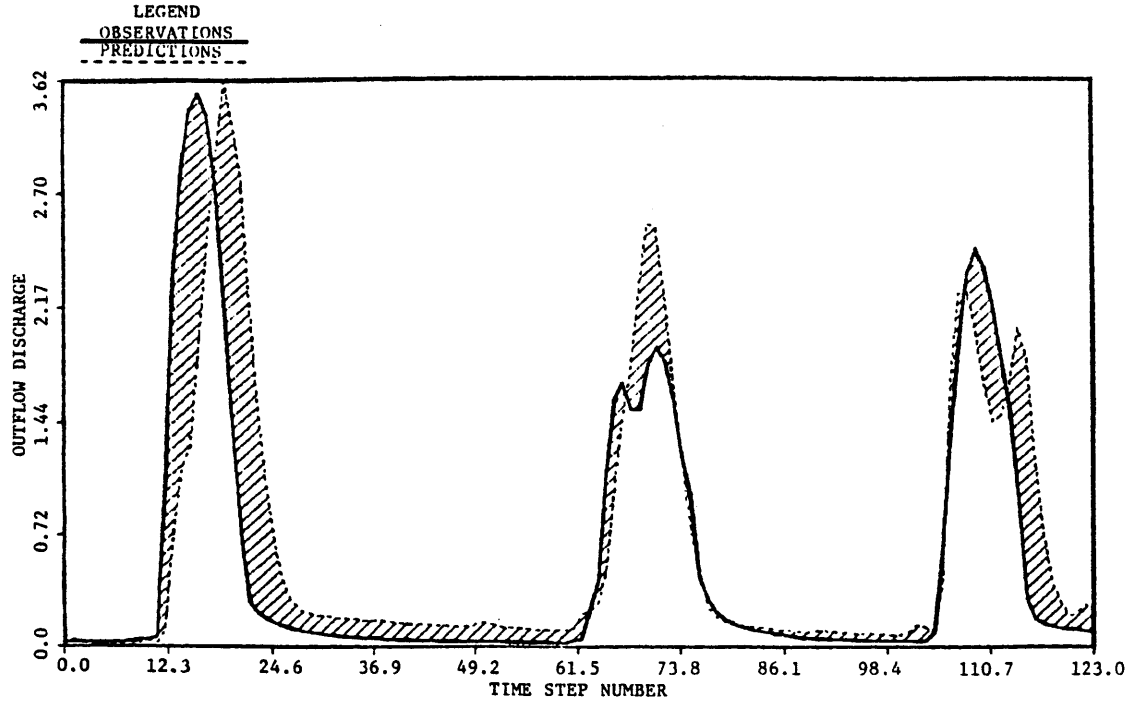

Figure 6.8 Stochastic Prediction of Discharge, Bird Creek, May 1960, EKF, Q-12

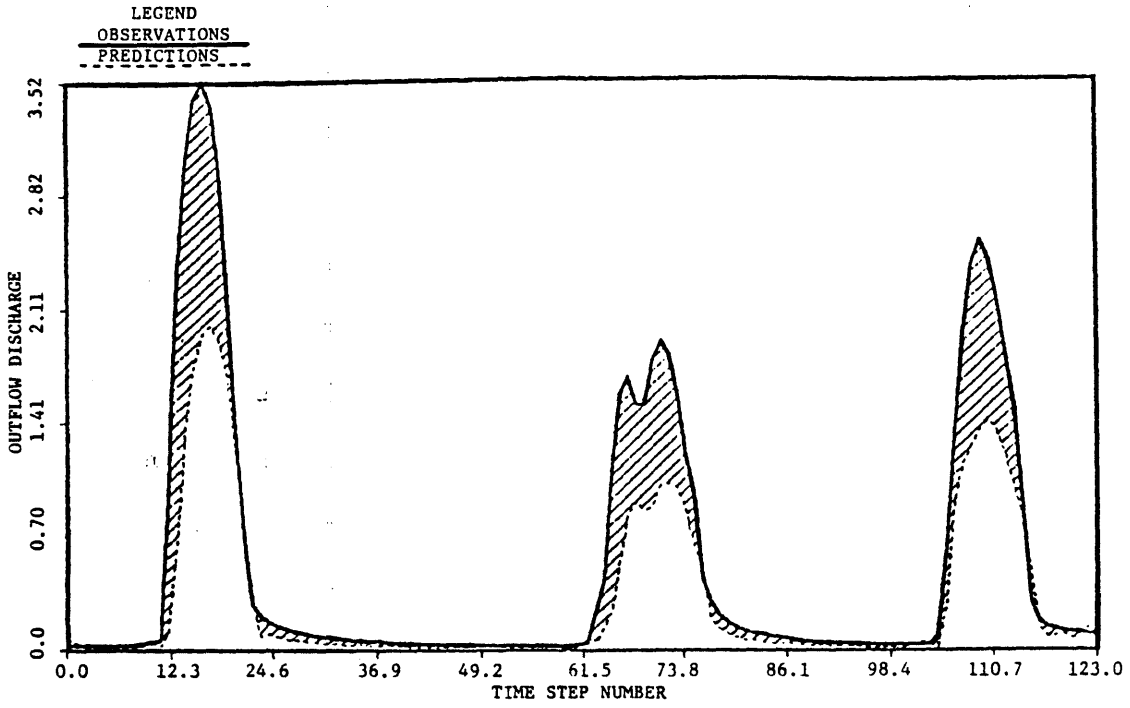

Figure 6.9 Stochastic Prediction of Discharge, Bird Creek, May 1960, EKF, Q-11

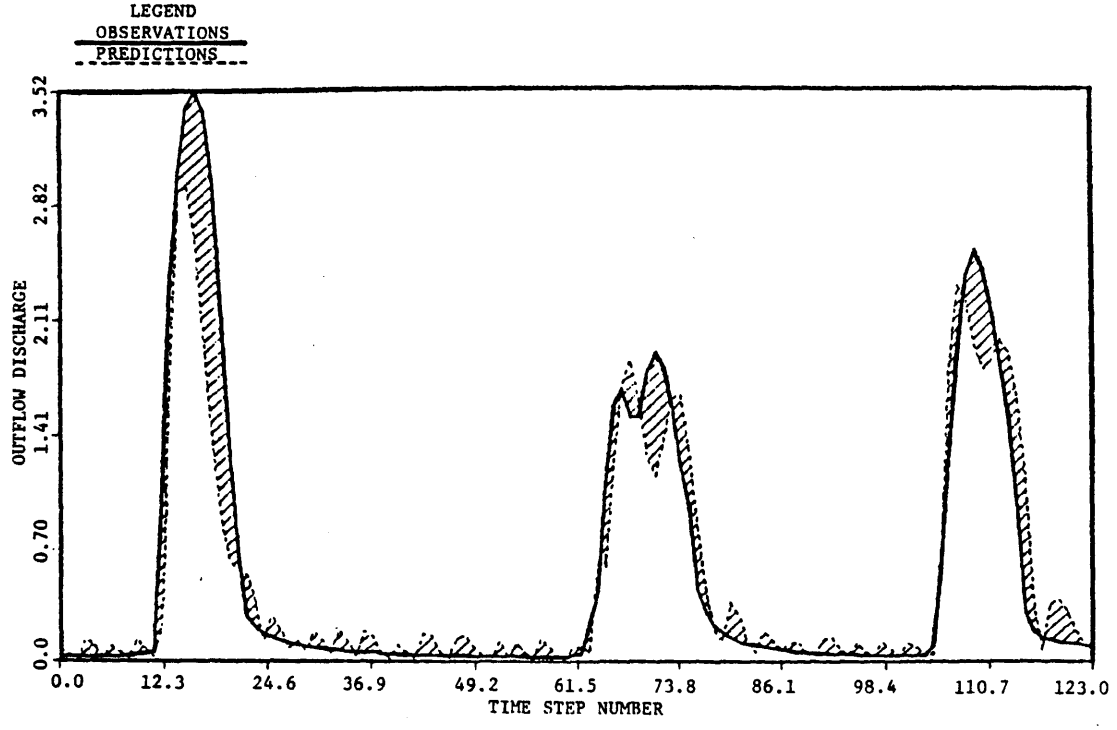

Figure 6.10 Stochastic Prediction of Discharge, Bird Creek, May 1960, EKF, Q-13

level 8 is changed at a time. The changes consist in setting estimated values which are at the upper bound to the lower bound and vice-versa, and changing values which are between the bounds to the lower bound.

As can be observed, the likelihood is affected only when elements on the precipitation and channel portions of the model are changed. The discharge least squares indices are insensitive to spectral density changes of states in the soil, and also to changes in the spectral density of the condensed water volume. The spectral density values for the channel are the most sensitive in least squares indices, although the likelihood of the model is not heavily affected.

The vicinity of the matrix Q of level 8 was further studied by setting all possible combinations of upper bound spectral density values to their lower bounds. The results obtained for the discharge least squares indices and model likelihood are shown in Table 6.10.

The results of Table 6.10 follow those of Table 6.9. Setting any spectral density values of the soil states to zero, does not affect either the model likelihood or the discharge least squares indices. By changing the spectral density value of the precipitation state to zero, the quality of the discharge predictions is only slightly decreased. The model likelihood is considerably decreased by having the precipitation model error covariance propagate with zero spectral density value. As can be seen in Figures 6.11 and 6.12, a larger spectral density for X_p gives larger precipitation predictions.

Table 6.9

Discharge Least Squares Indices and Model Log-Likelihood
One Dimensional Sensitivity, Q of Level 8

Spectral Standard Deviation Changed	Efficiency	Determination	Persistence	Extrapolation	Log Likelihood
Reference	0.94	0.95	0.44	-0.36	-615.3
X_p	0.933	0.934	0.318	-0.643	-1625.8
X_1	0.945	0.946	0.436	-0.359	-615.3
X_2	0.945	0.946	0.436	-0.357	-615.2
X_3	0.940	0.942	0.389	-0.471	-616.8
X_4	0.954	0.954	0.529	-0.135	-612.9
X_5	0.935	0.938	0.339	-0.590	-616.6
X_6	0.945	0.946	0.439	-0.352	-615.4
S_1	0.563	0.883	-3.47	-9.78	-669.7
S_2	-0.31	0.594	-12.42	-31.30	-693.1
S_3	0.563	0.845	-3.47	-9.77	-728.4

Table 6.10

Discharge Least Squares Indices and Model Log-Likelihood
High Dimensional Sensitivity, Q of Level 8

Spectral Standard Deviation Changed	Efficiency	Determination	Persistence	Extrapolation	Log Likelihood
Reference	0.94	0.95	0.44	-0.36	-615.3
X_p, X_1	0.933	0.934	0.318	-0.64	-1625.8
X_p, X_2	0.931	0.931	0.299	-0.69	-1626.3
X_p, X_5	0.932	0.933	0.305	-0.67	-1626.1
X_1, X_2	0.944	0.945	0.430	-0.37	- 615.4
X_1, X_5	0.939	0.941	0.376	-0.50	- 616.0
X_2, X_5	0.938	0.940	0.362	-0.54	- 616.1
X_p, X_1, X_2	0.933	0.933	0.311	-0.66	-1625.8
X_p, X_1, X_5	0.932	0.933	0.305	-0.67	-1626.1
X_p, X_2, X_5	0.931	0.931	0.291	-0.71	-1626.3
X_1, X_2, X_5	0.939	0.941	0.375	-0.50	- 615.9
X_p, X_1, X_2, X_5	0.931	0.932	0.291	-0.71	-1626.3

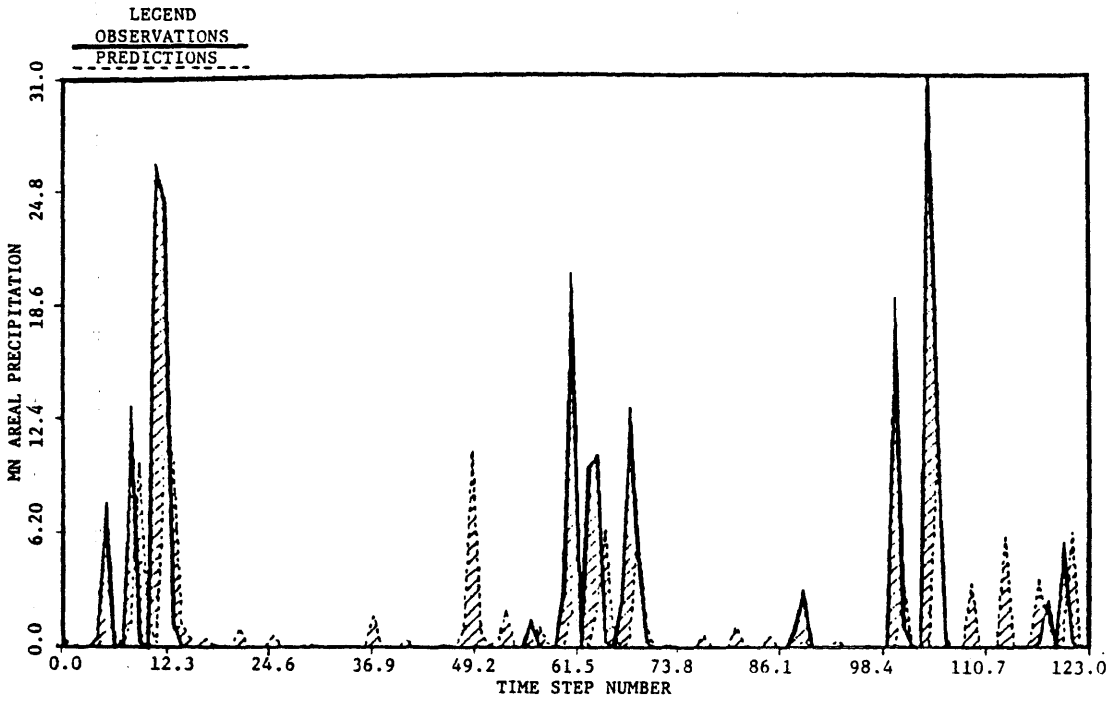

Figure 6.11 Stochastic Prediction of Precipitation, Bird Creek, May 1960, Q-8, with Q(1,1) = 0

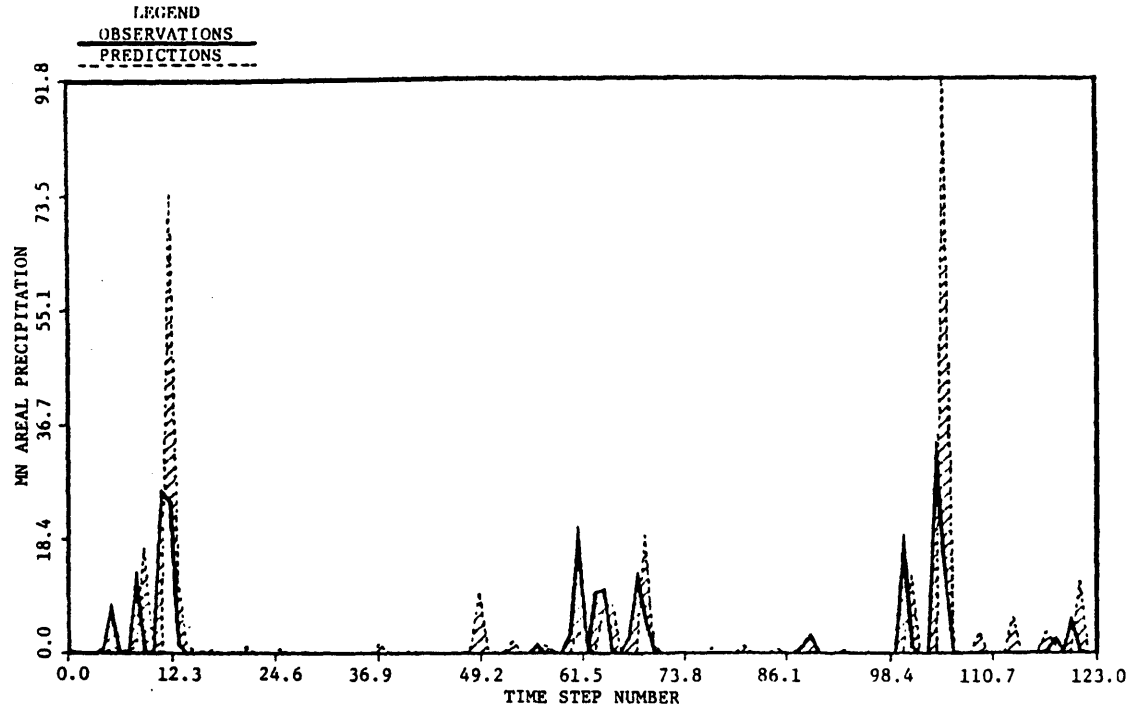

Figure 6.12 Stochastic Prediction of Precipitation, Bird Creek, May 1960, Q-8

When the spectral density element of precipitation is driven to zero, the physical model is fully believed and then its predicted error variance goes to zero. In this case, the residual variance for precipitation reduces to the mean areal precipitation observation variance (see Equation (5.9) and Table 4.1) and therefore takes a value of one. Figure 6.13 gives the standard deviations of the residuals of precipitation when the spectral density value provided by the approximate maximum likelihood method is used. Notice that the lower bound for those values is one. The log-likelihood for precipitation decreases when a zero spectral density value is used, because the sum of squares of residuals for this case is much bigger than the sum of the logarithms of residual mean areal precipitation variances when the spectral density is not zero (see Equation (5.8) for one observation).

Figures 6.14 to 6.23 show the evolution in time of the predicted states of the rainfall-runoff model, when using the spectral density diagonal matrix of level 8 with values of elements corresponding to states X_p, X_1, X_2, and X_5 set to their lower bounds. Since the precipitation and soil dynamics are fully believed, these graphs represent the deterministic evolution of those states. The only significant gain matrix elements are the ones related to the first and last channel reservoirs (see Figures 6.24 and 6.25). Notice the large magnitude of the gains on the first reservoir, which implies that what is observed as discharge comes primarily from the updating mechanism

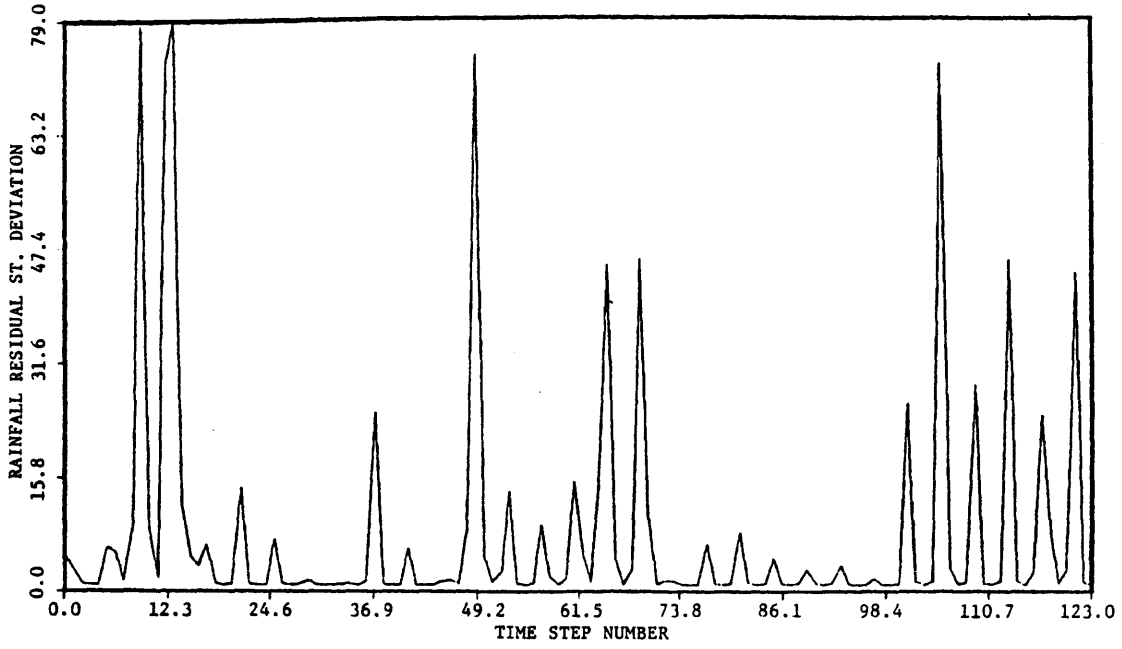

Figure 6.13 Precipitation Residuals Standard Deviations, Bird Creek, May 1960, Q-8

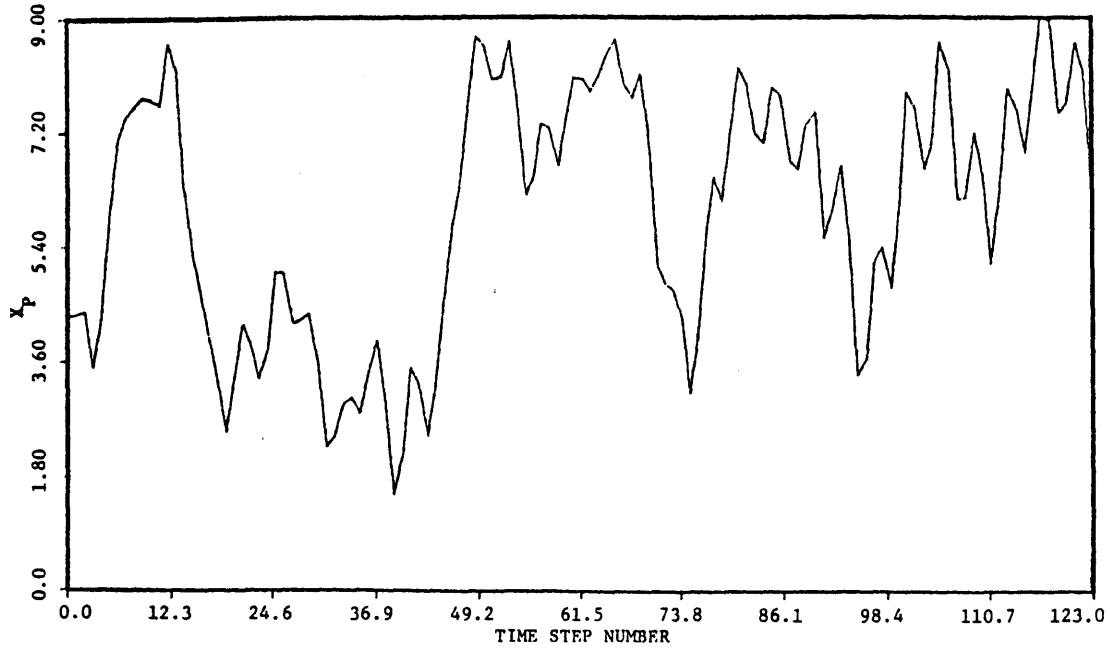

Figure 6.14 Predicted Trajectory of Condensed Water Volume, May 1960, Q-8, only channel non-zero

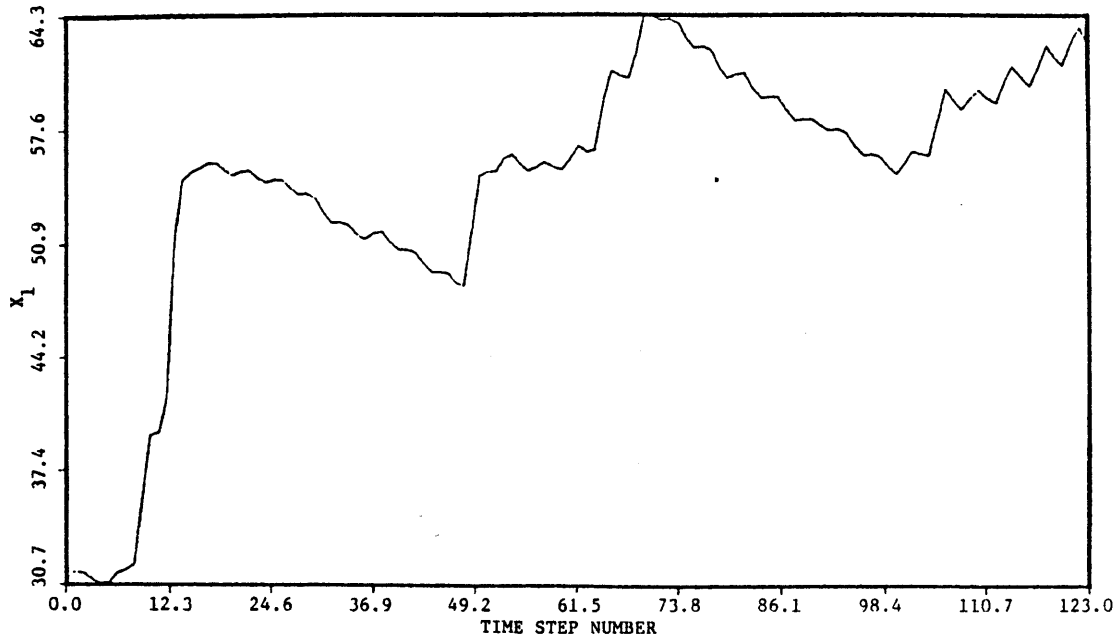

Figure 6.15 Predicted Trajectory of Upper Zone Tension Volume, May 1960, Q-8, only channel non-zero

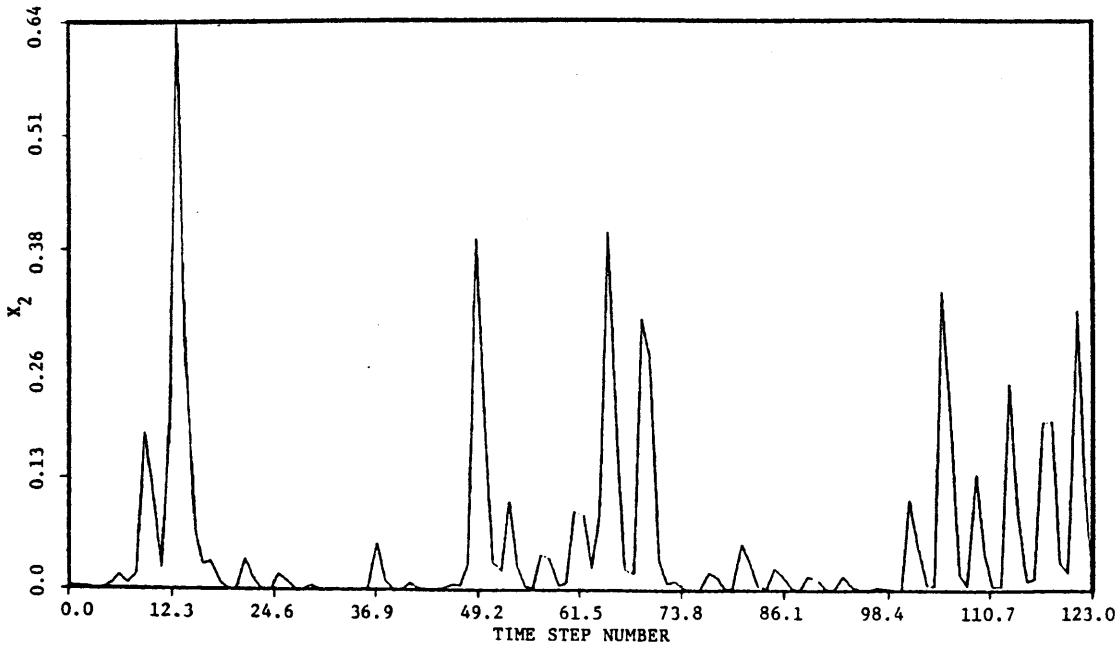

Figure 6.16 Predicted Trajectory of Upper Zone Free Volume, May 1960, Q-8, only channel non-zero

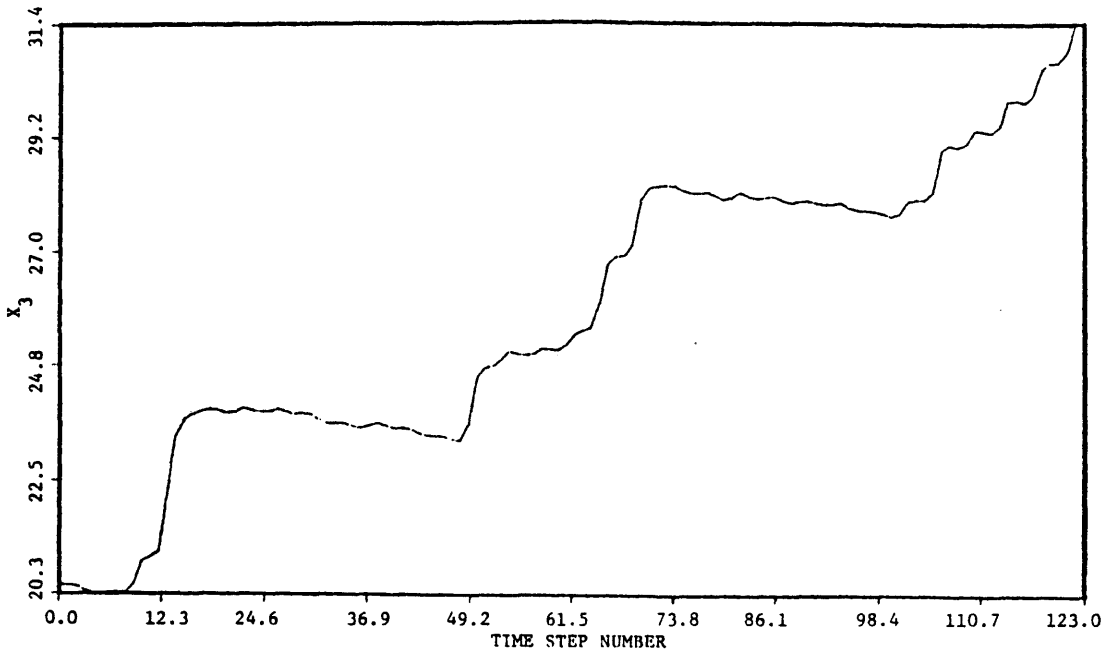

Figure 6.17 Predicted Trajectory of Lower Zone Tension Volume, May 1960, Q-8, only channel non-zero

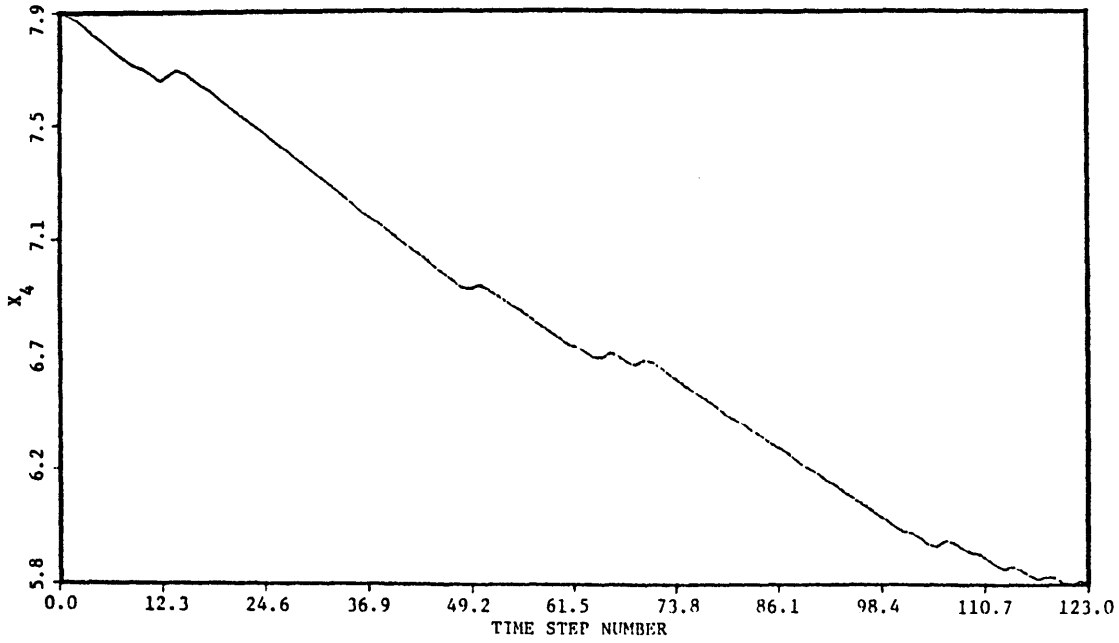

Figure 6.18 Predicted Trajectory of Lower Zone Free Primary Volume, May 1960, Q-8, only channel non-zero

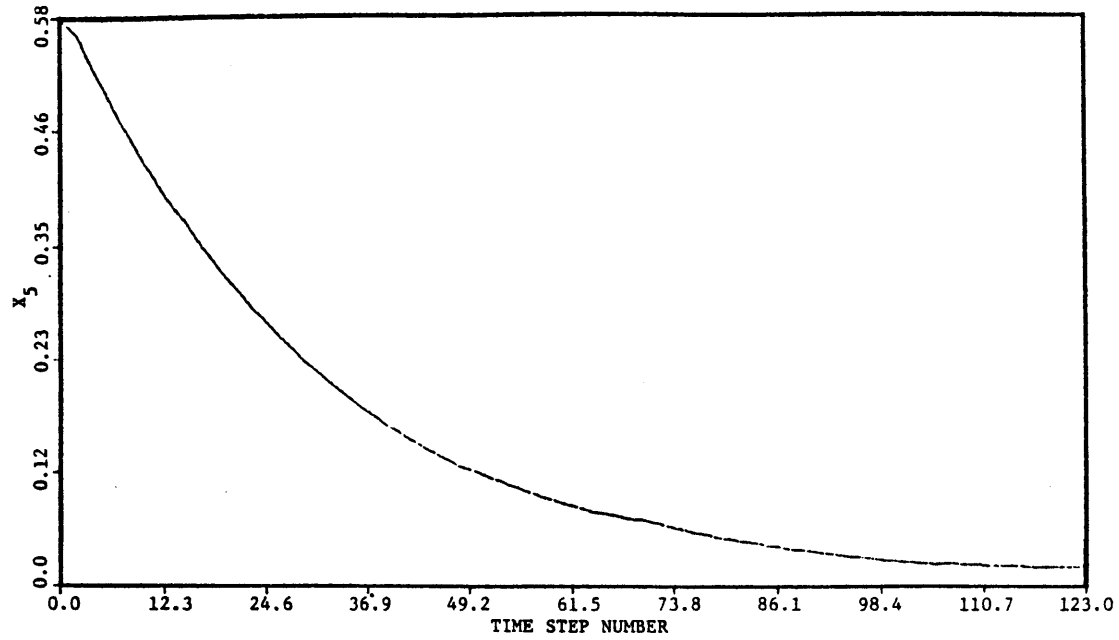

Figure 6.19 Predicted Trajectory of Lower Zone Free Secondary Volume, May 1960, Q-8, only channel non-zero

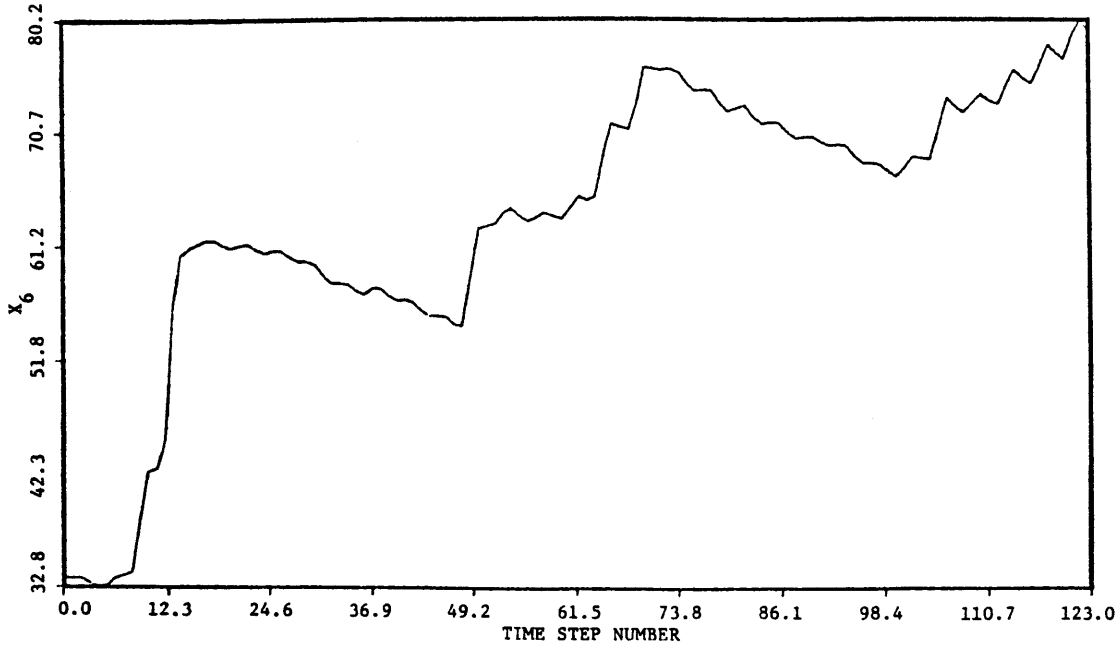

Figure 6.20 Predicted Trajectory of Additional Impervious Volume, May 1960, Q-8, only channel non-zero

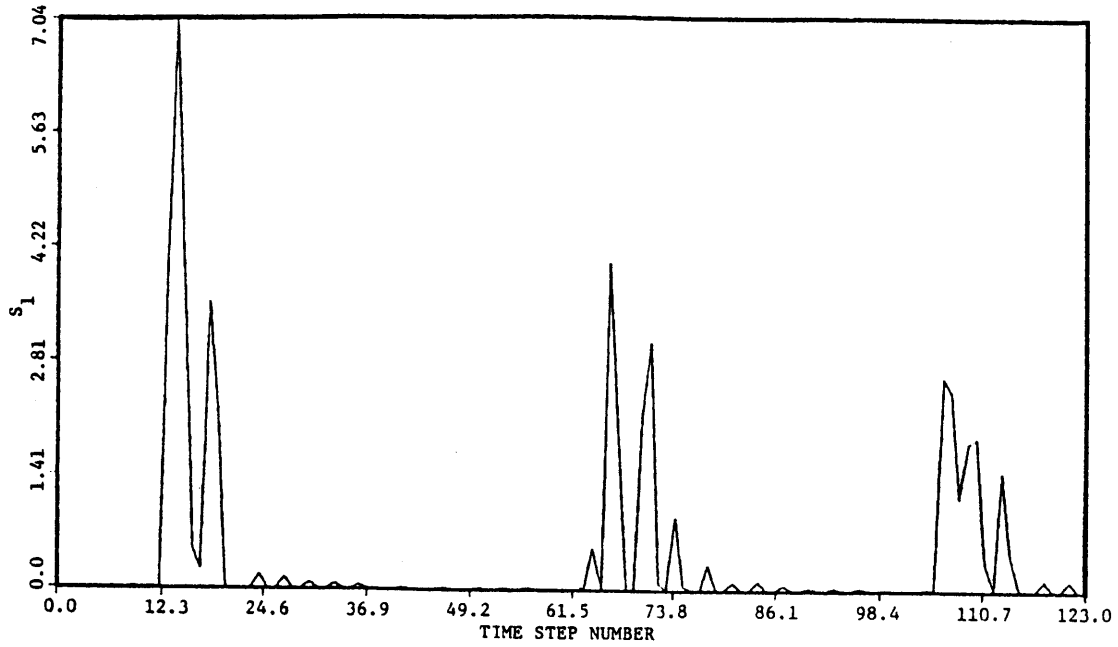

Figure 6.21 Predicted Trajectory of Volume on First Reservoir, May 1960, Q-8, only channel non-zero

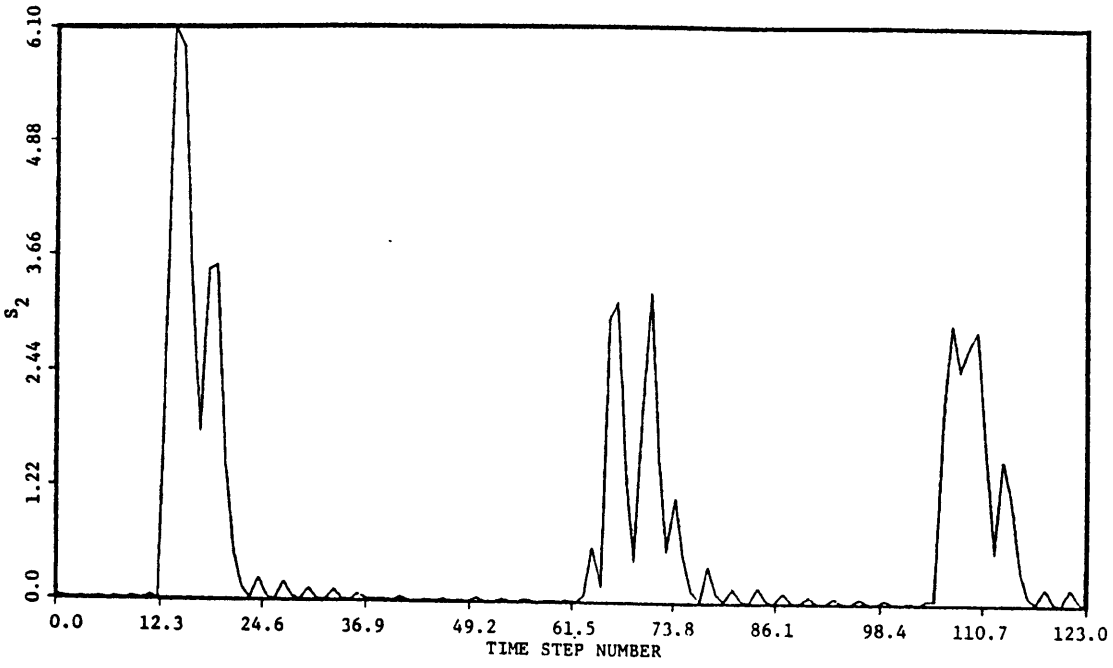

Figure 6.22 Predicted Trajectory of Volume on Second Reservoir, May 1960, Q-8, only channel non-zero

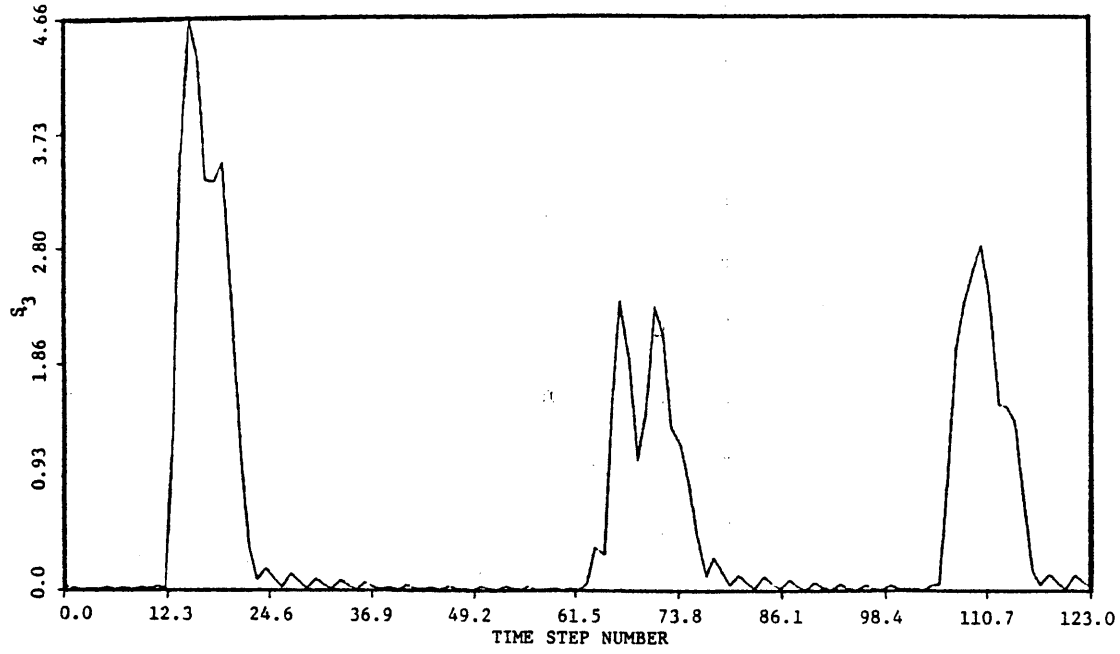

Figure 6.23 Predicted Trajectory of Volume on Third Reservoir, May 1960, Q-8, only channel non-zero

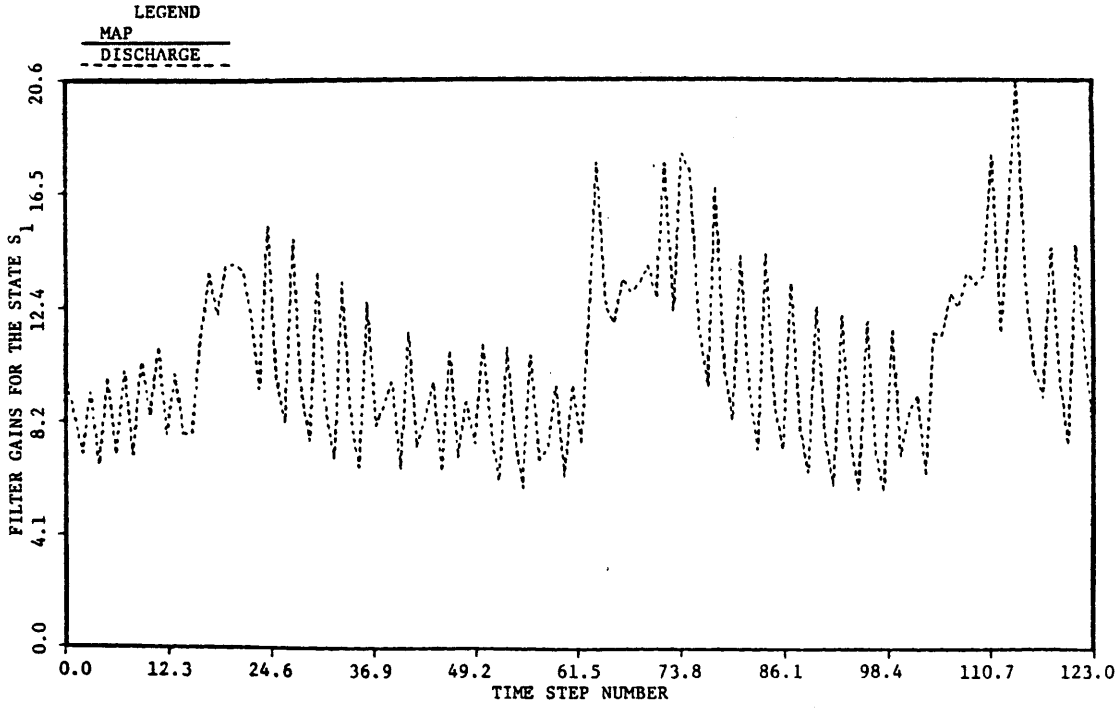

Figure 6.24 Filter Gains for the First Reservoir State, May 1960, Q-8, only channel non-zero

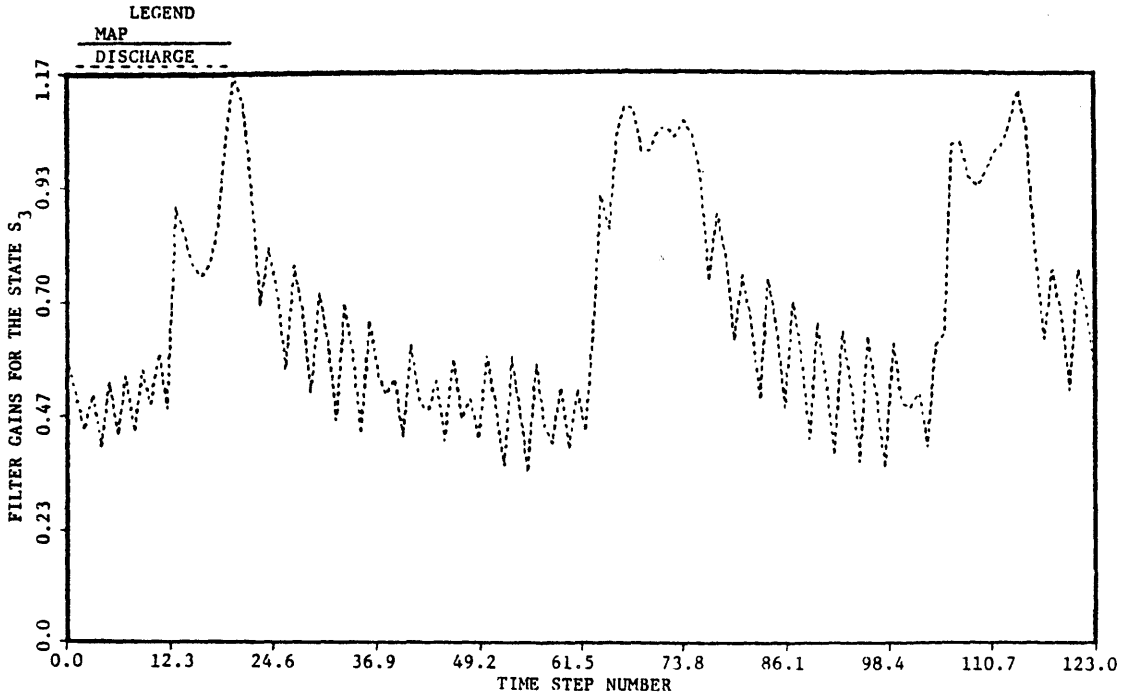

Figure 6.25 Filter Gains for the Third Reservoir State, May 1960, Q-8, only channel non-zero

of the filter and not from the soil output. Of course this is an undesirable feature, but recall that conservation of mass is not imposed at the updating step of the filter.

The fact that the filter is basically tracking the discharge observation is confirmed by looking at Figures 6.26 through 6.28, which represent extended forecasts of discharge. Notice the lag in the rise of the hydrograph and the sudden drop of the forecasts, based on past information of discharge. Observe, however, the good reproduction of the time to peak and peak magnitudes when predictions are made six hours ahead. Notice also that the extended forecasts produced using matrix Q of level 8 with all but channel values set to zero gives better results than previously found for the Q matrix of level 4 even when using the nonlinear filter smoothers (see Figures 4.30 to 4.33).

6.2.3 Sensitivity of the Approximate Maximum Likelihood Estimate on the Upper Bounds

Given that some of the spectral density values estimated by the approximate maximum likelihood procedure attain the prespecified upper bounds, the sensititivity of the estimates on such bounds was studied. Two upper bounds, besides the one in Table 6.1, were considered. A total of 124 time steps were used in the estimation, with the conditional information matrix used as the mechanism to iterate in

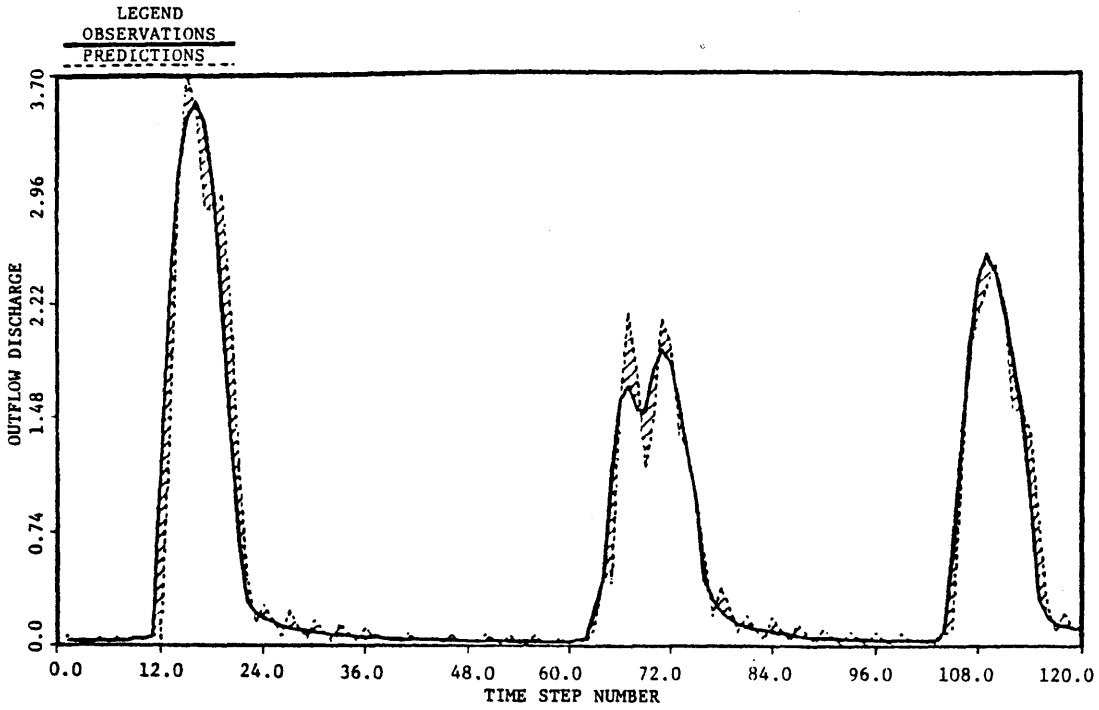

Figure 6.26 Extended Forecast of Discharge, Bird Creek, May 1960, Q-8, only channel non-zero, 6 hrs

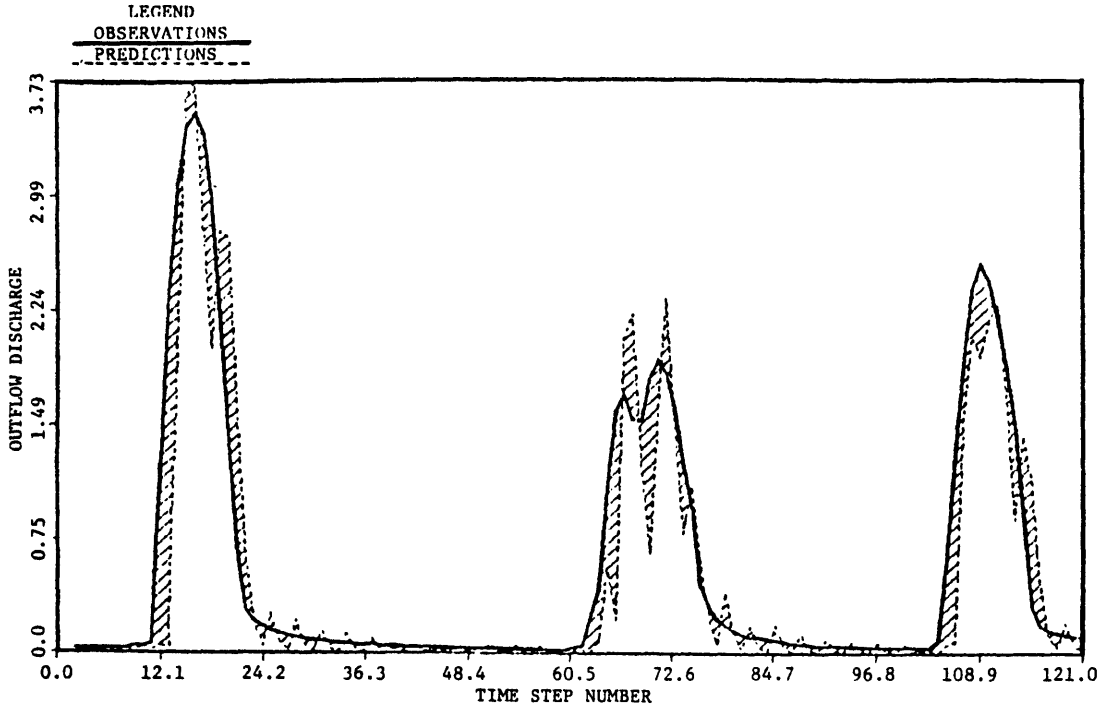

Figure 6.27 Extended Forecast of Discharge, Bird Creek, May 1960, Q-8, only channel non-zero, 12 hrs

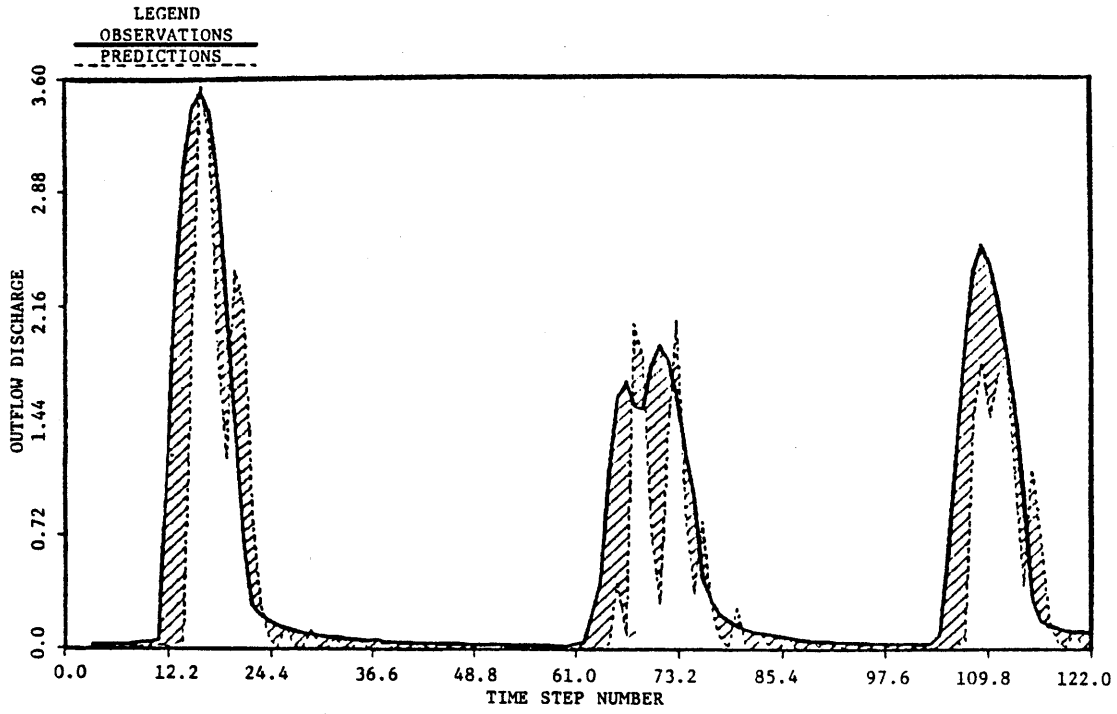

Figure 6.28 Extended Forecast of Discharge, Bird Creek, May 1960, Q-8, only channel non-zero, 18 hrs

Newton's method. The estimation was done using the spectral density matrix of level 0 as the initial condition for the procedure.

Table 6.11 includes the different upper bounds and the spectral density standard deviations obtained by imposing such bounds. Both cases were found convergent after the number of iterations shown on Table 6.11. Efforts to use a larger bound than the one given in the fourth column of this table failed; after few iterations the differential equations that propagate the error covariance could not be numerically integrated.

As can be observed in Table 6.11, the first set of bounds leads to convergence similar in pattern to those given (Table 6.2) for bounds in Table 6.1. However, the second set of limits led to convergence to a different pattern, with discrepancies found on parameters related to the states X_3, X_5, and S_2.

Table 6.12 contains the discharge least squares indices and the model log-likelihood when predictions are obtained using the convergent spectral density matrices of Table 6.11, i.e., matrices of levels 14 and 15. Table 6.12 also includes the results obtained by setting all spectral density values of non-channel states to the lower bound, and also the previously discussed results obtained with the upper bounds given in Table 6.1.

As the upper bound becomes larger, the obtained value for the likelihood function grows and the discharge least square indices become slightly better. If only positive spectral density values are

Table 6.11

Upper Bounds Sensitivity and Their Corresponding Approximate Maximum Likelihood Standard Deviation Estimates

State	Upper Bound	Q-14	Upper Bound	Q-15
X_p	40	40	200	200
X_1	95	95	200	200
X_2	25	25	100	100
X_3	130	10^{-5}	200	200
X_4	110	10^{-5}	200	10^{-5}
X_5	25	25	100	10^{-5}
X_6	120	10^{-5}	200	10^{-5}
S_1	20	13.8	40	0.951
S_2	10	10^{-5}	20	8.54
S_3	5	0.71	10	1.67
Initial Q	0		0	
Data Points	124		124	
Second Corrections	J		J	
Iterations	12		17	

J Conditional information matrix

Table 6.12

Discharge Least Squares Indices and Model Log-Likelihood for Variable Upper Bounds

Q-Level	Efficiency	Determination	Persistence	Extrapolation	Log Likelihood
14	0.934	0.936	0.324	-0.63	-943.7
8	0.945	0.946	0.437	-0.36	-615.3
15	0.958	0.958	0.570	-0.04	-486.4
14*	0.927	0.929	0.252	-0.80	-1626.8
8*	0.931	0.932	0.291	-0.71	-1626.3
15*	0.931	0.949	0.302	-0.68	-1731.2

*Spectral density values other than channel states set to zero.

allowed in the channel states, the global likelihood is decreased due to the lower precipitation residual variance, but as in the previous section excellent results are still obtained for discharge predictions.

Figure 6.29 shows the discharge predictions obtained using the largest upper bound, i.e., for Q of level 15. Due to the high spectral density value for the precipitation portion, a large predicted peak occurred at time step 100. However, overall predictions are excellent, with small timing errors on both the rising and falling portions of the hydrograph. Figure 6.30 depicts the discharge predictions when all spectral density values except those correspondent to the channel are set to zero. Notice the quality of the predictions.

Although the results of the approximate maximum likelihood procedure suggest that the only spectral density elements that are important are the ones corresponding to the channel states, it must be emphasized that these are only local results. If the spectral density values for channel states are off the approximate maximum likelihood values, the discharge predictions may then be sensitive to changes on spectral density values for other states. The results of Chapter 4 are one example where spectral density values of states not in the channel play a key role in the quality of the predictions.

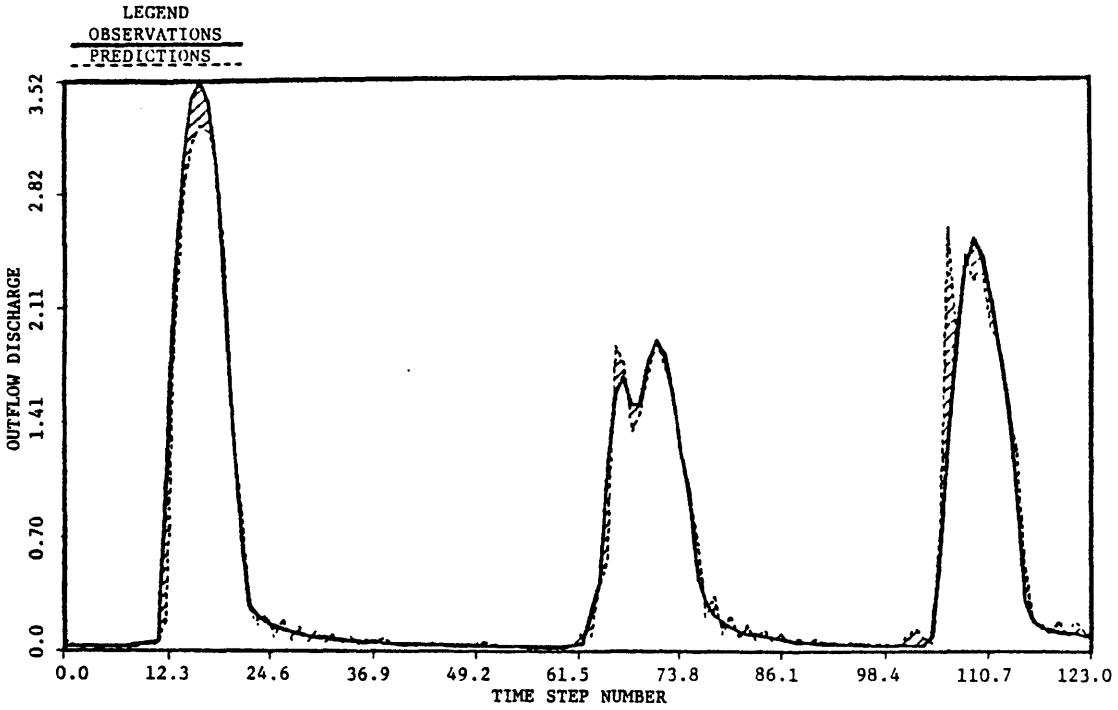

Figure 6.29 Stochastic Prediction of Discharge, Bird Creek, May 1960, Q-15

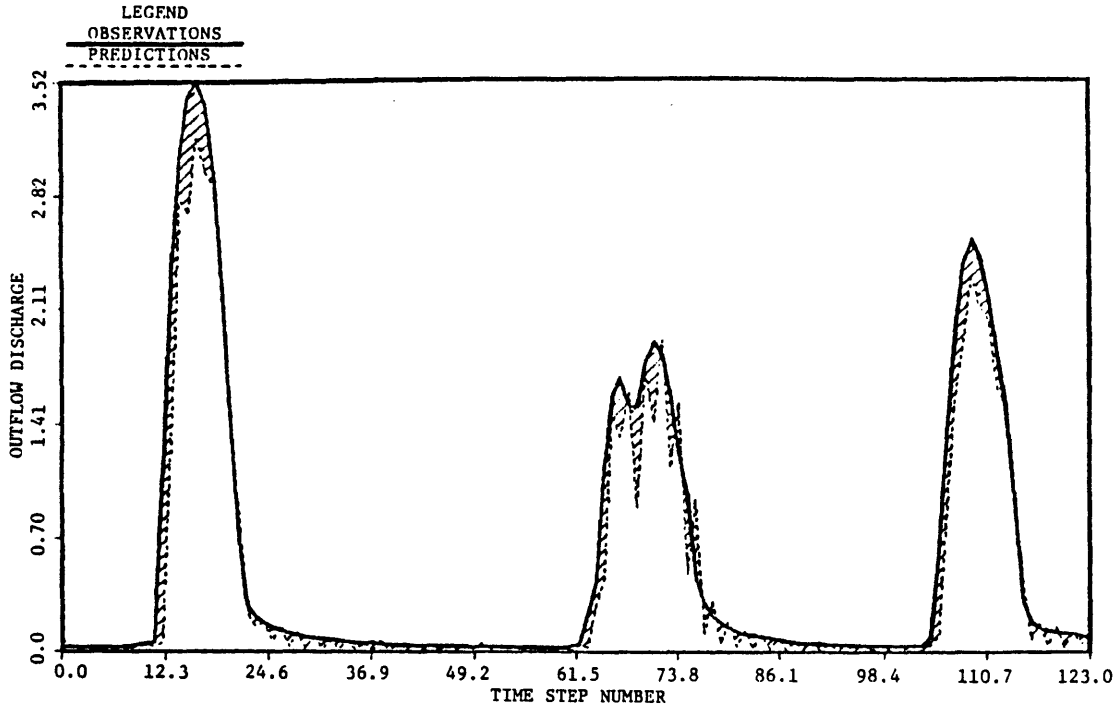

Figure 6.30 Stochastic Prediction of Discharge, Bird Creek, May 1960, Q-15 only channel non-zero

6.2.4 Results from the Sub-Optimal Explicit Maximum Likelihood Estimator

The explicit estimator described in Equation (5.48) was found convergent (using a total number of time steps N of 124) to the zero spectral density matrix. This implies that the predictions found by using the Q matrix given by such formula coincide with the deterministic propagation of the rainfall-runoff model, and therefore as in Chapter 4 the results badly underestimate the hydrograph peaks. The main reason for such a poor estimate is the fact that this simple estimate is obtained assuming that the system transition matrix is constant in time, a condition that is not valid for different flow regimes.

6.3 Results for Q Matrices Estimated from Consistency Conditions

Time varying and diagonal spectral density matrices Q(t) were obtained using consistency conditions on the residuals covariance matrix. Given that the physical model has two observations, and that the precipitation is mostly an input to the rest of the model, the Jazwinski's estimator (Equation (5.17)) provides only two independent conditions for elements in Q(t).

The two conditions used correspond to consistency of actual with expected variances of residuals. For this case the equations (5.51) have a simple solution: they are two simultaneous equations with two unknowns, with the characteristic matrix of the system being triangu-

lar. The independent equation provides the spectral density value for precipitation. Once this is obtained, its value is replaced in the other linear equation to obtain the spectral density value of any other prespecified state of the rainfall-runoff model.

Preliminary results suggested that the state to be used besides the condensed water volume should be such that discharge is sensibly affected. The estimator was then computed using either states in the channel or the upper zone free volume.

As with the approximate maximum likelihood procedure, this adaptive estimator was bounded below and above. Notice that small values in the transition matrix diagonal for the second selected state may translate into large values of Q(t), and hence the necessity of the upper bound (see Equation (5.51)).

Table 6.13 includes the discharge least squares indices when the Jazwinski's estimator is used every time step. Also included are the elements of matrix Q that are being changed from time to time and the Q-level matrix that defines the elements which are not being changed. Results obtained by not applying the Jazwinski's estimator, are also presented in such table under the heading "Reference." As is shown, performance may be improved by the use of this estimator, but no definite trends are obtained: for a given spectral density matrix, a given combination of states may improve performance, but that same combination may decrease performance for other spectral density matrices.

Table 6.13

Discharge Least Squares Indices.
Adaptive Estimation of Q Matrix Every Time Step

Q-Level	Elements Estimated	Efficiency	Determination	Persistence	Extrapolation
0	Reference	0.266	0.803	-6.51	-17.1
0	X_p, S_3	0.098	0.611	-8.23	-21.2
0	X_p, S_2	0.816	0.882	-0.88	-3.5
0	X_p, S_1	0.710	0.745	-1.97	-6.1
0	X_p, X_2	0.355	0.763	-5.60	-14.9
4	Reference	0.848	0.925	-0.55	-2.7
4	X_p, S_3	0.764	0.896	-1.42	-4.8
4	X_p, S_2	0.828	0.880	-0.76	-3.2
4	X_p, S_1	0.875	0.892	-0.28	-2.1
4	X_p, X_2	0.857	0.934	-0.46	-2.5
8	Reference	0.945	0.946	0.44	-0.36
8	X_p, S_3	0.838	0.854	-0.66	-2.99
8	X_p, S_2	0.936	0.937	0.35	-0.56
8	X_p, S_1	0.696	0.727	-2.11	-6.50
8	X_p, X_2	0.936	0.937	0.35	-0.55

As the reference performance improves, the estimator usefulness seem to decrease. The estimator may give great improvements for poor reference performance, as shown in Figure 6.31. Figures 6.32 and 6.33 show other cases for which good results were obtained.

Given the algebraic simplicity of the procedure, computational time is not considerably increased. Therefore, it is recommended to check several state combinations with past data and see which (if any) give together with a filtering procedure a useful forecasting tool.

Jazwinski's estimator was also employed assuming matrix Q is constant over periods of two and four time steps. Results for the obtained discharge least squares indices are shown in Table 6.14. The tendency of the results indicate that the more often matrix Q is changed the better. Notice that in some cases better results are obtained for the estimator applied every four time steps; however, in such cases there is no significant improvement over the reference performance (see Table 6.13). Although more information is being used by averaging the estimate over more than one time step, the rapid changes that occur in the hydrograph will not be reproduced if the currently used matrix Q does not present global hydrograph conditions (see Figure 6.34).

Consistency conditions of lags other than zero were incorporated to the estimator (see Equation (5.58)). The discharge least squares indices obtained when such conditions are added are included in Table

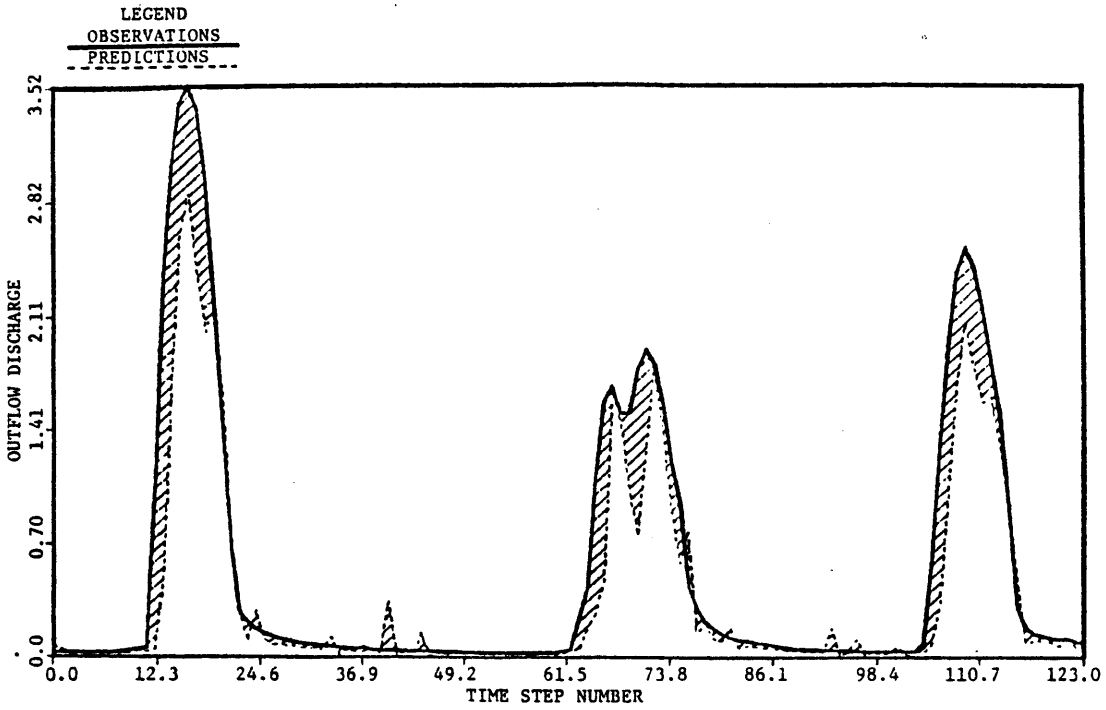

Figure 6.31 Adaptive Discharge Predictions, Bird Creek, May 1960, Q-0, States X_p, S_2, every time step

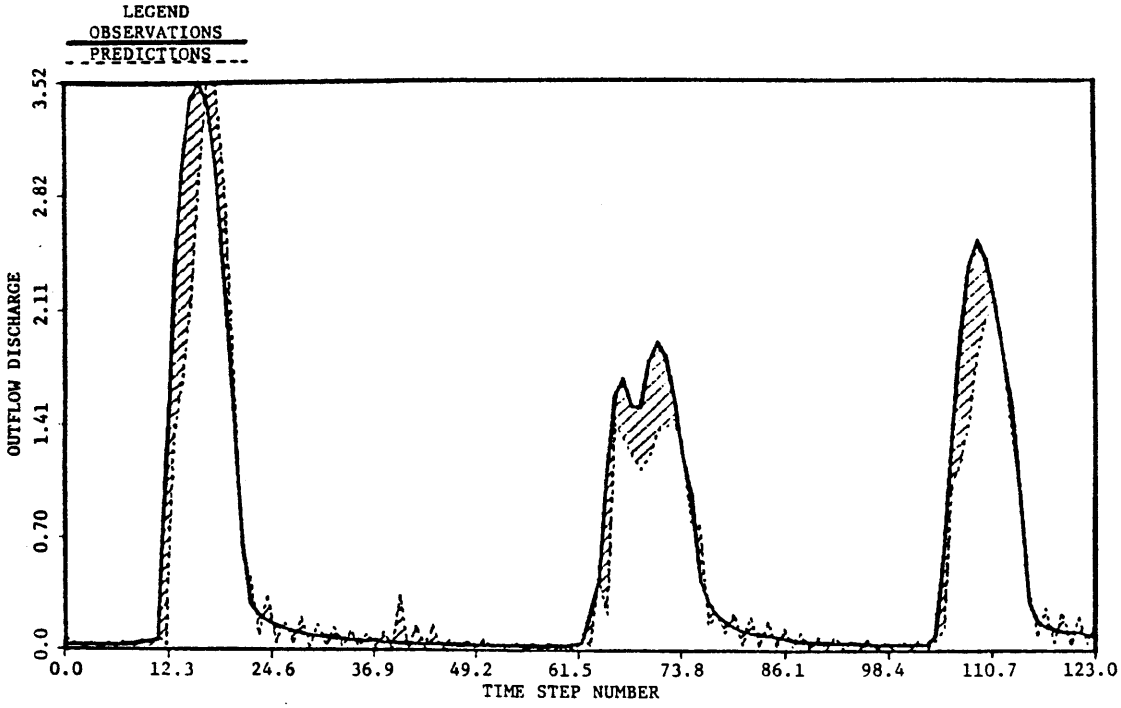

Figure 6.32 Adaptive Discharge Predictions, Bird Creek, May 1960, Q-4, States X_p, S_1, every time step

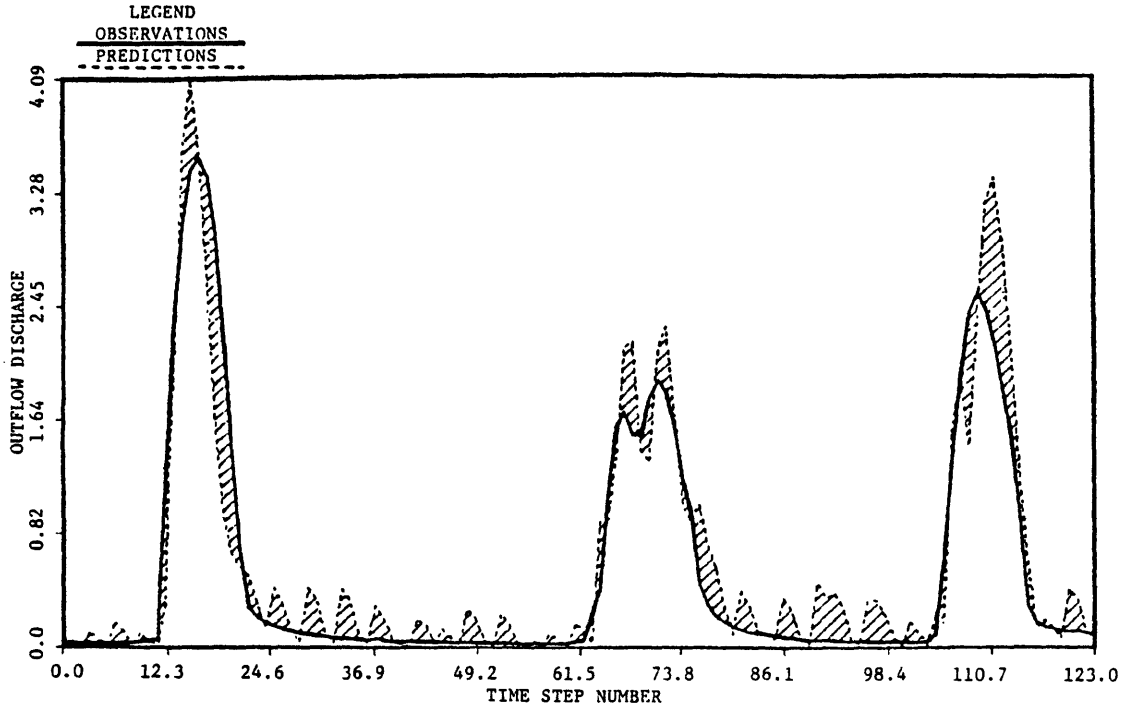

Figure 6.33 Adaptive Discharge Predictions, Bird Creek, May 1960, Q-8, States X_p,S_3, every time step

Table 6.14

Discharge Least Squares Indices.
Adaptive Estimation of Q Matrix,
Variable Estimation Lag

Q-Level	Elements Estimated	Esti-mation Lag	Efficiency	Determination	Persistence	Extrapolation
0	X_p, S_3	4	0.398	0.782	-5.1	-13.8
0	X_p, S_2	4	0.501	0.585	-4.1	-11.3
0	X_p, S_1	4	0.198	0.310	-7.2	-18.8
0	X_p, X_2	4	0.442	0.808	-4.7	-12.7
4	X_p, S_3	2	0.774	0.891	-1.3	-4.6
4	X_p, S_2	2	0.754	0.813	-1.5	-5.0
4	X_p, S_1	2	0.838	0.879	-0.6	-3.0
4	X_p, X_2	2	0.845	0.923	-0.6	-2.8
4	X_p, S_3	4	0.833	0.930	-0.7	-3.1
4	X_p, S_2	4	0.531	0.613	-3.8	-10.6
4	X_p, S_1	4	0.798	0.847	-1.1	-4.0
4	X_p, X_2	4	0.862	0.931	-0.4	-2.4
8	X_p, S_3	4	0.718	0.854	-1.9	-5.9
8	X_p, S_2	4	0.944	0.944	0.4	-0.4
8	X_p, S_1	4	0.548	0.602	-3.6	-10.1
8	X_p, X_2	4	0.943	0.944	0.4	-0.4

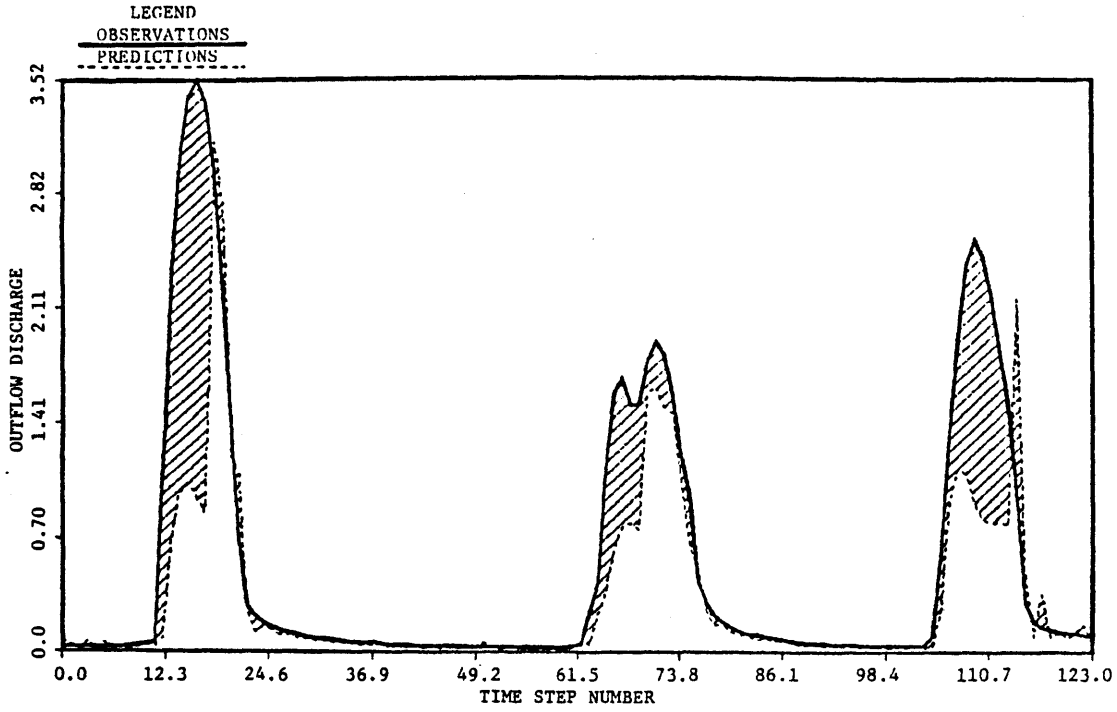

Figure 6.34 Adaptive Discharge Predictions, Bird Creek, May 1960, Q-4, States X_p,S_2, every 4 time steps

6.15. As is shown, no improvement resulted from having more conditions. Two reasons may explain this: first, the matrix Q is updated only after L+1 time steps where L is the number of additional lags considered; and second, given the way the estimator is defined, the consistency conditions on residuals at lag zero are used in the definition of conditions for higher lags, leading to no additional independent information.

6.4 Summary

This chapter describes the results of estimating the diagonal dynamics noise spectral density matrix for the rainfall-runoff model, using the procedures described in Chapter 5.

The approximate maximum likelihood method gave better results if the iterations were obtained by means of the conditional information matrix on Newton's method. As more information is included, a more reliable estimate is obtained. The final estimate was found sensitive to upper bounds imposed to the spectral density standard deviations. However, the estimate with all values equal to zero except for such elements corresponding to channel states was found to give excellent one-step ahead predictions (see Appendix C for an extensive analysis of the use of such a matrix). This estimate, however, had the undesirable property that the channel is driven primarily by the discharge observations and not from the water outflow from the soil

Table 6.15

Discharge Least Squares Indices.
Adaptive Estimation of Q Matrix Using
Consistency Conditions of Higher Lags

Q-Level	Elements Estimated	Efficiency	Determination	Persistence	Extrapolation
4	Reference	0.85	0.92	-0.55	-2.73
4	X_p, S_3, S_1	0.582	0.634	-3.28	-9.30
4	X_p, S_2, S_1	-4.47	0.323	-55.0	-133.9
4	X_p, X_2, S_1	0.758	0.761	-1.47	-4.96
4	X_p, S_2, S_1, S_3	-0.33	0.333	-12.7	-32.0
4	X_p, S_1, S_3, X_2	0.134	0.308	-7.9	-20.3
4	X_p, X_2, S_1, S_2	-3.96	0.321	-49.7	-121.1

component of the model, implying that perhaps with a simpler soil model, the same quality of results might be obtained.

The estimation of the spectral density matrix based on consistency conditions gave results that depend on the spectral density matrix that is used. Better results were obtained if matrix Q is changed every time step. The usefulness of the estimator tends to diminish as better reference values are used (obtained using a Q-matrix constant in time). Due to its low computational cost, the use of such estimator could be of help in cases where bad reference Q matrices are being used.

Chapter 7

FILTERING OF LARGE SCALE BASINS

7.1 Introduction

Serious computational problems may be encountered if the techniques presented in Chapter 3 are applied to a large scale system. This is primarily due to the large amount of calculations required in the propagation and updating of the error covariance matrix. If there are M subsystems and if on every one of them a model with n states is used, the composite state vector that describes the large scale system has nxM components, and therefore the error covariance matrix has dimension nxM by nxM. The number of computations required on the best case, the extended Kalman filter, grow as $(nxM)^3$. With n on the order of 10 for the rainfall-runoff model, a value of M greater than 5 may be problematic, especially if calculations for short forecast lead times are obtained using a mini- or microprocessor.

Procedures to deal with the computational burden due to the error covariance matrix have been given in the modern estimation theory literature. They represent a trade-off between computational efficiency and accuracy of the predictions.

Gelb (1974), in the section regarding suboptimal filter design, mentions the idea of prior specification of the filter gain matrix. If this can be done, the updating step becomes very simple. Also this implies that if only mean characteristics are of interest, only the state mean dynamic equations have to be solved.

Figures 7.1 to 7.4 show gain time traces with respect to the two observations for some of the states of the rainfall-runoff model obtained for the Bird Creek basin. As can be observed, it is not easy to approximate these traces with smooth functions of time.

An algorithm that estimates a portion of the state vector of a linear dynamic system was proposed by Sims (1974). The difficulties of applying this procedure lie on the specification of a decision mechanism that selects at every time step the representative components of the state vector. Only by extensive simulation studies, which comprehend diverse meteorological conditions, such decision algorithm may be defined.

Another way to decrease the computational burden due to the propagation of the error covariance matrix is to decouple states which naturally show weak connections. By doing this, it is possible to break a high-order filter into several mutually exclusive low-order filters. In the following section of this chapter, such an idea will be applied to the filtering of a large scale basin composed of several sub-basins.

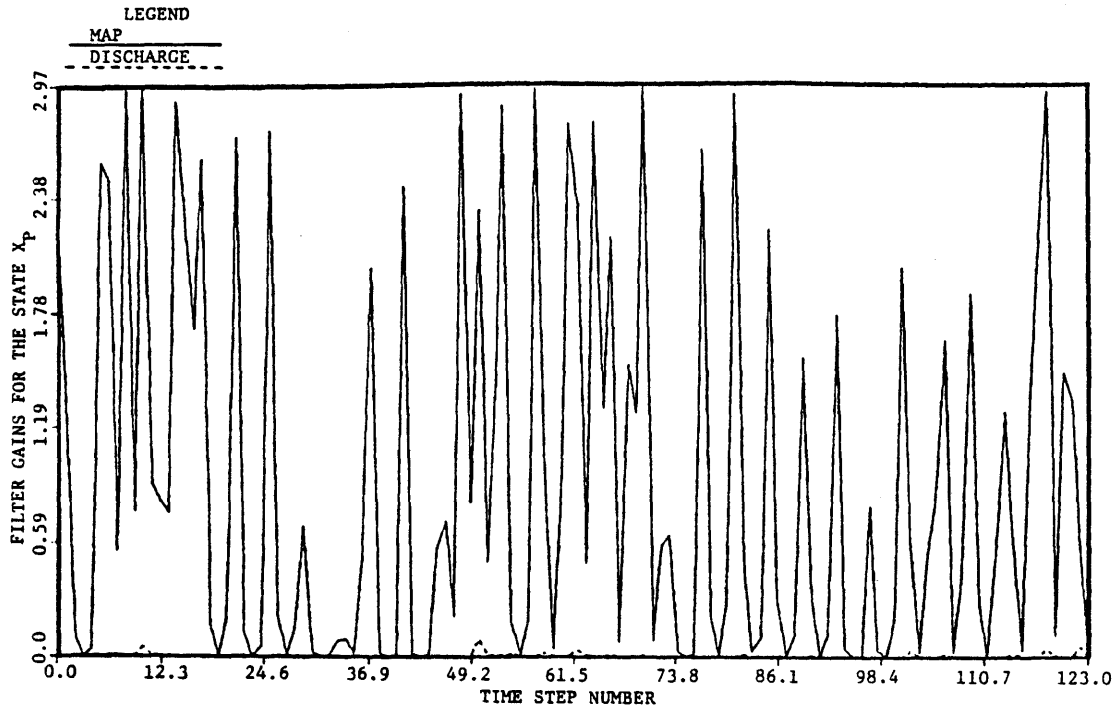

Figure 7.1 Filter Gains for the Condensed Water Volume, May 1960, Q-4

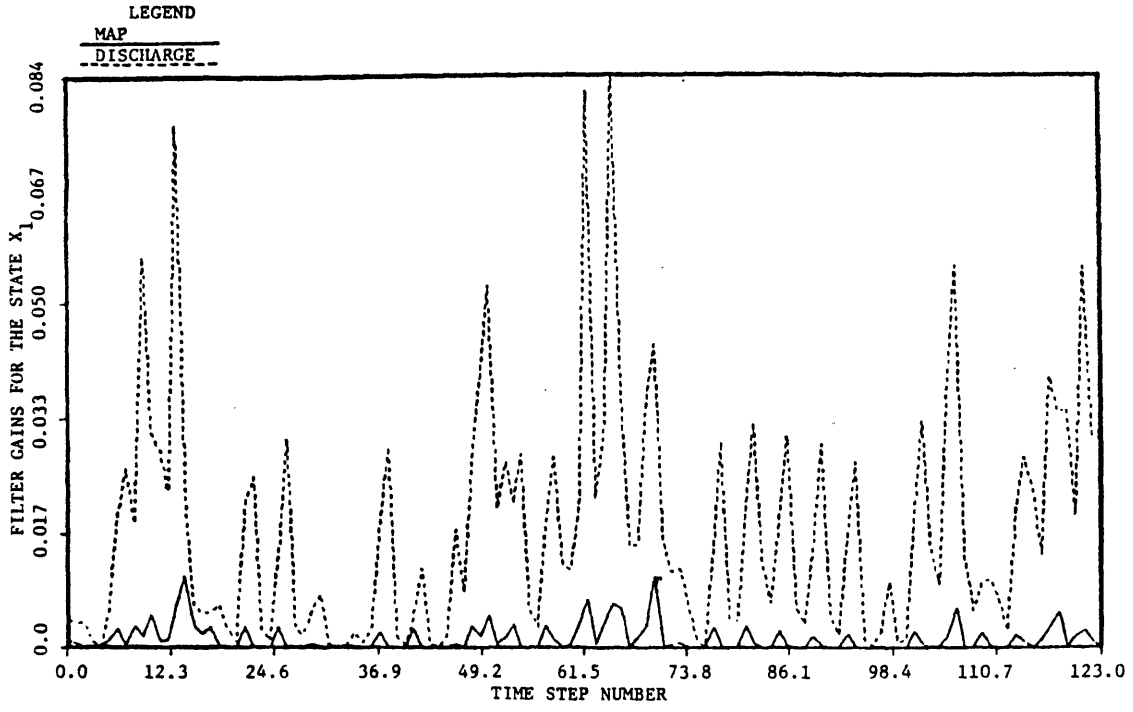

Figure 7.2 Filter Gains for the Upper Zone Free Volume, May 1960, Q-4

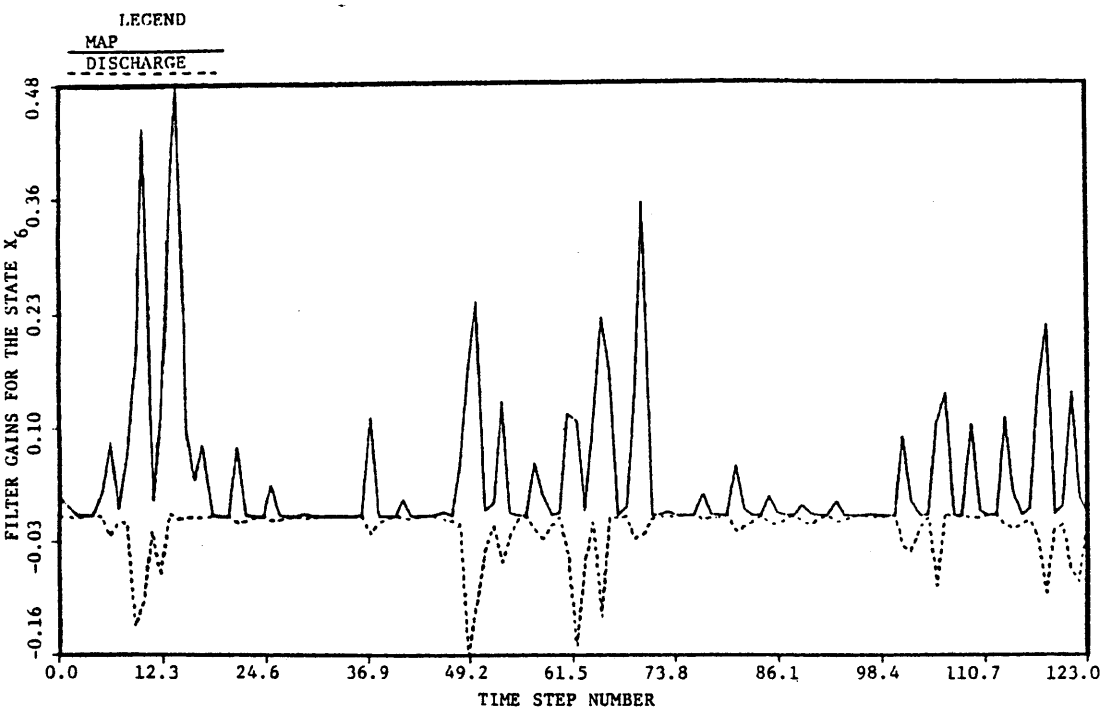

Figure 7.3 Filter Gains for the Additional Impervious Storage, May 1960, Q-4

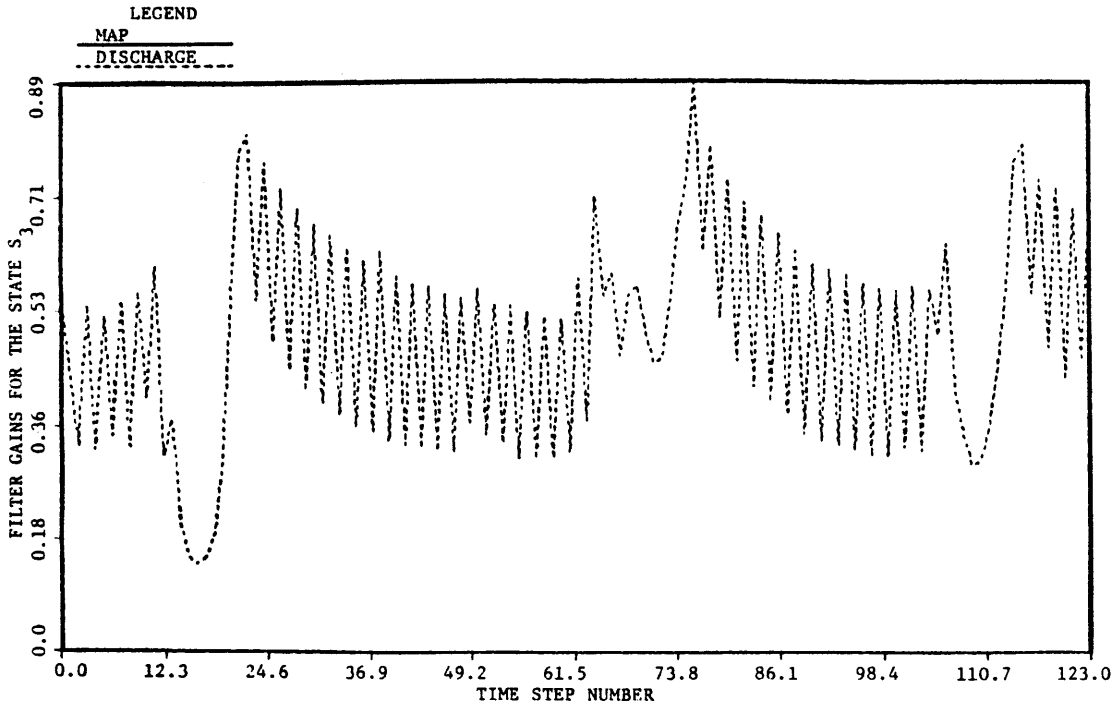

Figure 7.4 Filter Gains for the Third Channel State, May 1960, Q-4

7.2 Block Diagonal Decomposition Filters

A hypothetical large scale basin is shown in Figure 7.5 It is assumed that there are measurements of all input and observation variables, for all the sub-basins. The goal is to forecast mean areal precipitation and discharge on and from each of the sub-basins without treating the composite representation of all of them.

Two decomposition procedures which treat sub-basins separately were introduced by Puente, et al. (1983) and by Georgakakos (1983). Both procedures are based on the schematic representation of the large scale basin given in Figure 7.6. The nodes on this Figure represent the only physical interconnections taken into account by such procedures, e.g., discharges from upstream sub-basins that flow into downstream sub-basins. No dynamic connections between precipitation and soil states in different sub-basins are assumed.

Both methods first forecast upstream and then downstream sub-basins, using upstream discharge predictions as inputs to the channel component of respective downstream sub-basins. Because upstream discharge predictions not only affect the mean but also the variance of downstream flows, the two methods supplement the spectral density matrix of downstream sub-basins. This is done by adding a time varying component to the user's assigned spectral density matrix of downstream sub-basins, as in Equation (3.5), i.e.,

$$Q^d(t)' = F^d Q_u'(t) F^{d^T} + Q^d(t) \qquad (7.1)$$

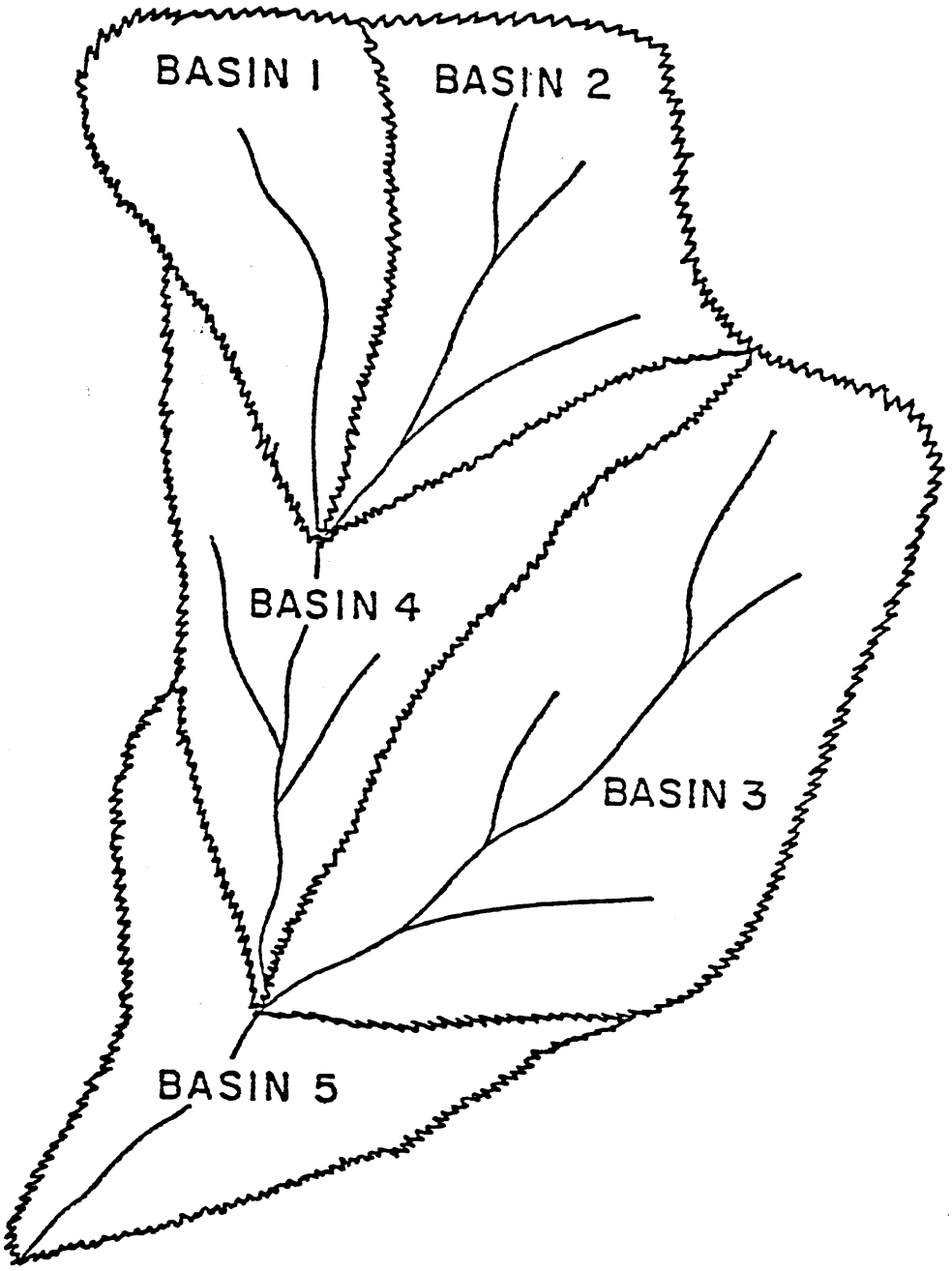

Figure 7.5 Hypothetical Large Scale Basin
(after Georgakakos and Bras, 1982)

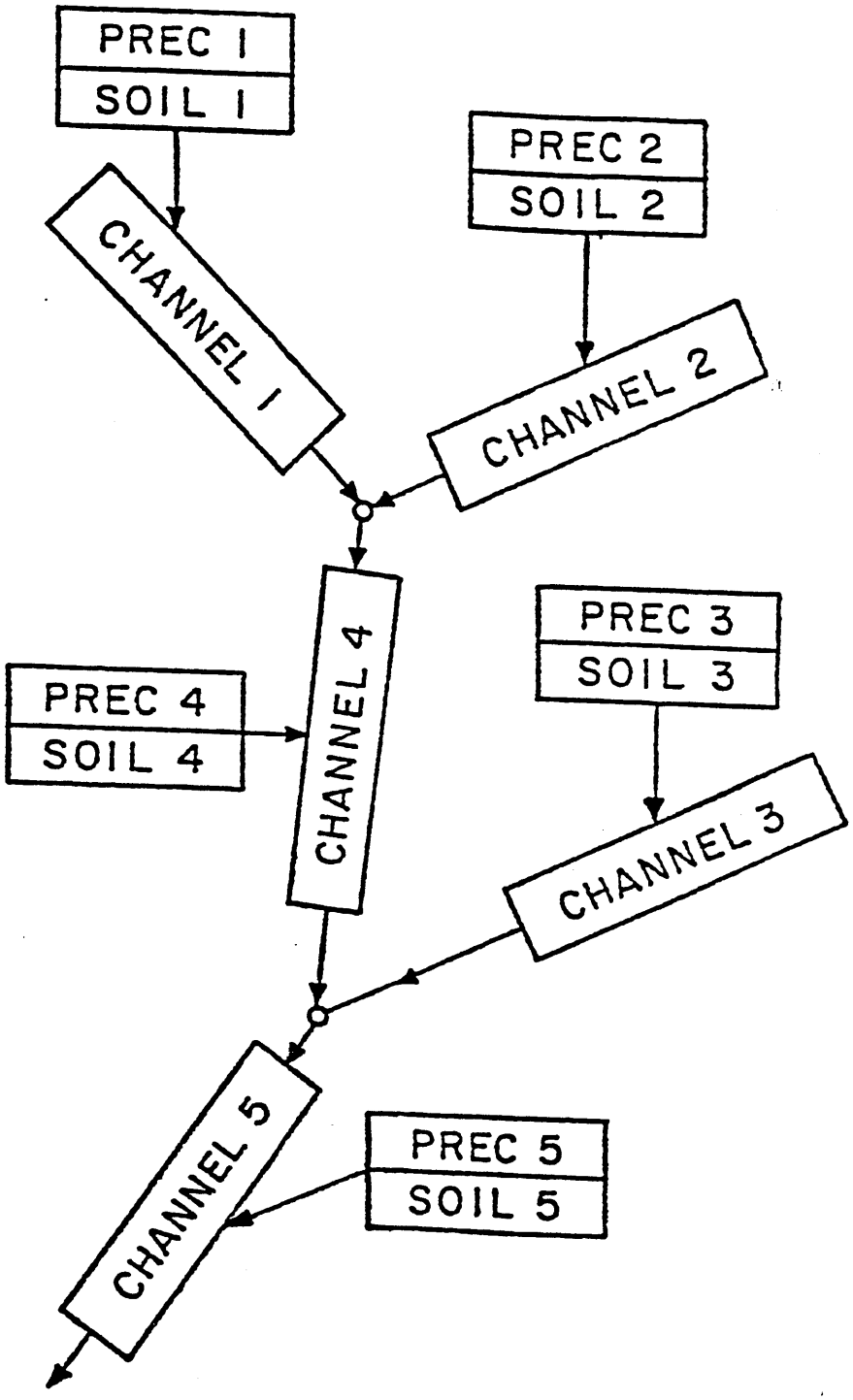

Figure 7.6 Schematic Representation of a Large Scale Basin (after Georgakakos and Bras, 1982)

where $Q'_u(t)$ denotes the upstream discharge input error at time t, F^d the downstream dynamics linearization matrix with respect to the upstream discharge input, and $Q^d(t)$ and $Q^d(t)'$ the originally assigned and discharge input-related spectral density matrices for the downstream sub-basin, respectively.

Because upstream discharges flow directly into the downstream river, the downstream linearizaation matrix F^d (of dimension n x 1) has non-zero values only for the downstream channel states. These non-zero elements are the channel dynamics inflow partitioning coefficients, e.g., for the ith channel state they equal P_i, see Equation (2.10).

Although the precipitation states in different sub-basins are not dynamically related, spatial correlations of their predicted errors may be obtained. Both decomposition methods consider the composite vector of precipitation states on the different sub-basins. The use of a non-diagonal spectral density error matrix for such vector would lead to a non-diagonal error covariance matrix of precipitation predictions, see Equation (3.7).

The difference between the two decomposition methods is that the one of Puente, et al. (1983) also decouples the dynamic equations within each sub-basin. Such procedure forecasts precipitation separately from the rest of the model, and uses the rainfall predictions as inputs to the soil and channel components. As with discharge inputs from tributary basins, the procedure of Puente, et al. (1983) adjusts the spectral density matrix of the soil-channel system by adding the time varying known error from the predicted rainfall inputs.

The decomposition method of Georgakakos (1983) does not decouple states within a basin and therefore accounts for correlations between the precipitation and the soil-channel states within each sub-basin.

Tables 7.1 and 7.2 include the prediction-updating cycles for the two decomposition methods. Notice that the required forecasting ordering (from upstream to downstream sub-basins) is not needed on the updating step.

Observe that both procedures update soil-channel states only from respective discharge observations. The two methods differ in that the procedure of Puente et al. (1983) updates the rainfall states only from precipitation observations, while the method of Georgakakos (1983) uses in addition discharge observations. Because Georgakakos' method computes the rainfall states updatings in two stages, i.e. first using precipitation observations (Step 3) and then using the respective discharge observation (Step 5), an additional step is supplemented (Step 4) in which the correlations between the rainfall and the other states within each sub-basin are maintained after the first stage of updatings.

Because the noise processes of partitioned subsystems and states are properly supplemented, these decomposition methods provide a theoretically sound solution of the filtering of the large scale system, Wood (1981).

The next chapter gives the results of using such block diagonal decomposition filters in a case study.

Table 7.1

Decomposition Algorithm of Puente, et al. (1983)

Step 1: Predict the mean and error covariance matrix of precipitation states in all sub-basins.

Step 2: Predict the means and error covariance matrices of soil-channel states for all sub-basins. Make the predictions following the river path (upstream to downstream), using respective precipitation predictions and respective upsteam discharge predictions from tributary sub-basins as inputs. Include spectral density matrix changes due to such inputs.

Step 3: Update the precipitation states mean and error covariance matrix, from available mean areal precipitation.

Step 4: Update the soil-channel states means and error covariance matrices for all sub-basins, using respective discharge observations.

Table 7.2

Decomposition Algorithm of Georgakakos (1983)

Step 1: Starting from upstream tributary basins, predict the state means and error covariance matrices of the rainfall-runoff model for every sub-basin. Use discharge predictions from tributary basins as inputs when necessary. Include spectral density matrix changes due to such inputs.

Step 2: Predict the error covariance matrix of precipitation states in different sub-basins.

Step 3: Update the mean and error covariance matrix of precipitation states, using observations of mean areal precipitation.

Step 4: Substitute the updated mean and error variance of the precipitation state in place of the predicted error variance for precipitation found in Step 1. In addition change the cross-covariance elements in the predicted error covariance matrix such that the correlations of precipitation and other states found on Step 1 are maintained using the precipitation variances of Step 3. The above changes are done for each sub-basin.

Step 5: Update the mean and error covariance matrices of the whole rainfall-runoff model for every sub-basin, using respective discharge observations.

Chapter 8

PRACTICAL USE OF DECOMPOSITION PROCEDURES

8.1 Introduction

The results of applying the block diagonal decomposition methods on a large basin are presented in this chapter. One step ahead predictions are considered. Also included are forecasts obtained by using global extended Kalman filters on the composite state vector formed by the states of each sub-basin's rainfall-runoff model.

8.2 Description of the Drainage Basin and of the Available Data

The large basin considered in this study belongs to the Potomac River basin with outlet at Millville, West Virginia. The basin is subdivided into five sub-basins located along the north and south forks of the Potomac River. Table 8.1 gives the name of the outlet of each sub-basin together with the sub-basin's area and average elevation. Figure 8.1 is a schematic view of the basin. The north fork runs through sub-basins with outlets at Cootes Store, Strasburg, and Millville; while the south fork runs through sub-basins with outlets at Lynnwood, Front Royal and Millville.

Instantaneous mean areal temperature, pressure, dew point and precipitation data were provided for each of the sub-basins by the NWS-Hydrologic Research Laboratory. The data sets were obtained aver-

Table 8.1

Potomac River Sub-Basins Characteristics

Sub-Basin	Area [Km^2]	Average Elevation [m]
Lynnwood	2808	600
Front Royal	1445	300
Cootes Store	544	700
Strasburg	1445	400
Millville	1632	200

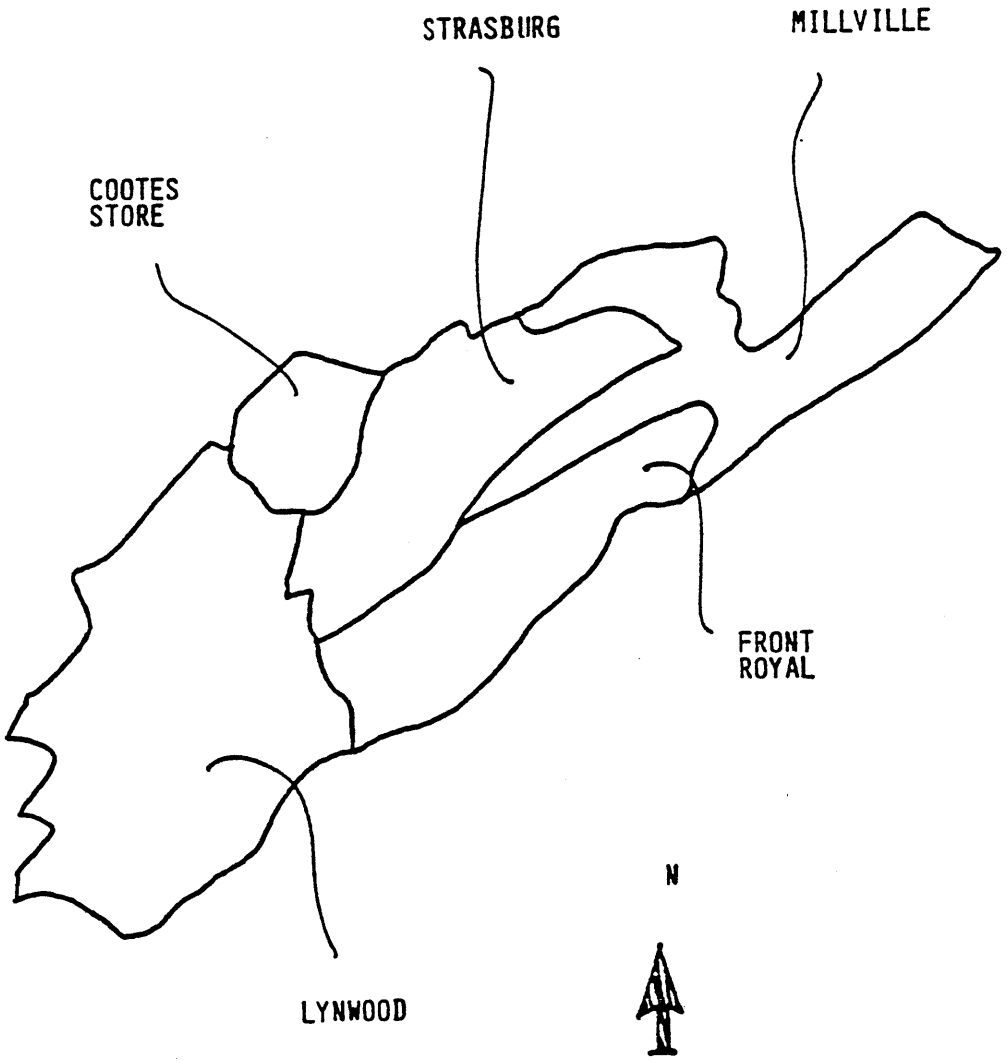

Figure 8.1 Sub-basin Network for the Potomac River Basin with outlet at Millville

aging point observations on and around the sub-basins, Georgakakos (1984).

Evapotranspiration demand was obtained from daily potential evapotranspiration data provided by the NWS. Instantaneous evapotranspiration was obtained weighting the daily values by 0, 0.33, 0.67, and 0, if the time interval in the day is respectively 0-6, 0-12, 12-18, and 18-24 hours.

Bi-hourly discharge values at the outlet of each sub-basin were obtained from local USGS offices for the period October 1969 to September 1971. Table 8.2 includes the minimum, maximum and average flows for each sub-basin. The sub-basins with outlets at Cootes Store and Millville are fast responding with characteristic times of 12 hours; sub-basins with outlets at Lynnwood and Front Royal have characteristic times of 18 hours; while the sub-basin at Strasburg is slow responding with characteristic time of 30 hours. Low flows in the large basin are frequent through the year.

Table 8.3 contains the parameters for the rainfall-runoff model on each of the sub-basins. These values were fixed in all the computations. The precipitation parameters are the location independent values given by Georgakakos (1982). The soil parameters were estimated by the NWS staff through manual calibration and daily data. The channel parameters preserve the routing characteristic times on each sub-basin and were obtained from input-output six-hourly data.

Table 8.2

Discharge Average, Maximum, and Minimum Values for the Potomac River Basin, October 1969 to September 1971

Sub-Basin	Discharge [cfs] Minimum	Maximum	Average
Lynnwood	182.0	21300	1017.5
Front Royal	250.0	41600	1539.0
Cootes Store	3.2	6520	187.5
Strasburg	88.0	12000	606.5
Millville	400.0	50700	2702.0

Table 8.3

Model Parameter Values for the Different

Sub-Basins on the Potomac Basin

Parameter	Lynnwood & Front Royal	Cootes Store	Strasburg	Millville
ε_1	1.65×10^{-3}	1.65×10^{-3}	1.65×10^{-3}	1.65×10^{-3}
ε_4	5.50×10^{-5}	5.50×10^{-5}	5.50×10^{-5}	5.50×10^{-5}
X_1^o	30	70	30	30
X_2^o	20	17	20	10
X_3^o	220	75	200	140
X_4^o	130	19	120	120
X_5^o	40	21	50	30
d_u	1.49×10^{-2}	1.20×10^{-2}	1.49×10^{-2}	1.49×10^{-2}
d'_ℓ	3.35×10^{-4}	1.27×10^{-3}	4.19×10^{-4}	4.19×10^{-4}
d''_ℓ	6.77×10^{-3}	5.80×10^{-3}	6.77×10^{-3}	9.30×10^{-3}
ε	40	220	40	40
Θ	1.4	3.5	1.4	1.4
P_f	0.2	0.2	0.1	0.2
μ	0	0	0	0
β_1	0	0.05	0	0
β_2	0.2	0.001	0.3	0.1

Table 8.3 (continued)

Parameter	Lynnwood & Front Royal	Cootes Store	Strasburg	Millville
m_1, m_2, m_3	2	2	2	2
n	3	2	5	2
P_1	1.0	1.0	1.0	1.0
P_2	0.0	0.0	0.0	0.0
P_3	0.0	--	0.0	--
P_4	--	--	0.0	--
P_5	--	--	0.0	--
a_1	1.0	1.0	1.0	1.0
a_2	1.0	1.0	1.0	1.0
a_3	1.0	--	1.0	--
a_4	--	--	1.0	--
a_5	--	--	1.0	--
m	0.8	0.8	0.8	0.8

The power functions, that approximate the threshold functions of the original Sacramento model, have all exponents equal to two for all sub-basins.

8.3 Deterministic Discharge Predictions on the Large Scale Basin

The months of October and November of 1970 were used to compute deterministic discharge predictions, decoupling states as in the decomposition procedure of Puente, et al. (1983). Observed precipitation values were used as inputs to the soil, and predicted discharge values became inputs to downstream sub-basins. Snow accumulation and ablation did not occur during this period of time.

The initial mean values used for the states on each of the sub-basins are included in Table 8.4. Figures 8.2 to 8.6 show the deterministic discharge observations and predictions on the various sub-basins (see Figures 8.7 to 8.11 for the observed rainfall). As can be seen, all sub-basins except the one with outlet at Cootes Store predict a big unrecorded discharge peak around time step 90. The basins predicted response is very rapid, as implied by the steeply rising and declining segments of the hydrographs. It is common for such sub-basins to overpredict discharge, with the sub-basin with outlet at Strasburg overpredicting the most. On the other hand, the sub-basin with outlet at Cootes Store gives predictions that do not exceed the observed discharges.

Table 8.4

Initial State Means for the Different Sub-Basins

on the Potomac Basin

State	Lynnwood & Front Royal	Cootes Store	Strasburg	Millville
X_p	2	2	2	2
X_1	5	10	5	5
X_2	5	5	5	2
X_3	10	10	10	10
X_4	10	10	10	10
X_5	10	10	10	10
X_6	5	5	5	5
S_1	10^{-2}	10^{-2}	10^{-2}	10^{-2}
S_2	10^{-2}	10^{-2}	10^{-2}	10^{-2}
S_3	10^{-2}		10^{-2}	
S_4			10^{-2}	
S_5			10^{-2}	

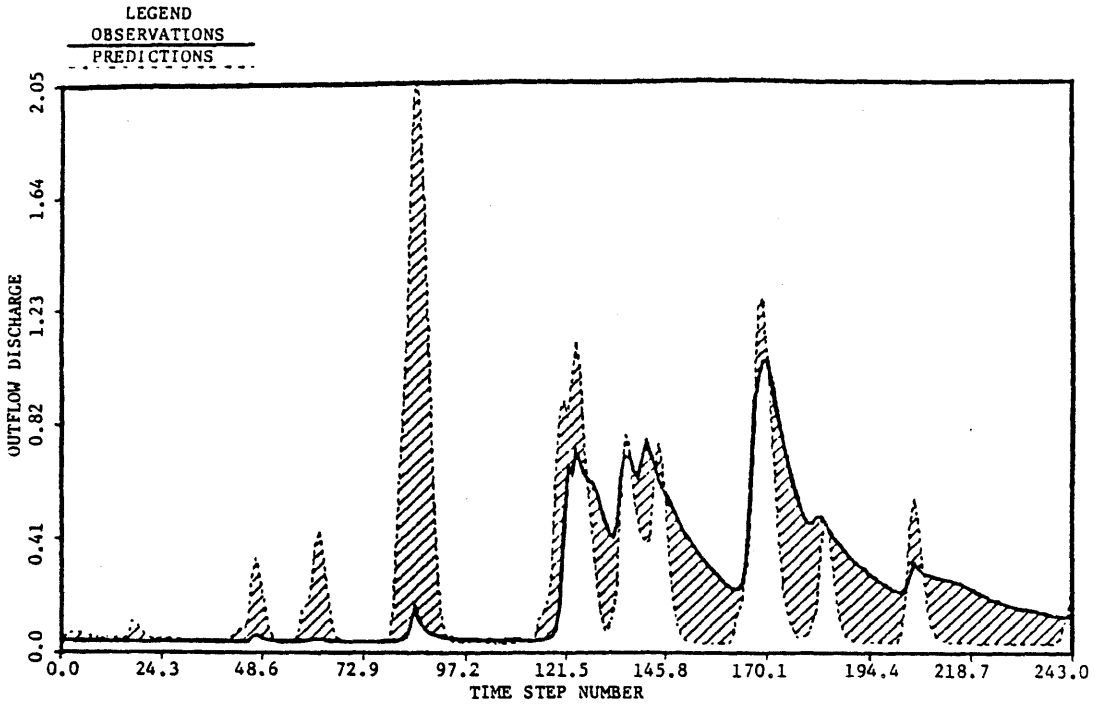

Figure 8.2 Deterministic Prediction of Discharge, Lynnwood, Observed Rainfall as Input, October-November 1970

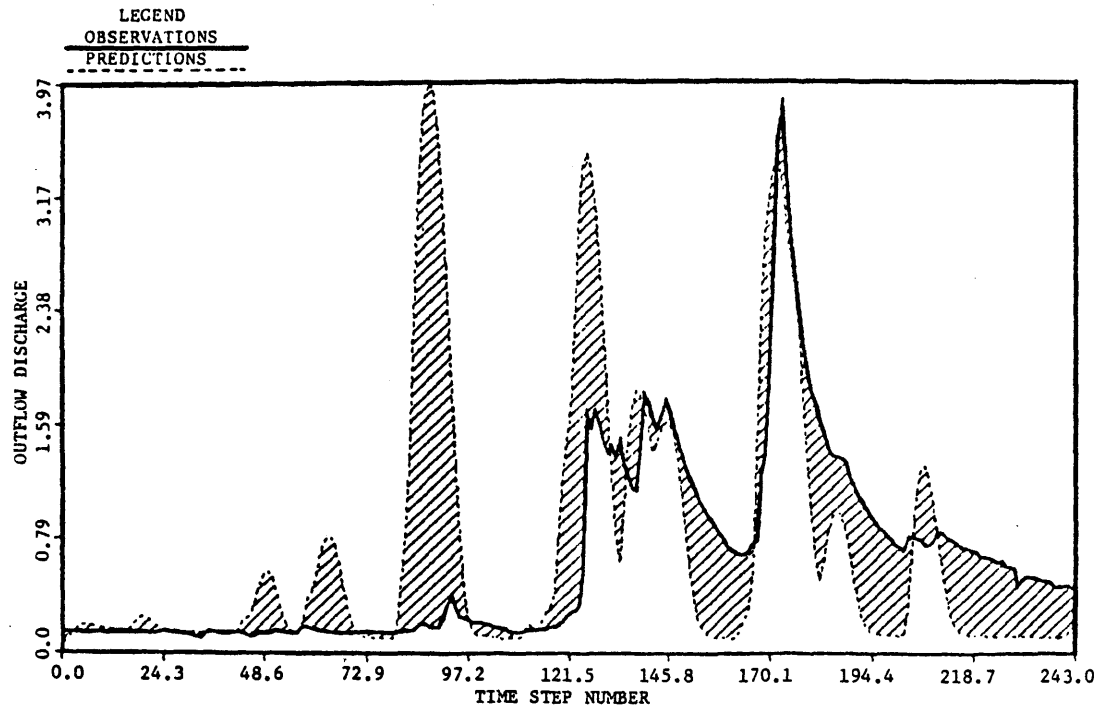

Figure 8.3 Deterministic Prediction of Discharge, Front Royal, Observed Rainfall as Input, October-November 1970

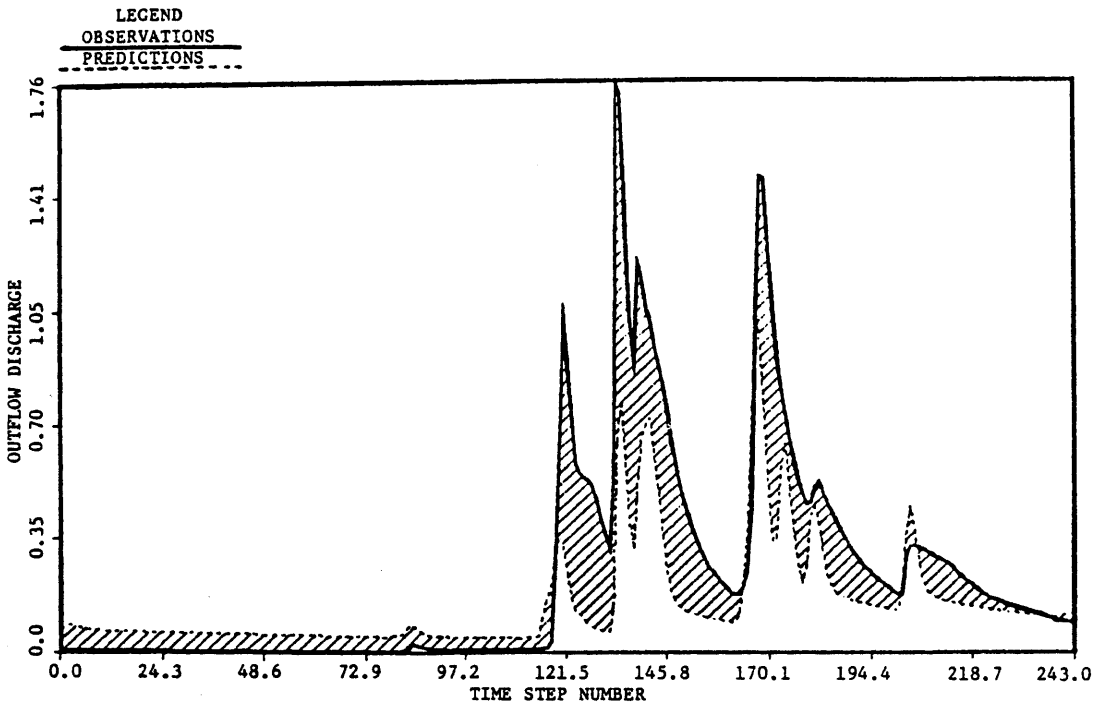

Figure 8.4 Deterministic Prediction of Discharge, Cootes Store, Observed Rainfall as Input, October-November 1970

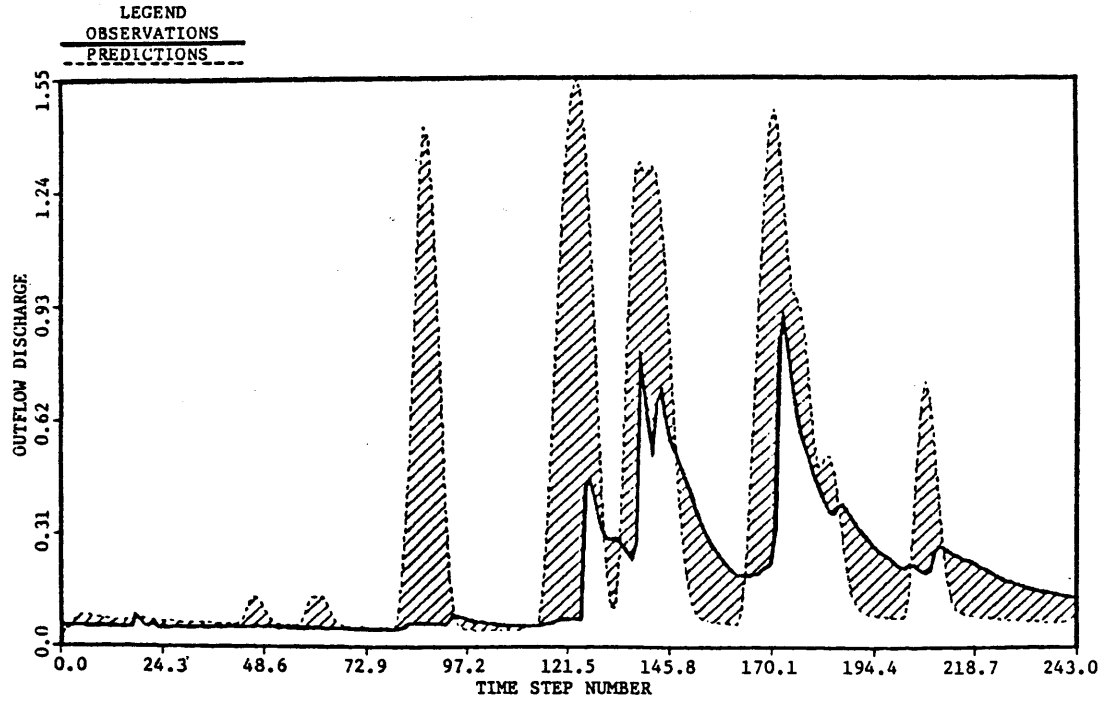

Figure 8.5 Deterministic Prediction of Discharge, Strasburg, Observed Rainfall as Input, October-November 1970

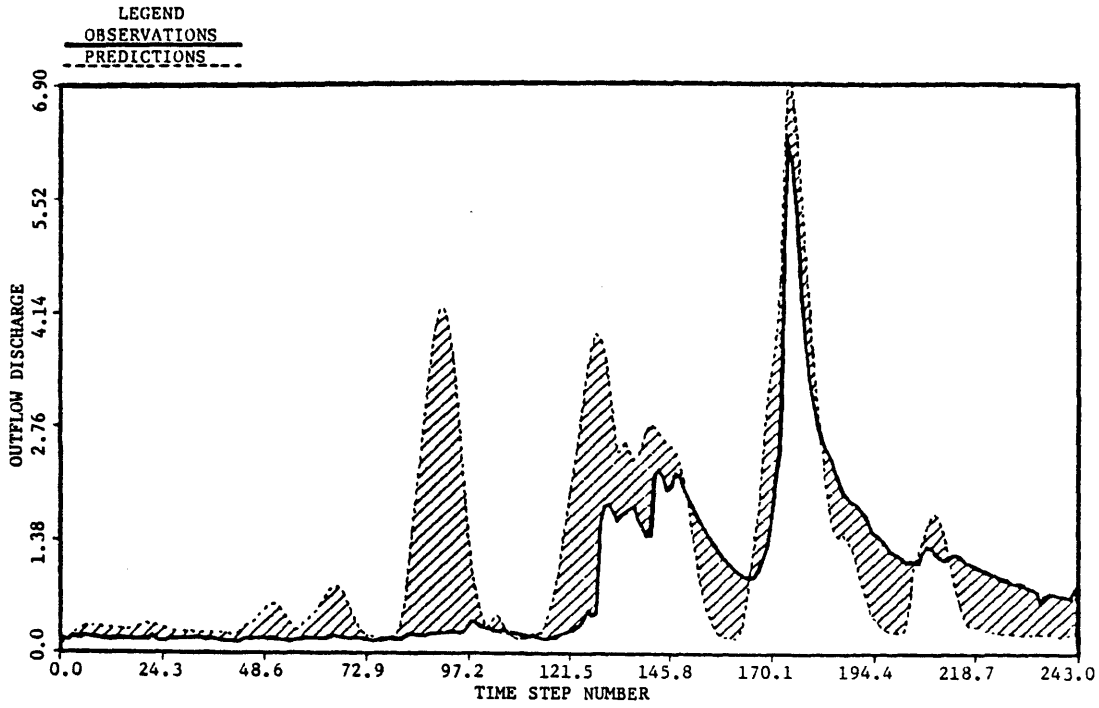

Figure 8.6 Deterministic Prediction of Discharge, Millville, Observed Rainfall as Input, October-November 1970

A possible explanation of the poor performance of the deterministic predictions is that the conceptual model parameters were not properly calibrated. For sub-basins other than Cootes Store the drainage coefficient of the upper zone, d_u, seems too big in contrast to the lower zone drainage coefficients, d'_ℓ and d''_ℓ, giving as a result low percolation to lower aquifers and high interflow. In addition, the upper zone tension capacities, X_1^o and X_2^o may be too small. For the sub-basin with outlet at Cootes Store the upper zone tension capacity, X_1^o, seems too large, producing high infiltration and therefore low discharge predictions.

Another possible cause of the discrepancies between the deterministic predictions and the discharge observations is that the rainfall records contain errors. There are no rainfall gages in the sub-basin with outlet at Cootes Store. But even for the rest of the sub-basins, which all contain rainfall gages, the transition for point data to areal averages could result in errors in the rainfall data.

8.4 Stochastic Predictions on the Large Basin

The conceptual rainfall-runoff model was used together with the filtering algorithms to produce predictions of mean areal precipitation as well as discharge over the large basin.

Table 8.5 shows the spectral density standard deviations used on each of the sub-basins. The values are based on the experience acquired from the results of Chapter 6. A diagonal spectral density matrix was assumed for the states of each sub-basin. Also, the dynamic precipitation noises for all sub-basins were assumed uncorrelated. The initial mean state vectors used on each sub-basin were the same employed on the deterministic discharge predictions, i.e., those of Table 8.4. The initial error covariance matrix for all sub-basins was taken diagonal, with standard deviations of 10^{-1} for precipitation and soil states and 10^{-4} for channel states. The observations noise covariance matrix of Table 4.5 was used for all sub-basins.

In addition to the block-diagonal decomposition procedures of Puente, et al. (1983) and Georgakakos (1983), two filters which use off-block diagonal information were employed. First, a global filter in two levels was obtained by forming a multivariable precipitation model (as in the decomposition procedure of Puente, et al. (1983)) whose predictions serve as rainfall inputs to a global soil-channel model that has as state vector the soil-channel states of all sub-basins. The procedure uses off-block diagonal information resulting from the linearization of channel equations with respect to tributary inflows. Such information provides off-block diagonal error covariances which allow the updating of soil-channel models not only from their respective discharge observations, but from discharges observed in other sub-basins as well. The second off-block diagonal filter

Table 8.5

Spectral Density Matrix Diagonal Standard Deviations for the Different Sub-Basins on the Potomac Basin

State	Lynnwood & Front Royal	Cootes Store	Strasburg	Millville
X_p	20	20	20	20
X_1	10	20	10	10
X_2	10	8	10	5
X_3	10^{-5}	10^{-5}	10^{-5}	10^{-5}
X_4	10^{-5}	10^{-5}	10^{-5}	10^{-5}
X_5	20	10	25	15
X_6	10^{-5}	10^{-5}	10^{-5}	10^{-5}
S_1	1.0	1.0	1.0	1.0
S_2	1.0	0.17	1.0	0.17
S_3	0.17		1.0	
S_4			1.0	
S_5			0.17	

considers all precipitation-soil-channel states as a global state; with updating on all sub-basins depending on all observations of mean areal precipitation and discharge.

The spectral density matrix of sub-basins with tributaries was adjusted by the inflows variance using Equation 7.1. Such equation was also employed to adjust the spectral density matrix of soil-channel models that use a separate multivariable precipitation model as input in the filtering procedure.

All filtering methods were applied to the Potomac River basin for the period starting October 12 and ending November 30 of 1970. All methods yielded the same precipitation predictions, shown in Figures 8.7 to 8.11. Excessive predictions occur in all sub-basins, especially on the first half of the period considered. As was found for the Bird Creek basin, the precipitation model inputs play a dominant role on the rainfall predictions. As a result, the updating portion of the filters has little effect. Possible causes for the overpredictions of precipitation are calibration errors on the rainfall model, and more likely errors resulting from the conversion of point input meteorologic data to areal averages.

Figures 8.12 to 8.31 show the discharge predictions for all sub-basins obtained when using the different filtering procedures. These figures are ordered according to the filtering mechanism as follows:

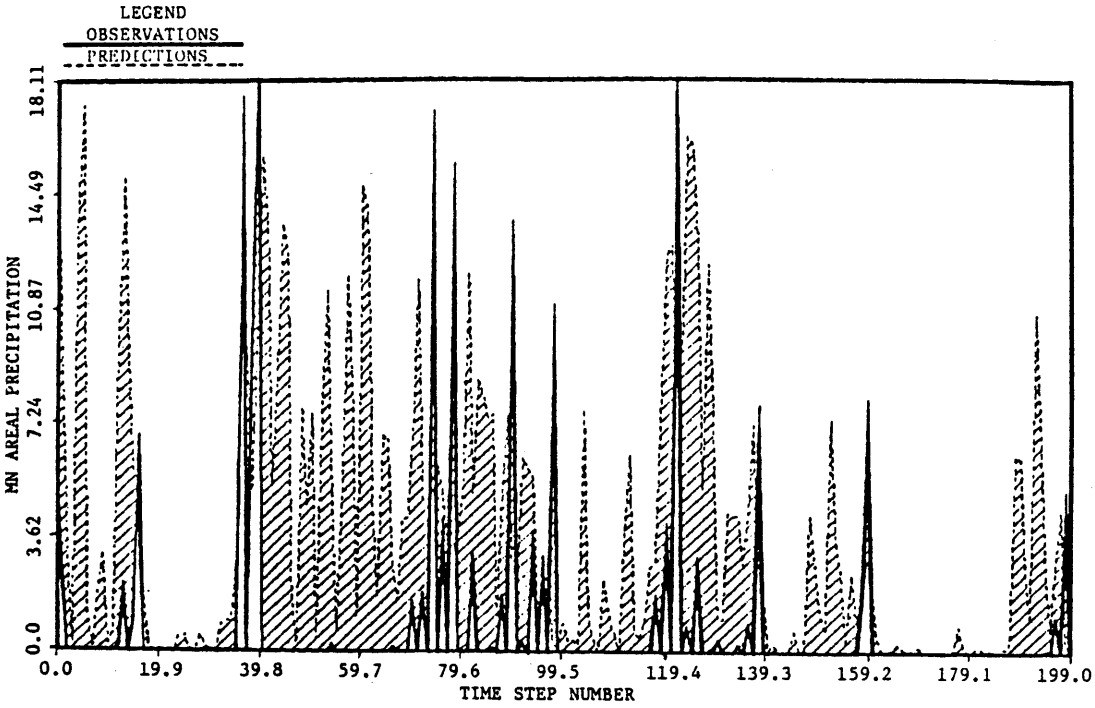

Figure 8.7 Stochastic Prediction of Precipitation, Lynnwood, October 12 to November 30, 1970

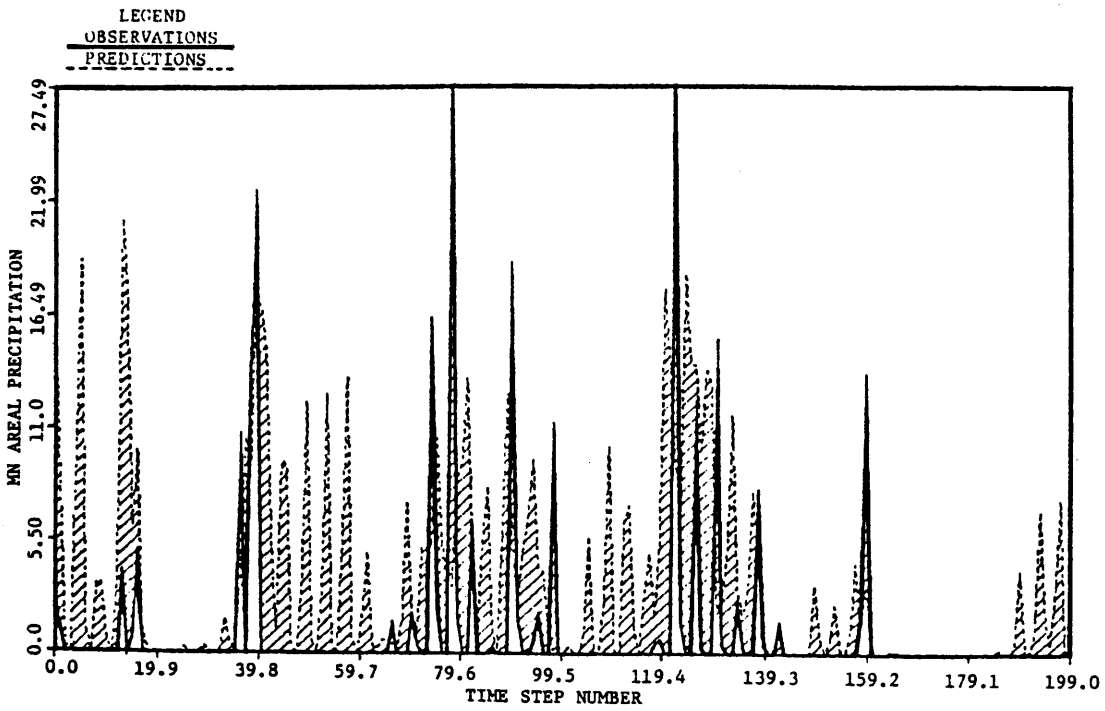

Figure 8.8 Stochastic Prediction of Precipitation, Front Royal, October 12 to November 30, 1970

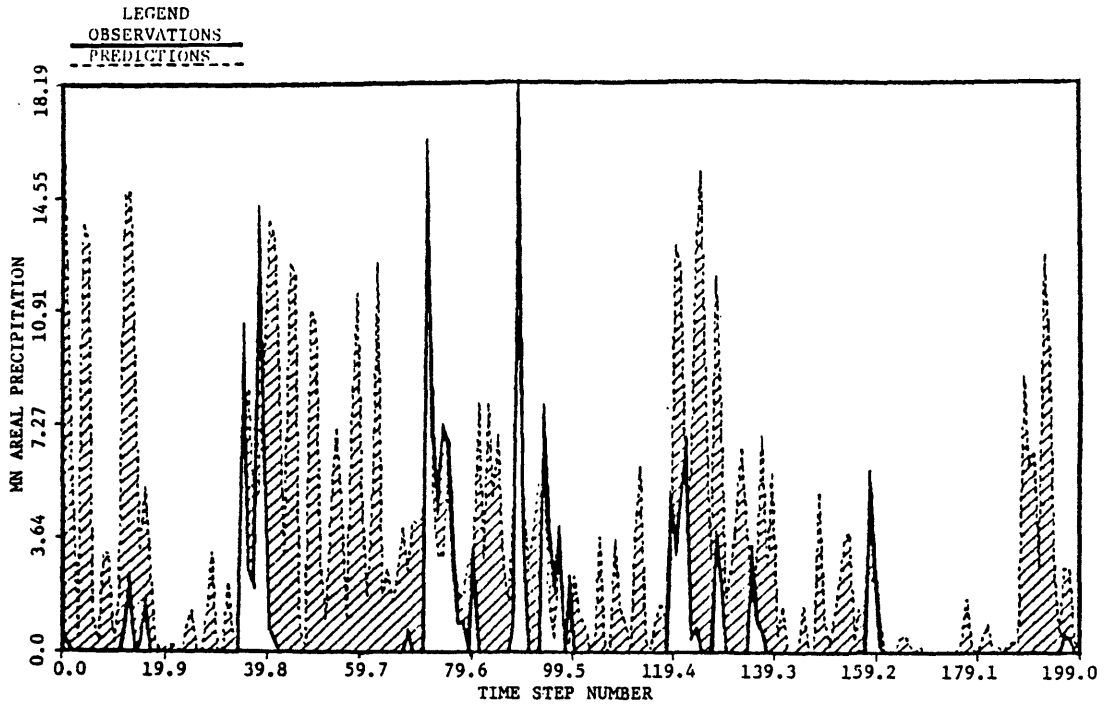

Figure 8.9 Stochastic Prediction of Precipitation, Cootes Store, October 12 to November 30, 1970

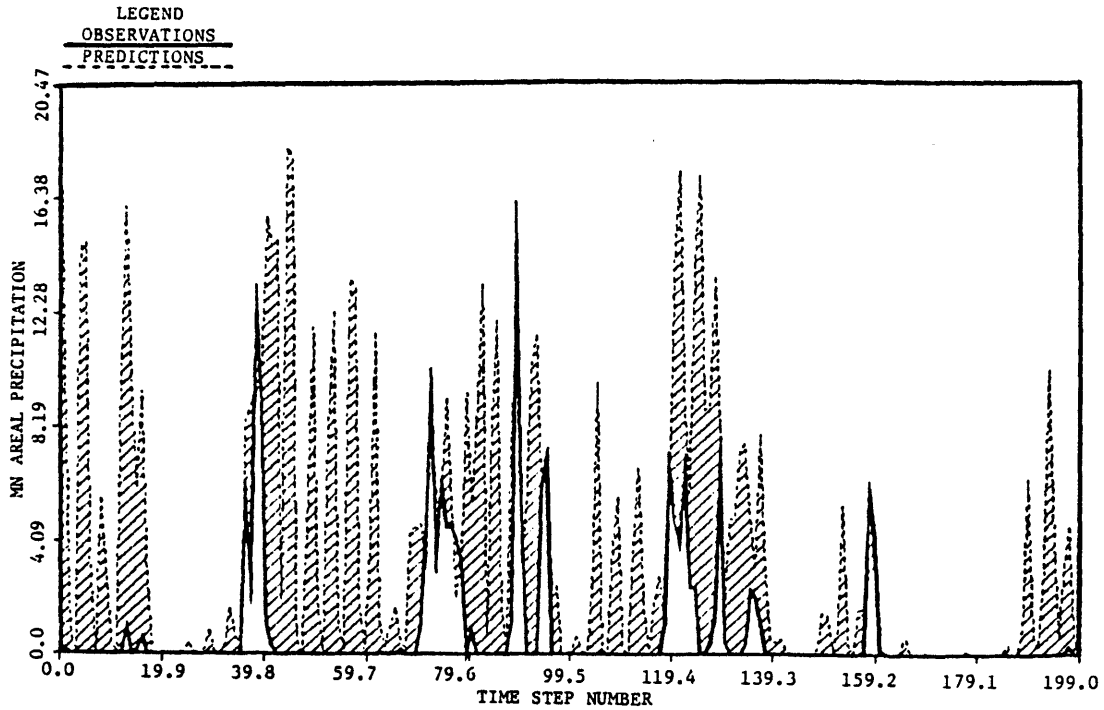

Figure 8.10 Stochastic Prediction of Precipitation, Strasburg, October 12 to November 30, 1970

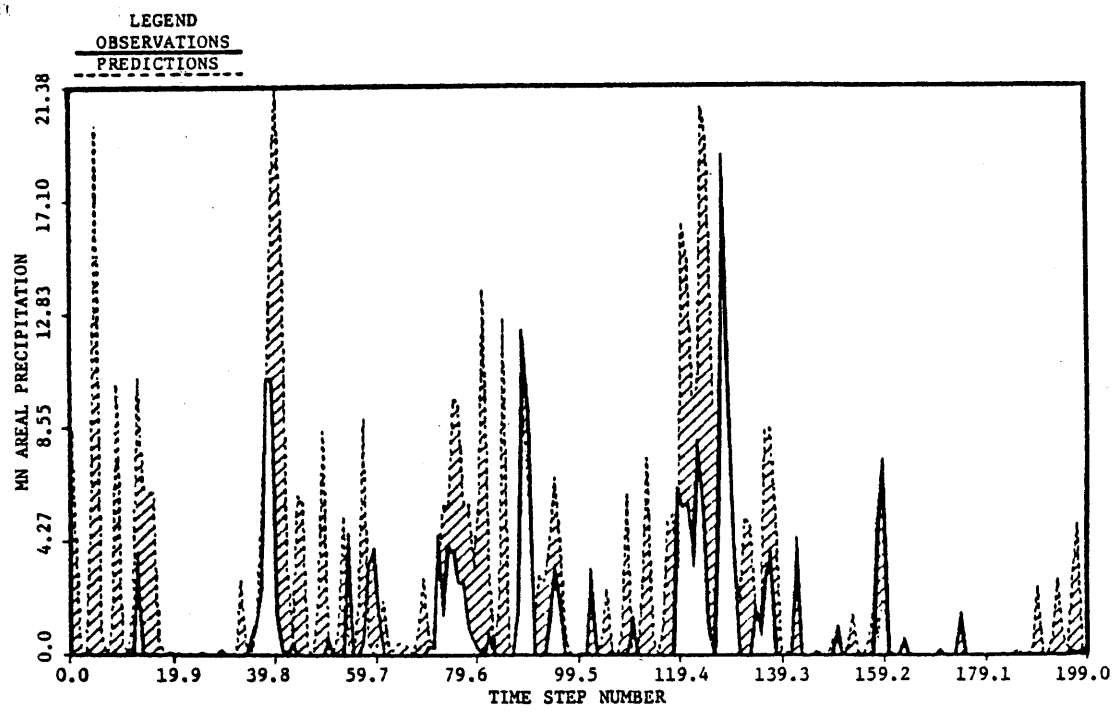

Figure 8.11 Stochastic Prediction of Precipitation, Millville, October 12 to November 30, 1970

the decomposition procedure of Puente, et al., the decomposition procedure of Georgakakos, the global filter in two levels, and the global filter.

As can be observed, rainfall excesses give discharge overpredictions. The filtering mechanisms provide better predictions than those obtained from deterministic propagation of the model dynamics, except for the sub-basin with outlet at Strasburg. Notice that for that sub-basin the deterministic predictions were in significant error, relative to excess volume. The precipitation model overpredicts rainfall resulting in even worst overpredictions, which could not be corrected by the filter. The filtering mechanisms could possibly result in better predictions at Strasburg with reduced observation error.

Very good discharge predictions were obtained using any of the filtering mechanisms for the sub-basins with outlets at Front Royal, Cootes Store and in particular at the outlet of the total basin at Millville. Notice that the excessive discharge predictions at Strasburg do not affect considerably the predictions at Millville.

Discharge predictions using the decomposition procedures show oscillatory behavior for low and some times medium flows in all sub-basins. This oscillations may be decreased by increasing the assumed discharge observation variance. Such periods are, however, non-existent when using any of the global filters. The use of discharge observations from other sub-basins therefore serves as a stabilizing mechanism.

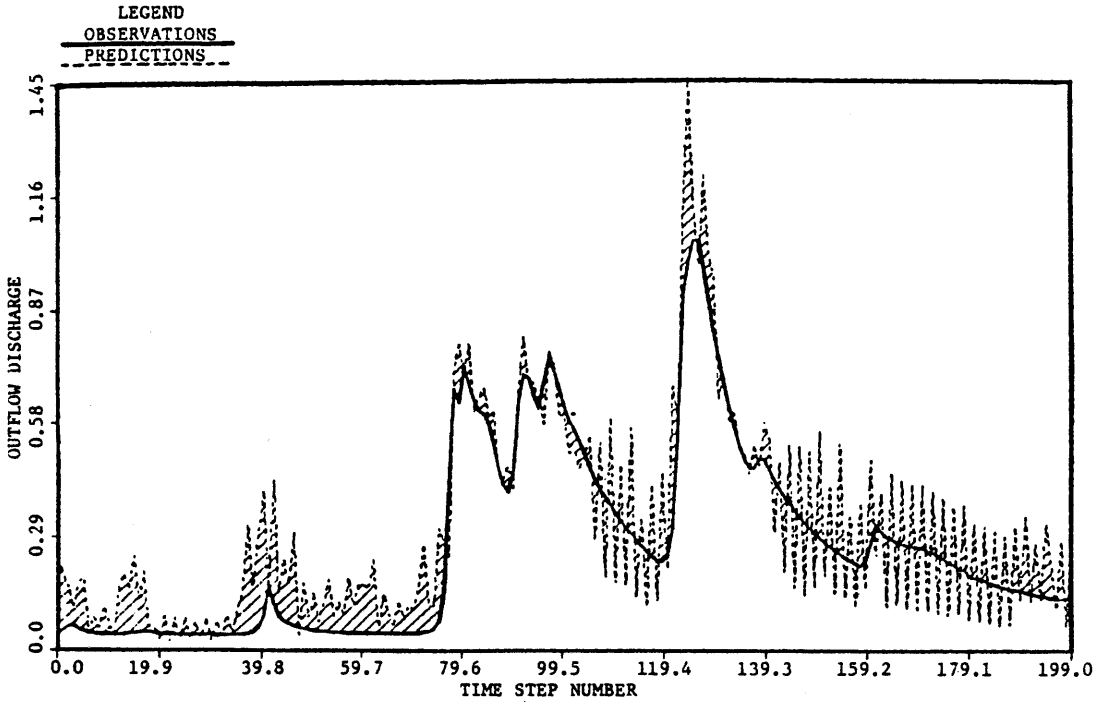

Figure 8.12 Stochastic Prediction of Discharge, Lynnwood, Decomposition Procedure of Puente, et al., October 12 to November 30, 1970

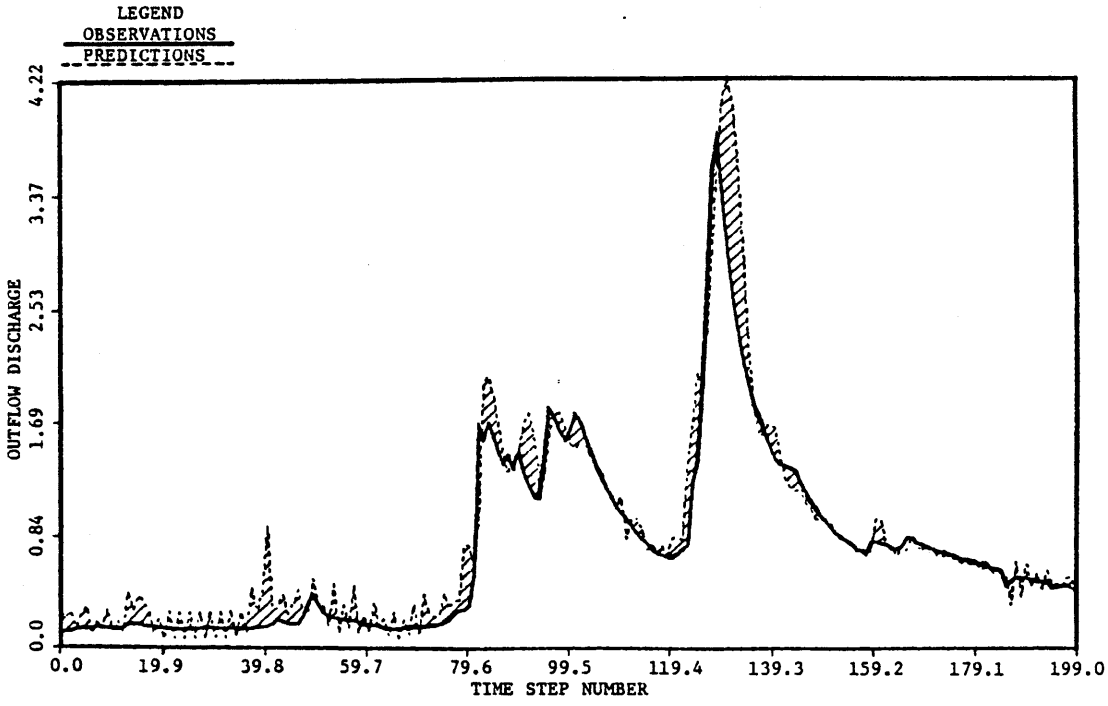

Figure 8.13 Stochastic Prediction of Discharge, Front Royal, Decomposition Procedure of Puente, et al., October 12 to November 30, 1970

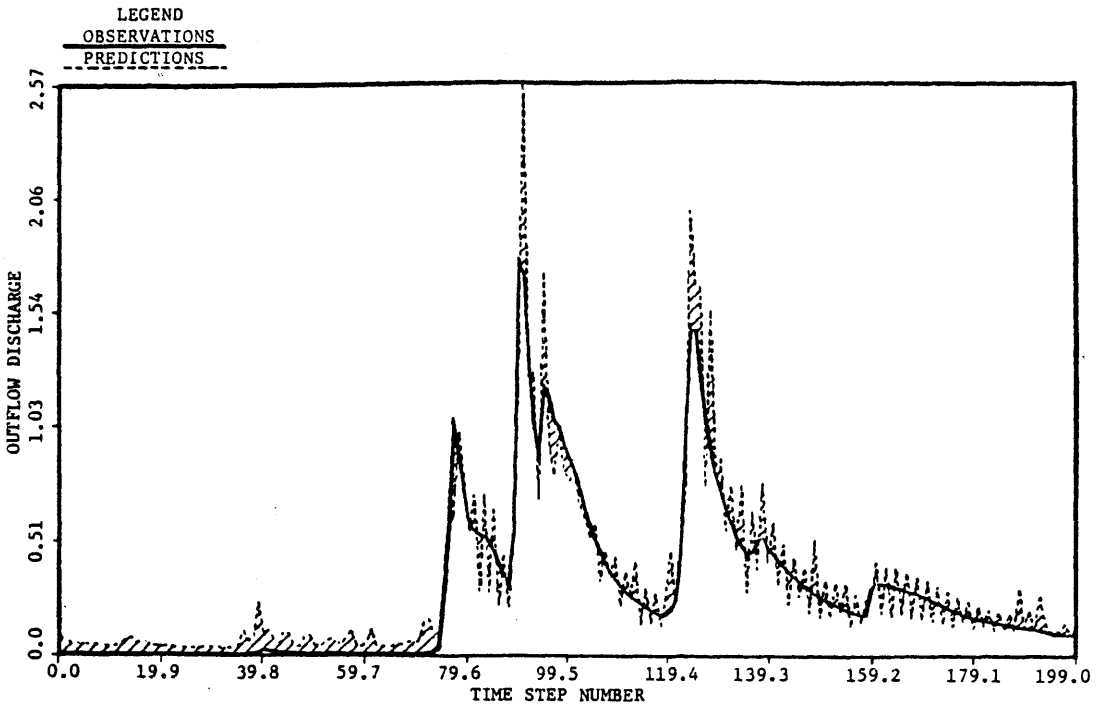

Figure 8.14 Stochastic Prediction of Discharge, Cootes Store, Decomposition Procedure of Puente, et al., October 12 to November 30, 1970

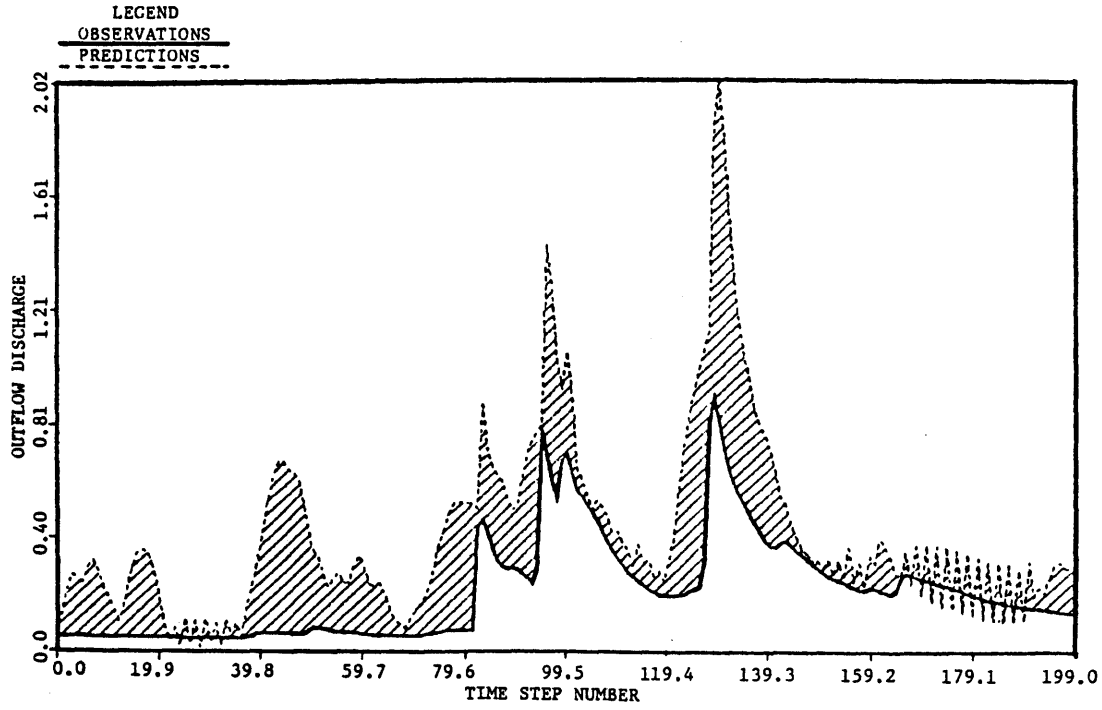

Figure 8.15 Stochastic Prediction of Discharge, Strasburg, Decomposition Procedure of Puente, et al., October 12 to November 30, 1970

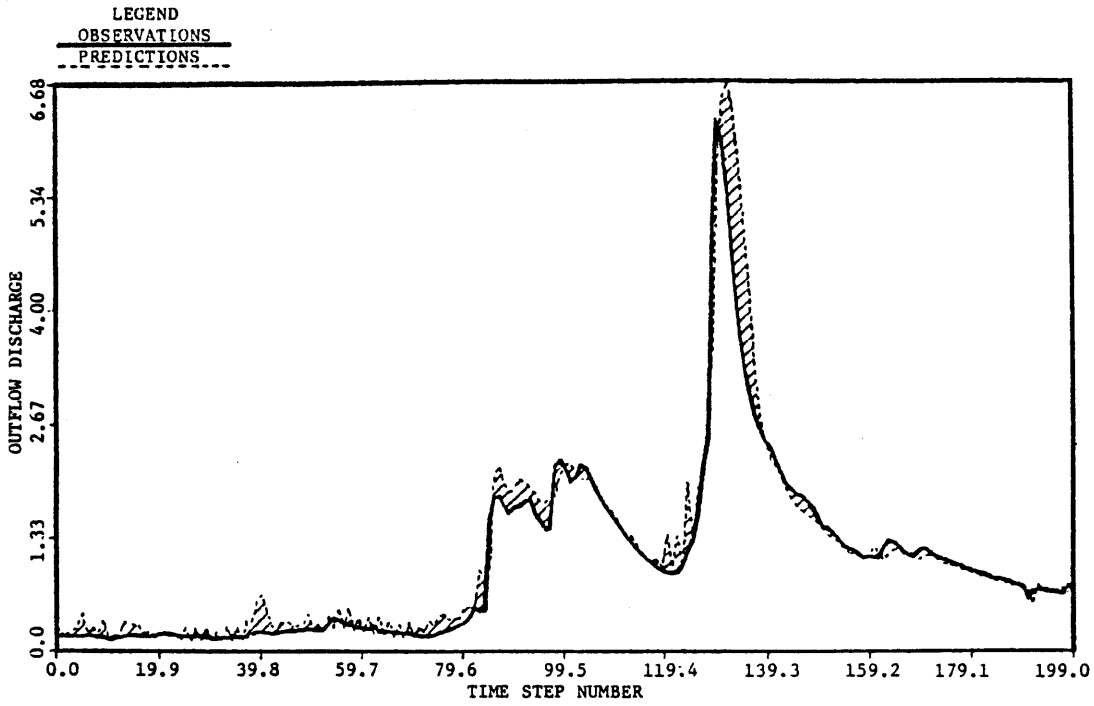

Figure 8.16 Stochastic Prediction of Discharge, Millville, Decomposition Procedure of Puente, et al., October 12 to November 30, 1970

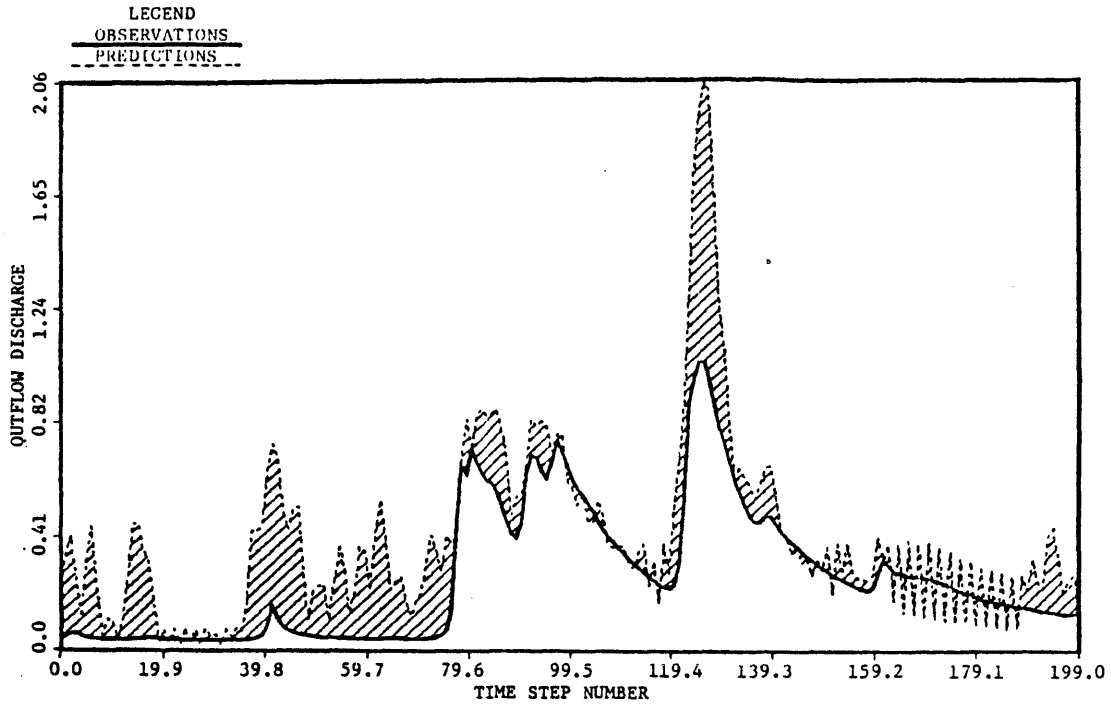

Figure 8.17 Stochastic Prediction of Discharge, Lynnwood, Decomposition Procedure of Georgakakos, October 12 to November 30, 1970

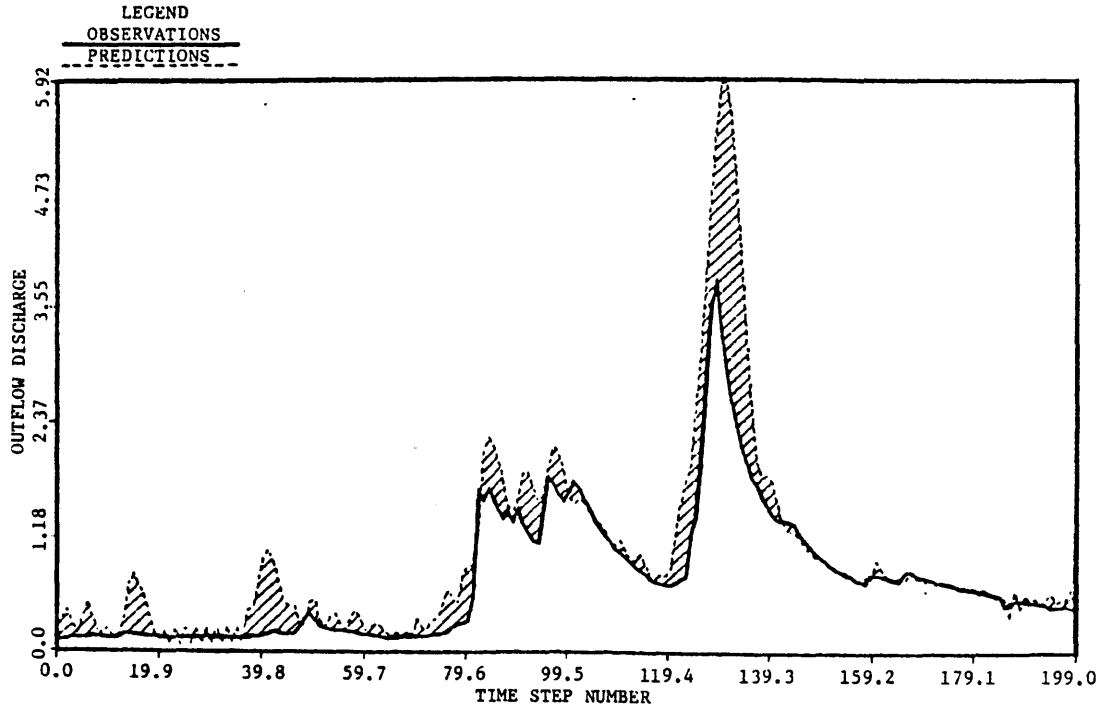

Figure 8.18 Stochastic Prediction of Discharge, Front Royal, Decomposition Procedure of Georgakakos, October 12 to November 30, 1970

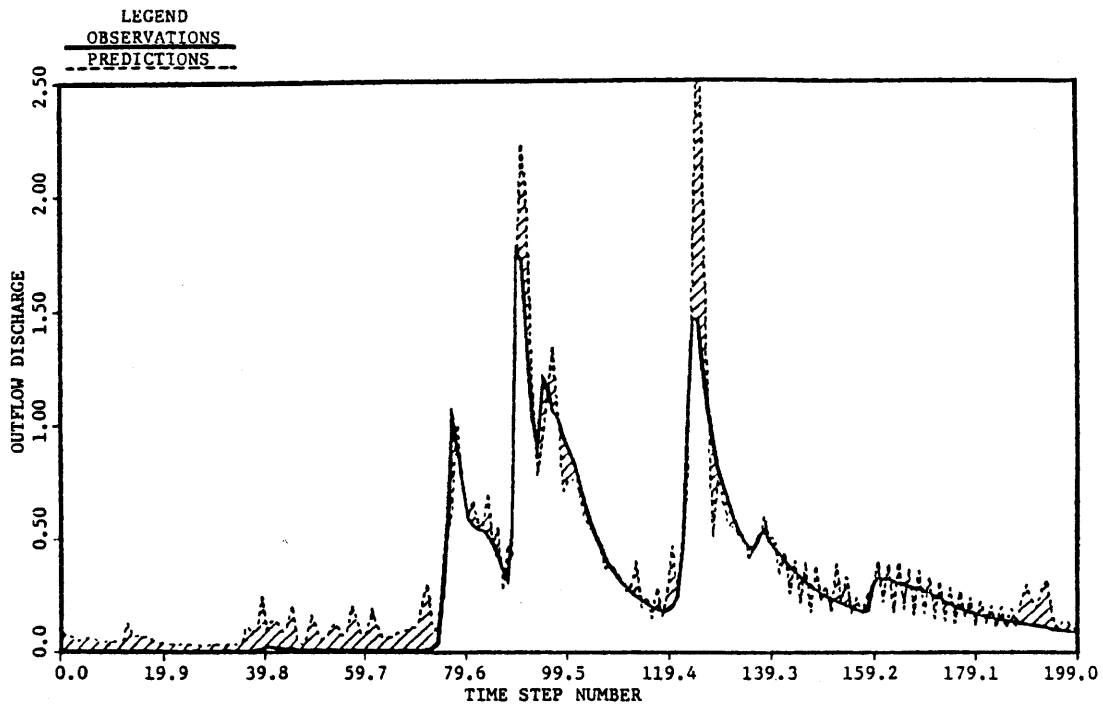

Figure 8.19 Stochastic Prediction of Discharge, Cootes Store, Decomposition Procedure of Georgakakos, October 12 to November 30, 1970

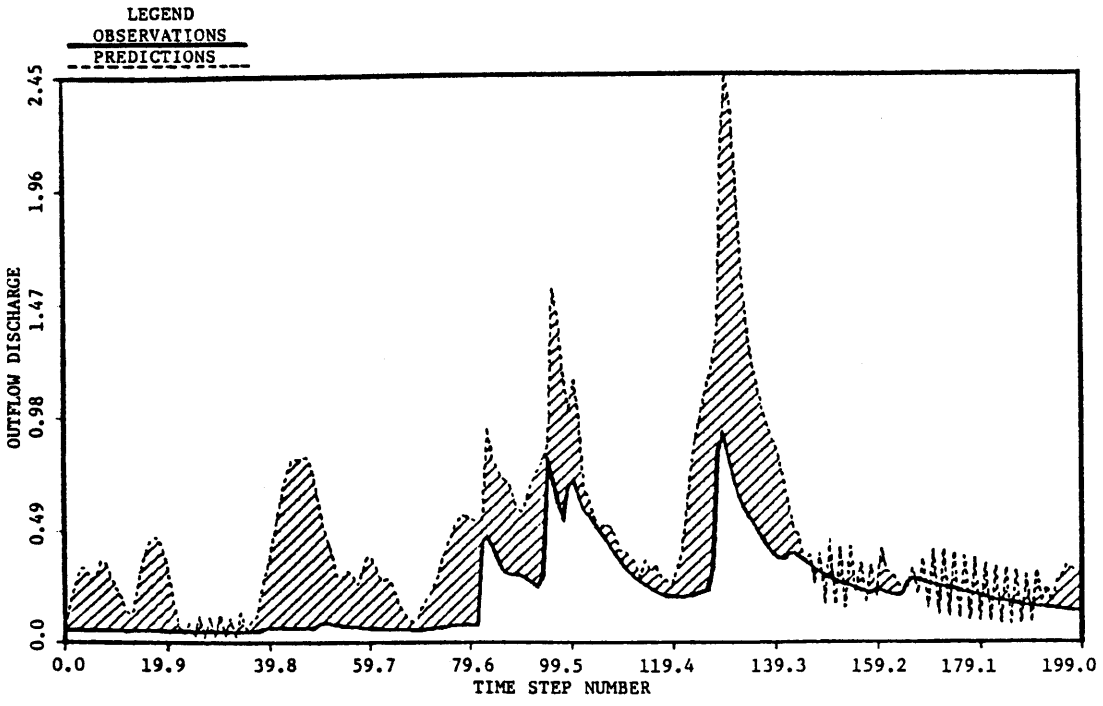

Figure 8.20 Stochastic Prediction of Discharge, Strasburg, Decomposition Procedure of Georgakakos, October 12 to November 30, 1970

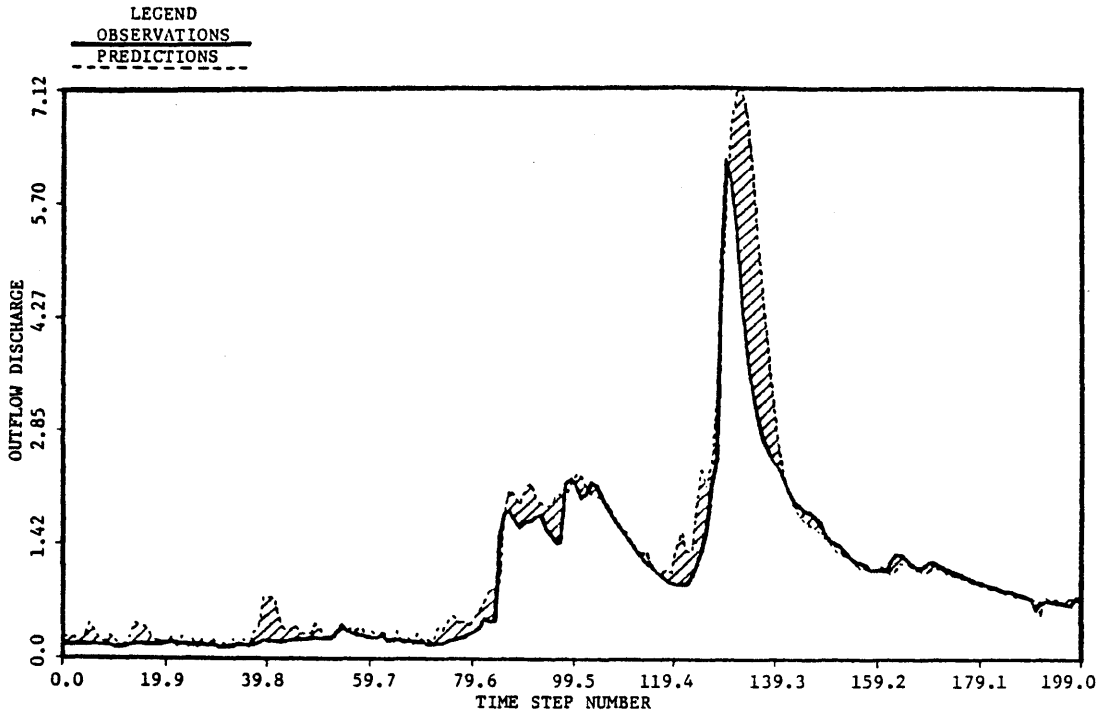

Figure 8.21 Stochastic Prediction of Discharge, Millville, Decomposition Procedure of Georgakakos, October 12 to November 30, 1970

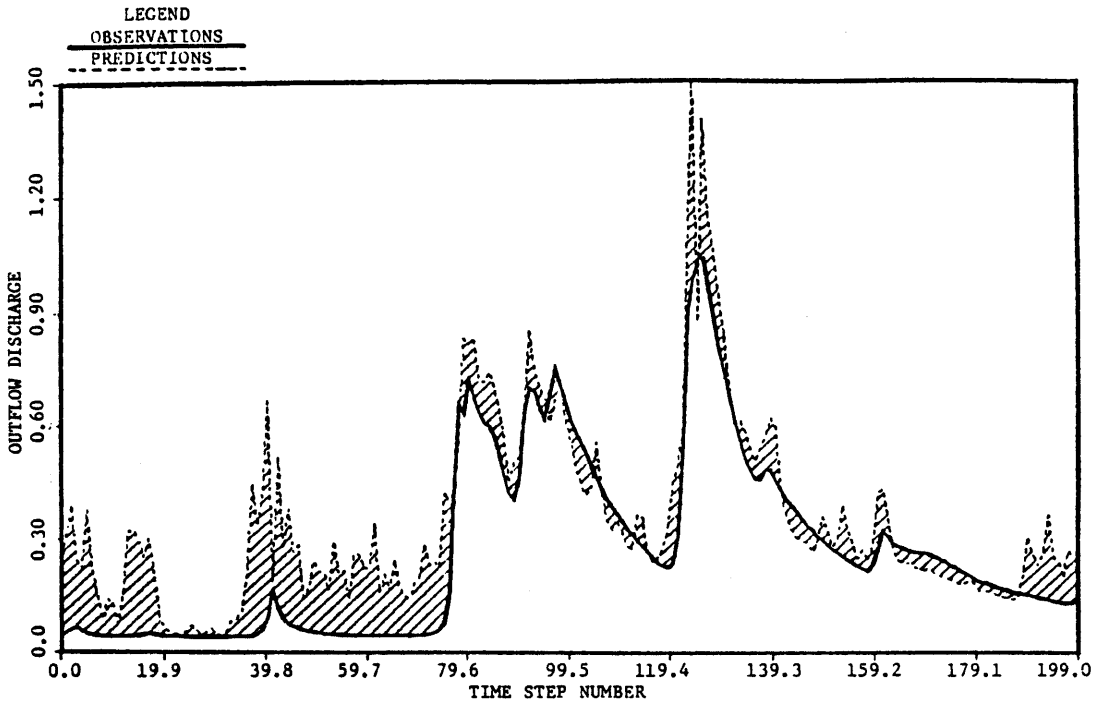

Figure 8.22 Stochastic Prediction of Discharge, Lynnwood, Global Filter in Two Levels, October 12 to November 30, 1970

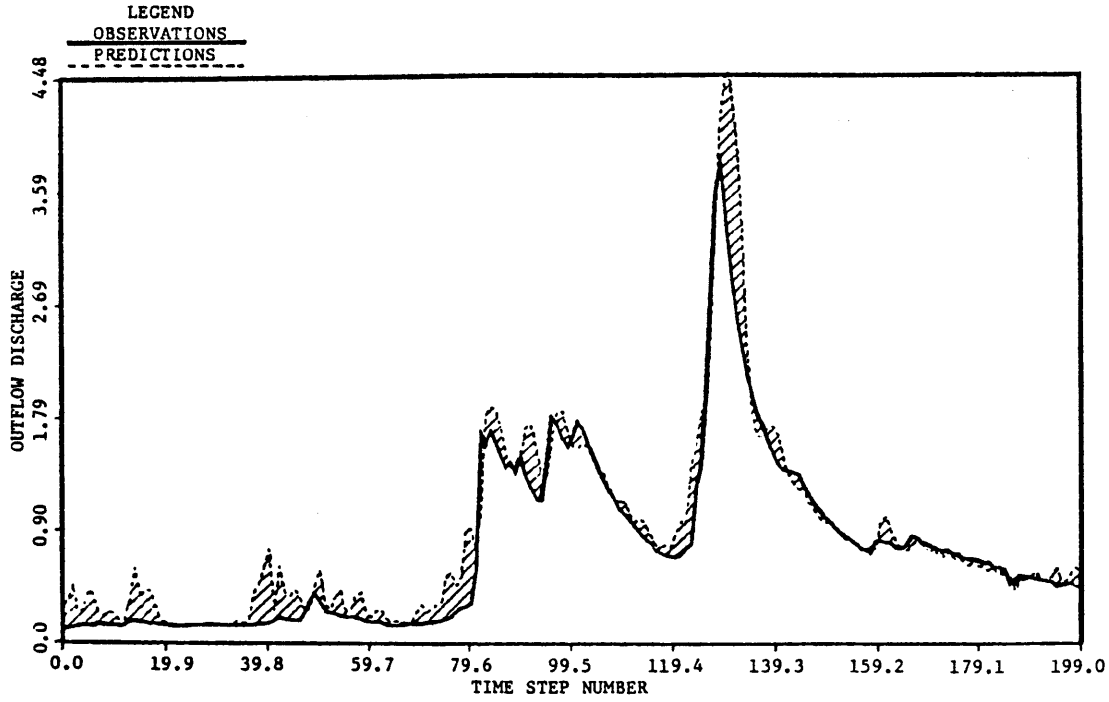

Figure 8.23 Stochastic Prediction of Discharge, Front Royal, Global Filter in Two Levels, October 12 to November 30, 1970

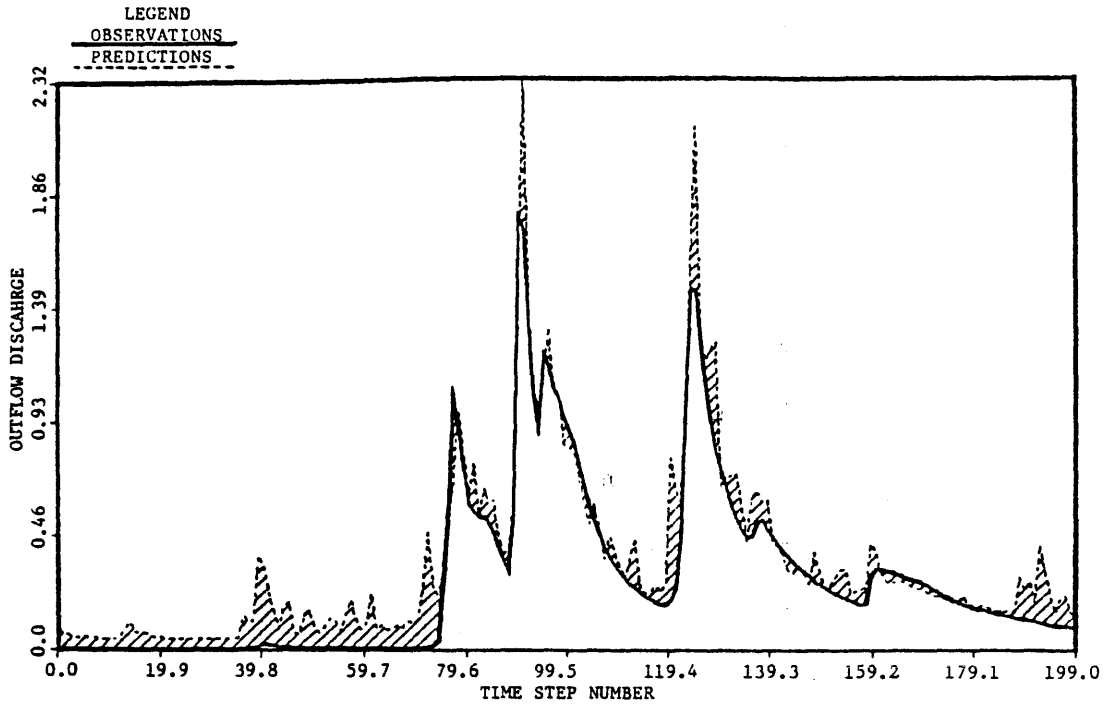

Figure 8.24 Stochastic Prediction of Discharge, Cootes Store, Global Filter in Two Levels, October 12 to November 30, 1970

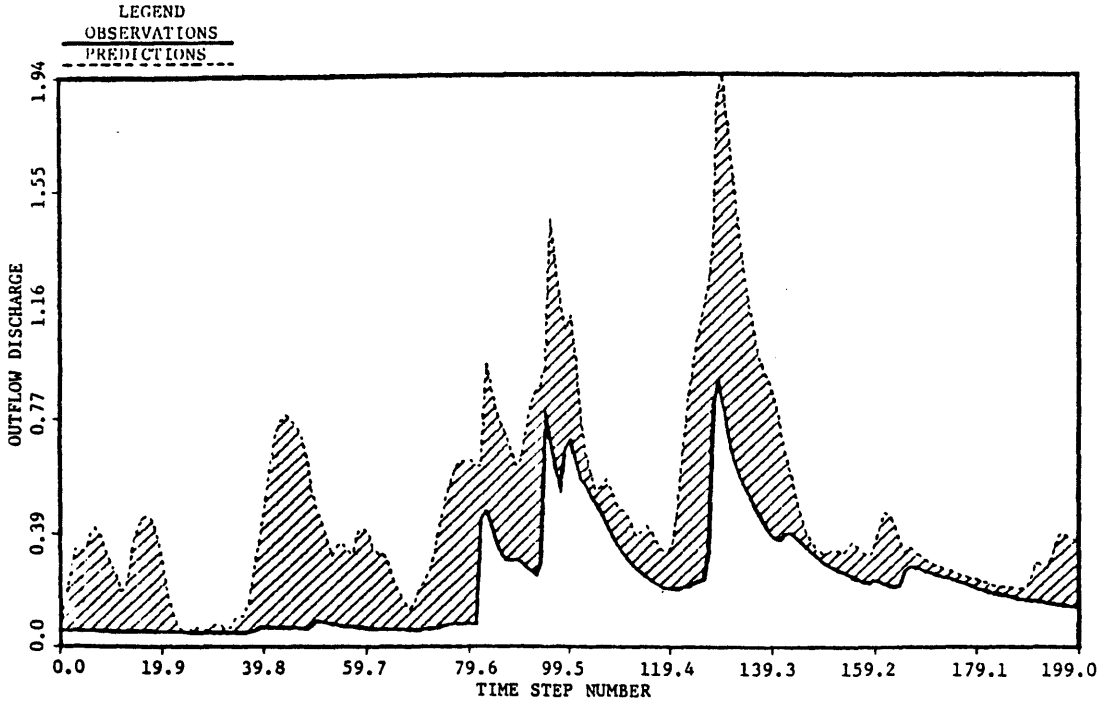

Figure 8.25 Stochastic Prediction of Discharge, Strasburg, Global Filter in Two Levels, October 12 to November 30, 1970

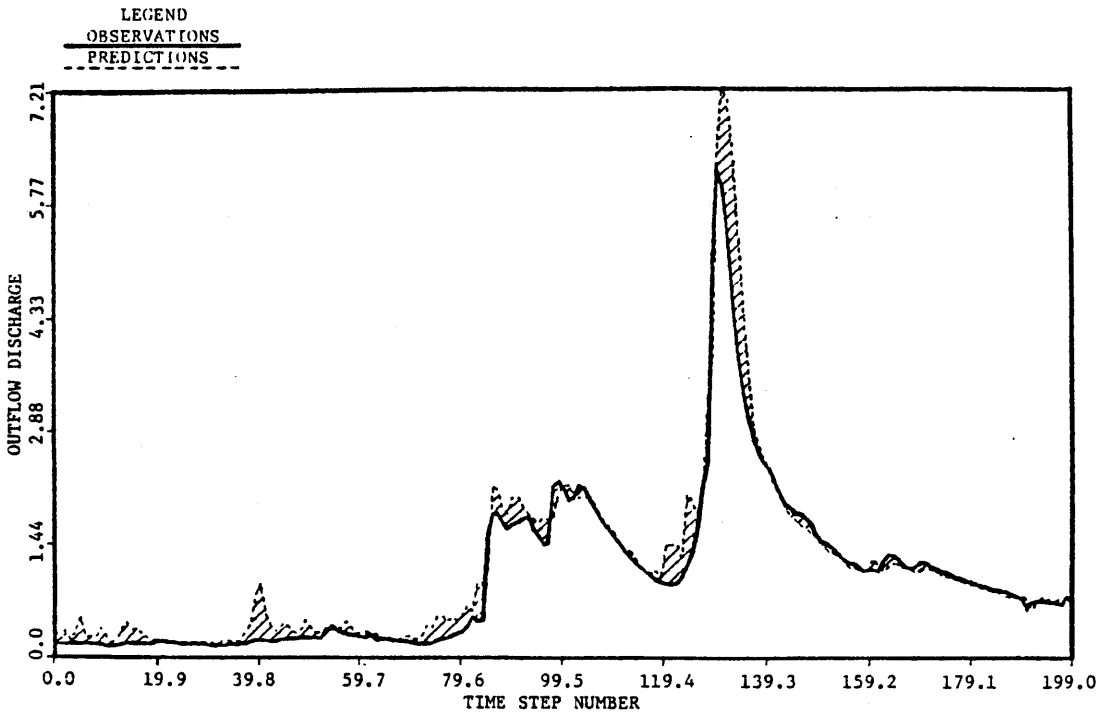

Figure 8.26 Stochastic Prediction of Discharge, Millville, Global Filter in Two Levels, October 12 to November 30, 1970

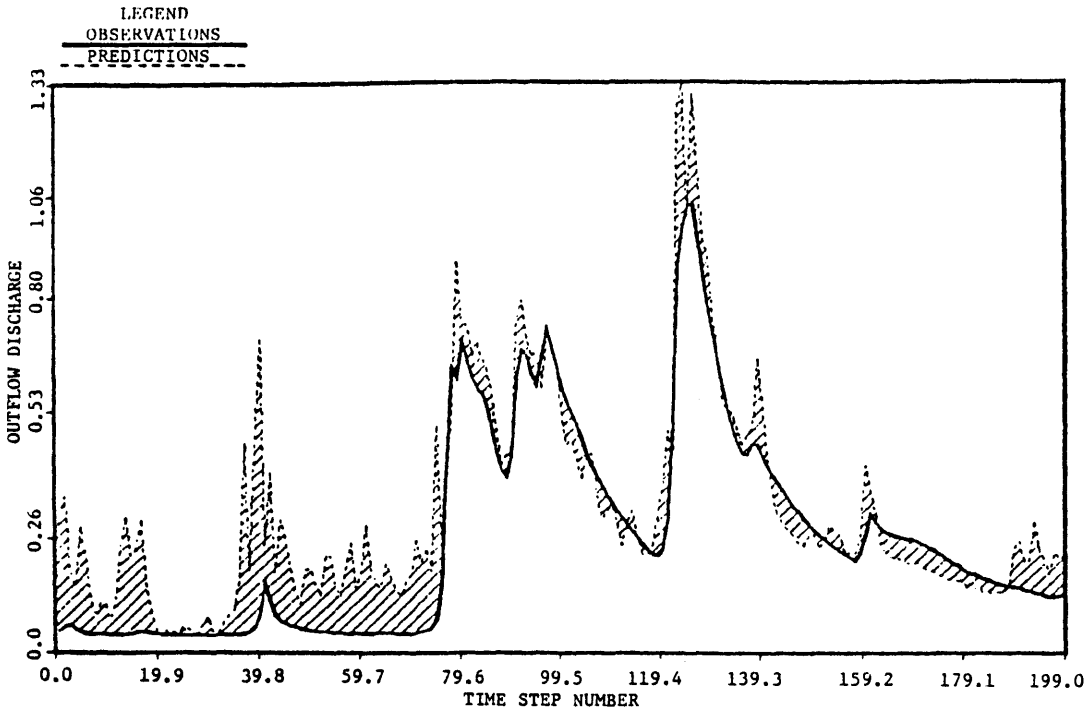

Figure 8.27 Stochastic Prediction of Discharge, Lynnwood, Global Filter, October 12 to November 30, 1970

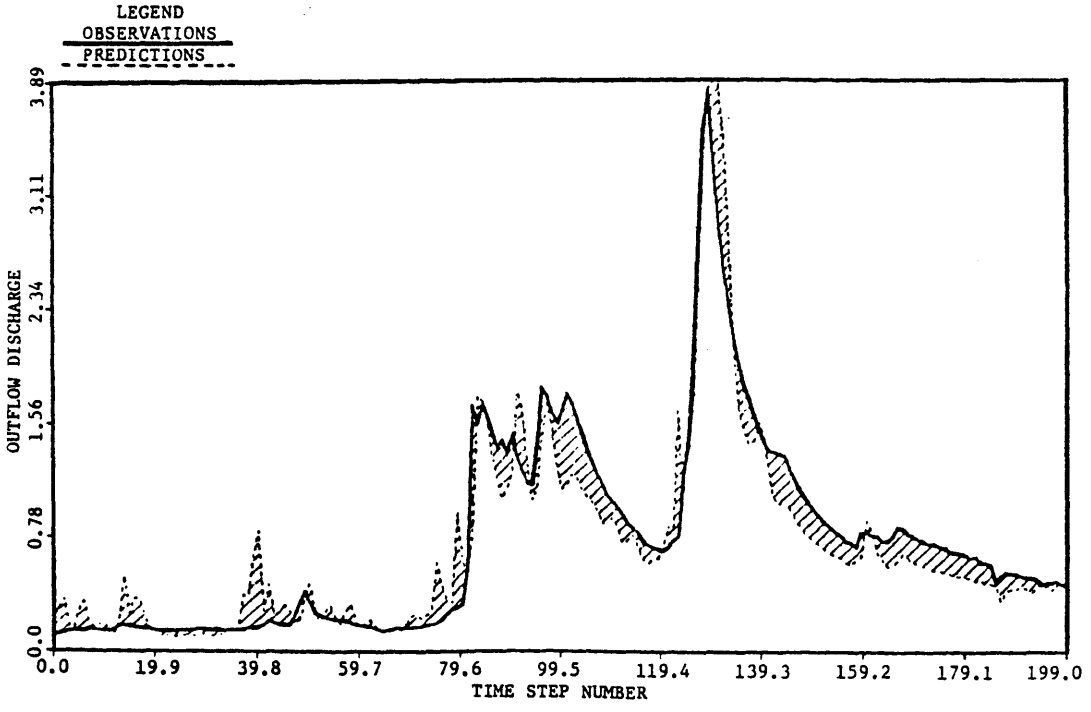

Figure 8.28 Stochastic Prediction of Discharge, Front Royal, Global Filter, October 12 to November 30, 1970

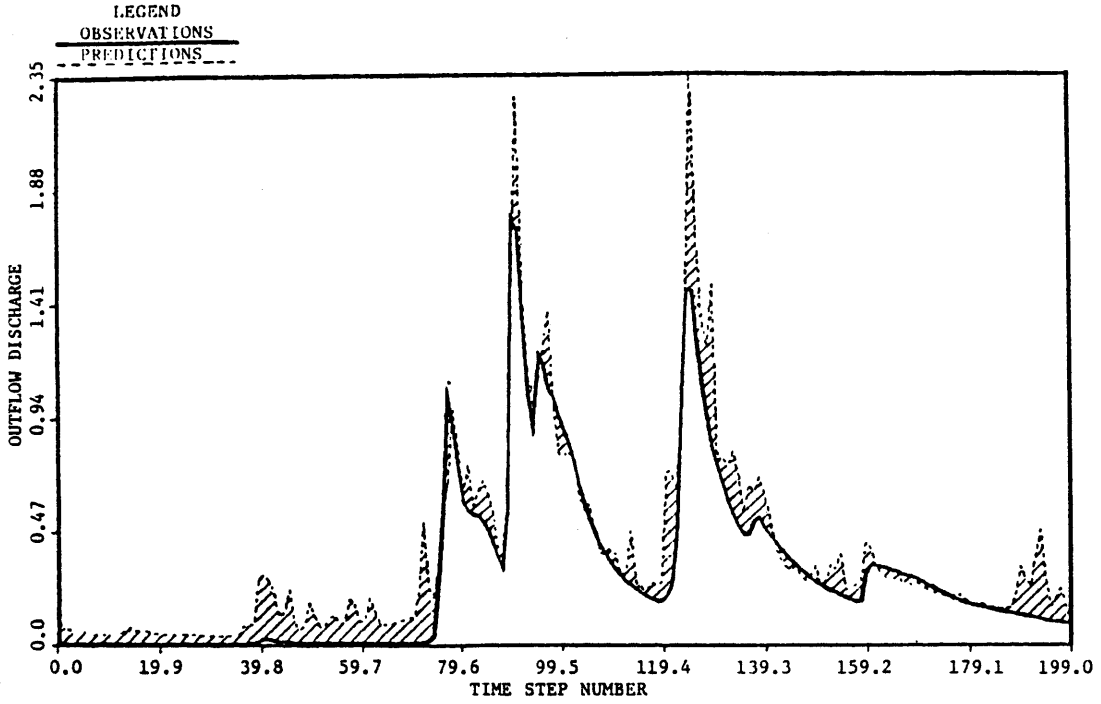

Figure 8.29 Stochastic Prediction of Discharge, Cootes Store, Global Filter, October 12 to November 30, 1970

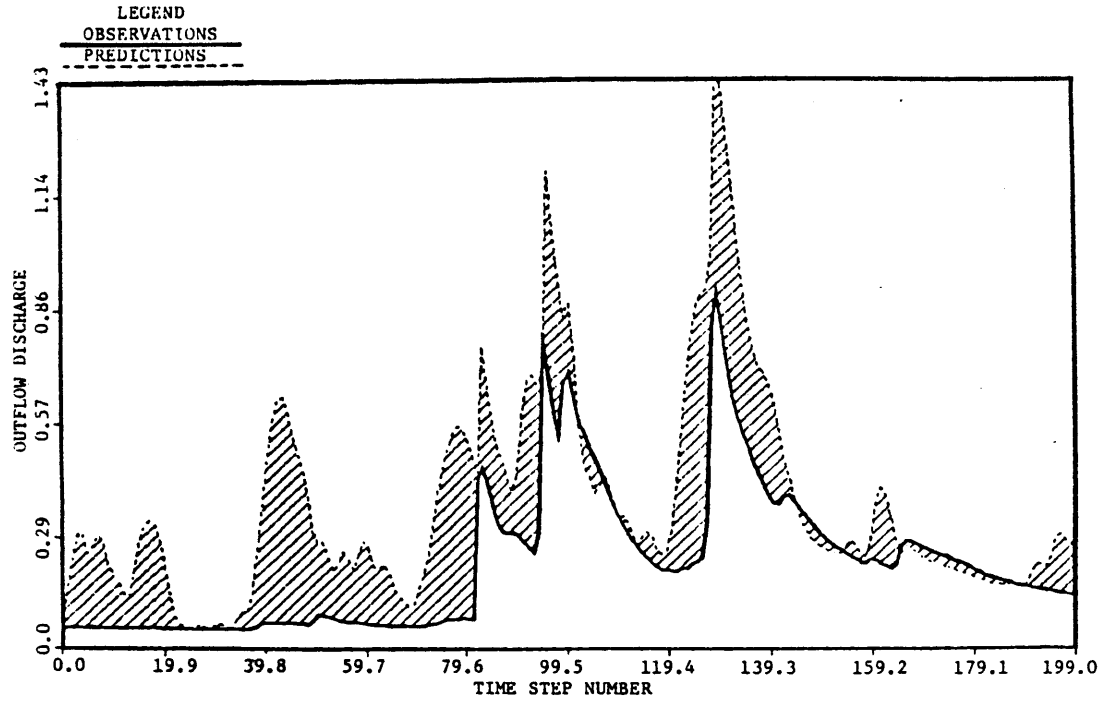

Figure 8.30 Stochastic Prediction of Discharge, Strasburg, Global Filter, October 12 to November 30, 1970

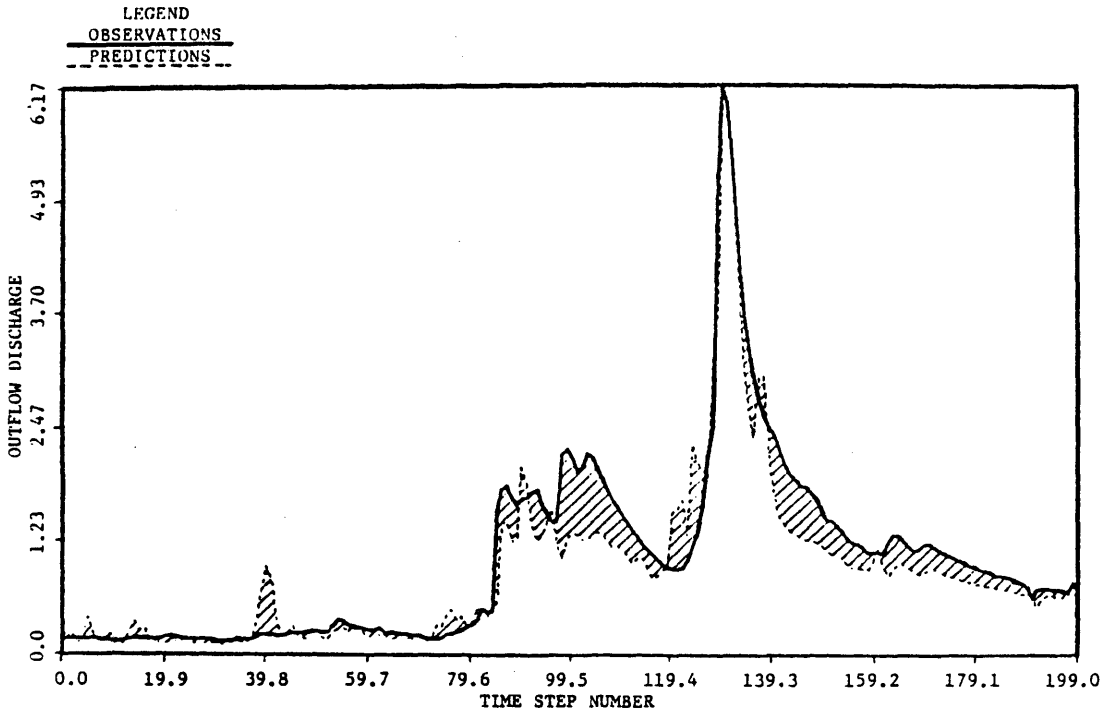

Figure 8.31 Stochastic Prediction of Discharge, Millville, Global Filter, October 12 to November 30, 1970

Slightly better predictions were found with the decomposition procedures of Puente, et al., (1983) over that of Georgakakos (1983). Computational time is about the same for both procedures. Notice, however, the better predictions obtained using the global filters.

Notice the very similar predictions obtained with the two global filters. This implies that upodating soil-channel states from precipitation observations has little effect compared to updatings from discharge observations, and that no major detrimental effects are caused by treating precipitation as an input to the soil-channel components.

Although improved predictions were obtained using the two global filters, the computational time they required was considerably higher, due to the error covariance propagation of the composite state vectors. Savings in such procedures may be achieved by filtering precipitation and soil components for each sub-basin separately and then by considering all channel states jointly.

8.5 Summary

This chapter includes the results of applying the block diagonal decomposition approaches to a case study. Results obtained using two global filters are also included.

Despite calibration errors on the rainfall-runoff model parameters, and apparent inconsistencies on the areal averaged inputs and precipitation observations, the decomposition procedures provide reasonable results except for a sub-basin where excessive predicted precipitation gives discharge overpredictions. The spectral density matrices of the dynamic noises on the different sub-basins were specified using the experience acquired from the approximate maximum likelihood results of Chapter 6. Appendix D presents the results obtained with the decomposition approaches, when the approximate maximum likelihood method described in Chapter 5 is applied to the decomposition case study.

The more expensive global Kalman filters gave better discharge predictions that do not oscillate, as was often the case for low flows when using the decomposition approaches.

Chapter 9

CONCLUSIONS AND RECOMMENDATIONS

9.1 Summary of Results

This work addressed three interconnected topics relevant to the real time forecasting of river flows. First, we studied if better predictions are obtained when more complex approximate nonlinear filters, other than the extended Kalman filter, are used in conjunction with a nonlinear conceptual rainfall-runoff model. The results, obtained for the Bird Creek basin in Oklahoma, showed that filters which use future state estimates to obtain improved state estimates in the past give generally better discharge predictions than the extended Kalman filter. Such nonlinear filter-smoothers follow better the model dynamic's nonlinearities, but at a higher computational cost. For the period under study the precipitation predictions underestimated the rainfall observations. This lack of water was overcome by the nonlinear filters during the updating step by "supplying" water to the different states of the conceptual hydrologic model. The improved predictions of the nonlinear filter-smoothers are due to increased moisture in the soil components. Oscillations on the discharge predictions, often found when using the extended Kalman filter, were reduced with the use of the nonlinear filter-smoothers, due to their lower discharge predicted variances.

It was shown that even the nonlinear filter-smoothers could give poor predictions if model errors are not properly specified. On the other hand, it was found that when the model dynamics errors are suitably quantified (a self-contained definition) no major improvement is found by using the nonlinear filter-smoothers over the simpler extended Kalman filter, despite the fact that the two nonlinear filters give different state trajectories. These results motivated the second topic of this work, namely how to properly quantify the errors inherent in the conceptual hydrologic model when using the extended Kalman filter.

A simplified maximum likelihood method and an adaptive procedure were developed to estimate the dynamics noise spectral density matrix of the model dynamic equations. The off-line approximate maximum likelihood method estimates a constant, in time, diagonal spectral density matrix. The joint probability density function of the observations, over a period of time, is maximized using Newton's method. The likelihood function derivatives, with respect to the unknown parameters, are computed assuming that their more important elements come from derivatives of the current discrete dynamics error covariance matrix. The adaptive procedure can only identify as many unknown error parameters as there are observations of the rainfall-runoff model, i.e., two. This estimator is based on internal consistency conditions of the filter residuals.

The results of estimating the model dynamics spectral density matrix for the Bird Creek basin were excellent when using the approximate maximum likelihood method. The estimate, however, had the undesirable property of having the channel primarily driven by previous discharge observations rather than the water outflow from the soil component of the conceptual model. Although excellent results were obtained for one-step ahead predictions, which are explicitly accounted for in the likelihood function, the extended discharge forecasts were simply tracking the observations. Although this is not appealing, no other spectral density matrix produced, when using the extended Kalman filter, better extended forecasts (to higher leads). Despite being inexpensive, when a good constant in time spectral density matrix is used as initial condition, the adaptive estimator does not necessarily give better predictions.

The third topic of study was the forecasting of flows on a large scale basin, composed of several interconnected sub-basins. Large amounts of calculations are required when forecasting techniques, such as the extended Kalman filter, are used to estimate the composite state vector that describes the large scale basin. An obvious way to reduce the computational burden is by decoupling those states in different sub-basins which have weak connections. Two decomposition algorithms which couple states in different sub-basins via precipitation or through the existing river network were presented. Instead of

working with the whole state error covariance matrix, these methods consider only block diagonal sub-matrices at a lower cost but also with a lower accuracy. The two block diagonal decomposition methods were introduced by Puente, et al. (1983) and by Georgakakos (1983). They differ in that the former procedure treats precipitation as an input to soil-channel models on each sub-basin, while the latter method conserves the state coupling between the precipitation state and states in the other components of the conceptual model.

The decomposition methods were used to forecast on five interconnected sub-basins of the Potomac River. Despite apparent calibration errors in the rainfall-runoff parameters and inconsistencies on the areal averaged meteorological inputs and precipitation observations, the decomposition approaches provided inexpensive and reasonable results for all sub-basins except one where excessive precipitation predictions gave discharge overpredictions.

The approximate maximum likelihood procedure of Chapter 5 was applied to estimate the spectral density matrices of sub-basins on the large scale basin. Although the likelihood function was increased for all sub-basins, the predictions do not look better than the ones obtained using the initial conditions. The likelihood increased due to changes in residual variances, but the residuals themselves were not decreased.

9.2 Recommendations for Future Research

The results obtained in this work stress the important role the precipitation component plays on discharge predictions. If precipitation is under (over) predicted, this will generally give under (over) predictions of discharge. Also timing errors on precipitation will generally transform into discharge timing errors. By using a filter, the model states are updated in a way that they explain better the current observations. If precipitation deficits (excesses) continue over the next time step, such deficits (excesses) will likely occur on discharge due to conservation of mass on the propagation stage of the filter. Because the updating is made after the observations are taken, the predictions will typically contain delays of at least one time step.

Notice that the previous considerations are valid even for soil-channel models whose parameters are calibrated such that they reproduce discharge observations when using the observed rainfall as an input. Therefore, the value of soil-channel models is closely related to the quality of the rainfall predictions.

The precipitation model of Georgakakos and Bras (1982) gives very good predictions when observations are available each hour. In the present study, data is available only every six hours, which goes beyond the characteristic time of the rainfall event. This results in behavior completely driven by the meteorological inputs. Filter updating then becomes ineffective. Research should continue on the area of rainfall modelling. Special emphasis should be given to the transitions from no rain to rain and from rain to no rain. Instead of

using fully believed observed input values, assumed perfectly observed, as in the present study, such inputs should be modelled and their predictions and variances used on the conceptual rainfall-runoff model to obtain a truly, real-time prediction. The creation of reliable data sets of meteorological inputs and rainfall observations is necessary.

The fact that the maximum likelihood results were found insensitive to soil updating suggests that a simpler scheme for the soil component, other than the Sacramento model, could be used in conjunction with the precipitation and channel components of the rainfall-runoff model. Simple soil models should be developed and used in real time discharge forecasting. Additional observations, other than rainfall and discharge, should be included in rainfall-runoff modelling. Upper soil storages measured using remote sensing represent a feasible approach in such a case. The work of Peck, et al. (1983) serves as framework for the use of remotely sensed data.

It is not clear how to discriminate between equally good predictions obtained from different state trajectories. It is not clear which dynamics noise parameters can be estimated from known observations. Although no problems in estimating dynamics noise variances were encountered in this work, identifiability problems may arise (conditional information matrix singular) if nondiagonal spectral den-

sity elements are estimated in addition to diagonal elements. Although it is known that additional observations generally lead to better state discrimination and more reliable estimates, these identifiability issues should be studied further.

Better extended forecasts by the conceptual rainfall-runoff model may be obtained if higher lead conditions are used in the approximate maximum likelihood procedure used to estimate the dynamics noise spectral density matrix. This could be accomplished by maximizing a weighted sum of observations taken every time step, two time steps and so on. Because the characteristic times of deep soil states is longer than six hours, such weighted maximum likelihood method should provide more accurate spectral density variances for such states, which may translate into better extended forecasts. Notice, however, that if precipitation deficits or excesses occur for long periods of time, the use of more lead on the estimation of the error on the rainfall-runoff model might not give better results.

The approximate maximum likelihood procedure used in this work employed the very simple Newton's method to iterate on the unknown spectral density matrix elements. The use of more complex methods, with adjustable step sizes, is the next step to provide better estimates. The work of Goldstein and Larimore (1980), Restrepo-Posada and Bras (1982) and Sorooshian, et al., (1982) is relevant in such case.

9.3 Computational Considerations

The major computational burden that is incurred when forecasting with approximate nonlinear filters and a large conceptual hydrologic model is due to the propagation in time of the model states mean and error covariance matrix. The main reasons for such computational load are: first, that there are many nonlinear differential equations that need to be numerically solved (110 for Bird Creek), and second that such equations are coupled together. When using the nonlinear filter-smoothers not only the number of computations increase due to repeated forwards-backwards cycles, but also storage is increased because forward trajectories are needed to linearize the backwards mean and error covariance dynamic equations.

Although the forecasting computational time for a single basin (for observations taken every six hours) is below the limits of real time forecasting (see Table 4.10), the simultaneous predictions on several basins require a more than proportional computational time due to the transfer of information between the several sites. This stresses the need of reliable and yet fast forecasting procedures.

Attempts to reduce forecasting computational time should be made. This could be accomplished by considering low order models (other than the Sacramento model), or by identifying meteorological conditions under which some equations of the Sacramento model could be decoupled or simplified. Model simplicity could be a function of the forecasting lead time to be considered.

Computational savings not only are important in the real time forecasting stage, but also during calibration of physical and noise parameters of the conceptual model. Such savings are particularly important if the maximum likelihood methodology is to be widely employed in practice.

REFERENCES

Abramson, Paul (1968), "Simultaneous Estimation of the State and Noise Statistics in Linear Dynamical Systems," Doctor of Science Thesis, Massachusetts Institute of Technology, Cambridge, MA.

Alspach, D. L. and H. W. Sorenson (1972), "Nonlinear Bayesian Estimation Using Gaussian Sum Approximations," IEEE Trans. Automatic Control, Vol. AC-17, No. 4, pp. 439-448.

Benjamin, J. R. and A. Cornell (1970), Probability, Statistics and Decision for Civil Engineering, McGraw-Hill, 684 pages.

Bergstrom, S. and A. Forsman (1973), "Development of a Conceptual Deterministic Rainfall Runoff Model," Nordic Hydrology, Vol. 4, No. 3.

Bergstrom, S. (1975), "The Development of a Snow Routine for the HBV-2 Model," Nordic Hydrology, Vol. 6, No. 2.

Brazil, L. E. and M. D. Hudlow (1981), "Calibration Procedures Used with the National Weather Service River Forecast System," In Water and Related Land Resource Systems, edited by Y. Y. Haines and J. Kindler, IFAC Symposium, Cleveland, Ohio, May 28-31, 1980, Pergamon, New York, pp. 457-466.

Bucy, R. S. and K. D. Senne (1971), "Digital Synthesis of Nonlinear Filters," Automatica, Vol. 7, pp. 287-298.

Denham, W. F. and S. Pines (1966), "Sequential Estimation When Measurement Function Nonlinearity is Comparable to Measurement Error," AIAA, J. 4, pp. 1071-1076.

Fjeld, M. and S. Aam (1980), "An Implementation of Estimation Techniques to a Hydrological Model for Prediction of Runoff to a Hydroelectric Power Station," IEEE Transactions on Automatic Control, Vol. AC-25, No. 2, pp. 151-163.

Gelb, A., editor (1974), Applied Optimal Estimation, The MIT Press, 374 pages.

Georgakakos, K. P. and R. L. Bras (1980), "A Statistical Linearization Approach to Real Time Nonlinear Flood Routing," Ralph M. Parsons Laboratory for Water Resources and Hydrodynamics, Department of Civil Engineering, M.I.T., Technical Report No. 256.

Georgakakos, K. P. and R. L. Bras (1982), "A Precipitation Model and Its Use in Real-Time River Flow Forecasting," Ralph M. Parsons Laboratory for Water Resources and Hydrodynamics, Department of Civil Engineering, M.I.T., Technical Report No. 286.

Georgakakos, K. P. (1982a), "Structure and Parameter Determination of a Hydrologically Useful Rainfall Prediction Model," paper presented at AGU Fall Meeting, San Francisco.

Georgakakos, K. P. (1982b), "TSFP User's Manual," National Weather Service Hydrologic Research Laboratory, Silver Springs, MD.

Georgakakos, K. P. (1983), "Stochastic Decomposition Schemes for the Real-Time Forecasting of River Flows in a Large Scale Basin," Technical Note No. 1, Hydrologic Research Laboratory, NWS, Silver Spring, MD.

Georgakakos, K. P. (1984), "Prototype Dataset for the Testing of Large River-Basin Decomposition Procedures," Hydrologic Research Laboratory, NWS, Silver Spring, MD.

Goldstein, J. D. and W. E. Larimore (1980), "Applications of Kalman Filtering and Maximum Liklihood Identification to Hydrologic Forecasting," Technical Report, The Analytic Science Corporation, Boston, MA.

Hassan, M. F., G. Salut, M. G. Singh, and A. Titli (1978), "A Decentralized Computational Algorithm for the Global Kalman Filter," IEEE Trans. Automatic Control, Vol. AC-23, No. 2, pp. 262-267.

Hostetler, L. and R. D. Andreas (1983), "Nonlinear Kalman Filtering Techniques for Terrain-Aided Navigation," IEEE Transactions on Automatic Control, Vol. AC-28, No. 3, pp. 315-323.

Jazwinski, A. H. (1966), "Filtering for Nonlinear Dynamical Systems," IEEE, Trans. Automatic Control, Vol. AC-11, pp. 765-766.

Jazwinski, A. H. (1968), "Limited Memory Optimal Filtering," IEEE Trans. Automatic Control, Vol. AC-13, No. 5, pp. 558-563.

Jazwinski, A. H. (1969), "Adaptive Filtering," Automatica, Vol. 5, pp. 475-485.

Jazwinski, A. H. (1970), Stochastic Processes and Filtering Theory, Academic Press, 376 pages.

Kalman, E. R. and S. R. Bucy (1961), "New Results in Linear Filtering and Prediction Theory," Journal of Basic Engineering, Transactions of the ASME, March, pp. 95-108.

Kitanidis, P. K. and R. L. Bras (1978), "Real Time Forecasting of River Flows," Ralph M. Parsons Laboratory for Water Resources and Hydrodynamics, Department of Civil Engineering, M.I.T., Technical Report No. 235.

Kushner, H. J. (1967), "Approximations to Optimal Nonlinear Filters," IEEE Trans. Automatic Control, Vol. AC-12, No. 5, pp. 546-556.

Liu, C. K. and W. Brutsaert (1978), "A Nonlinear Analysis of the Relationship Between Rainfall and Runoff for Extreme Floods," Water Resources Research, Vol. 14, No. 1, pp. 75-83.

Mendel, J. M. (1974), "Postflight Data Analysis by Means of Adaptive, Iterated, Extended Kalman Filtering," IEEE Trans. Automatic Control, Vol. AC-19, No. 5, pp. 1467-1474.

Nash, J. E. and J. V. Sutcliffe (1970), "River Flow Forecasting Through Conceptual Models: Part I -- A Discussion of Principles," J. of Hydrology, Vol. 10, pp. 282-290.

Noton, A. R. M. (1971), "Two-Level Form of the Kalman Filter," IEEE Trans. Automatic Control, Vol. AC-16, No. 2, pp. 128-133.

O'Connell, P. E. (Editor) (1980), "Real-Time Hydrological Forecasting and Control," Proceedings, 1st International Workshop Held at the Institute of Hydrology, Wallingford, England, July 1977.

Peck, E. L. (1976), "Catchment Modelling and Initial Parameter Estimation for the National Weather Service River Forecast System," NWS HYDRO-31.

Peck, E. L., E. R. Johnson and T. N. Keefer (1983), "Creating a Bridge Between Remote Sensing and Hydrologic Models," Final Report, Hydex Corporation for NASA.

Puente, C. E., J. B. Valdes and R. L. Bras (1983), "On-Line River Discharge Forecasting Using Filtering and Estimation Theory," Progress Report, September 1982 February 1983, Prepared for National Weather Service.

Restrepo Posada, P. J. and R. L. Bras (1982), "Automatic Parameter Estimation of a Large Conceptual Rainfall-Runoff Model: A Maximum Likelihood Approach," Ralph M. Parsons Laboratory for Water Resources and Hydrodynamics, Department of Civil Engineering, M.I.T., Technical Report No. 267.

Sastry, V. A. (1971), "Decomposition of the Extended Kalman Filter," IEEE Trans. Automatic Control, Vol. AC-16, pp. 260-261.

Schwartz, L. and E. B. Stear (1968), "A Computational Comparison of Several Nonlinear Filters," IEEE Trans. Automatic Control, Vol. AC-13, pp. 83-86.

Schweppe, F. C. (1973), Uncertain Dynamic Systems, Prentice Hall, Englewood Cliffs, NJ, 563 pages.

Sims, C. S. (1974), "An Algorithm for Estimating a Portion of the State Vector," IEEE Trans. Automatic Control, Vol. AC-19, pp. 391-393.

Smith, J. A., D. P. Sheer, and J. C. Schaake, Jr. (1982), "The Use of Hydrometeorological Data in Drought Management: Potomac River Basin Case Study," International Symposium on Hydrometeorology, American Water Resources Association.

Sorenson, H. W. and A. R. Stubberud (1968), "Nonlinear Filtering by Approximation of the Aposteriori Density," Int. J. Control, Vol. 8, No. 1, pp. 33-51.

Sorenson, H. W. (1980), Parameter Estimation, Principles and Problems, Volume 9, Control and Systems Theory, edited by Jerry M. Mendel, Marcel Dekker, Inc., 381 pages.

Sorooshian, S., V. K. Gupta, and J. L. Fulton (1982), "Evaluation of Maximum Likelihood Parameter Estimation Techniques for Conceptual Rainfall-Runoff Models: Influence of Calibration Data Variability and Length on Model Credibility," Water Resources Research, in press.

Sorooshian, S. (1983), "Surface Water Hydrology: On-Line Estimation," Reviews of Geophysics and Space Physics, Vol. 21, No. 3, pp. 706-721, U. S. National Report to International Union of Geodesy and Geophysics, 1979-1982.

Takara, K., S. Michiharu, and T. Takasao (1983), "A Stochastic Method of Real-Time Flood Prediction in a Basin Consisting of Several Sub-Basins," Journal of Hydroscience and Hydraulic Engineering, Vol. 1, No. 2, pp. 93-111.

Troutman, B. (1982), "An Analysis of Input Errors in Precipitation-Runoff Models Using Regressions with Errors in the Independent Variables," Water Resources Research, Vol. 18, No. 4, pp. 947-964.

Troutman, B. (1983), "Runoff Prediction Error and Bias in Parameter Estimation Induced by Spatial Variability of Precipitation," Water Resources Research, Vol. 19, No. 3, pp. 791-810.

Wishner, R. P., J. A. Tabaczynski, and M. Athans (1968), "On the Estimation of the State of Noisy Nonlinear Multivariable Systems," IFAC Symposium Multivariable Control Systems, Dusseldorf, West Germany.

Wishner, R. P., J. A. Tabaczynski, and M. Athans (1969), "A Comparison of Three Non-Linear Filters," Automatica, Vol. 5, pp. 487-496.

Wood, E. F. (1981), "Filtering of Partitioned Large Scale Hydrological Systems," Hydrological Science Bulletin, 26(1), pp. 33-46.

Yamada, T. (1980), "Comments on Two-Level Form of Kalman Filter," IEEE Trans. Automatic Control, Vol. AC-25, No. 4, pp. 856-857.

Appendix A

RAINFALL-RUNOFF MODEL FIRST ORDER LINEARIZATION MATRICES

This appendix includes the first order derivatives of the rainfall-runoff model. The derivatives of the station precipitation model are those of Georgakakos and Bras (1982), and are not reproduced here. The ordering of the model states and inputs are as in Table 4.1. The notation is also that of Table 4.1, with F and H denoting the linearization matrices of the dynamics[1] and observations with respect to the states, and F^u and H^u denoting the linearization matrices with respect to the inputs.

First the following notation is in order:

$$RX1M = \left(\frac{X_1}{X_1^o}\right)^{m_1} \tag{A.1}$$

$$RX2M = \left(\frac{X_2}{X_2^o}\right)^{m_2} \tag{A.2}$$

$$RX3M = \left(\frac{X_3}{X_3^o}\right)^{m_3} \tag{A.3}$$

$$y = 1 - \frac{X_3 + X_4 + X_5}{X_3^o + X_4^o + X_5^o} \tag{A.4}$$

---

[1] $F(i,j) = \dfrac{\partial f_i}{\partial X_j}$

$$C_1 = d'_\ell X_4^o + d''_\ell X_5^o \tag{A.5}$$

$$C_2 = d'_\ell X_4^o / C_1 \tag{A.6}$$

$$D3 = C_1 \cdot X_2 (1 + \varepsilon y^\theta) / X_2^o \tag{A.7}$$

$$D4 = \frac{C_1 \cdot \varepsilon X_2 \theta y^{\theta-1}}{[X_2^o (X_3^o + X_4^o + X_5^o)]} \tag{A.8}$$

$$D5 = \frac{C_1 \cdot \varepsilon X_2 \theta y^{\theta-1} (1 - P_f)(1 - RX3M)}{[X_2^o (X_3^o + X_4^o + X_5^o)]} \tag{A.9}$$

$$D6 = 1 - (1 - P_f)(1 - RX3M) \tag{A.10}$$

$$D7 = (C_2 \cdot X_5 / X_5^o - 1) X_4 / X_4^o + 1 \tag{A.11}$$

$$D8 = D4 \cdot D6 \cdot D7 \tag{A.12}$$

$$D9 = D4 \cdot D6 \cdot (1 - D7) \tag{A.13}$$

$$D10 = C_1 \cdot (1 + \varepsilon y^{\theta}) / X_2^o \tag{A.14}$$

$$RAT1 = \frac{X_6 - X_1}{X_3^o} \tag{A.15}$$

$$DF1 = 1 - RAT1^2 \tag{A.16}$$

The linearization elements are:

$$F(1,1) = - O(\underline{u}_p, \underline{\partial}_p) \tag{A.17}$$

$$F(2,1) = (1 - RX1M) \cdot \hat{\phi} \tag{A.18}$$

$$F(2,2) = -\hat{\phi} X_p m_1 X_1^{m_1 - 1} / (X_1^o)^m - u_e / X_1^o \tag{A.19}$$

$$F(3,1) = RX1M \cdot \hat{\phi} \cdot (1 - RX2M) \tag{A.20}$$

$$F(3,2) = m_1 \cdot \hat{\phi} X_p \cdot (1 - RX2M) \cdot X_1^{m_1 - 1} / (X_1^o)^{m_1} \tag{A.21}$$

$$F(3,3) = - RX1M \cdot \hat{\phi} \cdot X_p \cdot m_2 \cdot X_2^{m_2 - 1} / (X_2^o)^{m_2} - d_u - D10 \tag{A.22}$$

$$F(3,4) = D4 \tag{A.23}$$

$$F(3,5) = D4 \tag{A.24}$$

$$F(3,6) = D4 \tag{A.25}$$

$$F(4,2) = u_e \cdot X_3/[(X_1^o + X_3^o) \cdot X_1^o] \tag{A.26}$$

$$F(4,3) = D10 \cdot (1 - D6) \tag{A.27}$$

$$F(4,4) = -D3 \cdot (1 - P_f) m_3 X_3^{m_3 - 1} / (X_3^o)^{m_3}$$

$$- u_e (1 - X_1/X_1^o)/(X_1^o + X_2^o) - D5 \tag{A.28}$$

$$F(4,5) = -D5 \tag{A.29}$$

$$F(4,6) = -D5 \tag{A.30}$$

$$F(5,3) = D10 \cdot D6 \cdot D7 \tag{A.31}$$

$$F(5,4) = D3 \cdot D7 \cdot (1 - P_f) \cdot m_3 X_3^{m_3 - 1} / (X_3^o)^{m_3} - D8 \tag{A.32}$$

$$F(5,5) = -d_\ell' + D3 \cdot D6 \cdot (C_2 X_5/X_5^o - 1)/X_4^o - D8 \tag{A.33}$$

$$F(5,6) = D3 \cdot D6 \cdot C_2 \cdot X_4/(X_5^o \cdot X_4^o) - D8 \tag{A.34}$$

$$F(6,3) = D10 \cdot D6 \cdot (1 - D7) \tag{A.35}$$

$$F(6,4) = D3 \cdot (1 - P_f) \cdot (1 - D7) m_3 X_3^{m_3 - 1} / (X_3^o)^{m_3} - D9 \tag{A.36}$$

$$F(6,5) = D3 \cdot D6 \cdot (1 - C_2 X_5/X_5^o)/X_4^o - D9 \tag{A.37}$$

$$F(6,6) = -d_\ell'' - D3 \cdot D6 \cdot C_2 X_4/(X_5^o X_4^o) - D9 \tag{A.38}$$

$$F(7,1) = \{1 - (1 - DF1) \cdot RX1M\}\hat{\phi} - DF1 \cdot RX2M \cdot RX1M \cdot \hat{\phi} \tag{A.39}$$

$$F(7,2) = -\hat{\phi} X_p \{(1 - DF1) \cdot m_1 \cdot X_1^{m_1 - 1}/(X_1^o)^{m_1} - RX1M \cdot RAT1 \cdot 2/X_3^o\}$$

$$+ u_e \{(X_6 - X_1)/[X_1^o(X_1^o + X_3^o)] + (1 - X_1/X_1^o)/(X_1^o + X_3^o) - 1/X_1^o\}$$

$$- \hat{\phi} X_p RX2M \{DF1 \cdot m_1 X_1^{m_1 - 1}/(X_1^o)^{m_1} + RX1M \cdot 2 \cdot RAT1/X_3^o\} \tag{A.40}$$

$$F(7,3) = -\hat{\phi} X_p \cdot DF1 \cdot RX1M \cdot m_2 X_2^{m_2 - 1}/(X_2^o)^{m_2} \tag{A.41}$$

$$F(7,7) = -\hat{\phi}\, X_p \cdot RX1M \cdot RAT1 \cdot 2/X_3^o - u_e \left(1 - \frac{X_1}{X_1^o}\right) \frac{1}{X_1^o + X_3^o}$$

$$+ 2 \cdot RAT1 \cdot RX1M \cdot RX2M \cdot \hat{\phi} \cdot X_p/X_3^o \tag{A.42}$$

For $j=1,2,\ldots,n$:

$$F(7+j,1) = P_j \{\hat{\phi}\beta_2 + RAT1 \cdot RAT1 \cdot \hat{\phi} \cdot RX1M \cdot \beta_1 + \hat{\phi} \cdot RX1M \cdot RX2M \cdot$$

$$(1 - \beta_1 - \beta_2) + DF1 \cdot RX1M \cdot RX2M \cdot \hat{\phi}\beta_1\} \tag{A.43}$$

$$F(7+j,2) = P_j\{-2\cdot RAT1\cdot\hat{\phi}\cdot X_p\cdot RX1M\cdot\beta_1/X_3^o + RAT1^2\hat{\phi}X_p\cdot$$

$$\beta_1 m_1 X_1^{m_1-1}/(X_1^o)^{m_1} + \hat{\phi}X_p m_1 X_1^{m_1-1}/(X_1^o)^{m_1}\cdot RX2M(1-\beta_1-\beta_2)$$

$$+\hat{\phi}\,X_p\beta_1\cdot RX2M\cdot[DF1\cdot m_1 X_1^{m_1-1}/(X_1^o)^{m_1} + 2\cdot RAT1\cdot RX1M/X_3^o]\} \quad (A.44)$$

$$F(7+j,3) = P_j\{d_u(1-\beta_1-\beta_2) + \hat{\phi}X_p\cdot RX1M\cdot(1-\beta_1-\beta_2)m_2X_2^{m_2-1}/(X_2^o)^{m_2}$$

$$+ DF1\cdot RX1M\cdot\hat{\phi}X_p\cdot\beta_1 m_2 X_2^{m_2-1}/(X_2^o)^{m_2}\} \quad (A.45)$$

$$F(7+j,5) = P_j\{d'_\ell(1-\beta_1-\beta_2)/(1+\mu)\} \quad (A.46)$$

$$F(7+j,6) = P_j\{d''_\ell(1-\beta_1-\beta_2)/(1+\mu)\} \quad (A.47)$$

$$F(7+j,7) = P_j\{2\cdot RAT1\cdot\hat{\phi}X_p\cdot RX1M\cdot\beta_1/X_3^o\cdot(1-RX2M)\} \quad (A.48)$$

$$F(7+j,7+j) = -a_j\cdot mS_j^{m-1} \quad (A.49)$$

$$F(7+j,7+j-1) = a_{j-1}\cdot m\,S_{j-1}^{m-1},\ j=2,3,\ldots,n \quad (A.50)$$

$$H(1,1) = \hat{\phi}(\underline{u}_p, \underline{a}_p) \tag{A.51}$$

The linearization matrices with respect to temperature, pressure and dew-point temperature are included in Georgakakos and Bras (1982). The derivatives with respect to evapotranspiration are:

$$F^u(2,4) = -X_1/X_1^o \tag{A.52}$$

$$F^u(4,4) = -(1 - X_1/X_1^o)X_3/(X_1^o + X_3^o) \tag{A.53}$$

$$F^u(7,4) = -(1 - X_1/X_1^o)\left(\frac{X_6 - X_1}{X_1^o + X_3^o}\right) - X_1/X_1^o \tag{A.54}$$

Appendix B

RAINFALL-RUNOFF MODEL SECOND ORDER EXPANSION MATRICES

This appendix includes the nonzero second order derivatives of the rainfall-runoff model. The ordering of the model states is as in Table 4.1. The notation is as follows:

$$S(i,j,k) = \frac{\partial^2 f_k}{\partial X_i \partial X_j} \tag{B.1}$$

$$T(i,j,\ell) = \frac{\partial^2 h_\ell}{\partial X_i \partial X_j} \tag{B.2}$$

with f_k and h_ℓ indicating the k^{th} dynamic function and the ℓ^{th} observations function, respectively. Note that for a fixed function, these matrices are symmetric.

In addition to the notation of Appendix A, the following notation is required:

$$FX1 = m_1(m_1 - 1)\, X_1^{m_1-2}/(X_1^o)^{m_1} \tag{B.3}$$

$$FX2 = m_2(m_2 - 1)\, X_2^{m_2-2}/(X_2^o)^{m_2} \tag{B.4}$$

$$FX3 = m_1 X_1^{m_1-1}/(X_1^o)^{m_1} \tag{B.5}$$

$$FX4 = m_2 X_2^{m_2-1} / (X_2^o)^{m_2} \tag{B.6}$$

$$FX5 = C_1 \cdot \varepsilon \cdot \theta \cdot y^{\theta-1} / [(X_3^o + X_4^o + X_5^o) \cdot X_2^o] \tag{B.7}$$

$$FX6 = C_1 \cdot \varepsilon\theta(\theta - 1) y^{\theta-2} / [X_2^o (X_3^o + X_4^o + X_5^o)^2] \tag{B.8}$$

$$FX7 = m_3 X_3^{m_3-1} / (X_3^o)^{m_3} \tag{B.9}$$

$$FX8 = C_1 \cdot (1 + \varepsilon y^{\theta}) / X_2^o \tag{B.10}$$

$$FX9 = m_3(m_3 - 1) X_3^{m_3-2} / (X_3^o)^{m_3} \tag{B.11}$$

$$FX10 = (C_2 \cdot X_5 / X_5^o - 1) \cdot 1 / X_4^o \tag{B.12}$$

The elements of the second-order matrices are:

$$S(1,2,2) = - \hat{\phi} \cdot FX3 \tag{B.13}$$

$$S(2,2,2) = - \hat{\phi} X_p \cdot FX1 \tag{B.14}$$

$$S(1,2,3) = \hat{\phi} \cdot FX3 \ (1 - RX2M) \tag{B.15}$$

$$S(1,3,3) = - \hat{\phi} \cdot RX1M \cdot FX4 \tag{B.16}$$

$$S(2,2,3) = \hat{\phi}X_p \cdot FX1 \cdot (1 - RX2M) \tag{B.17}$$

$$S(2,3,3) = -\hat{\phi}X_p \cdot FX3 \cdot FX4 \tag{B.18}$$

$$S(3,3,3) = -\hat{\phi}X_p \cdot RX1M \cdot FX2 \tag{B.19}$$

$$S(3,4,3) = FX5 \tag{B.20}$$

$$S(3,5,3) = FX5 \tag{B.21}$$

$$S(3,6,3) = FX5 \tag{B.22}$$

$$S(4,4,3) = -FX6 \cdot X_2 \tag{B.23}$$

$$S(4,5,3) = -FX6 \cdot X_2 \tag{B.24}$$

$$S(4,6,3) = -FX6 \cdot X_2 \tag{B.25}$$

$$S(5,5,3) = -FX6 \cdot X_2 \tag{B.26}$$

$$S(5,6,3) = -FX6 \cdot X_2 \tag{B.27}$$

$$S(6,6,3) = -FX6 \cdot X_2 \tag{B.28}$$

$$S(2,4,4) = u_e/[X_1^o(X_1^o + X_3^o)] \tag{B.29}$$

$$S(3,4,4) = -FX8 \cdot (1 - P_f)FX7 - (1 - P_f)(1 - RX3M) \cdot FX5 \quad (B.30)$$

$$S(3,5,4) = -(1 - RX3M) \cdot FX5 \cdot (1 - P_f) \quad (B.31)$$

$$S(3,6,4) = -(1 - RX3M) \cdot FX5 \cdot (1 - P_f) \quad (B.32)$$

$$S(4,4,4) = -D3 \cdot (1 - P_f)FX9 + 2.0 \cdot FX5 \cdot X_2 \cdot (1 - P_f) \cdot FX7 + FX6 \cdot X_2(1 - P_f)(1 - RX3M) \quad (B.33)$$

$$S(4,5,4) = FX5 \cdot X_2(1 - P_f)FX7 + FX6 \cdot X_2(1 - P_f)(1 - RX3M) \quad (B.34)$$

$$S(4,6,4) = S(4,5,4) \quad (B.35)$$

$$S(5,5,4) = FX6 \cdot X_2(1 - P_f)(1 - RX3M) \quad (B.36)$$

$$S(5,6,4) = S(5,5,4) \quad (B.37)$$

$$S(6,6,4) = S(5,5,4) \quad (B.38)$$

$$S(3,4,5) = FX8 \cdot D7(1 - P_f)FX7 - FX5 \cdot D6 \cdot D7 \quad (B.39)$$

$$S(3,5,5) = FX8 \cdot D6 \cdot FX10 - FX5 \cdot D6 \cdot D7 \quad (B.40)$$

$$S(3,6,5) = FX8 \cdot D6 \cdot C_2 \cdot X_4/(X_4^o X_5^o) - FX5 \cdot D6 \cdot D7 \tag{B.41}$$

$$S(4,4,5) = FX6 \cdot X_2 \cdot D6 \cdot D7 + D3 \cdot D7 \cdot FX9 \cdot (1 - P_f) - 2 \cdot FX5 \cdot X_2 (1 - P_f) FX7 \cdot D7 \tag{B.42}$$

$$S(4,5,5) = -FX5 \cdot X_2 \cdot D6 \cdot FX10 + FX6 \cdot X_2 \cdot D6 \cdot D7 + D3 \cdot FX10 \cdot FX7 \cdot (1 - P_f) - FX5 \cdot X_2 \cdot D7 \cdot FX7 \cdot (1 - P_f) \tag{B.43}$$

$$S(4,6,5) = -FX5 \cdot X_2 \cdot D6 \cdot C_2 X_4/(X_4^o X_5^o) + FX6 \cdot X_2 \cdot D6 \cdot D7 + D3 \cdot C_2 X_4/(X_4^o \cdot X_5^o) \cdot (1 - P_f) \cdot FX7 - FX5 \cdot X_2 \cdot D7 (1 - P_f) \cdot FX7 \tag{B.44}$$

$$S(5,5,5) = FX6 \cdot X_2 \cdot D6 \cdot D7 - 2 \cdot FX5 \cdot X_2 D6 \cdot FX10 \tag{B.45}$$

$$S(5,6,5) = -FX5 \cdot X_2 \cdot D6 \cdot C_2 \cdot X_4/(X_4^o X_5^o) + FX6 \cdot X_2 \cdot D6 \cdot D7 + D3 \cdot D6 \cdot C_2/(X_4^o X_5^o) - FX5 \cdot X_2 D6 \cdot FX10 \tag{B.46}$$

$$S(6,6,5) = FX6 \cdot X_2 \cdot D6 \cdot D7 - 2.0 \cdot FX5 \cdot X_2 \cdot D6 \cdot C_2 \cdot X_4/(X_4^o X_5^o) \tag{B.47}$$

$$S(3,4,6) = FX8 \cdot (1 - D7)(1 - P_f) \cdot FX7 - FX5 \cdot D6 (1 - D7) \tag{B.48}$$

$$S(3,5,6) = - FX8 \cdot D6 \cdot FX10 - FX5 \cdot D6(1 - D7) \quad (B.49)$$

$$S(3,6,6) = -FX8 \cdot D6 \cdot C_2 X_4/(X_4^o X_5^o) - FX5 \cdot D6(1 - D7) \quad (B.50)$$

$$S(4,4,6) = -2 \cdot FX5 \cdot X_2(1 - D7) \cdot (1 - P_f) \cdot FX7 + FX6 \cdot X_2 D6(1 - D7)$$

$$+ D3(1 - D7)FX9 \cdot (1 - P_f) \quad (B.51)$$

$$S(4,5,6) = FX5 \cdot X_2 \cdot D6 \cdot FX10 + FX6 \cdot X_2 \cdot D6(1 - D7) -$$

$$- D3 \cdot FX10 \cdot FX7(1 - P_f) - FX5 \cdot X_2(1 - D7)(1 - P_f) \cdot FX7 \quad (B.52)$$

$$S(4,6,6) = FX5 \cdot X_2 D6 \cdot C_2 \cdot X_4/(X_4^o X_5^o) + FX6 \cdot X_2 \cdot D6(1 - D7)$$

$$- D3 \cdot FX7(1 - P_f) C_2 X_4/(X_4^o X_5^o) - FX5 \cdot X_2(1 - D7)(1 - P_f)FX7 \quad (B.53)$$

$$S(5,5,6) = FX5 \cdot X_2 D6 \cdot FX10 + FX6 \cdot X_2 \cdot D6(1 - D7) + FX5 \cdot X_2 D6 \cdot FX10 \quad (B.54)$$

$$S(5,6,6) = FX5 \cdot X_2 \cdot D6 \cdot C_2 \cdot X_4/(X_4^o X_5^o) + FX6 \cdot X_2 \cdot D6(1 - D7)$$

$$- D3 \cdot D6 \cdot C_2/(X_4^o X_5^o) + FX5 \cdot X_2 \cdot D6 \cdot FX10 \quad (B.55)$$

$$S(6,6,6) = 2 \cdot FX5 \cdot X_2 \cdot D6 \cdot C_2 \cdot X_4/(X_4^o X_5^o) + FX6 \cdot X_2 D6(1 - D7) \quad (B.56)$$

$$S(1,2,7) = -\hat{\phi}\cdot RAT1^2\cdot FX3 + 2\cdot RAT1/X_3^o\cdot RX1M\cdot\hat{\phi}$$
$$- DF1\cdot X_2/X_2^o FX3\cdot\hat{\phi} - 2\cdot RAT1/X_3^o\cdot RX1M\cdot RX2M\cdot\hat{\phi} \quad (B.57)$$

$$S(1,3,7) = -\hat{\phi}\cdot DF1\cdot RX1M\cdot FX4 \quad (B.58)$$

$$S(1,7,7) = -2\cdot RAT1/X_3^o\cdot RX1M\cdot\hat{\phi} + 2\cdot RAT1/X_3^o\cdot RX1M\cdot RX2M\cdot\hat{\phi} \quad (B.59)$$

$$S(2,2,7) = -\hat{\phi}X_p RAT1^2 FX1 + \hat{\phi}X_p\cdot FX3\cdot 4.0\cdot RAT1/X_3^o - \hat{\phi}X_p\cdot RX1M\cdot 2/(X_3^o)^2$$
$$- 2\cdot\phi\cdot u_e/(X_1^o[X_1^o + X_3^o]) - \phi X_p RX2M\cdot DF1\cdot FX1$$
$$- \hat{\phi}X_p RX2M\cdot FX3\cdot 4.0\cdot RAT1/X_3^o + \hat{\phi}X_p RX2M\cdot 2/(X_3^o)^2\cdot RX1M \quad (B.60)$$

$$S(2,3,7) = -\hat{\phi}X_p\cdot FX4\cdot(DF1\cdot X3 + RX2M\cdot 2.0\cdot RAT1/X_3^o) \quad (B.61)$$

$$S(2,7,7) = -\hat{\phi}X_p FX3\cdot 2\cdot RAT1/X_3^o + \hat{\phi}X_p\cdot RX1M\cdot 2.0/(X_3^o)^2$$
$$+ u_e/(X_1^o[X_1^o + X_3^o]) - \hat{\phi}X_p\cdot RX2M\cdot(RX1M\cdot 2/(X_3^o)^2$$
$$- FX3\cdot 2.0\cdot RAT1/X_3^o) \quad (B.62)$$

$$S(3,3,7) = -\hat{\phi}X_p\cdot FX2\cdot DF1\cdot RX1M \quad (B.63)$$

$$S(3,7,7) = \hat{\phi}X_p\cdot RX1M\cdot FX4\cdot 2.0\cdot RAT1/X_3^o \quad (B.64)$$

$$S(7,7,7) = -2.0 \cdot \hat{\phi} X_p \cdot RX1M/(X_3^o)^2 + \hat{\phi} X_p RX1M \cdot RX2M \cdot 2.0/(X_3^o)^2 \quad (B.65)$$

For j=1,2,...,n:

$$\begin{aligned} S(1,2,7+j) = P_j\{&\hat{\phi}\beta_1 \cdot RAT1^2 FX3 - \hat{\phi}\beta_1 \cdot 2 \cdot RAT1 \cdot RX1M/X_3^o \\ &+ \hat{\phi} FX3 \cdot RX2M \cdot (1 - \beta_1 - \beta_2) + DF1 \cdot RX2M \cdot FX3 \cdot \hat{\phi}\beta_1 \\ &+ 2.0 \cdot RAT1 \cdot RX1M \cdot RX2M \cdot \hat{\phi} \cdot \beta_1/X_3^o\} \end{aligned} \quad (B.66)$$

$$S(1,3,7+j) = P_j\{\hat{\phi} \cdot RX1M \cdot FX4(1 - \beta_1 - \beta_2) + DF1 \cdot FX4 \cdot RX1M \cdot \hat{\phi} \cdot \beta_1\} \quad (B.67)$$

$$\begin{aligned} S(1,7,7+j) = P_j\{&2.0 \cdot RAT1 \cdot \hat{\phi} \cdot \beta_1 \cdot RX1M/X_3^o \\ &- 2.0 \cdot RAT1 \cdot RX1M \cdot RX2M \cdot \hat{\phi} \cdot \beta_1/X_3^o\} \end{aligned} \quad (B.68)$$

$$\begin{aligned} S(2,2,7+j) = P_j\{&\beta_1 \cdot X_p \hat{\phi}([1 - DF1] \cdot FX1 - FX3 \cdot 4.0 \cdot RAT1/X_3^o \\ &+ RX1M \cdot 2/(X_3^o)^2) + \hat{\phi} \cdot X_p \cdot RX2M \cdot FX1 \cdot (1 - \beta_1 - \beta_2) \\ &+ \beta_1 \cdot X_p \cdot \hat{\phi} \cdot RX2M \cdot (FX3 \cdot 4.0 \cdot RAT1/X_3^o - RX1M \cdot 2.0/(X_3^o)^2 \\ &+ DF1 \cdot FX1)\} \end{aligned} \quad (B.69)$$

$$\begin{aligned} S(2,3,7+j) = P_j\{&\hat{\phi} X_p (1 - \beta_1 - \beta_2) FX3 \cdot FX4 \\ &+ \hat{\phi} X_p \beta_1 \cdot FX4(RX1M \cdot 2 \cdot RAT1/X_3^o + DF1 \cdot FX3)\} \end{aligned} \quad (B.70)$$

$$S(2,7,7+j) = P_j\hat{\phi}X_p\{\beta_1 \cdot FX3 \cdot 2.0 \cdot RAT1/X_3^o - \beta_1 \cdot RX1M \cdot 2/(X_3^o)^2$$
$$+ \beta_1 \cdot RX2M(RX1M \cdot 2.0/(X_3^o)^2 - FX3 \cdot 2.0 \cdot RAT1/X_3^o)\} \quad (B.71)$$

$$S(3,3,7+j) = P_j \cdot \hat{\phi}X_p \cdot FX2\{RX1M \cdot (1 - \beta_1 - \beta_2)$$
$$+ \beta_1 \cdot RX1M \cdot DF1\} \quad (B.72)$$

$$S(3,7,7+j) = -P_j \cdot \beta_1 \cdot X_p \cdot \hat{\phi} \cdot RX1M \cdot FX4 \cdot 2.0 \cdot RAT1/X_3^o \quad (B.73)$$

$$S(7,7,7+j) = P_j \cdot X_p \cdot \hat{\phi} \cdot 2.0 \cdot RX1M/(X_3^o)^2 \cdot \beta_1(1 - RX2M) \quad (B.74)$$

$$S(7+j,7+j,7+j) = -a_j m(m-1)S_j^{m-2} \quad (B.75)$$

$$S(7+j-1,7+j-1,7+j) = a_{j-1} \cdot m(m-1)S_{j-1}^{m-2} \quad , \quad j=2,\ldots,n \quad (B.76)$$

$$T(7+n,7+n,2) = a_j m(m-1)S_n^{m-2} \quad (B.77)$$

Appendix C

BROAD COMPARISON OF DISCHARGE PREDICTIONS USING DIFFERENT SPECTRAL DENSITY MATRICES

The spectral density matrices used in the following comparison are the matrix of level 4 (see Table 4.4) and a modified matrix of level 8 (see Table 6.2). The latter was found by setting all state variances to zero except those corresponding to the states of the channel. The eight different time intervals of Table C.1 were considered. All runs were made using the initial conditions employed in Chapter 6. As in Chapters 4 and 6, no error was attributed to the inputs.

Tables C.2, C.3, and C.4 present the residual statistics, normalized residual statistics and least square indices for discharge, respectively. Figures C.1 to C.16 show the predictions obtained in the different runs with the different spectral density matrices.

As it is observed, the spectral density matrix of level 8 with all but channel elements set to zero gives consistently better results than the Q matrix of level 4. Notice that although the matrix of level 8 was found using maximum discharges of 3.52 mm (see Figures C.11 and C.12) and a total of 124 data points, the use of such matrix gives reasonably good predictions for hydrographs with higher peaks (see Figures C.13 and C.15) for periods of time longer than one month data. Only the record event of run No. 4 was not properly reproduced.

Table C.1

Time Intervals Used In Comparisons

Run No.	Initial Date	Final Date
1	Mar 1/58	Apr 30/58
2	May 1/58	Jun 30/58
3	Jul 1/59	Jul 31/59
4	Sep 1/59	Oct 30/59
5	Mar 1/60	Apr 30/60
6	May 3/60	Jul 2/60
7	May 1/61	Jun 30/61
8	Jul 1/61	Aug 30/61

Table C.2

Discharge Residual Statistics for Different Runs

Run No.	Mean	Variation Coefficient	Skewness	Autocorrelations Lag-1	Lag-2	Lag-3	Lag-4
1	-0.014	-7.68	0.404	-0.093	-0.340	0.325	0.004
2	-0.004	-5.01	-1.62	-0.298	-0.032	0.195	-0.204
3	-0.008	-20.4	1.03	0.108	-0.183	0.022	-0.067
4	0.270	6.61	7.40	0.879	0.631	0.385	0.224
5	-0.009	-11.0	1.99	-0.027	-0.455	0.060	0.058
6	-0.0004	-381.3	1.46	0.382	-0.179	-0.081	0.165
7	0.003	69.7	2.68	0.446	-0.146	-0.146	0.029
8	0.018	12.1	3.07	0.566	0.029	-0.066	0.139
Q-level 8 with all but channel elements set to zero							
1	0.017	9.90	0.708	-0.587	0.833	-0.568	0.681
2	-0.003	-13.9	-2.72	-0.600	0.361	-0.276	0.190
3	0.066	3.70	1.52	0.284	0.537	0.039	0.141
4	0.431	4.93	6.24	0.915	0.741	0.558	0.429
5	0.014	10.0	1.79	-0.397	0.784	-0.395	0.640
6	0.058	4.19	3.33	0.644	0.709	0.397	0.387
7	0.120	4.00	4.90	0.840	0.794	0.562	0.461
8	0.169	3.64	3.64	0.911	0.831	0.658	0.515
Q-level 4							

Table C.3

Discharge Normalized Residual Statistics for Different Runs

Run No.	Mean	Variation Coefficient	Skewness	Autocorrelations Lag-1	Lag-2	Lag-3	Lag-4
1	-0.027	-6.66	-0.257	-0.060	-0.359	0.303	0.017
2	-0.006	-5.12	-3.42	-0.306	0.034	0.203	-0.204
3	-0.025	-11.5	0.912	0.150	-0.201	0.035	-0.047
4	0.147	6.57	5.43	0.883	0.697	0.548	0.422
5	-0.019	-8.62	0.154	0.032	-0.487	0.003	0.131
6	-0.009	-32.7	-0.239	0.404	-0.215	-0.102	0.189
7	-0.008	-50.4	1.65	0.417	-0.189	-0.137	0.056
8	0.023	16.0	2.74	0.582	0.033	-0.072	0.126
Q-level 8 with all but channel elements set to zero							
1	-0.0001	-6230.0	0.37	-0.602	0.840	-0.578	0.700
2	-0.027	-8.13	-4.95	-0.514	0.330	-0.269	0.196
3	0.173	5.07	1.01	0.117	0.530	-0.041	0.178
4	0.329	4.49	3.37	0.833	0.846	0.698	0.727
5	-0.014	-40.3	1.53	-0.446	0.781	-0.431	0.662
6	0.129	5.72	2.29	0.444	0.714	0.276	0.430
7	0.245	4.33	2.70	0.588	0.800	0.445	0.562
8	0.315	3.98	2.62	0.776	0.827	0.602	0.555
Q-level 4							

Table C.4

Discharge Least Squares Indices for Different Runs

Run No.	Efficiency	Determination	Persistance	Extrapolation
1	0.909	0.915	0.141	-0.66
2	0.839	0.878	0.251	0.28
3	0.937	0.940	0.617	0.32
4	0.615	0.746	-3.00	-3.94
5	0.915	0.926	0.130	-0.36
6	0.938	0.939	0.291	-0.65
7	0.931	0.931	-0.060	-1.24
8	0.961	0.964	0.332	-0.62
Q-level 8 with all but channel elements set to zero				
1	0.768	0.774	-1.191	-3.24
2	0.264	0.537	-2.42	-2.29
3	0.858	0.889	0.146	-0.52
4	0.443	0.757	-4.80	-6.15
5	0.834	0.836	-0.697	-1.66
6	0.863	0.923	-0.570	-2.66
7	0.715	0.841	-3.37	-8.23
8	0.690	0.891	-4.25	-11.7
Q-level 4				

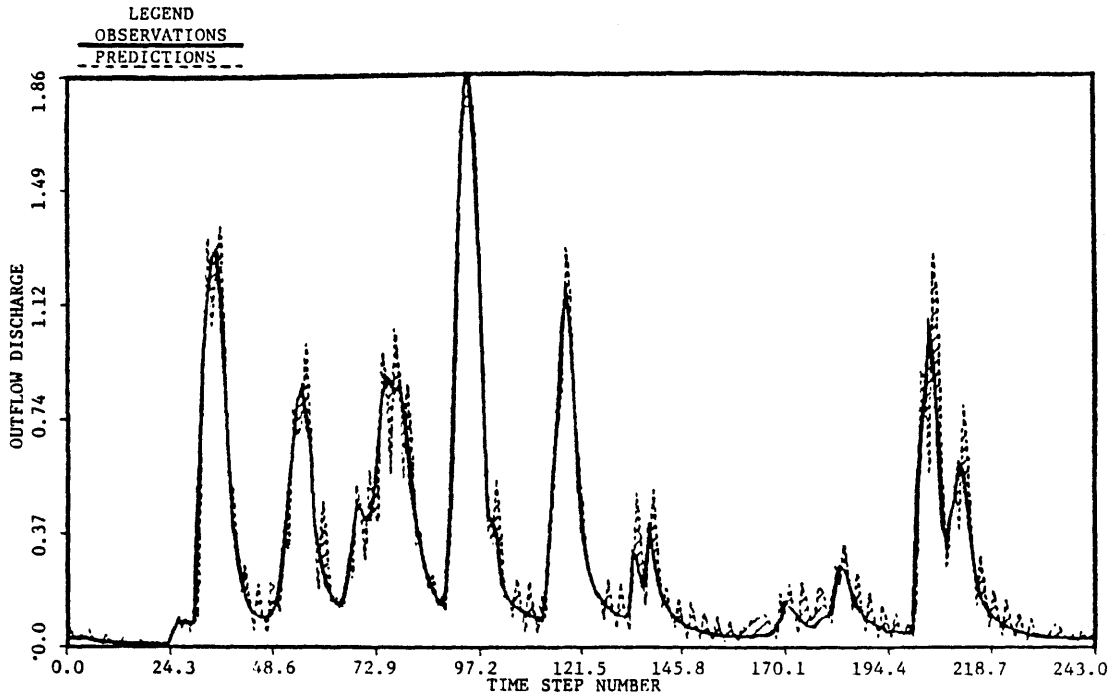

Figure C.1 Stochastic Prediction of Discharge, Bird Creek, Run No. 1, EKF, Q-8, only channel non-zero

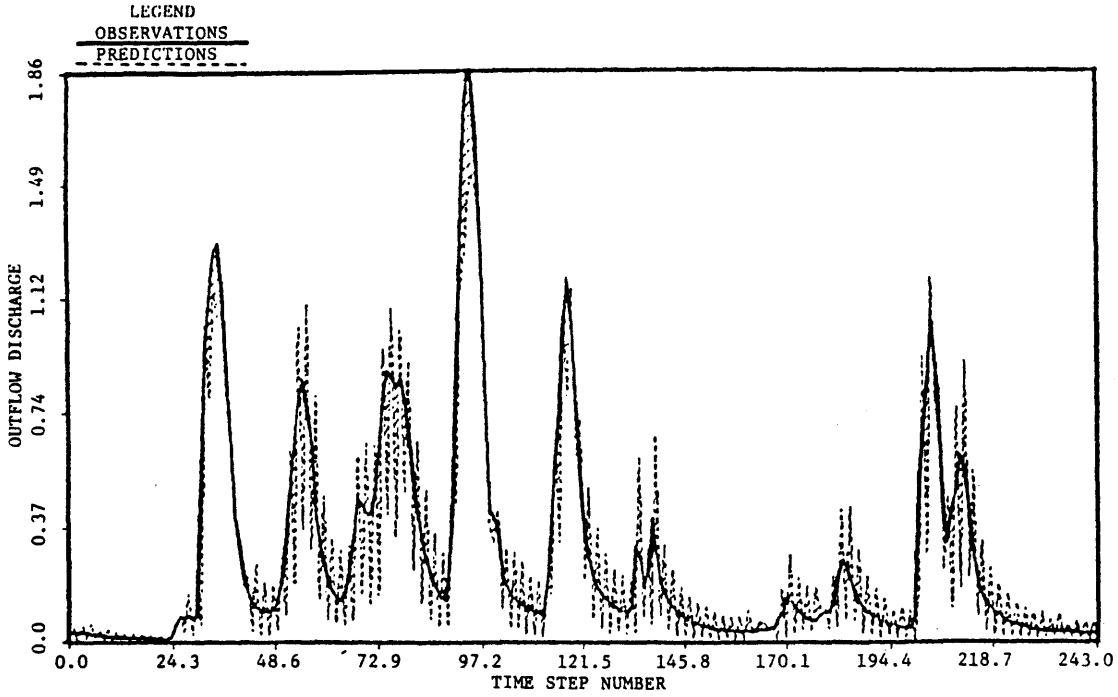

Figure C.2 Stochastic Prediction of Discharge, Bird Creek, Run No. 1, EKF, Q-4

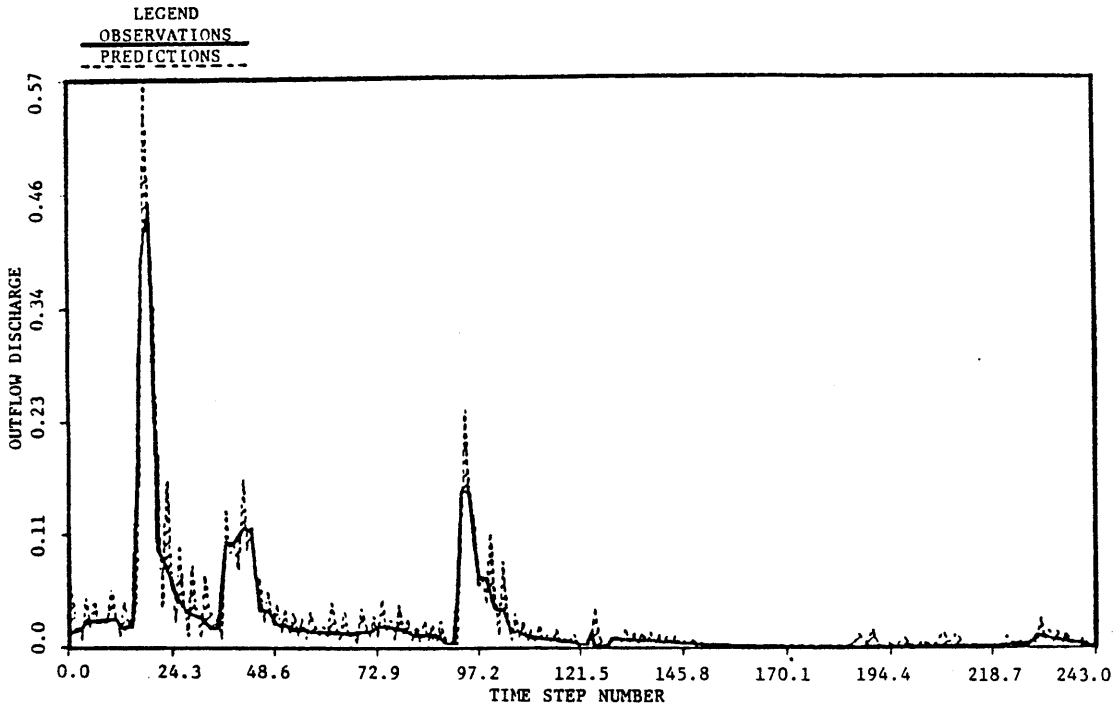

Figure C.3 Stochastic Prediction of Discharge, Bird Creek, Run No. 2, EKF, Q-8, only channel non-zero

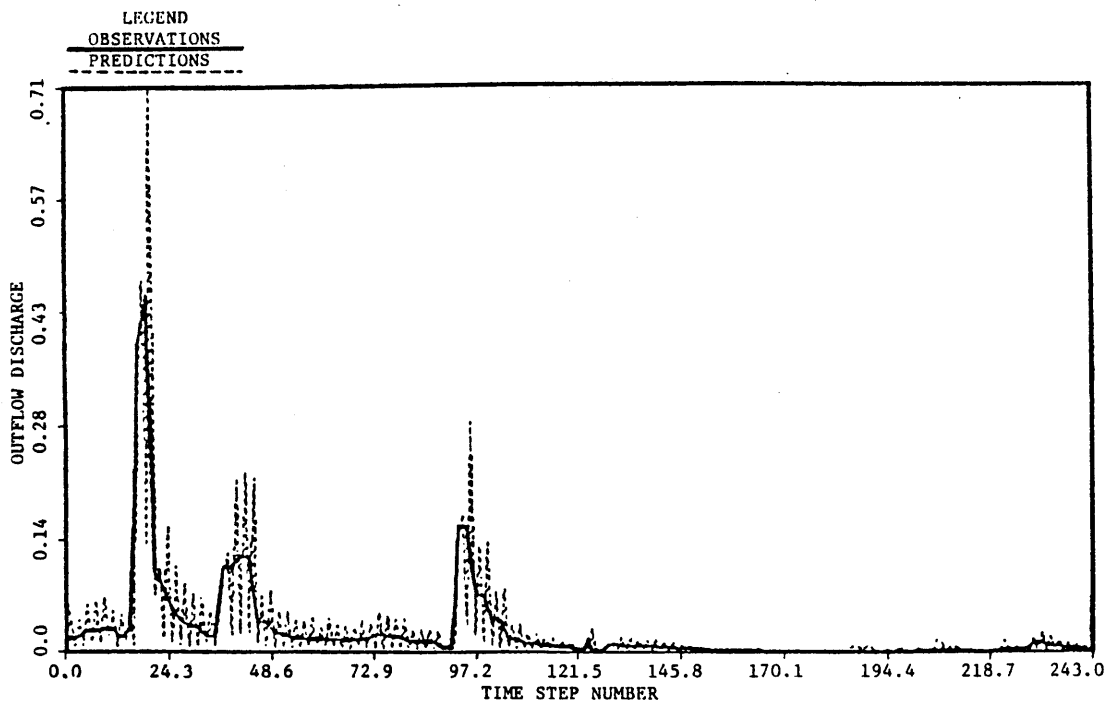

Figure C.4 Stochastic Prediction of Discharge, Bird Creek, Run No. 2, EKF, Q-4

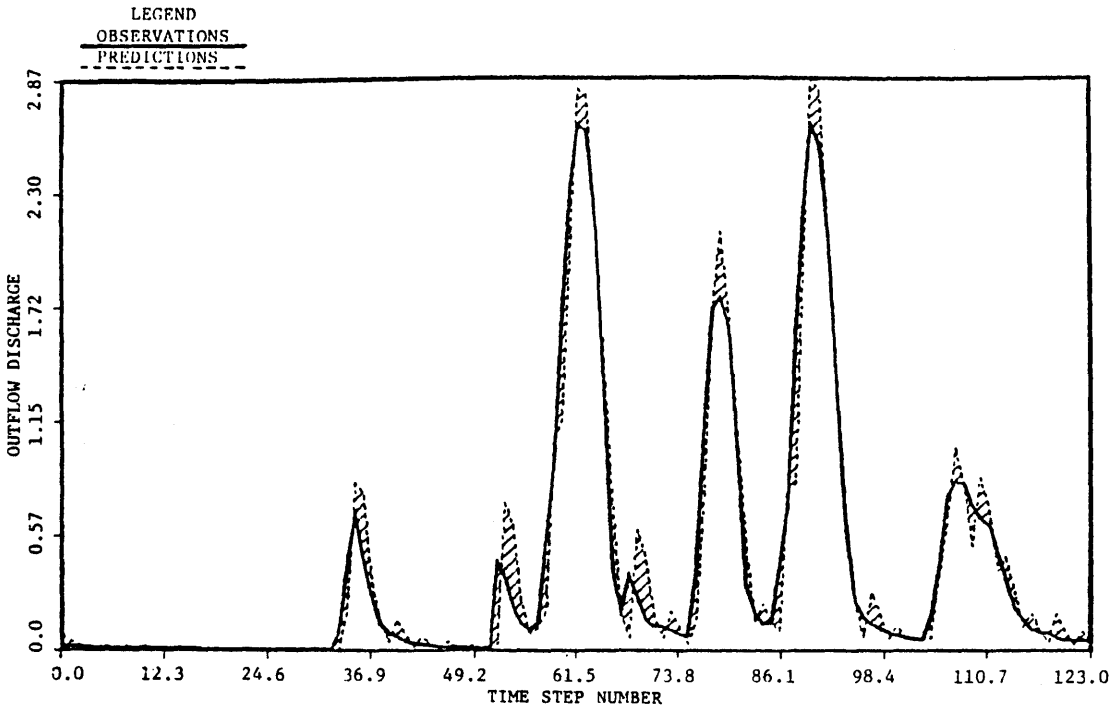

Figure C.5 Stochastic Prediction of Discharge, Bird Creek, Run No. 3, EKF, Q-8, only channel non-zero

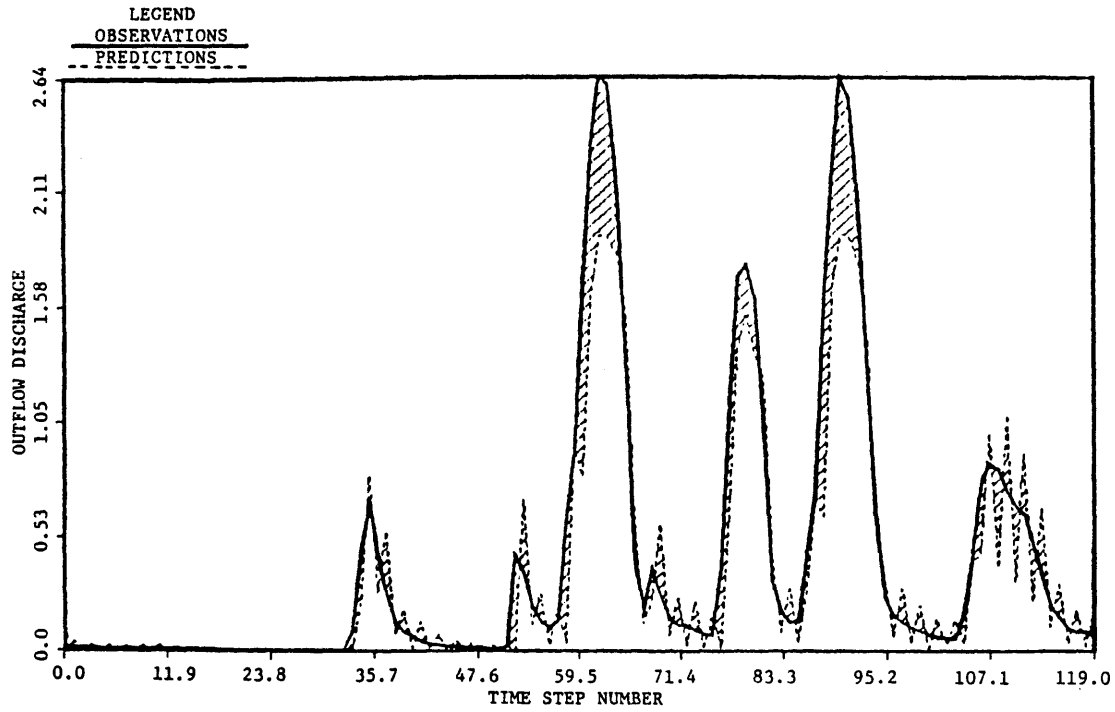

Figure C.6 Stochastic Prediction of Discharge, Bird Creek, Run No. 3, EKF, Q-4

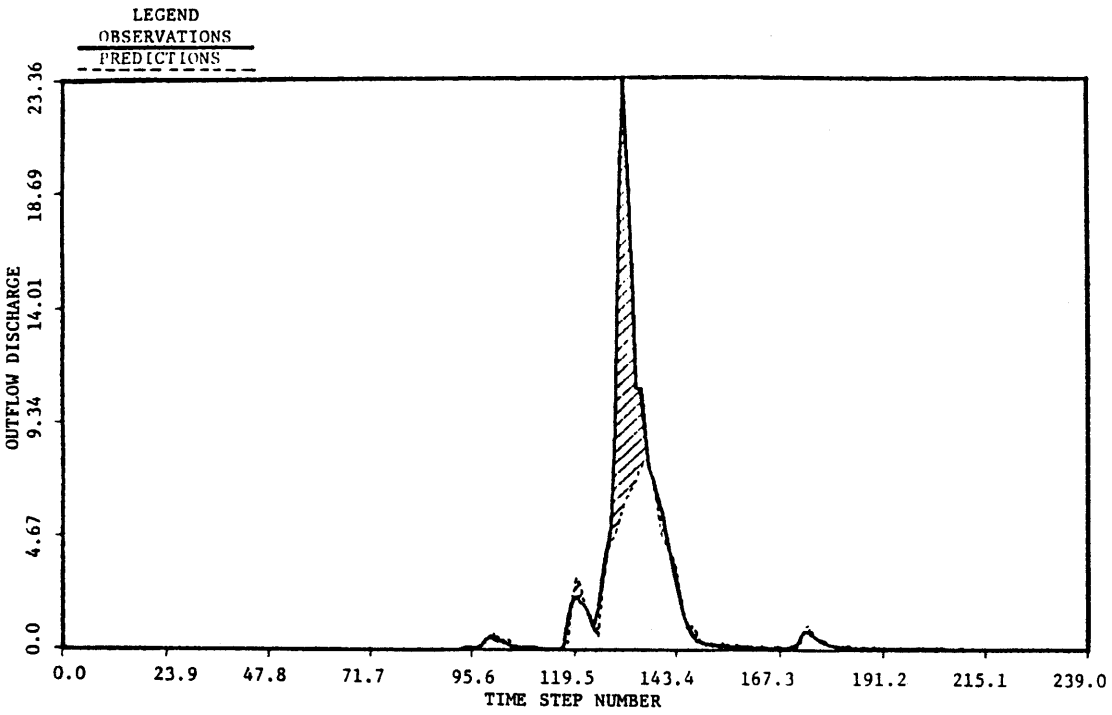

Figure C.7 Stochastic Prediction of Discharge, Bird Creek, Run No. 4, EKF, Q-8, only channel non-zero

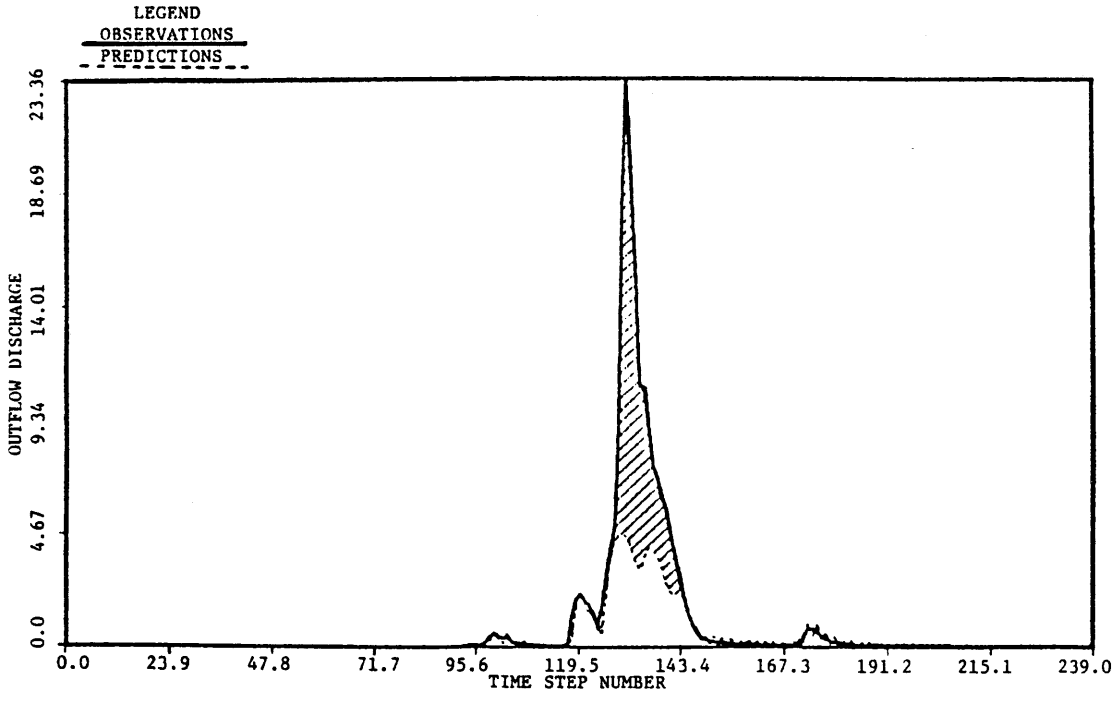

Figure C.8 Stochastic Prediction of Discharge, Bird Creek, Run No. 4, EKF, Q-4

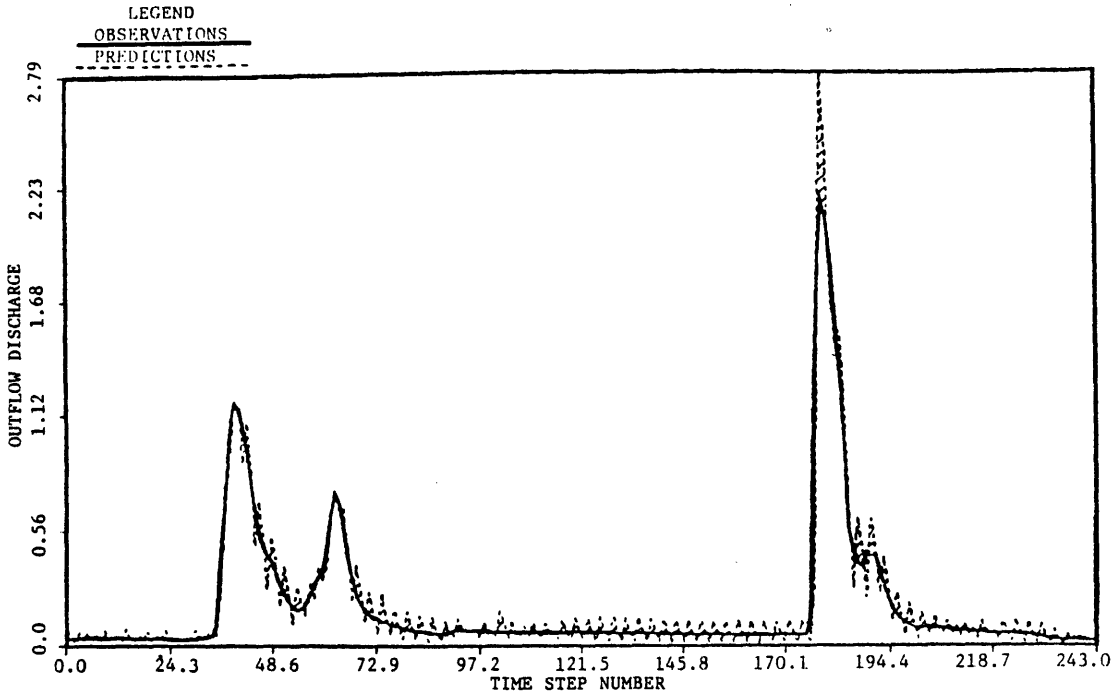

Figure C.9 Stochastic Prediction of Discharge, Bird Creek, Run No. 5, EKF, Q-8, only channel non-zero

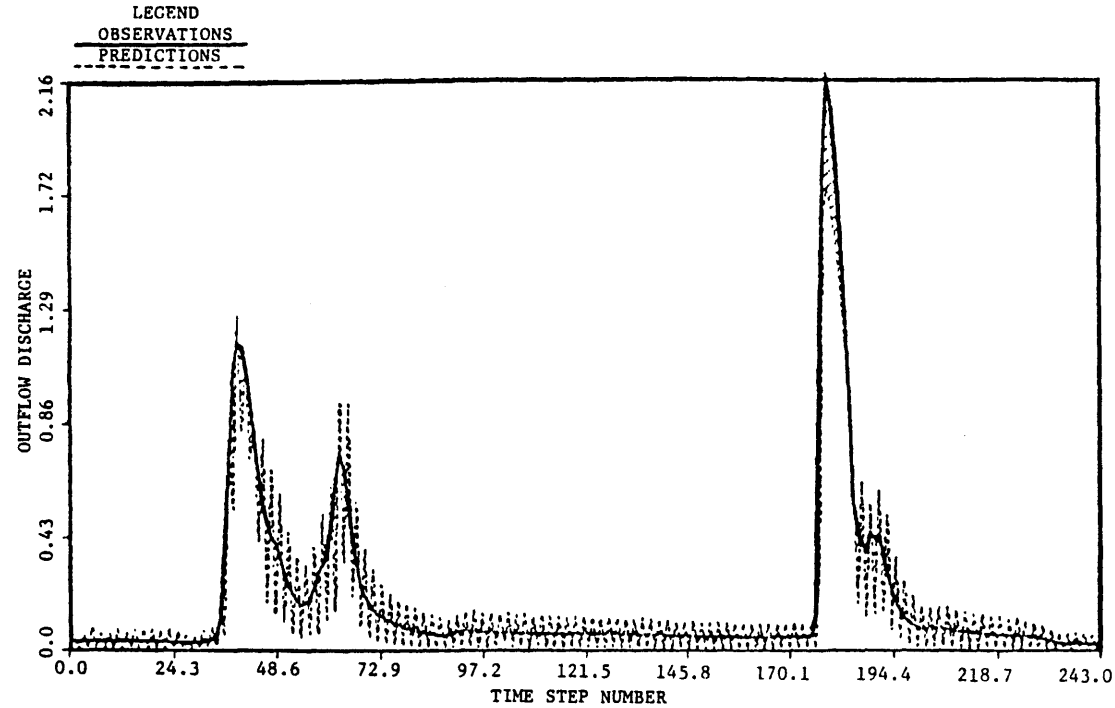

Figure C.10 Stochastic Prediction of Discharge, Bird Creek, Run No. 5, EKF, Q-4

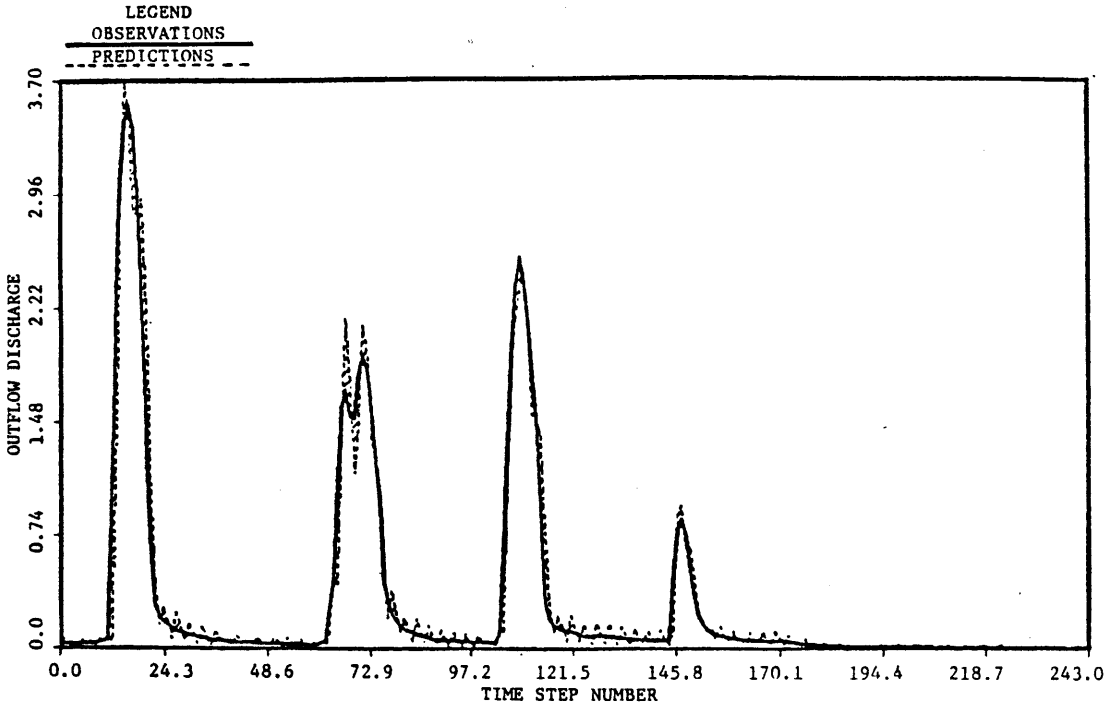

Figure C.11 Stochastic Prediction of Discharge, Bird Creek, Run No. 6, EKF, Q-8, only channel non-zero

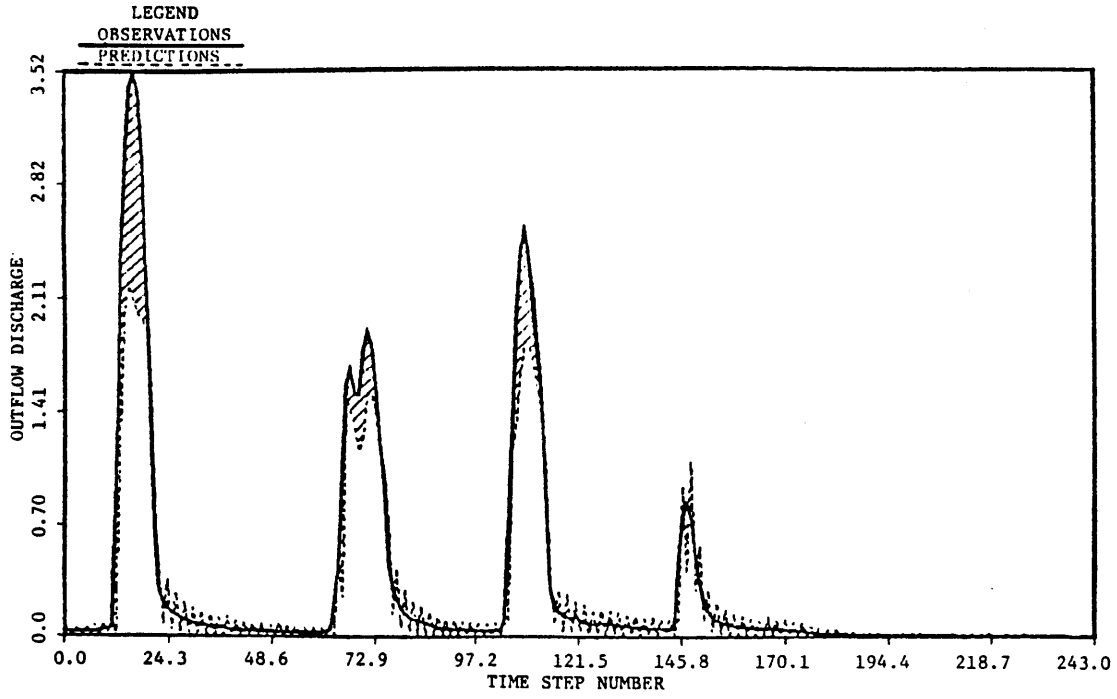

Figure C.12 Stochastic Prediction of Discharge, Bird Creek, Run No. 6, EKF, Q-4

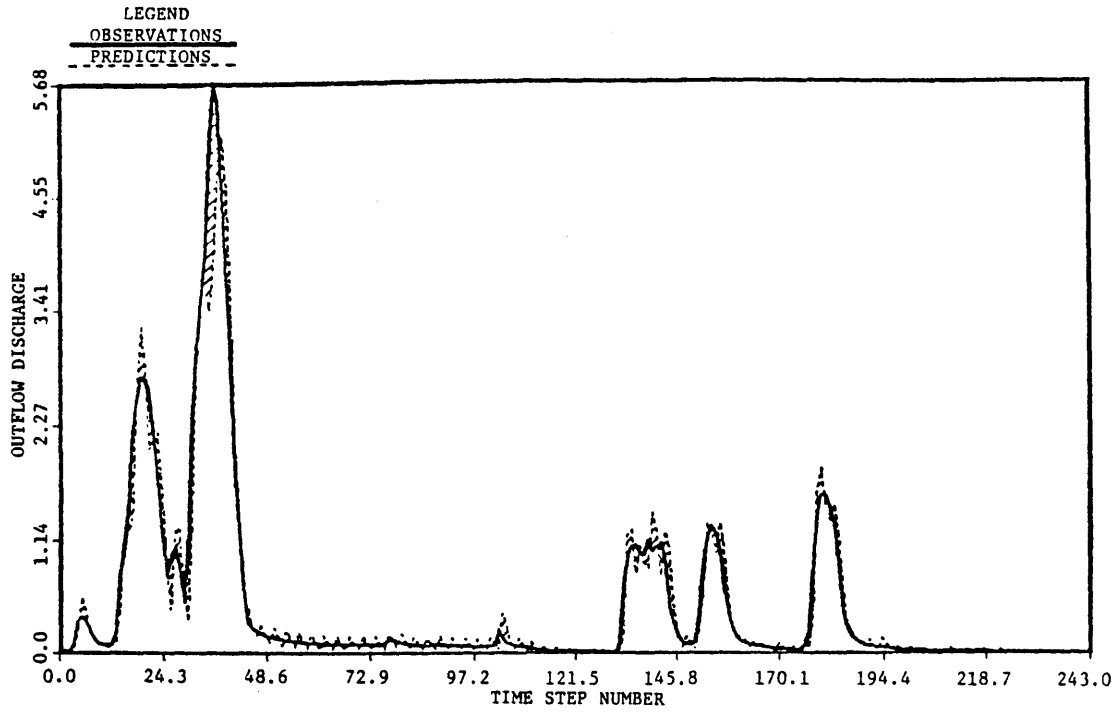

Figure C.13 Stochastic Prediction of Discharge, Bird Creek, Run No. 7, EKF, Q-8, only channel non-zero

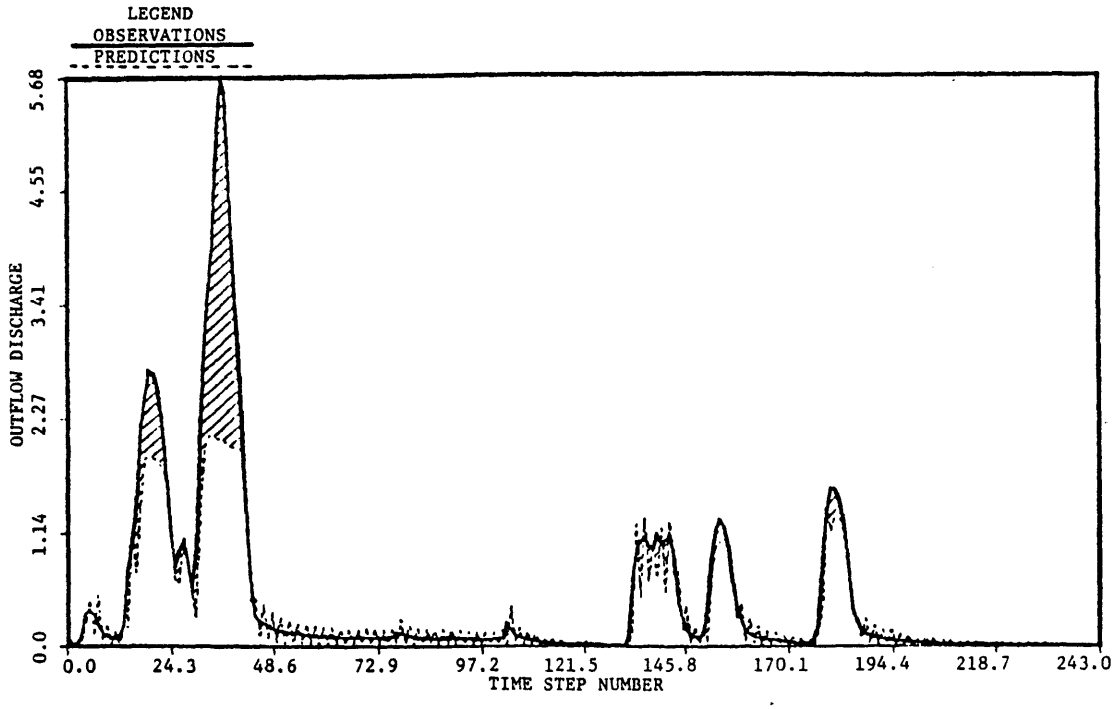

Figure C.14 Stochastic Prediction of Discharge, Bird Creek, Run No. 7, EKF, Q-4

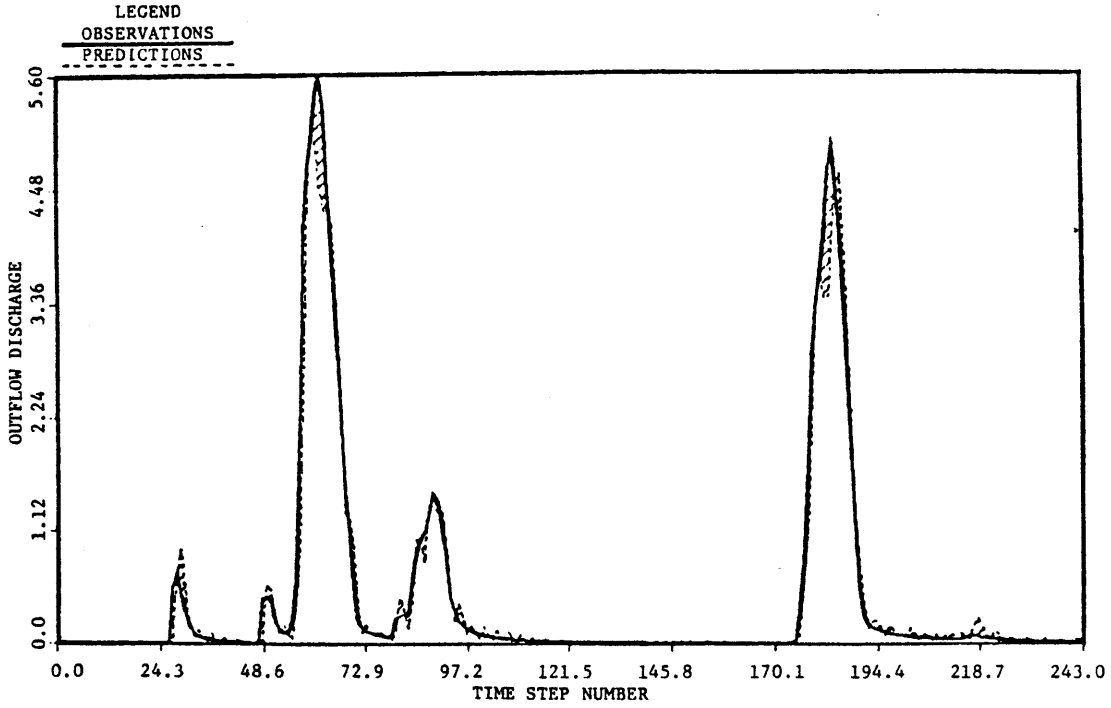

Figure C.15 Stochastic Prediction of Discharge, Bird Creek, Run No. 8, EKF, Q-8, only channel non-zero

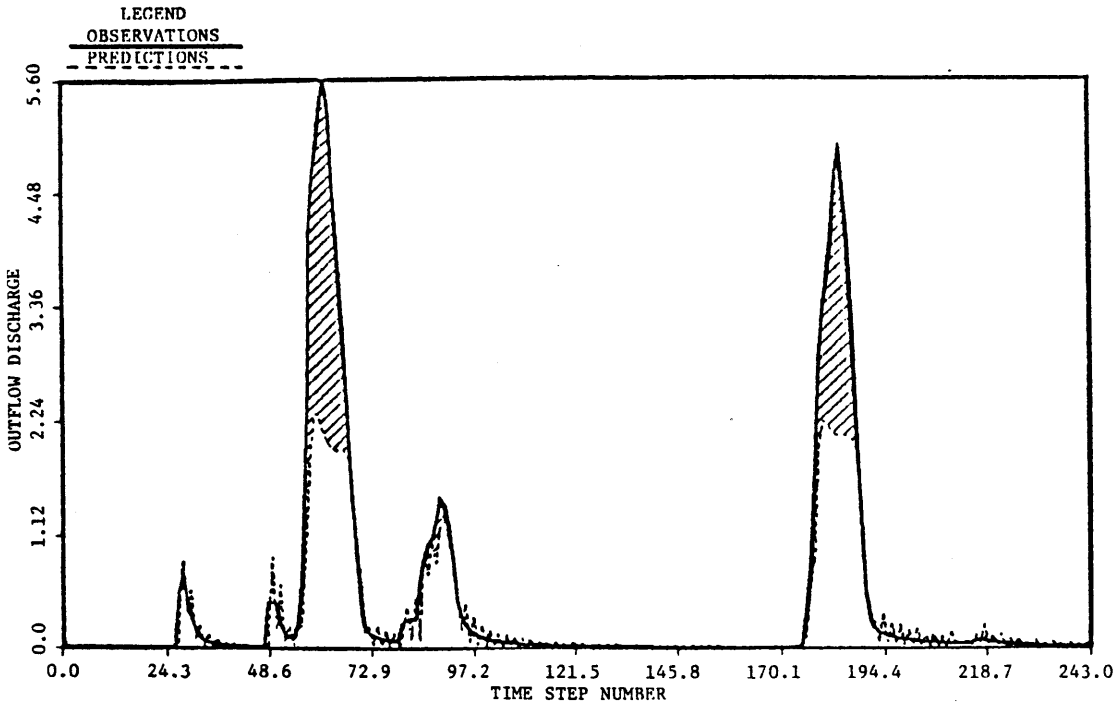

Figure C.16 Stochastic Prediction of Discharge, Bird Creek, Run No. 8, EKF, Q-4

Figure C.17 show, for the different matrices, a histogram of the difference in time between the predicted and observed hydrograph peaks, for the eight runs made. Observed peaks higher than 0.43 mm/6 hrs. are included in that figure. Figure C.18 depicts, for the significant peaks, the percent error in predicting the peak magnitude. Such percent error is defined by:

$$\left(\frac{\text{Predicted Peak - Observed Peak}}{\text{Observed Peak}}\right) \times 100$$

Notice that about 50% of the peaks time to peak was correctly forecasted irrelevant of the spectral density matrix used. Although timing is not considerably different for the two spectral density matrices, the peak magnitudes are better preserved with the Q matrix of level 8 with only non-zero channel values. Notice that with the modified matrix of level 8, 38.9% of the peak magnitudes were predicted with less than 10 percent error, and 92% of the cases were predicted with errors less than 30%. This matrix, however, tends to overpredict the peak magnitude, while the Q matrix of level 4 tends to underestimate the bigger peaks.

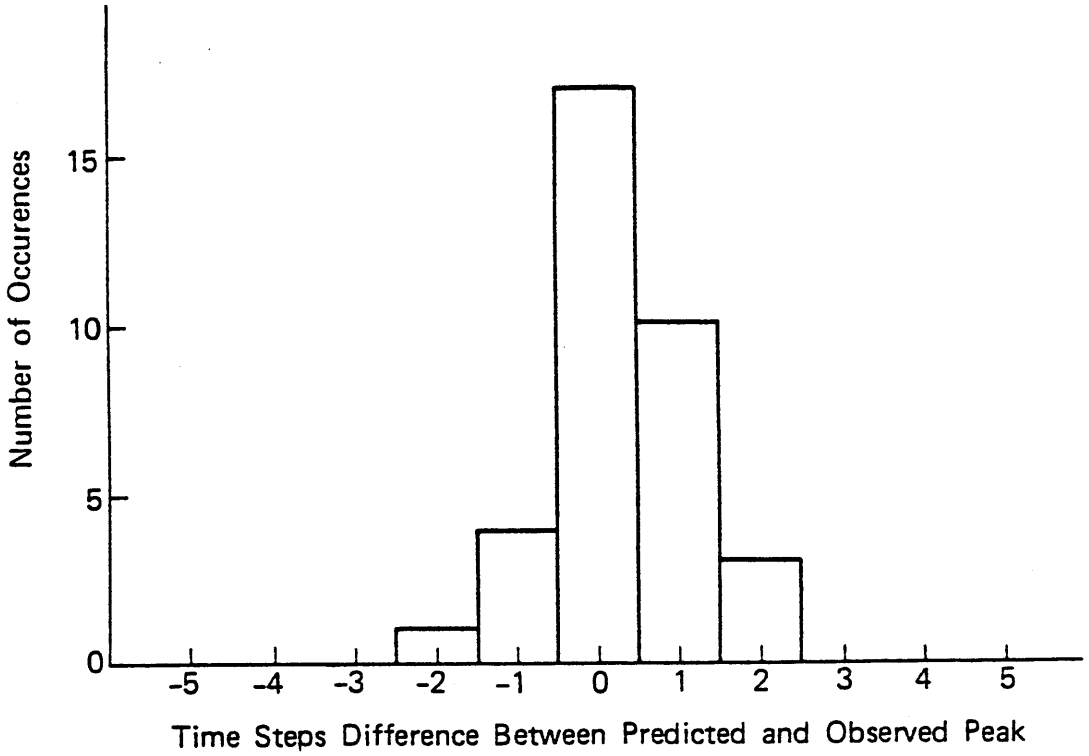

(a)

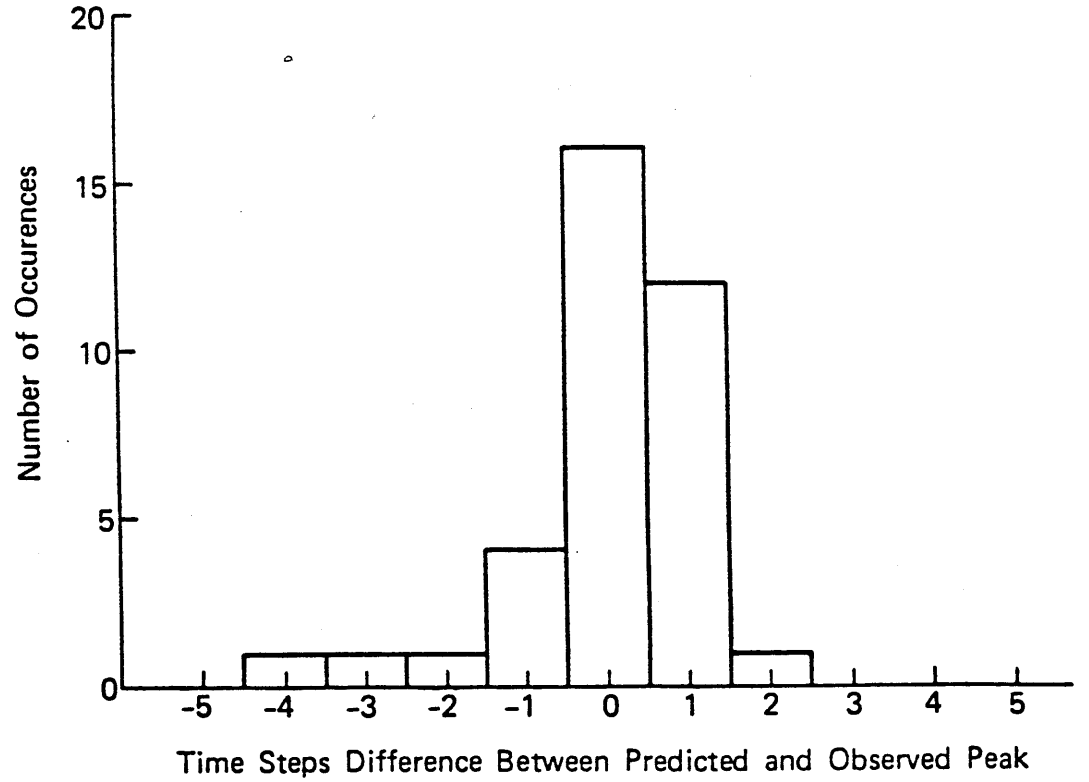

(b)

Figure C.17 Histogram of the Difference in Time Between Predicted and Observed Peak
(a) Q-8 with all but channel values set to zero
(b) Q-4

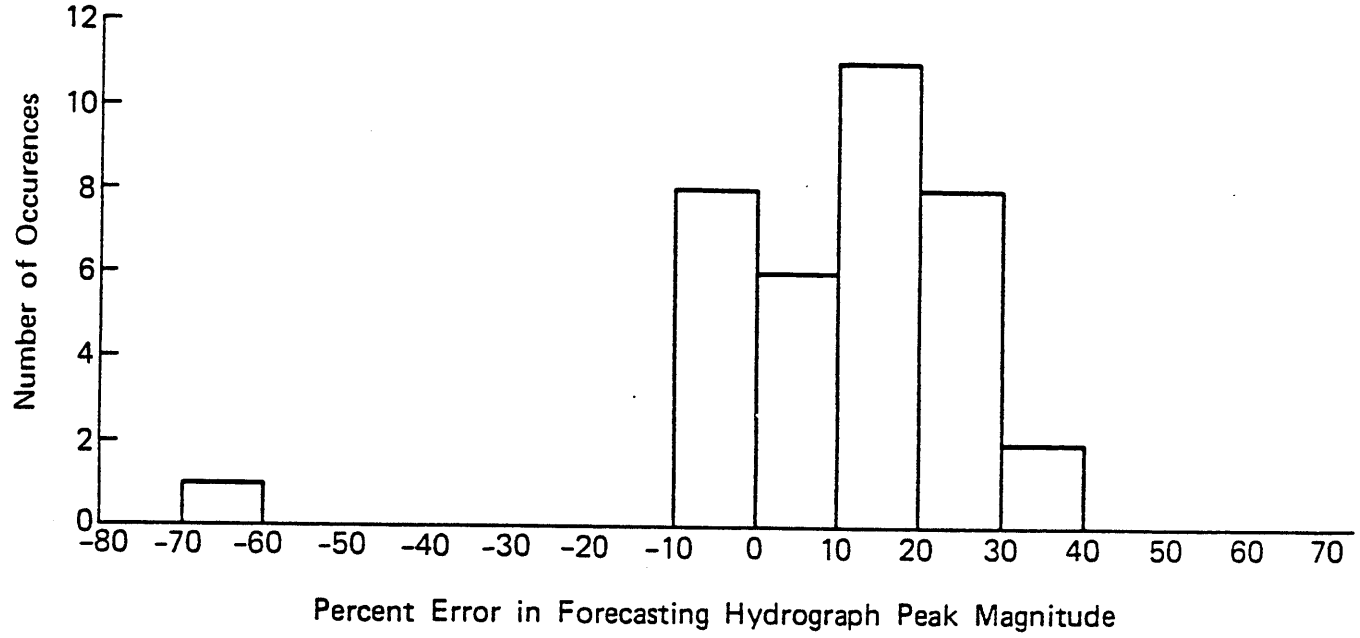

(a)

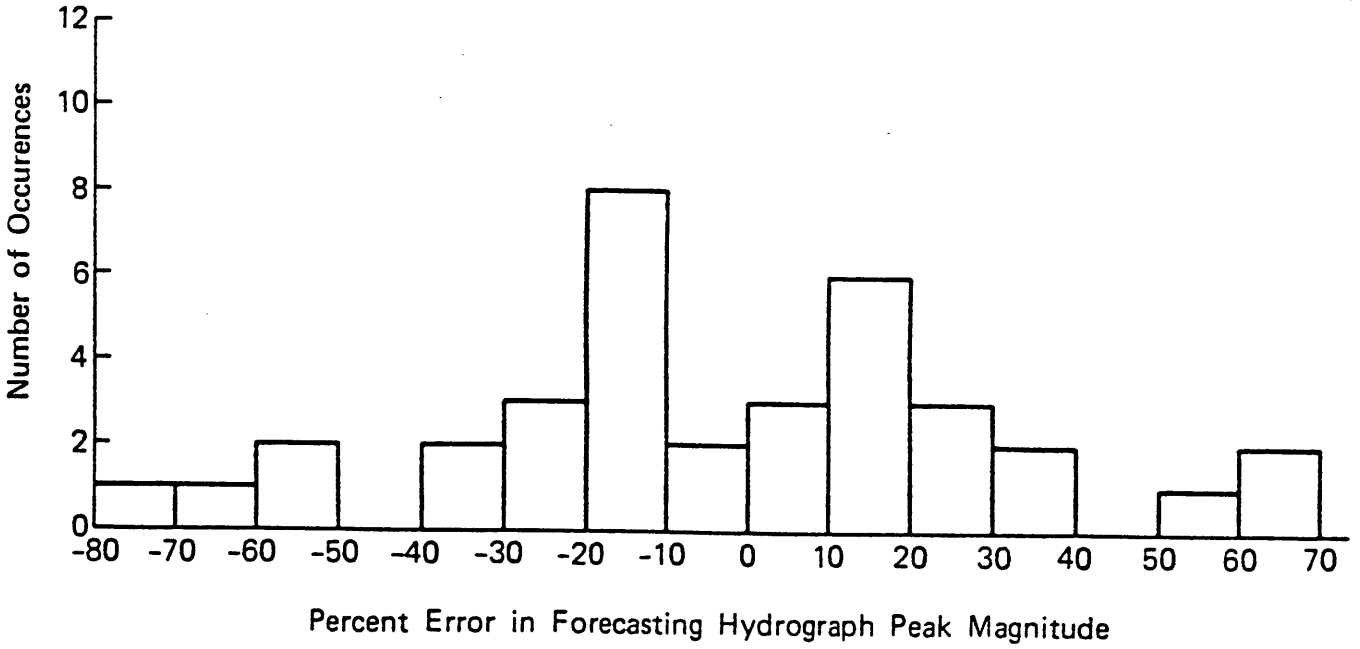

(b)

Figure C.18 Histogram of the Percent Error in Forecasting Hydrograph Peak Magnitude
(a) Q-8 with all but channel values set to zero
(b) Q-4

Appendix D

APPROXIMATE MAXIMUM LIKELIHOOD ESTIMATION ON THE POTOMAC BASIN

The results obtained when using the approximate maximum likelihood method of Chapter 5 to estimate the diagonal spectral density matrices of the large basin on the Potomac River are presented in this Appendix. The decomposition procedure of Georgakakos (1983) served as the filtering mechanism used in the computations. Although the spectral density matrix of upstream sub-basins affects the spectral density matrix of downstream tributary sub-basins, the precipitation and discharge observations likelihood were maximized on an individual basis. The initial spectral density matrices were those on Table 8.5. The upper bounds shown in Table D.1 were used to prevent unrealistically high estimates. Table D.2 contains the final spectral density matrices and the initial and final log-likelihood values found on each sub-basin. The approximate maximum likelihood procedure used the conditional information and Newton's method in its search algorithm. Due to cost and time restrictions the computations were carried for only 10 iterations on each sub-basin. However, as can be observed in Table D.2, the likelihood increased in all cases.

Figures D.1 to D.10 show the discharge predictions on the Potomac basin when using the decomposition procedures of Georgakakos (1983)

Table D.1

Spectral Density Matrices Upper Bounds on the Potomac Basin

State	Cootes Store	All Others
X_p	30	30
X_1	70	40
X_2	25	25
X_3	80	180
X_4	30	130
X_5	45	45
X_6	160	160
S_1	50	50
S_2	50	50
S_3		50
S_4		50
S_5		50

Table D.2

Spectral Density Estimates and Log-Likelihoods on the Potomac River

State	Lynnwood	Front Royal	Cootes Store	Strasburg	Millville
X_p	21.8	24.8	20.2	16.7	10^{-5}
X_1	40	40	40	40	40
X_2	25	25	10^{-5}	10^{-5}	10^{-5}
X_3	10^{-5}	10^{-5}	10^{-5}	10^{-5}	10^{-5}
X_4	130	130	30	130	130
X_5	10^{-5}	45	10^{-5}	10^{-5}	10^{-5}
X_6	160	10^{-5}	154.3	10^{-5}	160
S_1	10^{-5}	0.542	0.977	49.8	28.5
S_2	0.482	0.805	0.207	2.45	4.53
S_3	1.332	0.895		45.9	
S_4				10^{-5}	
S_5				1.99	
Initial Log-Likelihood	-963.1	-1496.1	-485.5	-575.1	-974.4
Final Log-Likelihood	-409.9	-416.7	-294.9	-350.0	-478.0

and Puente, et al. (1983), respectively, with the spectral density matrices of Table D.2. As can be observed, the predictions do not necessarily look better than those obtained using the initial spectral density matrices; see Figures 8.12 to 8.21. Notice that although for the sub-basin at Strasburg slightly better results were now obtained; the sub-basin at Lynnwood now gives oscillatory predictions due to the high spectral density variance used at its last channel state, see Table D.2. The likelihood was increased due to changes in residual variances but not due to lower residuals.

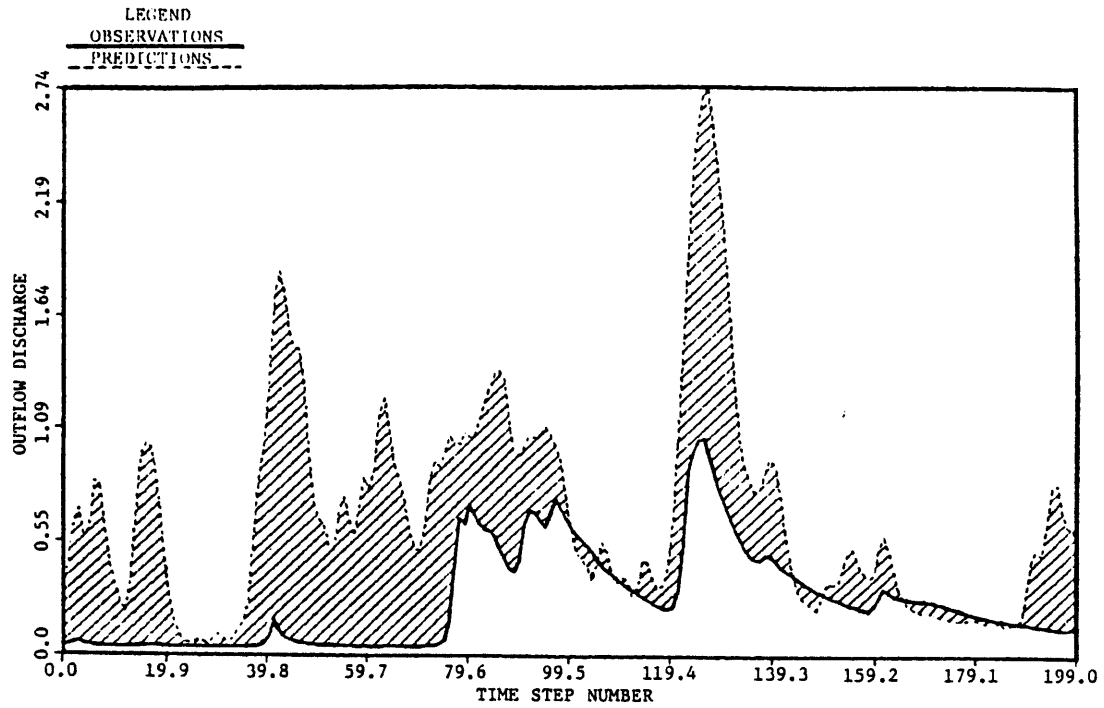

Figure D.1 Stochastic Prediction of Discharge, Lynnwood, Decomposition Procedure of Georgakakos, October 12 to November 30, 1970, Maximum Likelihood

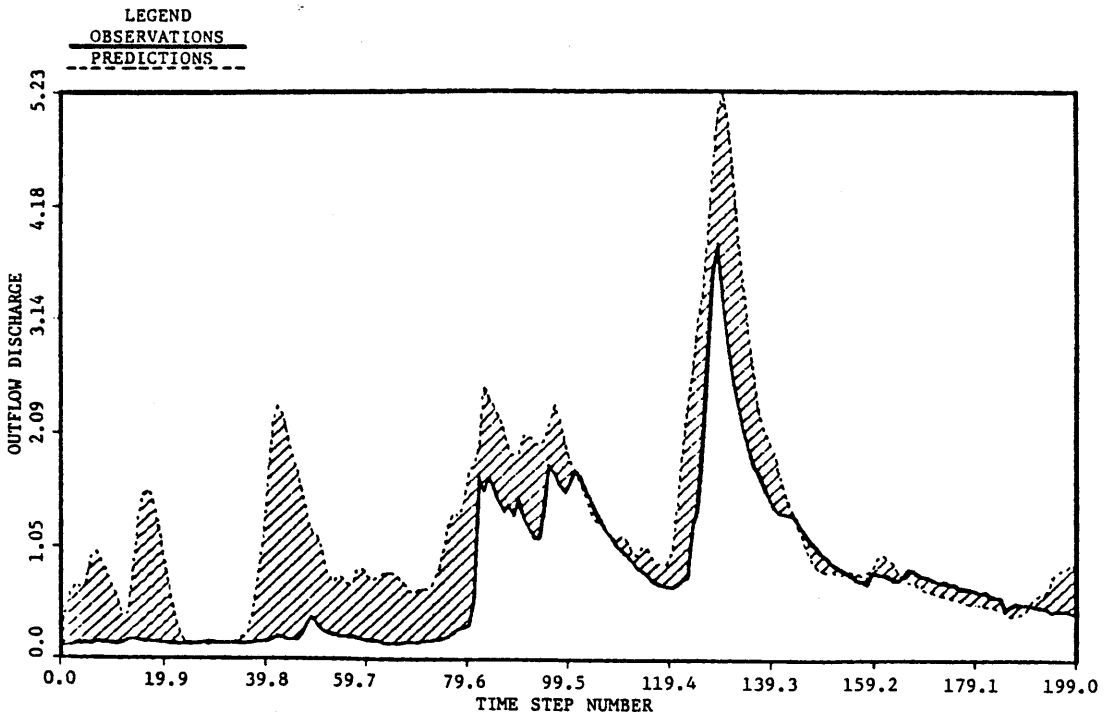

Figure D.2 Stochastic Prediction of Discharge, Front Royal, Decomposition Procedure of Georgakakos, October 12 to November 30, 1970, Maximum Likelihood

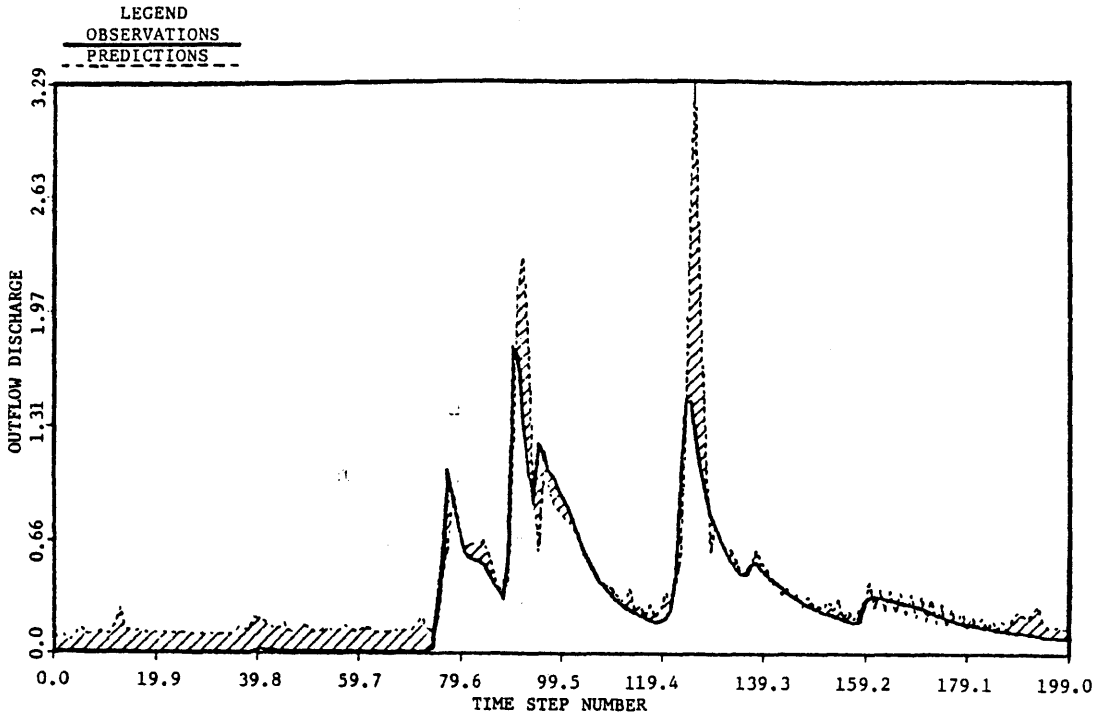

Figure D.3 Stochastic Prediction of Discharge, Cootes Store, Decomposition Procedure of Georgakakos, October 12 to November 30, 1970, Maximum Likelihood

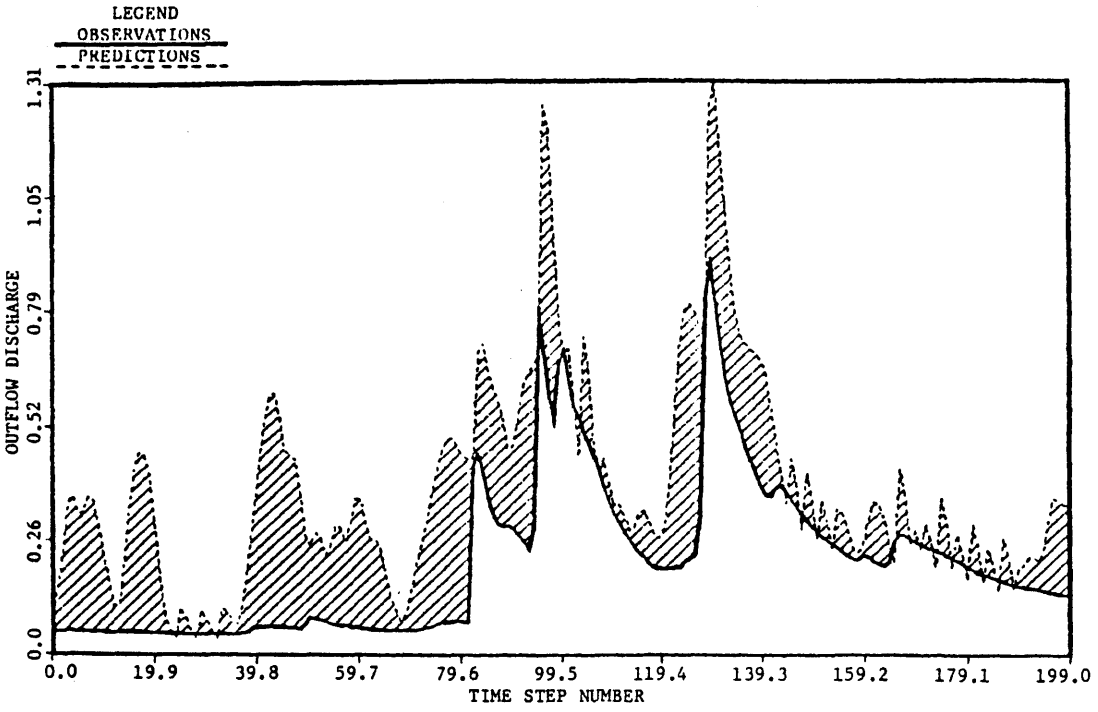

Figure D.4 Stochastic Prediction of Discharge, Strasburg, Decomposition Procedure of Georgakakos, October 12 to November 30, 1970, Maximum Likelihood

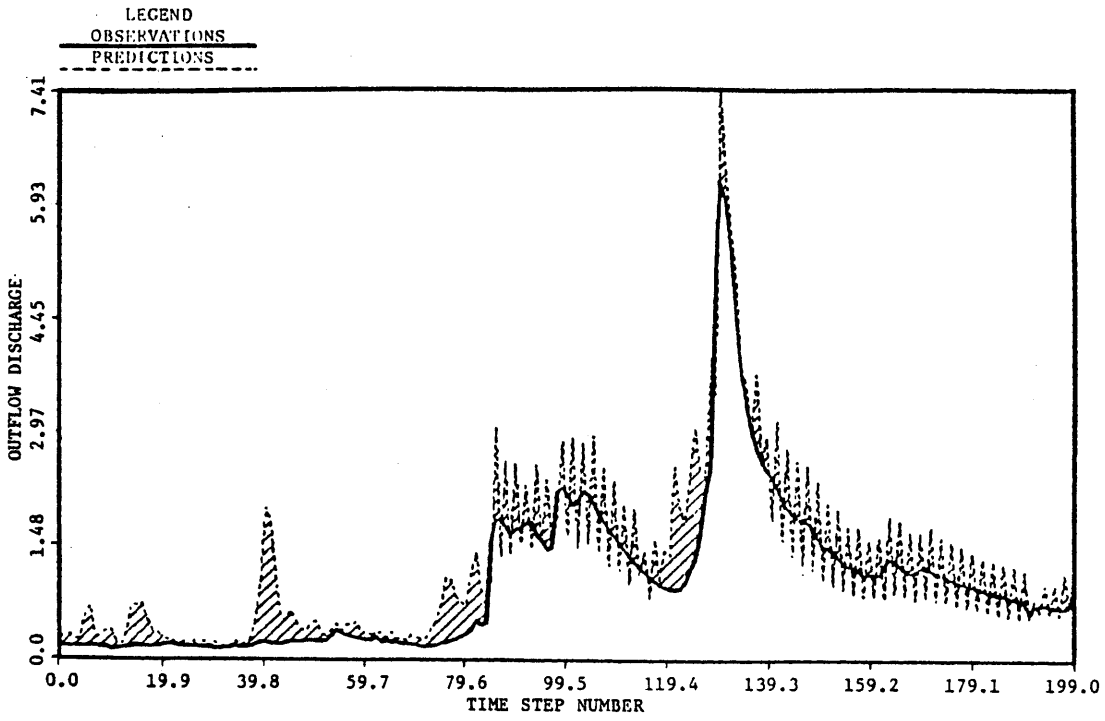

Figure D.5 Stochastic Prediction of Discharge, Millville, Decomposition Procedure of Georgakakos, October 12 to November 30, 1970, Maximum Likelihood

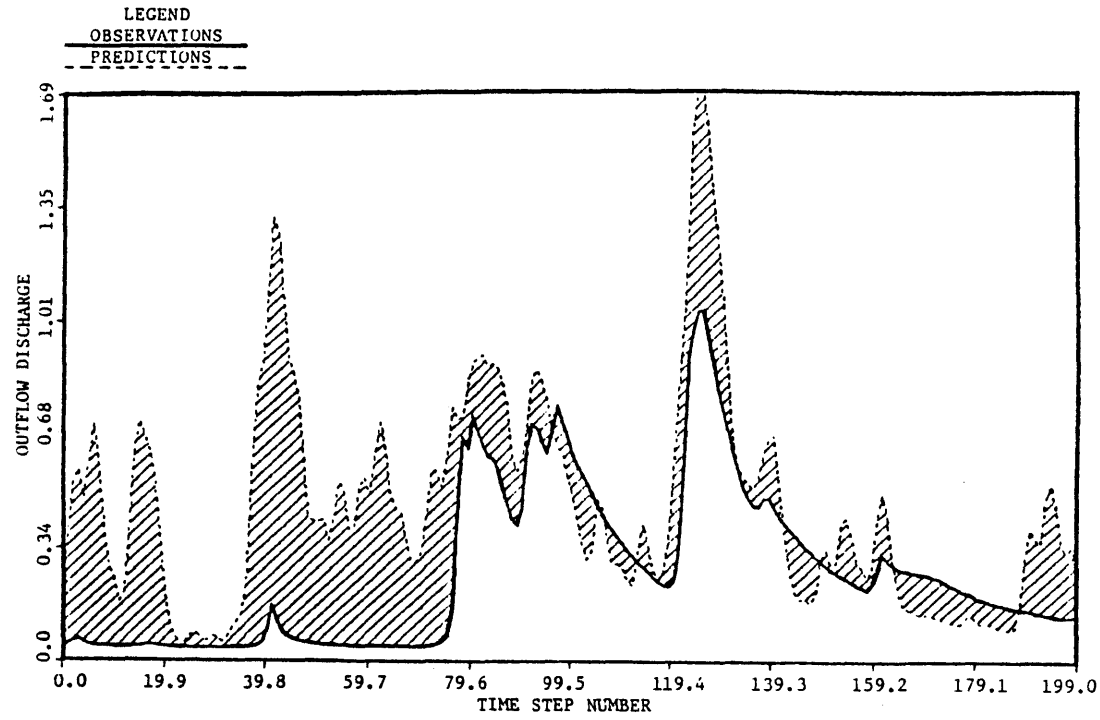

Figure D.6 Stochastic Prediction of Discharge, Lynnwood, Decomposition Procedure of Puente, et al., October 12 to November 30, 1970, Maximum Likelihood

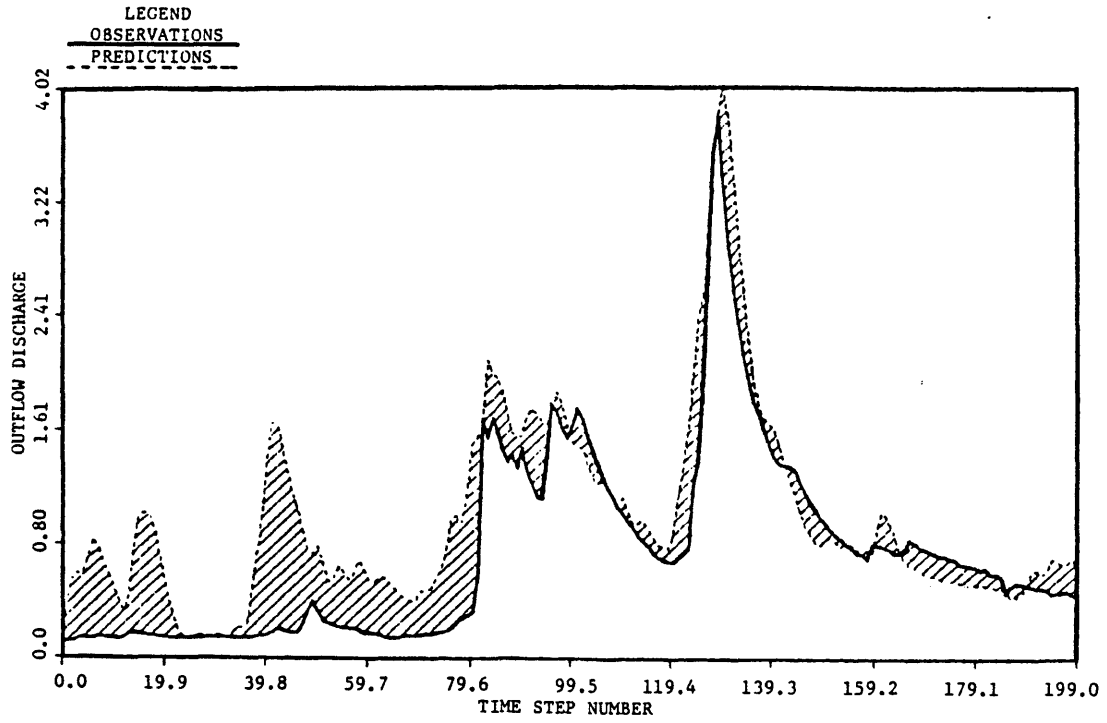

Figure D.7 Stochastic Prediction of Discharge, Front Royal, Decomposition Procedure of Puente, et al., October 12 to November 30, 1970, Maximum Likelihood

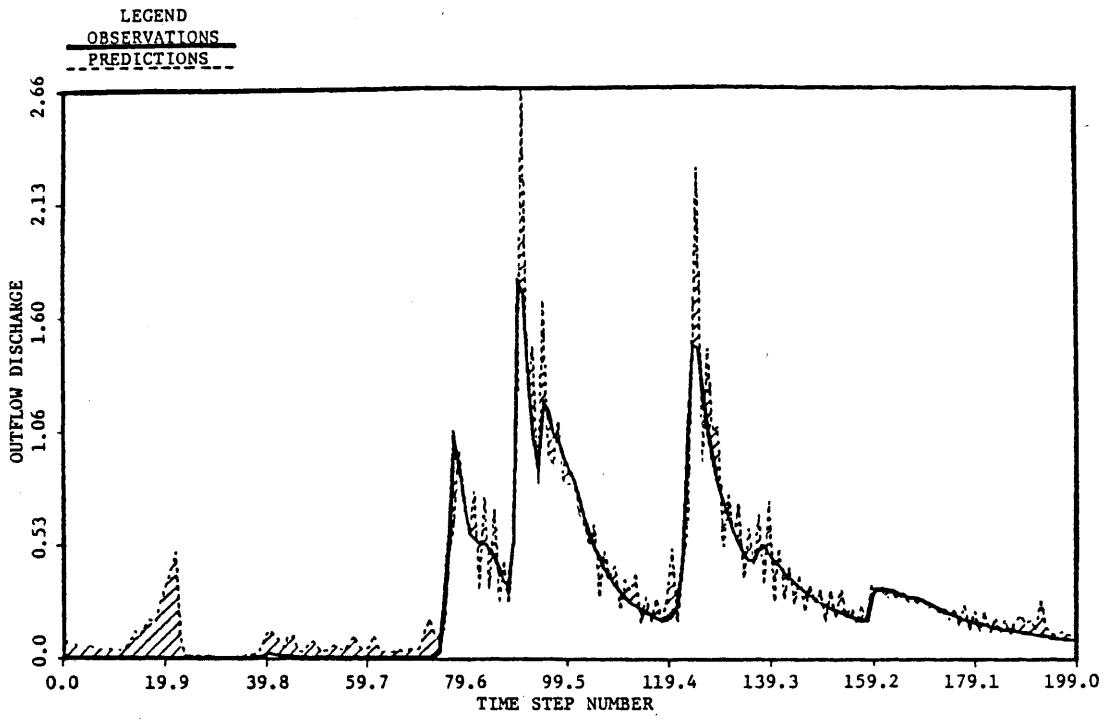

Figure D.8 Stochastic Prediction of Discharge, Cootes Store, Decomposition Procedure of Puente, et al., October 12 to November 30, 1970, Maximum Likelihood

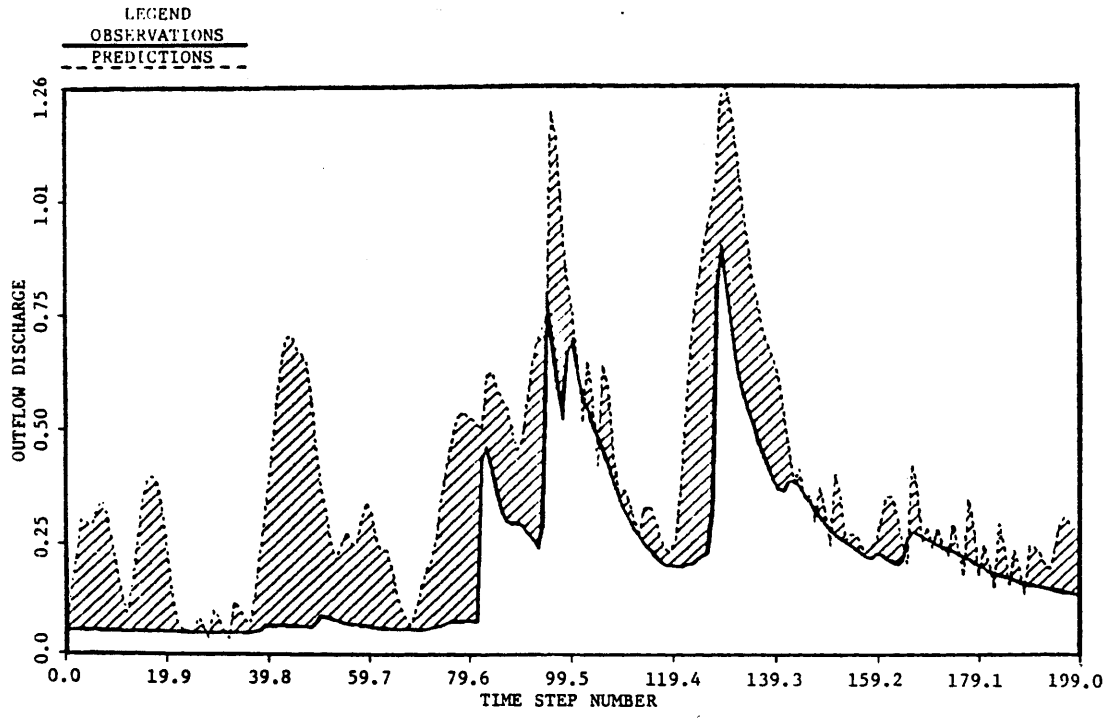

Figure D.9 Stochastic Prediction of Discharge, Strasburg, Decomposition Procedure of Puente, et al., October 12 to November 30, 1970, Maximum Likelihood

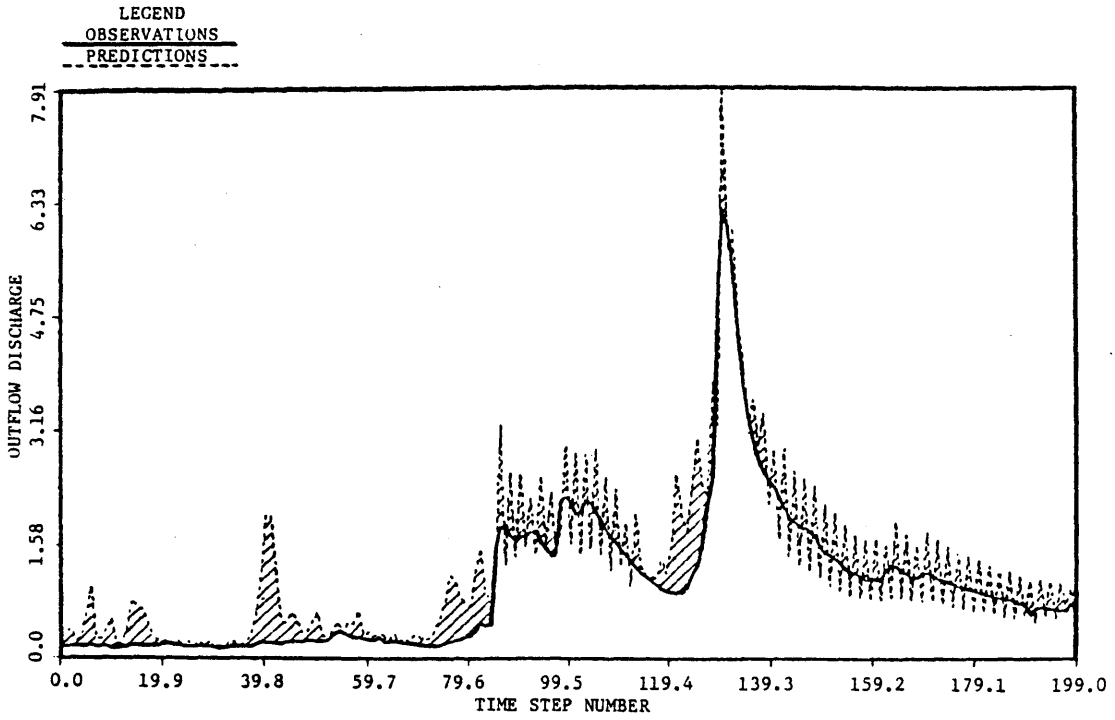

Figure D.10 Stochastic Prediction of Discharge, Millville, Decomposition Procedure of Puente, et al., October 12 to November 30, 1970, Maximum Likelihood